Characterising the interaction of fragments derived from Bcl-xL, Bax and Bid with lipid membranes

Ana Jesús García Sáez

Valencia, Marzo de 2005

Memoria presentada para optar al grado de Doctora en Bioquímica

Agradecimientos

Tengo la impresión de que llegué a un laboratorio y me iré de otro. Y cuando me acuerdo de todos estos años, estoy contenta. Contenta de lo que he hecho, de lo que he aprendido, y de la gente maravillosa que he conocido. Y si al final la historia acaba en tesis, pues mira, mejor que mejor :-)

Mil gracias a Jesús. Sin ti esta tesis no sería posible. Gracias por dejarme participar en tu proyecto, por dedicarme tanto tiempo, por guiarme y dejarme ir sola en los momentos justos, por la discusión científica, por la crítica, por enseñarme mil cosas que no caben en unas líneas... Es difícil imaginar un director de tesis mejor.

Gracias también a los otros "jefes"... A Ismael, no sólo por lo que te toca de tesis, que no es poco, sobretodo si me acuerdo de Lep y compañía... También por las ayudas varias durante todos estos años, y por las discusiones, las risas, y el colegueo en general. Gracias a Quique, por ser uno de los mejores profesores que he tenido, por enrolarme en el mundo de las proteínas, por llevarme por ahí, por los burri-burris, y como no, por la colaboración científica, sobretodo en lo que a los péptidos se refiere. Y gracias a Cucha, porque siempre estás dispuesta a echar una mano.

Gran parte de la felicidad que he disfrutado en estos años se la debo a las princesas, gracias por la amistad sin límites que me habéis dado. Es imposible escribir en unas líneas todo lo que os tendría que agradecer... Gracias a Ana Rizos, por la luna y por las estrellas, por esa dulzura especial que tú emanas, por las lecciones de estilo, por los momentos de placer en forma de colonia, y como no, por tu gran ayuda con los péptidos. Gracias a Mar, mi madre del lab (te estamos saliendo de hijas...), por enseñarme a ser un poquito polite y a ver las cosas desde otros ángulos... y qué decir de la biología molecular, de los protocolos bien seguidos y de las mil sugerencias para las mil consultas, si es que no son más. Y gracias también a Puig, siempre tan parsirimoniosa y fenomenal. Por hacerme sonreír (y reírme a carcajadas) cada día, por compartir tu sabiduría peptídica, dicroica y hachepelecética, compañera de poyata, germana de lab i mestra de valencià. Tienes una sensibilidad especial para hacer sentir bien a los demás.

Un par de kilos de gracias se las lleva también Ana Saurí. Porque no sólo hemos compartido vidas científicas paralelas, sino también una gran amistad, inolvidables momentos té, interesantes conversaciones y asesoramiento científico en general. Al señor D. Paco Taberner, también muchas gracias. Por las charlas de ciencia y de no ciencia, y por tener siempre una idea a punto para cada traspiés experimental. Y tú Luis, coge todas las gracias que puedas, que harás corto. Gracias por la culturilla musical, por los tés tan divertidos, y por escucharme y

escucharme y escucharme... has sido el auténtico sufridor de anaenfasetesis. Pero nos hemos hecho amigos, verdad?

Y no creáis que me olvido del resto de la gente del lab. Tengo gracias para los que estaban cuando llegué: para Mayte, la fuerza manchega, para Marçal, mi padre del lab, para Belenchi y Tere, porque nos hemos divertido dentro y fuera del trabajo, y para Gema y nuestras charlas de trapos. Y también para los que siguen: para Dunja, por sus pasteles tan buenos, y por su asesoramiento lingüístico y profesional, y para mis compañeros apoptóticos, Gustavo, el "becario perfecto", y para Santi, por descubrirnos a Cálico Electrónico (mucha suerte!!!). Mención especial para las técnico del lab, porque probablemente no os he agradecido antes vuestra colaboración diaria, y os aseguro que ha sido de mucho level. Gracias sobretodo a Cris, por la grata compañía y por la vidilla que le das al lab, y a Ali, por tu uso genuino del vocabulario y tu buen humor constante. A la recién llegada María, mucha suerte.

Gracias a la gente del Departamento, a Ana P. y a Aurora, aliadas especiales en esta fase-tesis, a Ana Ruiz, a Juan y sus piropos, a Elena, M^{a}Angels y el resto de los del lab de arriba, que con cualquier excusa os hago visitillas, a Ramón, por la ayuda con algunos protocolos, y a Maribel, por las mitocondrias y los experimentos con el oxímetro, a Juan Carlos por ayudarme a compaginar las estancias con las prácticas, a María y Toni, por las cosillas más burocráticas, y a J.R. por el hígado de rata, entre otras cosas. Mil gracias a Juanjo Calvete por las medidas de masas y a Tano por el diseño de la portada.

A special place in my heart is for the people I met in Trento. Grazie mille a Gianfranco, per darmi la possibilità di lavorare nel suo laboratorio, per una benvenuta cosi bella e per l'importante contributo in questo lavoro. A Mauro, sempre caro e divertente, grazie per aiutarmi in tutto momento, anche quando non avevi il tempo. Tantissime grazie a Manu, perche mi hai insegnato tutti i misteri delle vescicole e dell'FTIR (parte di questo lavoro è tuo), per dedicarmi il tuo tempo con il sorriso permanente nella faccia, ma sopratutto per tanti momenti divertenti pieni di ridere e per la tua grande amicizia. Grazie a Romi i a Corrado, amici miei, per portarmi a sciare, al lago, a salire una montagna, in giro per tutto il Trentino, a feste di compleanno con neve da per tutto, o all'aperto in state, o in refuggio di montagna in autunno, o nel palazzo delle Albere con i caipiroska di fraggola... un saluto anche per Walter e gli altri. Danke, grazie, thanks, Christoph, für deine Hilfe mit den PLM, aber du weisst, überalles für die "Abendbiere" und für so viele lustige und schöne Momenten, die wir zussamen verbracht haben. Grazie a Roby, per essere cosi simpatica e per l'aiuto con il filmino, a Cris, sempre pronta per il divertimento, a Rossi, dolce e cara ragazza, alla forte Gabri, e anche a Michele (Miguelito il chimico), a Laura, Andrea, Massimiliano, Claudia, a Raffaela

e la sua paella, al sempre amabile Massimo e a tutti gli altri. Thanks also to the other ospiti I met, to Katarina, or how to make a friend in two weeks, to Sabina, the girl who knows perfectly what she wants, and to Mariusz, grande puffo, always ready for a beer. Grazie mille a Rossella e Giovanni, grande cuoco, anche al piccolo Tommaso, per insegnarmi italiano, per le bellissime (e buonissime) cene, e per farmi sentire come a casa. Vi porto a tutti nel cuore.

Montones de gracias para mis amigüitos de la vida real. Gracias María, porque me has demostrado que una buena amistad se mantiene a pesar del tiempo y de la distancia, y porque aún estoy echando de menos tus ganas de reír, tu hiperactividad, y esas conversaciones interminables y llenas de sinceridad. Gracias Laura y Paula, por estar ahí para cualquier cosa, amigas desde siempre y para siempre, qué más se puede pedir!!! Aquí entran también los respectivos de algunas de las de arriba, como Jordi, Massimo, Mora y Pedro. Y no me olvido de los amiguicos de Buñol siti, sobretodo del Alfre y de las chicas de las cenas/cervecicas de los viernes, ni de la peña de San Antón, con tantas ganas de marcha!

Pero sobretodo gracias a Carlos, por ser la persona que mejor me entiende del mundo. Por respetarme siempre, por ser mi principal punto de apoyo y por estos años de felicidad que venimos compartiendo.

Y un gracias infinito para mi familia, mis hermanos Gloria y Luis, y mis padres, por respetar y apoyar mi contundente "Mamá, quiero ser científica", porque me habéis hecho como soy, y porque siempre estáis ahí, para lo que haga falta.

Abbreviations

pBcl2, proteins of the Bcl-2 family

OMM, outer mitochondrial membrane

TM, transmembrane

tBid, active C-terminal part of Bid after caspase 8 cleavage

Lep, engineered model membrane protein derived from leader peptidase of E. coli

AP, glycosyltransferase acceptor peptide

ISP, inhibitor of the signal peptidase.

BH, Bcl-2 homology domain

MOM, mitochondrial outer membrane

ER, endoplasmic reticulum

LUVs, large unilamellar vesicles

Bid-α6, peptide including the fragment α6 from Bid

Bax-α5, peptide including the fragment α5 from Bax

CD, circular dichroism

TFE, trifluoroethanol

SDS, sodium dodecylsulfate

FTIR, Fourier-transformed infrared spectroscopy

PA, phosphatidic acid

PC, egg phosphatidylcholine

ATR, attenuated total reflection

R, dichroic ratio

S, form factor

γ, tilt angle

TFA, trifluoroacetic acid

L/P, lipid to peptide ratio

PLM, planar lipid membrane

DPhPC, diphytanoyl-sn-glycerophosphocholine

P+/P-, permeability ratio between cations and anions

PE, phosphatidylethanolamine

PS, phosphatidylserine

CL, cardiolipin

LPC, lysophosphocholine

pyPC, pyrene-PC

FD-20, fluorescein labelled dextrans of 20 kDa

FD-70, fluorescein labelled dextrans of 70 kDa

Contents

Part I.

Introduction

1. The object of study

Biological membranes are structural elements essential for living organisms. They are non-covalent assemblies of amphipatic molecules organised in two leaflets to form asymmetric bilayers. Although lipids are their principal components, they contain also proteins and carbohydrates. These sheet-like structures surround closed volumes, acting as permeability barriers to polar molecules and defining the distinct cellular compartments.

However, this function alone would not require the complex lipidic and proteic composition found in natural membranes. In this chapter, we will summarise the composition of biological membranes and describe briefly their structural and physical-chemical properties, to end up focusing on those that are of special interest for this work.

The proteins embedded in the lipid bilayer control the flux of molecules and information, acting as pumps, channels, receptors, energy transducers and enzymes. Additionally it has also become evident that lipids perform a number of important functions in the cellular physiology, acting as secondary messengers in signaling pathways or cofactors for enzyme activity.

1.1. The lipidic component

Lipids are amphipatic molecules, barely soluble in water and highly soluble in organic solvents such as chloroform. They are the main constituents of biomembranes, but have several other biological roles: Lipids are used as fuel molecules, constitute highly concentrated energy stores and act as signal molecules. Phospholipids, glycolipids and cholesterol are the major types of membrane lipids.

1.1.1. Types of lipids

Phospholipids

Phospholipids can be understood as molecules consisting of four components: fatty acids, a platform molecule to which the fatty acids are attached, a phosphate

group and an alcohol attached to the phosphate. The long acyl chains of the fatty acids are highly hydrophobic, whereas the rest of the molecule is constituted by polar groups, forming a hydrophilic head that can interact with the aqueous environment. The platform holding the fatty acids can be glycerol, giving rise to phosphoglycerides, or sphingosine, which originates sphingolipids J.M. Berg (2002).

In the *phosphoglycerides*, the hydroxyl groups on positions C1 and C2 of the glycerol are esterified with the carboxyl groups of two fatty acids, and the C3 hydroxyl group is esterified with phosphoric acid. This molecule is the simplest phosphoglyceride and is called phosphatidic acid (PA). Several alcohols can form a ester bond with the phosphatidic acid giving rise to phosphatidylserine (PS), phosphatidylethanolamine (PE), phosphatidylcholine (PC), phospatidylglycerol (PG) and phosphatidylinositol (PI), depending on the alcohol esterified. Cardiolipin (CL), a lipid located exclusively in the inner mitochondrial membrane and in the intermembrane contact sitesGarcia Fernandez et al. (2002), presents a dimeric structure with four acyl chains and two phosphate groups. The structures of these molecules are shown in figure 1.1.

The most common *sphingolipid* is sphingomyelin, in which the amino group of the sphingosine is amidated with the carboxyl group of a fatty acid, and the primary hydroxyl group is sterified to phosphoryl choline.

Glycolipids

Glycolipids are sugar-containing lipids, based also on a sphingosine molecule. Like in sphingomyelin, the amino group of sphingosine is acetylated by a fatty acid, but the primary hydroxyl group of the alcohol is linked to one or more sugars. If only one molecule of glucose or galactose is linked, the glycolipid is called cerebroside and is the simplest glycolipid. When glycolipids contain more complex and branched sugar chains, they are called gangliosides. Glycolipids are oriented asymmetrically, with the sugar residues always on the extracellular side of the membrane.

Cholesterol

Cholesterol is quite different from the other lipids. It is a steroid, with a structure containing four linked hydrocarbon rings. It has a hydrocarbon chain on one end of the steroid molecule, and a hydroxyl group on the other end. Cholesterol is absent in prokaryotes, and is found at several proportions in eukaryotic membranes. It is oriented parallel to the acyl chain of phospholipids, with the hydroxyl group interacting with the polar head groups.

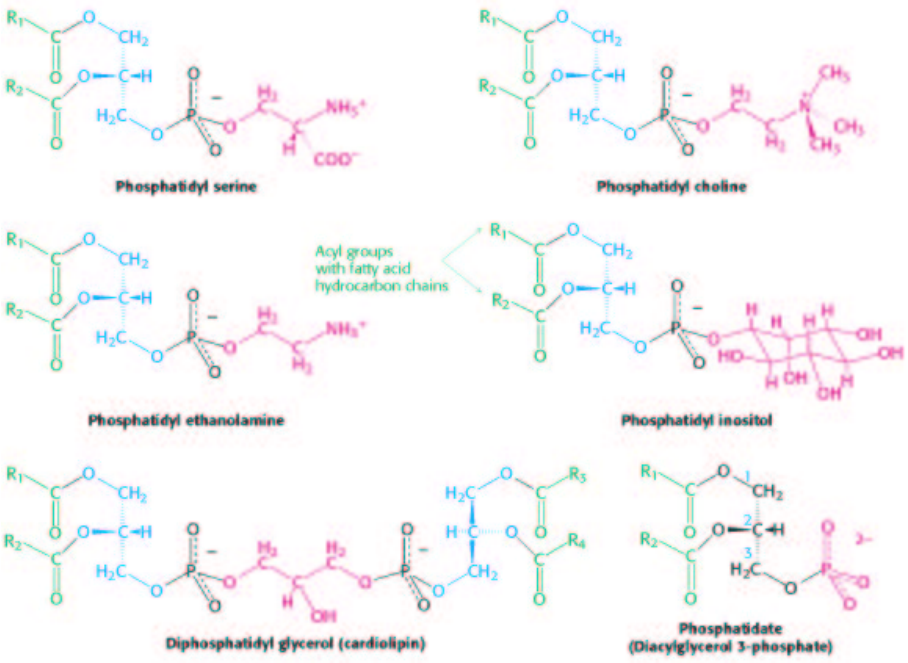

Figure 1.1.: Schematic representation of the structures of the phosphoglycerides normally found in biomembranes. The acyl groups, with hydrocarbon chains depicted as R1 and R2, are shown in green. The phosphate groups are represented in black, except in the case of phosphatidate (PA), which is shown in pink. The glycerol backbone in the Fischer projection is shown in blue, and in black in the case of PA. The alcohols sterified with the phosphate group are shown in pink. (Adapted from J.M. Berg (2002))

The *fatty acids* which are linked to the lipids establish the properties of the hydrophobic nucleus, such as the thickness and fluidity of the bilayer. They are hydrocarbon chains of several lengths and degrees of unsaturations which contain a terminal carboxyl group.

1.1.2. Lipid organisation in aqueous environments: Lipid phases and polymorphism

The amphipatic nature of the lipidic molecules is the main responsible of their organisation in aqueous environments. The polar head groups tend to interact with the aqueous solvent, while the hydrophobic tails favor the interaction between themselves. The *hydrophobic effect* is the major driving force, leading to exclusion of water molecules from the hydrophobic interior. In addition, Van der Waals attractive interactions induce the tight packing between the hydrocarbon chains, and finally, electrostatic and hydrogen-bond forces favor the interaction between the polar head groups and water molecules J.M. Berg (2002).

Studies in simple lipidic systems have allowed the characterisation of their structural properties in a number of environmental conditions. When lipids are dispersed in an aqueous environment, they adopt a great variety of liquid-crystalline phases, which optimise the hydrophobic effect and their geometric packing constraints. Some examples of these phase structures are the normal (oil-in-water) fluid lamellar L_α phase, the inverse (water-in-oil) hexagonal H_{II} phase or the inverse bicontinuous cubic Pn3m phase, schematic representations of this phases are shown in figure 1.2 . The normal lamellar phase is a 2D phase with a sheet-like structure formed by two monolayers of lipids, which bury their hydrocarbon chains and expose their headgroups to the aqueous environment. The H_{II} phase is also a 2D structure, where the lipids aggregate in long cylinders packed with a hexagonal geometry. Water molecules are contained inside the cylinders, with the headgroups exposed to them, and the fluid acyl chains fill the remaining space. The cubic phases are isotropic 3D structures with cubic symmetry. The bicontinuous phases are formed by draping a continuous lipid bilayer Seddon and Templer (1995).

Phase transitions

At low temperatures and water contents, most lipids adopt a crystalline lamellar L_c phase, where the molecules are long- and short-range ordered. Another ordered phase observed is the gel phase, which many lipids form at low temperatures and in the presence of water. In gel phases, the acyl chains are still ordered in a *trans*

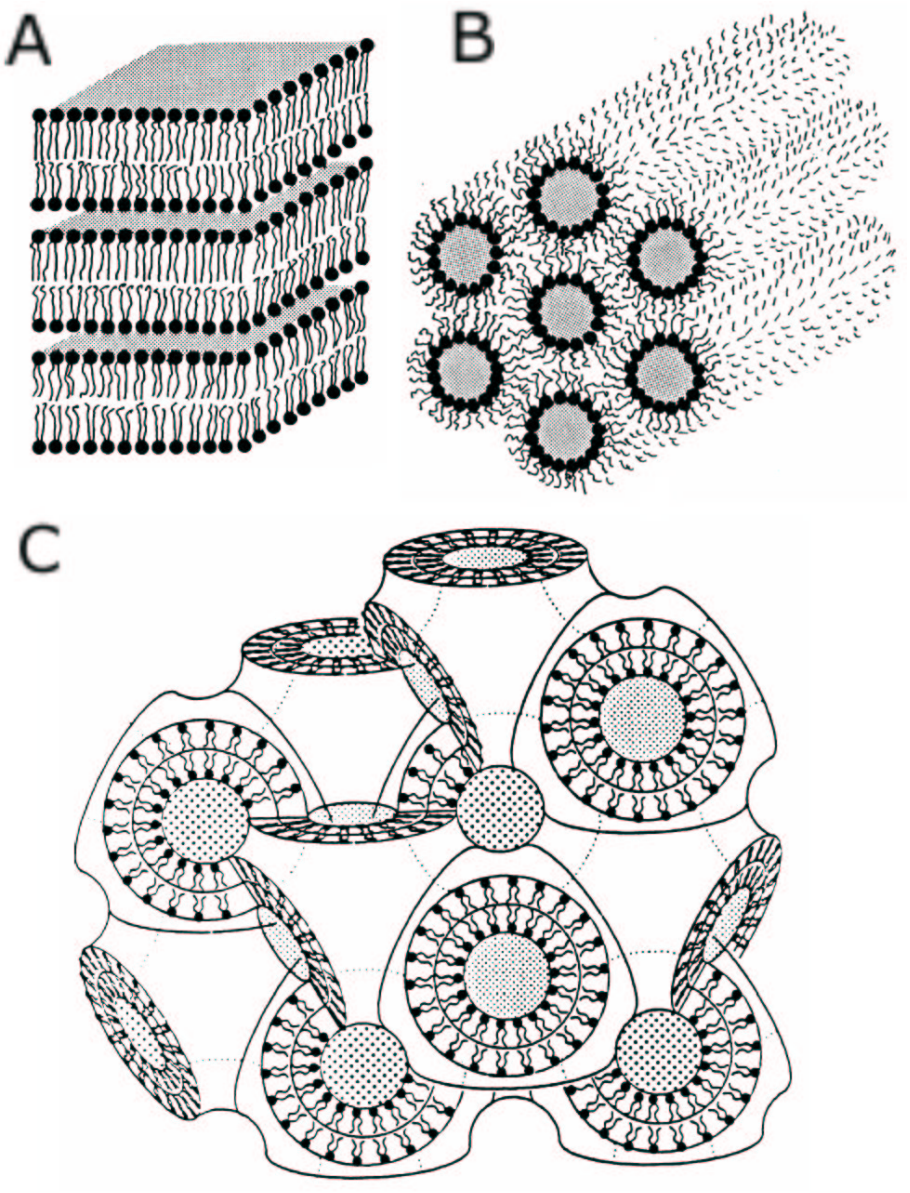

Figure 1.2.: Examples of lyotropic structures. A) L_α fluid lamellar phase. B) Inverse hexagonal H_{II} phase. C) Inverse bicontinuous cubic Pn3m phase. Adapted from Seddon and Templer (1995) .

conformation, but are able to rotate around their long axis. The L_β gel phase is characterised by the acyl chains arranged normal to the bilayer, but other possibilities have been described, such as the $L_{\beta'}$ phase, with the hydrocarbon chains tilted, the interdigitated $L_{\beta I}$ phase, of the $P_{\beta'}$ ripple phase, where the lamellae are periodically undulated Seddon and Templer (1995).

As the temperature increases, there is a linear increase of the lipid cross-sectional area in the gel phase. At a critical point, known as the *melting temperature* T_m, there is an abrupt expansion of the lipid cross-sectional area, accompanied by a decrease in the bilayer thickness, which is associated with a transition to a fluid-like state. Most lipids melt to the fluid lamellar L_α phase, which is characterised by higher disorder and rapid lateral diffusion. Upon heating lipid systems in the L_α phase, transitions to non-lamellar structures are observed. However, in some lipid systems the transition from the gel phase leads directly to non-lamellar fluid structures like the H_{II} or the cubic phases Seddon and Templer (1995).

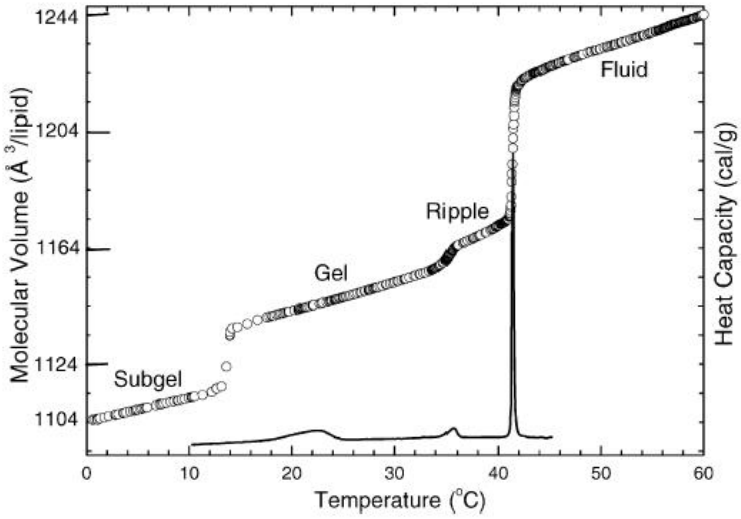

Figure 1.3.: Experimental evidences of phase transitions. Molecular volume (open circles) and heat capacity (solid lane) vs. temperature for DPPC bilayer in excess water, from Tristram-Nagle and Nagle (2004).

At very high dilutions in water, micellar solutions can be formed. These structures are translationally disordered discontinuous isotropic phases, characterised by nearly spherical shapes with a hydrophobic core and the lipid headgroups exposed to the solvent. Phospholipids form these phases at extremely low con-

centrations, due to steric repulsions between the two acyl chains. Phospholipids with short acyl chains and lysophospholipids have a higher propensity to form micelles.

Lipid polymorphism

The ability and propensity of each lipid to form the different structural phases is known as *lipid polymorphism* Seddon and Templer (1995). The nature of the headgroups is the major determinant of this property. The main factor is the effective polarity of the headgroup, which depends on its ability to interact with water molecules and to bind to other headgroups. For example, water solvation increments the T_m and disfavors the formation of inverted non-lamellar phases, as in the case of phophatidylcholines, which is in clear contrast to the case of phosphatidylethanolamines. The presence of charges and the steric effects of the headgroups are secondary factors not to be obviated. In addition, increasing the length of the hydrocarbon chains increases the hydrophobicity and the chain-chain interactions, thus increasing the melting temperature and favoring inverse non-lamellar phases, while the presence of unsaturations has the opposite effect. Water content and temperature are the major environmental parameters affecting the stability of the different phases that lipids can adopt. Other relevant conditions include the presence of divalent cations, organic molecules or the pH.

The various lipid phases observed are characterised by different intrinsic curvatures of the monolayers, which express the spontaneous bending properties of a monolayer and result of the best lipid packing. As a consequence, the lipid polymorphism can be simplified to a shape-structure concept, as schematically depicted in figure 1.4.

Cylindrical lipids, which have a headgroup cross-sectional area similar to that of the acyl chains, tend to form lamellar phases, as in the case of PC. However, if the cross-sectional area of the headgroup is larger than that of the hydrocarbon chains, the micellar phase is favored and the lipid is said to have an intrinsic positive monolayer curvature. This is the case of lysolipids and most detergents. In contrast, when the cross-sectional area of the polar headgroup is smaller than that of the acyl chains, other non-lamellar structures are preferred, with a net negative intrinsic curvature, like the H_{II} or the cubic phases, which are formed by lipids like PE. In this shape-structure simplification, the overall shape of the lipids not only depends on their chemical structure, but also on environmental parameters that have been observed to affect the phase formation, as described above van den Brink-van der Laan et al. (2004).

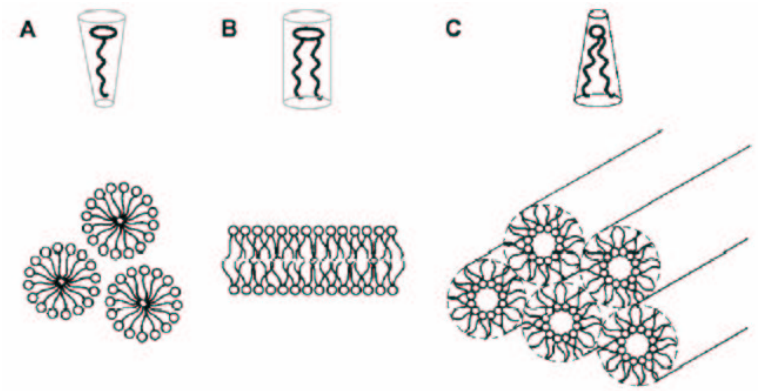

Figure 1.4.: Shape-structure concept of lipid polymorphism. A) Molecules with overall inverted conical shape, such as detergents, form structures with positive curvature, like micelles. B) Molecules with overall cylindrical shape tend to adopt lamellar arrangements, such as the $L_\alpha$phase. C) Molecules with an overall conical shape prefer to organise into structures with negative curvature, like the H_{II} phase. (From van den Brink-van der Laan et al. (2004)).

Lipid organisation in natural membranes

In biological membranes, lipids are organised in lamellar structures similar to the L_α phase, which self-assemble spontaneously. As a consequence, membranes display some features of biological relevance: they are cooperative, self-sealing structures, that tend to be extensive and to close on themselves forming compartments. However, the enormous amount of different lipids that arises from the combination of the diverse acyl chains and polar head groups have different phase-forming properties and determine the features of the membranes they make. In fact, lipidic polymorphism is biologically relevant, since it is involved in the local formation of non-lamellar structures, like those connected to the processes of membrane fusion, the formation of lipidic pores or the organisation of tight junctions van den Brink-van der Laan et al. (2004). In addition, the presence of non-lamellar lipids may influence the flexibility and the barrier properties of the bilayer, or affect the folding or the function of membrane proteins, as it has been reported in the case of protein kinase C Senisterra and Epand (1993), phospholipase A_2 R.B. Cornell (1996), rhodopsin Botelho et al. (2002) or the mitochondrial adenine nucleotide transporter Streicher-Scott et al. (1994).

1.2. The proteic component

The permeability barrier in the membrane depends mainly on the lipidic component, but almost all the other membrane functions are performed by specific proteins. Membranes performing different functions contain different sets of proteins. Thus, the protein content differs between different biomembranes, and varies largely from less than 20%, as in myelin, to near 75% in energy-transduction membranes.

Proteins associate with membranes to different extents. Depending on the ease they can be dissociated, they are classified as integral or peripheral membrane proteins. The first ones usually span the lipid bilayer and interact extensively with the hydrophobic nucleus of the membrane. Only reagents that can compete efficiently for these nonpolar interactions, such as detergents or organic solvents, can release them. The later are proteins bound to the membrane mainly through electrostatic and hydrogen-bond interactions with the polar head groups of lipids. Dissociation can be accomplished by eliminating these interactions, with a high salt concentration, the presence of a denaturing agent, or a pH change. Some peripheral proteins can associate to the membrane through interaction with the surface of integral proteins, on either the cytosolic or the extracellular side of the membrane. Others can be anchored through a covalent bond with a fatty acid, such as a farnesyl or a palmitoyl group attached to a cysteine, or a glycosyl phosphatidylinositol group bound to the carboxyl terminus.

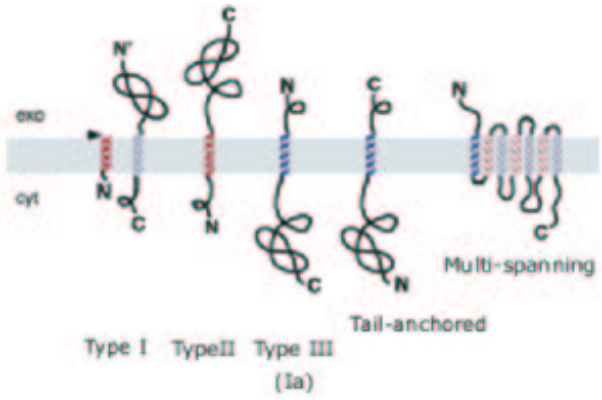

Figure 1.5.: Types of membrane proteins. Classification of membrane proteins according to the number and topology of transmembrane segments they contain (adapted from Higy et al. (2004)).

Depending on the regions spanning the bilayer, integral membrane proteins can be classified as monotopic, bitopic or polytopic (multi-spanning), as schematically shown in figure 1.5. Monotopic proteins are further classified in type I, type II and type III proteins, and tail-anchored proteins (see 1.2.1), depending on the position and the orientation of the transmembrane segment (figure 1.5).

1.2.1. Protein insertion in biological membranes

In general, membrane proteins are characterised by the presence of extensive hydrophobic regions, and do not have a stable structure in the aqueous environment of the cytoplasm. Thus, complex and precise mechanisms have been developed in the cell to control structural stability, folding ans localisation of membrane proteins. Two classes can be distinguished, depending on how association with the membrane is performed with respect to protein synthesis.

Co-translational insertion

The majority of membrane proteins are incorporated to the cellular membranes during their synthesis. Nascent proteins of this type typically contain a N-terminal signal sequence of hydrophobic character. At the beginning of the translation of the mRNA, as soon as the signal sequence is synthesised and exposed to the cytosol, it will be recognised by a specific GTPase known as the Signal Recognition Particle (SRP). Binding of the signal sequence to the SRP pauses translation, causing the ribosomal complex to translocate to the endoplasmic reticulum (ER). At the surface of this organelle, the SRP recognises a membrane bound SRP receptor (SR), which is dynamically associated with the translocon complex. The SRP-SR interaction drives their dissociation from the ribosome in a GTP-dependent reaction. Then, the ribosomal complex containing the nascent signal peptide is transferred to the translocon, where translation continues.

The translocon is a large protein complex in the ER membrane which is responsible of the insertion and assembly of the nascent polypeptide in the bilayer. The main components of the translocon are the heterotrimer Sec61 and TRAM. Additionally, it contains associated enzymatic activities, such as the glycosyl transferase and the signal peptidase, which perform post-translational modifications, as well as other important proteins like calnexin, which is an ER membrane chaperone, or BiP, which has been implicated in translocon sealing White and von Heijne (2004).

Post-translational insertion

Some proteins insert in the membrane independently of the machinery of the translocon. In this case, integration to the membrane occurs after they have been synthesised and folded in the cytoplasm. These proteins have a stable structure in aqueous solution, and protect their hydrophobic regions from the hydrophilic environment until they insert. Two types of proteins can be distinguish: those who have a stable structure soluble in the cytosol, and the tail-anchored proteins. The first ones usually suffer a conformational change to adopt a stable structure in the hydrophobic environment of the membrane. Moreover, these proteins interact initially with the membrane interface, with very different properties from those of the hydrophobic nucleus. Although these proteins are not continuously inserted in the lipidic bilayer, they are common in biological membranes and perform important functions, such as infection, defense or signal transduction in apoptosis.

On the other hand, *tail-anchored (TA) proteins* are integral membrane proteins that span the lipidic bilayer through a single hydrophobic domain located in the C-terminal region, while the remaining polypeptidic chain is folded into a functional soluble domain oriented to the cytosol. They localise to all the cellular membranes, where they perform a variety of functions involved in protein localisation, membrane traffic, lipid biosynthesis or controlled cell death High and Abell (2004). TA proteins lack an N-terminal signal sequence and their insertion in the membrane is translocon independent. They synthesised in the cytosol and are targeted and inserted into the cellular membranes in a post-translational fashion, using a novel insertion pathway Borgese et al. (2003).

The information determining the specificity of membrane targeting is essentially located within the C-terminal anchoring domain, which emerges the ribosome at the end of translation Borgese et al. (2003). Once liberated from the ribosome, TA proteins must discriminate between the mitochondrial outer membrane (OMM) (or the chloroplast membrane in plants) and the endoplasmic reticulum (ER) membranes. The TA proteins targeted to other cellular membranes will be delivered there through the secretory pathway from the ER. The OMM-targeting sequence is characterised by a relatively short hydrophobic region flanked by basic residues. In contrast, TA proteins lacking specific C-terminal sequences will be targeted only to the ER membrane. Those proteins with weak OMM-targeting signals will be targeted to both the OMM and the ER. In the ER membrane, the properties of the hydrophobic tail, and probably the cytosolic domain, will determine the final destination of the protein in the secretory pathway.

The concrete mechanism of membrane insertion of the anchor domain remains unclear. Some proteins, like synaptobrevin I Kutay et al. (1995) and VAMP IB

Lan et al. (2000), have been reported to require ATP to insert in microsomes and the OMM, respectively. However this is not the case of other TA proteins like cytochrome b_5 and Bcl-2 Kim et al. (1997). In some instances, the ATP dependence has been associated to the activity of chaperones, but neither their identity nor their concrete role (prevention of aggregation, membrane targeting or both) have been clarified so far. The specificity of the targeting has led to the suggestion that other, yet unknown proteins are involved in the insertion process, although differences in the lipidic composition between the membranes might also play a role Borgese et al. (2003).

1.2.2. Structure and folding of membrane proteins

The lipid bilayer can be considered as a solvent to integral membrane proteins, since it provides the hydrophobic environment essential for them to acquire their active conformation. Membrane proteins usually aggregate in aqueous environments, thus difficulting the processes of purification and handling. This has been so far the major handicap for the study of membrane proteins and the main reason for the slower progress in this field, compared to water soluble proteins.

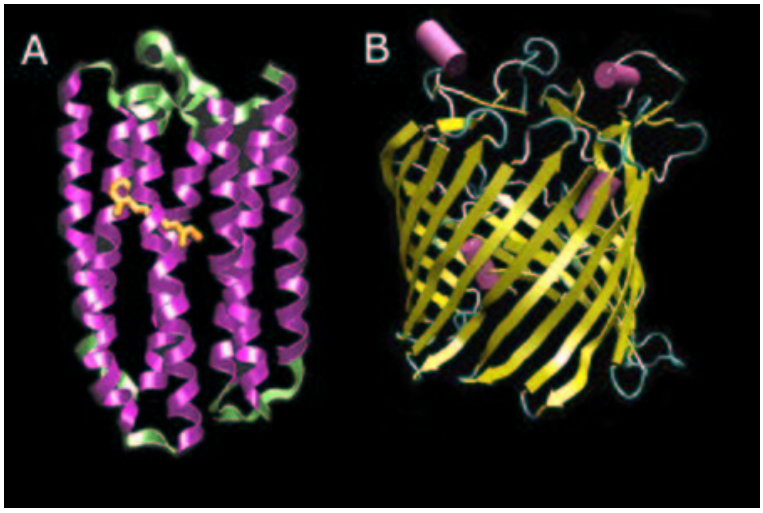

Figure 1.6.: Structures of membrane proteins. A) pSRII, example of α-helical arrangement and B) porin, example of β-barrel organisation. (From http://www.uth.tmc.edu/cmb/index.html)

In contrast to proteins residing in aqueous media, membrane proteins are

immersed in an asymmetric environment, with domains surrounded by the hydrophobic core of the lipid bilayer, regions residing a solvated polar head-group zone and other parts exposed completely to the aqueous solvent. The interaction with such different dielectric environments determines of the structure and functionality of membrane proteins.

The polypeptidic domains located in the interface region of the bilayer participate in strong polar interactions of electrostatic nature and hydrogen bonds with the lipid headgroups nearby. In contrast, the hydrophobic core of the membrane has a very low dielectric constant, which that energetically disfavors the presence of charges and polar groups. This determines the higher proportion of non-polar amino acids and the preferred adoption of secondary structures with maximum number of hydrogen bonds in the regions of the proteins buried within the hydrocarbon region of the bilayer. As a consequence, the length of the hydrophobic sequences in membrane proteins tends to correlate with the thickness of the hydrocarbon region. When this condition is not fulfilled, unfavorable "hydrophobic mismatch" exists, and the lipids and the protein will reorganise to try to minimise this effect. In addition, membrane proteins minimise the area exposed to the membrane to avoid disruption of lipid chain packing Scarlata (2004).

These general ideas correlate well with statistical analysis of the primary structure of membrane proteins. Residues in the membrane spanning domains are mainly of non-polar character. On this basis, a number of hydrophobicity scales have been proposed to evaluate the potential of the different amino acids to reside within the core of the membrane (see 4.1). Some residues interact with both the interface and the hydrocarbon regions of the membrane: Aromatic amino acids, like tryptophan and tyrosine, have been described to act as anchoring residues, accommodating mainly in the interfacial region of the bilayer. while lysines buried in the hydrophobic region of the bilayer, orientate their long polar side chains to the interphase.

In the structures of membrane proteins known so far, there is a preferred organisation into α-helices and β-sheets, which are regular elements of secondary structure where the maximum number of hydrogen bonds of the backbone groups can be satisfied. During their synthesis in the translocon complex, the hydrophobic domains of nascent proteins are thought to be stabilised by membrane chaperones, likely TRAM or calnexin. In the case of helical fragments, they may reversibly partition to the membrane and associate between them before the synthesis is completed. In contrast, β-sheet structures might assemble prior to insertion in the membrane, in a more complex process Scarlata (2004).

Organisation of membrane proteins into tertiary and quaternary structures probably follows the same rules as in soluble proteins. Interactions between el-

ements of secondary structure tend to optimise the packing, and diverse strategies have been observed. In some cases, singular dimerisation motives including G and C_β-branched residues (like GVXXGV in glycophorine A) have been described to form complementary interacting surfaces allowing close packingOrzaez et al. (2004). Polar and hydrogen bonding interactions can also take place between transmembrane (TM) α-helices. In addition, it has been proposed that the antiparallel organisation of TM helices allows favorable interactions between the helix dipoles. Finally, helix tilting allows the organisation into a highly packed, left-handed coiled-coil Scarlata (2004).

1.3. Organisation of biomembranes: Beyond the fluid mosaic model

In 1972 Singer and Nicholson proposed the fluid mosaic model to explain the membrane structure. This model highlights the dynamic and fluid properties of the biomembranes, where constituent elements can diffuse laterally, thus forming two-dimensional solutions of oriented proteins and lipids. Although very useful to understand may properties of the biological membranes, this model, with two smooth surfaces separating polar and apolar regions, is not sufficiently accurate. X-ray and neutron diffraction have shown that membranes form planar structures with a time-averaged spatial distribution of structural groups Wiener and White (1992). As represented schematically in figure 1.7, the thermal motion of molecules gives rise to a heterogeneous environment. In addition, the thickness of the two hydrated interfaces, 15Å each, is similar to that of the hydrocarbon core, thus being enough to accommodate folded or unfolded polypeptide chains. The interfaces are also a chemically heterogeneous environment, where groups of different properties coexist, allowing a rich number of non-covalent interactions. Computational simulations yield three dimensional pictures of bilayers showing a high level of disorder and conformational fluctuations, but keeping a tight packing and good van der Waals contacts that give rise to a crowded hydrophobic environment and explains the permeability properties of the membrane (see 1.7D).

1.4. The asymmetry of biological membranes

Biological membranes are structurally and functionally asymmetric, and highly variable in their lipidic and proteic composition. This composition is characteristic of every cellular membrane. As shown in table 1.1, the different organelles in an eukaryotic cell contain the same classes of lipids, but at a distinct molar ratio.

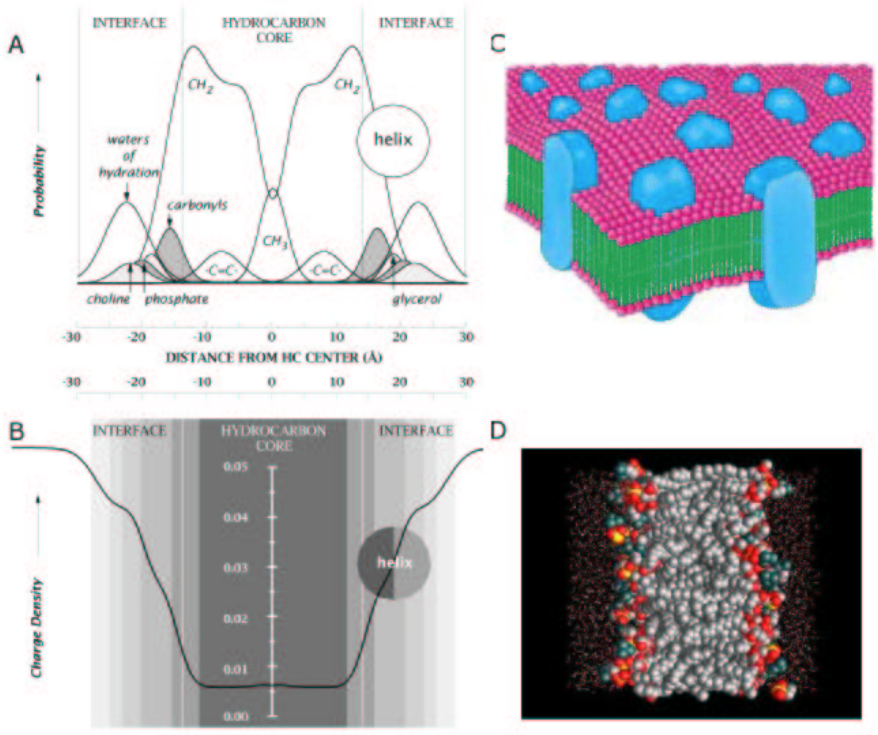

Figure 1.7.: Organisation of biomembranes. A) The representation of the liquid-crystallographic structure of a L_α-phase DOPC bilayer. The time-averaged transbilayer distributions of the quasi-molecular groups shown can be thought of as probability or number densities. The areas under the peaks are equal to the number of structural groups per lipid molecule. B) Polarity profile of the fluid DOPC bilayer derived from A, which represents the average density of atomic partial charges, both positive and negative, calculated by weighting the absolute values of the charge densities by the number density and group volume at each position across the bilayer (from Wiener and White (1992)). C) Scheme of the fluid mosaic model proposed by Singer and Nicholson. D) Molecular graphic of a computational simulation of a DOPC bilayer (from http://moose.bio.ucalgary.ca).

There are also differences in the number of unsaturations of the lipid acyl chains in different cellular membranes. The ER contains the higher level of unsaturation, with a 45%, whereas the Golgi apparatus contains 36% and the plasmatic membrane has 29% Keenan and Morre (1970).

Table 1.1.: Lipid composition in the different organelles from rat liver. The values refer to the molar percentage of each lipid. n.d.: not detected. (Data from van Meer (1989)).

Phospholipid %(mol/mol)	Mitochondrial membrane	Endoplasmic reticulum	Plasmatic membrane	Lysosomal membrane
SM	0.5	2.5	16.0	20.3
PC	40.3	58.4	39.3	39.7
PI	4.6	10.1	7.7	4.5
PS	0.7	2.9	9.0	1.7
PE	34.6	21.8	23.3	14.1
CL	17.8	1.1	1.0	1.0
LysobiPA	0.2	n.d.	n.d.	7.0
CHOL/phospholipid	0.03	0.08	0.4	0.5

The lipid composition of plasmatic membranes varies among the two monolayers. Concretely, PS and PE are mainly found on the cytoplasmic leaflet, while PC and SM predominate on the outer leaflet Zachowski (1993). This transversal asymmetry arises mainly from the activity of an ATP-dependent translocase, which specifically translocates PS and PE inwards. As a consequence, there is a passive outward lipid flux, which also affects the redistribution of PC, SM and cholesterol Frickenhaus and Heinrich (1999). Additionally, transversal asymmetry exists also for membrane proteins. They are synthesised and inserted in the membranes in an asymmetric manner, and do not rotate from one leaflet to the other. This membrane asymmetry is maintained because flip-flop, or transversal diffusion, is very low in the case of lipids and has not been observed for proteins, as a change in the orientation would require a too high energetic cost. In addition, membranes are always synthesised by the growth of preexisting membranes.

There is also lateral asymmetry in the membranes, as lipids are not distributed uniformly in the bilayer plane Binder et al. (2003). Thus domains characterised by distinct lipidic compositions and physical properties, have been observed. In natural membranes, a type of lipidic domains, called rafts, have been identified.

These membrane regions are resistant to detergents and contain a high concentration of sphingomyelin and cholesterol. The interaction of cholesterol with the phospholipids generates liquid ordered phases and fluid phases in the bilayer. Liquid ordered phases condensate preferentially over the fluid phases and sphingomyelin enriches in the ordered phase, leading to domain formation. Rafts act as receptor and anchoring domains to certain membrane proteins. Other types of lipidic domains of different composition may exist on natural membranes, generating defined regions with concrete functional features.

Membranes can be regarded as dynamic supramolecular aggregates. Both the lipidic and proteic composition of the different cellular membranes are regulated in response to the different physiological conditions of the cell. The huge diversity of possible combinations of head groups and acyl chains allows fine tuning of the lipidic composition. This composition is controlled by the cell through a number of enzymatic activities, such as phospholipases, acylases or flipases participate in the mechanisms of regulation.

Moreover, lipids and many membrane proteins experiment continuous lateral diffusion. Proteins vary in their lateral mobility. Some proteins are almost fixed in the membrane, as fibronectin, which is anchored to the cytoskeleton, whereas others diffuse nearly as much as lipids, like in the case of rhodopsin Wey et al. (1981).

1.5. Alteration of the structural integrity of membranes

Biomembranes form closed environments were conditions can be maintained, allowing the development of cellular metabolism. However, cellular and organularorganellar activities also require a regulated exchange of material with the external milieu. Two general processes are involved in trafficking across the membrane barrier: membrane fusion and membrane permeabilisation.

1.5.1. Membrane fusion

Membrane fusion is essential for intracellular membrane traffic. It is involved in a number of important cellular processes, including synaptic transmissions, hormone secretion, exocytosis, endocytosis, protein and membrane sorting, fertilisation and cellular division.

For membrane fusion to occur, the structure of the bilayer must be altered. The process begins at the point of fusion with monolayer merging and the loss

of the lamellar organisation, which appears to be mediated by lipids that favor formation of hexagonal phases. Transient intermediate structures, known as stalks, appear and connect the two extern leaflets of the opposing membranes. Destabilisation of the two connecting monolayers and exposition of hydrophobic groups are next required. This leads to points of hemifusion, where the lipids in the external leaflets are mixed, and the process ends with the association of the internal monolayers, resulting in the formation of fusion pores which connect the two lumen volumes previously separated Yang and Huang (2002).

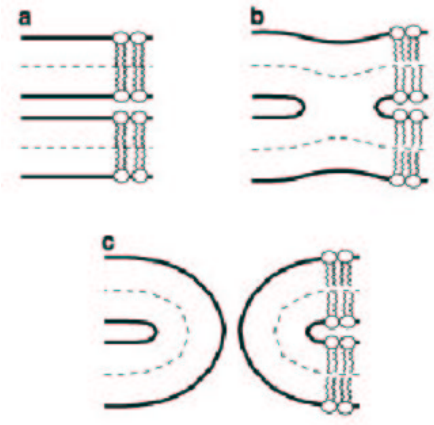

Figure 1.8.: Schematic representation of the process of membrane fusion. Two close bilayers (a) form an intermediate structure called stalk (b) prior to formation of the fusion pore Yang and Huang (2002).

Membrane fusion is not an efficient process, and the help of protein molecules, commonly known as fusion proteins is normally needed. These proteins are able to destabilise the lipid bilayer and induce membrane fusion. The SNARE (soluble N-ethylmaleimide-sensitive factor attachment protein receptor) proteins, which mediate intracellular fusion processes, and the viral fusion proteins, which are essential for the infection mechanism of membrane coated viruses are two examples of well-characterised families of fusion proteins.

1.5.2. Membrane permeabilisation

The permeabilisation of lipid membranes allows the flux of hydrophilic molecules between the interior and the exterior of the cellular compartments. It is essential for cell life, as it is involved in many important processes, like the entrance of

nutrients into the cell, the maintenance of the electrochemical potential for the generation of energy, the import of proteins to organelles, the ionic homeostasis, the excretion of toxic metabolic products, the defence mechanisms against pathogens or the regulation of the physiological cell death.

Many types of proteins are able to permeabilise lipid membranes. Most of them are constitutively inserted in the membrane, where they organise and form stable and highly regulated structures which are assembled using the translocon machinery. These include ion channels, pumps, transporters, carriers and protein translocator complexes.

However, a group of pore-forming polypeptides, involved directly or indirectly in cell death, have a constitutive water soluble structure and insert in the membrane to exert their lethal poration function. This is the case of antibiotic peptides, bacterial pore-forming toxins (PFTs) and regulators of apoptosis of the Bcl-2 family. Because of their relevance in the present work, this latter group of porating polypeptides is discussed in more detail.

Bacterial PFTs are proteins with a molecular mass higher than 30 kDa, which porate membranes mainly by two mechanisms Heuck et al. (2001): Some of them, upon interaction with the membrane, organise into β-barrels, which are well defined stable structures that cross the hydrophobic region of the membrane. In *β-barrel channels*, an hydrophilic pore is created in the core of the structure by polar amino acids oriented to it, and hydrophobic amino acids interacting with the hydrocarbon region. Examples of this group are the staphylococcal α-toxin, the cholesterol-dependent cytolysis or the anthrax toxin.

The second strategy involves a group of multidomain toxins which form pores lined by α-helices, like in the case of colicins, δ-endotoxins and the diphtheria toxin. In the case of colicins, they contain a receptor binding domain, a translocation domain and a pore-forming domain. In aqueous environment, the pore-forming domain adopts a globular structure formed by a hairpin of hydrophobic α-helices in the apolar core, which are surrounded by other amphipatic α-helices. Interaction of the pore forming domain with lipid membranes triggers a large conformational rearrangement, which is followed by helix elongation and insertion into the bilayer. The structural reorganisation involves the unfolding of the globular domain and exposition of the hydrophobic hairpin, which inserts in the membrane while the other helices form an extended network on the bilayer interface, in agreement with the umbrella-like model of insertion, shown in figure 1.9. This membrane-bound intermediate corresponds to the closed state of the pore, which, in the presence of a trans-positive potential, evolves to an open state characterised by extensive helix insertion, as represented in figure 1.9 Zakharov et al. (2004). The proteins of the Bcl-2 family, which are involved in programmed

cell death, show a structural organisation in water similar to the pore forming domain of these toxins, and are able to form pores likely by means of a comparable mechanism.

The actinoporins constitute third class of PFTs. They are smaller proteins (18-20 kDa) which organise into a β-sandwich with two flanking helices, of which the N-terminal one is responsible of membrane insertion and pore formation. Recent studies have suggested that the proteins of this group form toroidal pores Anderluh et al. (2003); Malovrh et al. (2003), a mechanism which had been previously proposed for some antimicrobial peptides (see below). Additionally, such mechanism has been also proposed for the permeabilising action of Bax Terrones et al. (2004), a proapoptotic member of the Bcl-2 family, and Cramer and colleagues have also proposed a mechanism based on a toroidal pore for the action of colicins in recent publications Zakharov et al. (2004); Sobko et al. (2004).

Antimicrobial peptides are smaller molecules, usually with molecular weights between 1 and 5 kDa, and permeabilise membranes through similar but less constrained strategies. Some of them follow poration mechanisms comparable to the β-barrel-forming PFTs, like protegrin Heller et al. (2000), while others exhibit a channel activity based on helical structures. Among these, the *barrel stave model* describes the action of alamethicin Yang et al. (2001) and other peptaibols (chugh02). According to this model, the helices insert in the membrane either as monomers or oligomers, and then recruit additional monomers. The helices are amphipatic and expose their hydrophilic face to the proteic lumen of the formed pore, while their hydrophobic face is oriented to the hydrocarbon region of the membrane.

Other helical antimicrobial peptides, like magainin Ludtke et al. (1996) or melittin Yang et al. (2001), have been described to form partially lipidic pores, known as *toroidal pores*. In these structures, the rim of the pore is formed both by lipid and protein molecules. The two leaflets of the membrane are in contact and form a continuous sheet, with positive monolayer curvature perpendicular to the plane of the bilayer and negative monolayer curvature in the plane of the membrane. The organisation of the protein molecules in the pore is yet not well-known, but they can be considered to lay always embedded on the polar surface of the membrane, with variable insertion in hydrocarbon region of the bilayer.

A more generic model of membrane destabilisation, the *carpet model*, has been also suggested for helical peptides like dermaseptins La Rocca et al. (1999) or cecropins Gazit et al. (1994). Upon binding to the membrane, the amphipatic peptides expose their polar face to the solvent and their hydrophobic face interact with the hydrocarbon region of the membrane. When sufficient peptide molecules are bound to the bilayer, transient pores can be formed, which eventually lead to

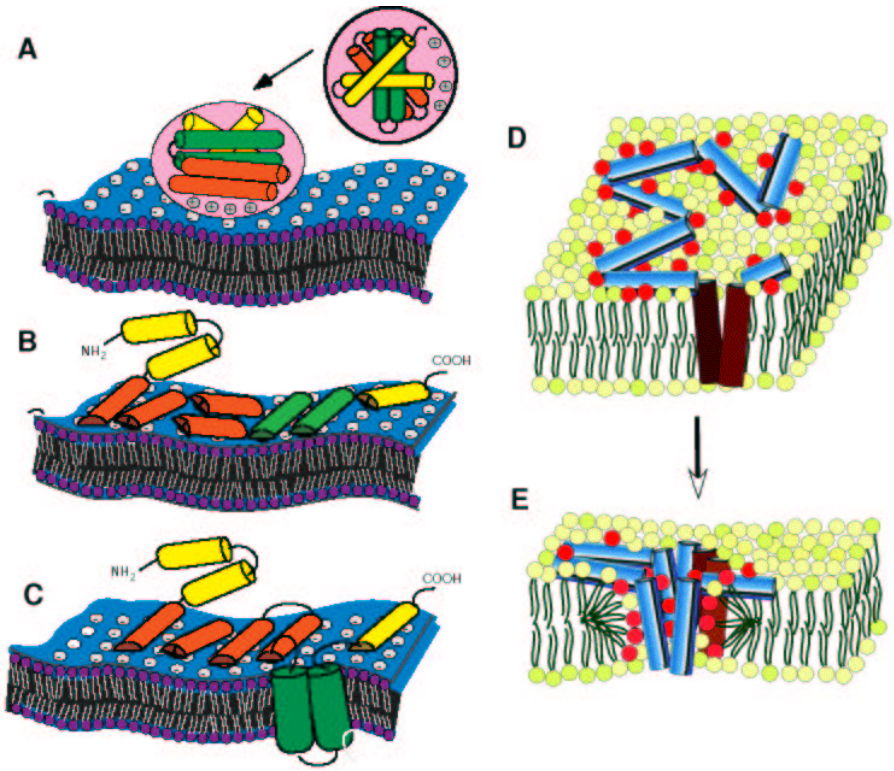

Figure 1.9.: Models of membrane insertion and pore formation for colicins. In A to C the model of umbrella-like insertion is schematically depicted. Interaction with the membrane (A) triggers a conformational rearrangement to an unfolded state (B) prior to membrane insertion of the hydrophobic central hairpin (C) (from Elkins et al. (1997)). This membrane bound intermediate (D) corresponds to the close state of the channel. Application of a trans-positive potential is applied gives rise to extensive insertion of the helices and transition to the open state (D) (adapted from Sobko et al. (2004)).

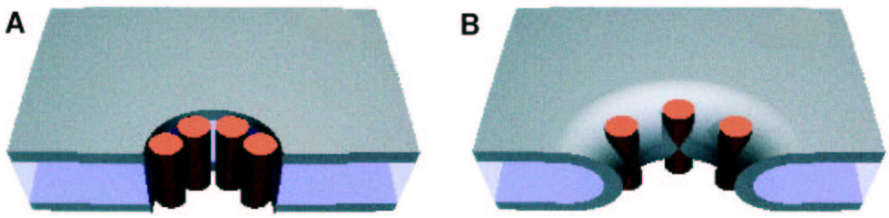

Figure 1.10.: Schematic representation of the barrel-stave model (A) and the toroidal model (B). The dark layers represent the head-group region of the bilayer and the cylinders represent the peptides (adapted from Shai (2002)).

membrane disruption in a detergent-like mechanism.

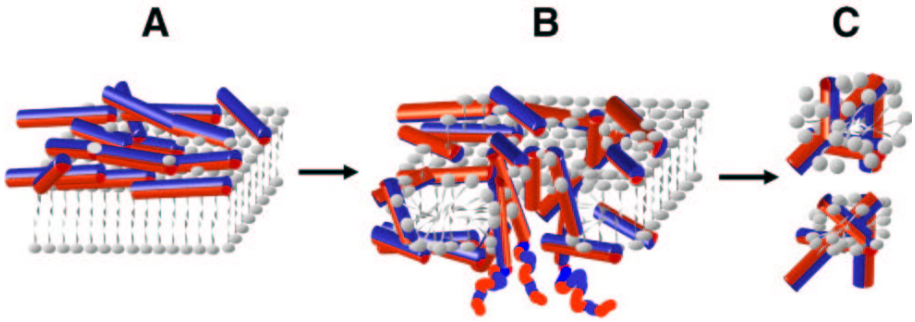

Figure 1.11.: Schematic representation of the carpet model of membrane permeabilisation. A) Amphipatic peptides bind to the membrane with their non-polar side facing the hydrocarbon region of the membrane and their polar side oriented to the solvent. B) At a certain peptide/lipid threshold, transient pores form in the membrane, that can lead to membrane disruption, as shown in C) (from Shai (2002)).

Molecular model of lipidic pore formation

The model of toroidal pore proposed for the above peptides and proteins is based on previous studies of pores in pure lipid membranes. When a pure lipid bilayer is set under tension, pores are formed, likely at points of nucleation defects, through a still unclear mechanism. In contrast, the energetics and dynamics of the open

pore are well understood. The energy of the pore, E_R, is given by the expression Lee et al. (2004):

$$E_R = \Im 2\pi r - \sigma \pi r^2 \tag{1.1}$$

where the first term represents the energy necessary to create the rim of the pore, and is proportional to the length of the pore edge, while the second term represents the work done by the membrane tension to open the pore, which is proportional to the pore area. Thus, $\Im$ is the line tension (energy cost per unit length of the edge), r is the radius of the pore, and σ is the membrane tension. Then, a pore in a pure lipid bilayer is unstable: The membrane tension is the driving force to open the pore, and the line tension is the driving force to close it. As a consequence, at r smaller than $\Im/\sigma$, the pore tends to close, and at r larger than $\Im/\sigma$ the pore tends to expand indefinitely.

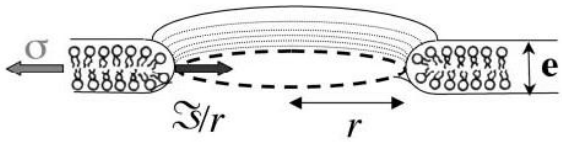

Figure 1.12.: Representation of a lipidic pore. $\Im/r$ is the line tension term tending to close the pore, σ is the membrane tension tending to expand it, and r is the radius of the pore (from Karatekin et al. (2003)).

According to this model, pore forming peptides probably exert their action by a mechanism which involves the generation of membrane tension, and the stabilisation of the open pore associated to a decrease of the line tension Lee et al. (2004).

Based on these considerations and other experimental evidences, the group of Huang has proposed a model for the action of helical and β-sheet antimicrobial peptides, known as the *two-state model* Huang (2000). This model distinguishes two membrane-bound states of binding to lipid bilayers, one inactive S state at low protein to lipid ratios (P/L), and one active I state at P/L ratios above a P/L threshold. In the S state, the peptides are bound to the bilayer and cause membrane thinning in an energetically favorable process. They are embedded in the polar region and increase the area of the bilayer. As the volume of the hydrocarbon region is constant, its thickness decreases proportionally to the surface increase and to the peptide concentration, and creates a tension on the bilayer. At the P/L threshold, the membrane thinning is energetically very unfavorable,

and the pore state is the energetically favored. In the pore state, peptides bind preferentially to the rim of the pore, where they are assumed not to cause membrane tension and to decrease its line tension. As a consequence, transferring the peptide from the surface to the pore edge reduces the membrane tension. If the peptide concentration at the rim of the pore is constant, increasing the radius of the pore increases the number of peptide molecules at the pore edge, and thus reduces the membrane tension in a feedback process that makes the pore stable Huang et al. (2004).

Antimicrobial peptides are mostly positively charged and selectively interact with bacterial membranes, which exhibit negative charges on their membrane surface, and not with eukaryotic membranes, whose membranes are predominantly neutral. However different peptides act preferentially against different pathogens. The gives an explanation for such observations, since the P/L threshold depends on lipid composition, and thus, influences on the efficiency of the antimicrobial peptides to kill cells.

2. The biological problem

2.1. Apoptosis

Programmed cell death is defined as "a sequence of events based on cellular metabolism that lead to cell destruction". There are several forms of programmed death described to date, such as autophagy and necrosis-like cell death, but undoubtedly, apoptosis is the type of programmed cell death that has been investigated in more detail Assuncao Guimaraes and Linden (2004).

Apoptosis is a conserved process that plays a central role in physiological cell death of pluricellularmulticellular organisms. It is necessary for cell recycling and normal tissue homeostasis, which is maintained through a balance between cell proliferation and cell death. It is of special importance in animal development, tissue regeneration, correct functioning of the immune system and in the control and behaviour of pathological states Kerr et al. (1972). The apoptotic process develops through a complex biochemical pathway that is activated when is physiologically required typically in response to a number of abnormal conditions, like cell cycle malfunctioning, toxicity, or at the periphery of acute lesions. A failure in the control of apoptosis leads to misregulation of cell death Thompson (1995). This may provoke excessive cell proliferation, which has been implicated in cancer and autoimmune processes Johnstone et al. (2002), or disproportionate cell death, related to degenerative disorders such as Alzheimer or Parkinson diseases Mattson (2000). Due to the social impact of these diseases, research of apoptosis has experienced an enormous development in the past few years, making it a preferred focus for drug discovery. Both the activation and inhibition of apoptosis may be of interest for therapeutic use Reed and Tomaselli (2000); Nicholson (2000).

2.1.1. The apoptotic phenotype

Apoptosis was first described as a concrete way of cell death, characterised by a well-defined set of morphological changes, as shown in figure 2.1. These include cell shrinkage, plasma membrane blebbing, loss of integrity of organelles, condensation and fragmentation of DNA and formation of the so-called apoptotic bodies

Hengartner (1997).

The apoptotic bodies are membranous vesicles that enclose the cellular contents. Individual cells undergoing apoptosis are eventually removed through phagocytosis by macrophage cells located in the vicinity. This "clean" process was understood as a physiological cell suicide, in contrast necrotic cell death, which is an uncontrolled process that affects extensive populations of cells. In this case, cell death is characterised by cytoplasm swelling, destruction of the organelles and the plamatic membrane, leading to the release of intracellular contents and inflammatory response.

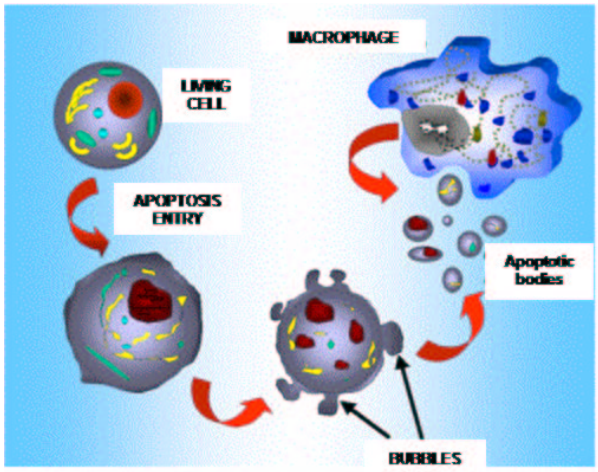

Figure 2.1.: Changes in cell morphology occurring during apoptosis. Induction of apoptosis leads to cell shrinkage, followed by membrane blebbing and formation of the apoptotic bodies, which are engulfed by the macrophages nearby.

2.1.2. Actors of apoptosis

The apoptotic phenotype is controlled through a complex biochemical pathway which is genetically encoded and highly conserved Vaux et al. (1994); Huang et al. (2000). Extensive studies over the last decades have led to the elucidation of the main components of the apoptotic machinery, revealing the complexity of the process. However, many obscure aspects of the pathway still remain to be explained.

The complete process of apoptosis involves a large number of different proteins, mainly located in the cell membrane, the cytoplasm, the mitochondrion and the

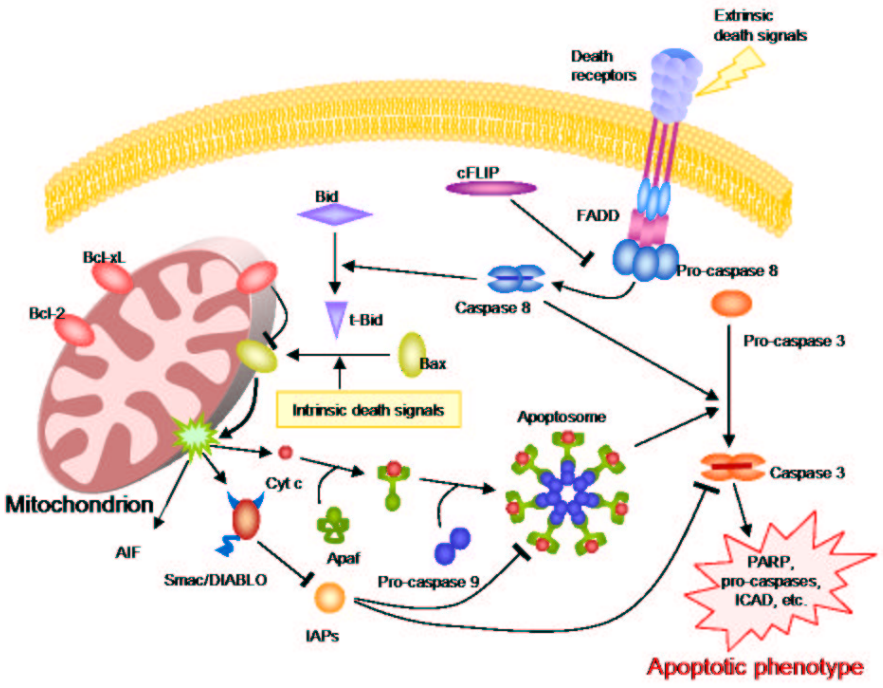

Figure 2.2.: Biochemical routes to apoptosis. The main protagonists in signal transduction pathways of mammalian apoptosis are depicted schematically.

nucleus. According to their role, these proteins can be classified as receptors, adaptors, regulators and executioners.

A family of cysteine aspartyl proteases, called caspases, carries out the progressive dismantling of the cell that occurs during apoptosis Thornberry and Lazebnik (1998). They are the main executioners of cell death and cleave selectively a concrete set of target proteins in a coordinated manner, ultimately leading to the apoptotic death. Caspases are highly conserved through evolution and share similarities in their amino acid sequences, structures and substrate specificities Earnshaw et al. (1999). At least 14 caspases have been described to date. Some of them are not involved in apoptosis, but participate in the activation of cytokines and in the inflammatory response, like caspase-1 (also known as interleukin-1-β-converting enzyme or ICE). Regarding the substrates of caspases, more than 60 have been described so far. Among them, we find procaspases, cell cycle regulators, cytoskeleton proteins, DNAses, transcription factors, signaling molecules,

and proteins of the Bcl-2 family (see section 2.3). Some of these substrates are essential proteins that become inactive upon caspase cleavage, but they can also be structural proteins that loose their function in the cleaved state, or apoptotic proteins that become activated after being processed by caspases.

Caspases are synthesised as inactive pro-enzymes, known as procaspases, that are activated by proteolytic cleavage. Thus, they can be activated by other caspases of even self-activated under certain conditions. They can be classified into two major groups: effector caspases, like caspases 3 and 7, which are responsible for the disassembly of cellular components, or initiator caspases, like caspases 8 and 9, which are responsible for activation of effector caspases3. When the cell is prompted to die, caspases are activated through a proteolytic amplifying cascade, that constitutes a point of no return for the cell fate.

Procaspases contain two domains: a prodomain of variable length and a conserved protease domain made of a small (p10) and a large (p20) subunit, joined by a flexible linker that contains the cleavage site for caspase activation. Initiator and inflammation related caspases have long prodomains that are important for activation. In contrast, effector caspases have short prodomains that seem to be dispensable. According to the model of induced proximity, the mechanism of activation of initiator caspases involves oligomerisation of caspase precursors, aided by adaptor proteins Muzio et al. (1998). In the complex, the digestion site and the active site come in close proximity, which allows autoprocessing. This is the case of the apoptosome complex, that allows activation of caspase 9[1] Srinivasula et al. (1998). On the other hand, effector caspases are transactivated by initiator caspases in a two-step process Chai et al. (2001). First, a partially active intermediate is generated by cleavage at the linker region, and in the second step the intermediate cleaves itself at the level of the short prodomain to generate the fully active enzyme. The active caspase enzyme is a heterotetramer formed by two molecules of processed caspases. In some cases, effector caspases are also able to auto-activate, contributing to the cascade of signal amplification.

Because of the potentially dramatic consequences of a malfunctioning of apoptosis, both, activation and activity of caspases, are highly controlled through complex pathways Chang and Yang (2000); Goyal (2001). Once processed, caspase activity is regulated by specific inhibitors known as IAPs (inhibitors of apoptosis proteins), such us X-IAP, which inhibits both caspase 3 and 9. IAPs bind directly

[1] The apoptosome is a macromolecular complex made of seven molecules of an adaptor protein called Apaf-1 (apoptotic protease activating factor 1), which associate with seven molecules of cytochrome c. The complex is then more flexible and can bind ATP, and recruit several molecules of caspase 9, which are processed in the complex, giving rise to the active holoenzyme, which cleaves and activates caspase 3.

to caspases and inhibit them through the baculovirus IAP repeat (BIR) domains, and are thought to inhibit residual caspase activity in healthy cells Huang et al. (2001). Their action is counteracted by proteins like SMAC (second mitochondrial activator of caspases), also known as DIABLO (direct IAP binding protein with low pI), that sequesters IAimmunePs allowing normal activity of caspases Du et al. (2000); Ekert et al. (2001); Liu et al. (2000).

2.1.3. Pathways for caspase activation

Caspase processing and activation is regulated mainly by two routes, known as the extrinsic and the intrinsic (or mitochondrial) pathways, shown schematically in figure 2.2. The extrinsic pathway gathers specific apoptotic signals coming from the extracellular environment and has revealed essential for the normal function of the immune system Ashkenazi and Dixit (1998). The signaling molecules belong to the superfamily of the tumor necrosis factor (TNF), like TNFα, Fas/CD95 and Apo2 ligand/TRAIL, which activate the corresponding membrane bound receptors from the TNF/NGF receptor family, such as TNFR1, Fas/CD95 and Apo2. After recruiting the apoptotic ligands in the extracellular side, these death receptors (DR) form trimers in the plasmatic membrane. The DR clusters interact in the cytosolic side with an adaptor protein called FADD (Fas-associated death domain protein) to form the so-called death inducing signaling complex (DISC), which recruits multiple initiator procaspase-8 molecules and facilitates their autoproteolytic activation through the mechanism of induced proximity (see above). Then caspase-8 activates procaspases 3 and 7, and the cell enters a point of no return. Processing of procaspase 8 can be inhibited by c-FLIPP, a degenerate caspase homologue that binds to FADD.

The intrinsic pathway responds to most apoptotic signals, and is crucial for stress-induced and genotoxic-induced cell death Jiang and Wang (2004). It is triggered by the release of proapoptotic proteins from the mitochondrial intermembrane space, which include cytochrome c Liu et al. (1996), SMAC/DIABLO Du et al. (2000); Verhagen et al. (2002), Omi/HtrA2 Suzuki et al. (2001), Apoptosis Inducing Factor (AIF) Susin et al. (1996) and Endonuclease G (EndoG) Li et al. (2001). The major consequence is the formation f the apoptosome complex, leading to the activation of caspase 9. A large family of proteins, known as the Bcl-2 proteins, controls this process at the mitochondrial outer membrane.

2.2. A cross-road at mitochondria

In 1996, a protein known as apoptosis inducing factor, AIF, was found to normally reside in the mitochondria, and exit to the cytosol during apoptosis Susin et al. (1996). Almost simultaneously, it was discovered that cytochrome c, a small electron carrier involved in the redox chain connected to the oxidative phosphorylation, can be released from the mitochondrial intermembrane space to work as an apoptotic factor Liu et al. (1996). Since then, many other apoptotic proteins have been reported to be released from the mitochondria during apoptosis, including SMAC/DIABLO Verhagen et al. (2002); Du et al. (2000), Omi/HtrA2 Suzuki et al. (2001), and EndoG Li et al. (2001).

Soon, it was shown that mitochondria are at a cross-road of the apoptotic route, constituting the main check-point of the intrinsic apoptotic pathway and providing a connection between the extrinsic and intrinsic pathways through the Bid regulator Luo et al. (1998) (see section 2.3.3).

During apoptosis, mitochondria undergo several morphological changes, that affect the structure of the mitochondrial membranes, and the physiology of these organelles. Effects like lipid peroxidation Keller et al. (1998), remodeling of cristae and contact sites Scorrano et al. (2002), and mitochondrial fission have been observed in connection to apoptosis Oakes and Korsmeyer (2004).

But clearly, the main role of mitochondria in the process of apoptosis is to provide a compartment that under normal conditions keeps closed a number of important pro-death factors, to be released in a regulated manner as a consequence of apoptotic signals.

Among the proapoptotic proteins of mitochondrial origin, SMAC/DIABLO acts by freeing caspases from their specific inhibitors, IAPs Verhagen et al. (2000); Du et al. (2000). This function is also performed by Omi/HtrA2, a mitochondrial serine protease that cleaves and inactivates IAPs Suzuki et al. (2001). AIF and EndoG G are implicated in caspase independent pathways to apoptosis related to DNA fragmentation and chromatin condensation. But the major role of mitochondria is thought to be related to the activation of the apoptosome initiator complex for which the release of cytochrome c is essential Jiang and Wang (2004).

2.3. The Bcl-2 family of proteins: guards of the mitochondrial fate

Bcl-2 (B-cell lymphoma/leukemia-2) was first described as an oncogene related with human tumors and it was later connected to apoptosis due to its homology

with the CED-9 protein of *C. elegans* Hockenbery et al. (1990). Several proteins have been described to date as Bcl-2-like proteins, also involved in apoptosis and containing up to four Bcl-2 homology (BH) domains. They constitute the Bcl-2 family of proteins. Figure 2.3 shows the conserved regions and the BH domains of some members of the family.

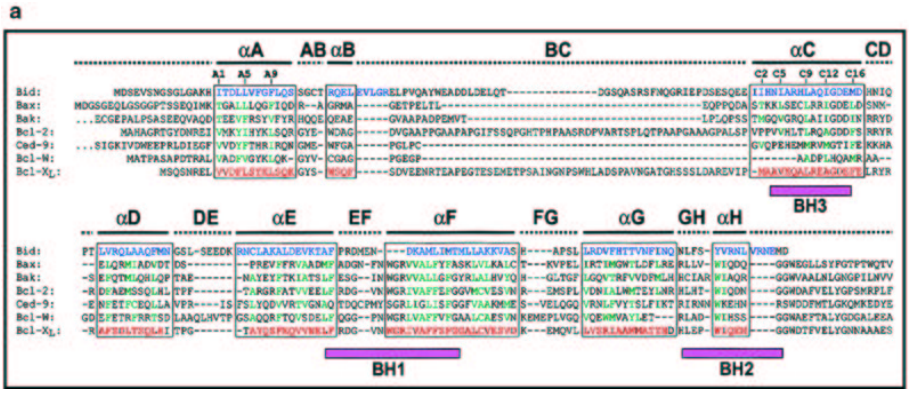

Figure 2.3.: Sequence aligment of some Bcl-2 members. Conserved residues in the helical regions are squared and coloured in green (with respect to residues from Bid and Bcl-xL, which are coloured in blue and red, respectively), homology domains are underlined with a violet bar and the helical regions named with letters at the top line. (From McDonnell et al. (1999))

Despite their sequence homology, different proteins of the Bcl-2 family have opposing functions regarding apoptosis. Thus, some of them are proapoptotic and induce the death pathway in response to apoptotic stimuli, while others are antiapoptotic and protect the cell from programmed cell death by counteracting the proapoptotic Bcl-2 proteins Adams and Cory (2001). The family of Bcl-2 proteins can be classified in three groups, depending on their BH domains, as shown in figure 2.4.

Antiapoptotic members such as Bcl-2 and Bcl-xL (type I Bcl-2 proteins) present all four homology domains BH1-BH4. Proapoptotic members, however, can be of two types: type II Bcl-2 proteins, like Bax and Bak, which have BH1, BH2 and BH3 domains, and type III Bcl-2 proteins, like Bid and Bim, also known as BH3-only proteins, because they only possess this homology domain. The BH1, BH2 and BH3 domains form a hydrophobic cleft that is a common feature of type I and II proteins and constitutes a binding site of the BH3 domain of other Bcl-2 proteins Sattler et al. (1997). This interaction is responsible of the homo- and

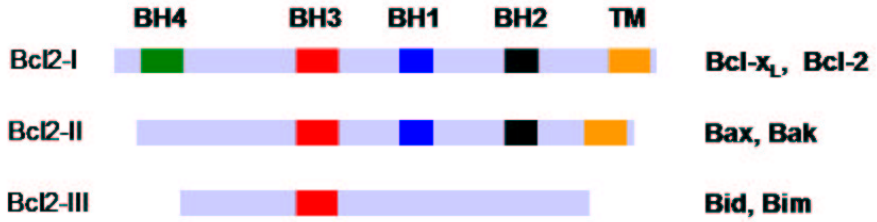

Figure 2.4.: The three subgroups of proteins of the Bcl-2 family and their most representative members. The BH domains and the C-terminal hydrophobic domain are indicated.

heterodimerisation patterns showed among different members of the family Zha et al. (1996); Hanada et al. (1995). The antagonistic effect between pro- and anti-apoptotic members of the family is thought to be connected to their ability to interact with each other through the BH3 domain of types II and III and the hydrophobic docking cleft found at the surface of type I Bcl-2 proteins Oltvai et al. (1993). This interaction based mechanism is viewed either as a way to sequester proapoptotic factors by membrane anchored type-I Bcl-2 proteins Cheng et al. (2001), or a way to inactivate these latter antiapoptotic regulators by proapoptotic ones Kelekar et al. (1997). Either case leads to a model of mutual neutralisation, where the ratio of pro versus antiapoptotic Bcl-2 proteins determines apoptosis induction Oltvai et al. (1993); Boise et al. (1993).

Multiple lines of evidence connect the function of these proteins to their subcellular localisation and their association with membranes. Some of them localize constitutively at intracellular membranes, as the mitochondrial outer membrane (MOM) (Bcl-2, Bcl-xL, Bak) and the nuclear and endoplasmic reticulum (ER) membranes (Bcl-2, Bcl-xL), while others are soluble in the cytosol and translocate to the MOM in response to apoptotic stimuli (Bcl-w, Bax, Bid, Bim) Gross et al. (1999); Hockenbery et al. (1990); Wolter et al. (1997). The constitutive membrane-bound proteins contain a hydrophobic C-terminal domain that controls their localisation Priault et al. (1999); Nguyen et al. (1993). This C-terminal segment acts as a constitutive anchor to the cytoplasmic side of outer membrane of mitochondria, the nucleus or the endoplasmic reticulum. However, some soluble proteins, like Bax, contain also a C-terminal hydrophobic domain that is partially buried in a hydrophobic cleft on the surface of the protein. These latter proteins are normally soluble in the cytosol, but under apoptotic signals the C-terminal

domain is thought to become exposed and to promotes protein insertion in the mitochondrial membrane Nechushtan et al. (1999).

The main role of the proteins of the Bcl-2 family involves the control of the release of the apoptotic factors from the mitochondria. As explained above, this affects the assembly of the apoptosome by regulating the presence of cytochrome c in the cytosol. Additionally, they regulate the release from the mitochondria of SMAC/DIABLO and Omi/HtrA2, and AIF and EndoG, which are involved in overcoming caspase inhibition by IAPs, and in the induction of DNA fragmentation, respectively.

In addition to the selective permeabilisation of the MOM, the induction of the mitochondrial permeability transition pore, through regulation of Ca2+ release from the ER stores and Ca2+ uptake by the mitochondria Esposti and Dive (2003); Oakes et al. (2003) has been related to the action of the Bcl-2 proteins. In either case, their function appears closely related to pore formation activity. Moreover, Bcl-2, Bax and Bak have been found at the ER membrane, where they control apoptosis initiation dependent on the activation of caspase 12 Zong et al. (2003). This new apoptotic pathway appears to be connected with the regulation of intracellular calcium fluxes Nutt et al. (2002); Scorrano et al. (2003). An increase in the presence of Bcl-2 at the ER membrane produces a decrease in the concentration of $Ca^{2+}$and then, in the cellular Ca^{2+}responses, thus protecting cells against some apoptotic stimuli. In contrast, the increase of Bax at the ER membrane has been related with an increment in the concentration of Ca^{2+}at the ER lumen and in the cellular Ca^{2+}responses, increasing the mitochondrial uptake of Ca^{2+} and promoting apoptosis. It is not yet understood whether this mechanism is due to the direct action of the Bcl-2 proteins or it is a consequence of the interaction with other proteins. But it seems to be independent of the central hydrophobic hairpin of the Bcl-2 proteins, while interactions with the inositol-3-phosphate receptor (IP3R), may be involved.

2.3.1. Bcl-2 protein have water soluble structures

The activation of the proteins of the Bcl-2 family is largely connected to their ambivalent folding properties, being stable both in water and lipidic media, but only the structure of the inactive, water soluble forms of Bcl-xL Muchmore et al. (1996), Bcl-2 Petros et al. (2001), Bax Suzuki et al. (2000) and Bid Chou et al. (1999)McDonnell et al. (1999) are known so far.

The first structure described was that of Bcl-xL Muchmore et al. (1996), lacking the C-terminal membrane anchoring domain, which showed a compact fold formed by seven α-helices and a long flexible loop between helices $\alpha 1$ and $\alpha 2$ (see

figure 2.5, B). Water soluble Bcl-xL is arranged in three layers of helices, in such a way that two central α-helices, namely $\alpha 5$ and $\alpha 6$, are flanked on one side by $\alpha 3$ and $\alpha 4$, and on the other side by $\alpha 1$, $\alpha 2$ and $\alpha 7$. The central helices $\alpha 5$ and $\alpha 6$ contain mainly hydrophobic amino acids, and are organised into an antiparallel hairpin. This structure corresponds to the fold class of toxins' membrane translocation domains in the SCOP classification, and concretely, resembles the membrane insertion domains of colicins and diphtheria toxin. Additionally, the BH1, BH2 and BH3 domains organise close in the space and generate a hydrophobic cleft, which later was shown to be site of interaction with the BH3 domains of other Bcl-2 proteins.

When the structures of the water soluble forms of Bid and Bax were resolved, they resulted to be surprisingly similar. Both Bax and Bid organise also into helical folds with a central hydrophobic hairpin of helices in the core of the protein, surrounded by other amphipatic helices, which are exposed to the solvent. Nine α-helices give rise to the water soluble structure of Bax Suzuki et al. (2000) (figure 2.5, C), where helices $\alpha 5$ and $\alpha 6$ form the hydrophobic hairpin, and helix $\alpha 9$ is the homologous to the C-terminal hydrophobic domain lacking in the structure of Bcl-xL. In this protein, $\alpha 9$ is buried in the hydrophobic cleft formed by the BH1, BH2 and BH3 domains, which show orientations slightly different from those of Bcl-xL.

In the case of Bid Chou et al. (1999); McDonnell et al. (1999), it presents eight helices, of which helices $\alpha 6$ and $\alpha 7$ form the central hairpin homologue to $\alpha 5\alpha 6$ in Bcl-xL and Bax (figure 2.5, D). As Bid contains only the BH3 domain, it lacks the hydrophobic cleft found in Bcl-xL and Bax, but the overall organisation is almost identical to them. Although practically preserved, the structure of cleaved Bid, which is the active form of the protein, exposes a larger area in the BH3 domain and in the region of the hydrophobic hairpin.

Constructing coherent models of pores formed by Bcl-2 proteins is hindered by the lack of structural information about the membrane inserted conformation of these proteins. A large conformational rearrangement has been reported to be involved in the interaction of these proteins with lipid membranes and detergent micelles Suzuki et al. (2000); Losonczi et al. (2000); Oh et al. (2005). In addition, the large structural transition from a globular, water soluble, to a membrane inserted species appears to be a regulated process, where different members of the Bcl-2 family interplay to give a final outcome of activation or inhibition of apoptosis Oltvai et al. (1993).

Although the high resolution structures of the membrane inserted proteins are yet unresolved, several other observations have provided some insight into the organisation of the Bcl-2 in lipid environments. NMR experiments with Bcl-xL in

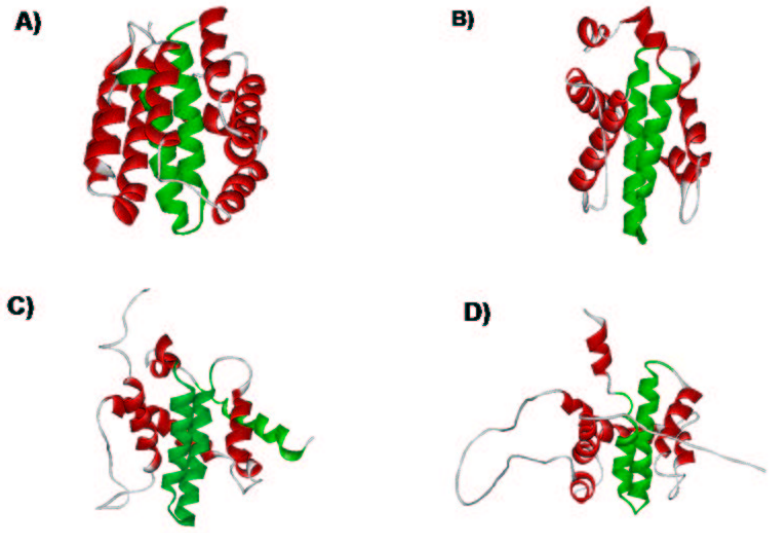

Figure 2.5.: Soluble structures of Bcl-2 proteins in comparison with the pore forming domain of colicin E1. Figures have been built from the corresponding PDB files. Exposed helical domains are shown in red and the two putative homologue central α-helices are shown in green. A) Soluble pore-forming domain of colicin E1. B) Soluble form of human Bcl-xL without the C-terminal anchoring domain. C) Soluble form of human Bax, C-terminal domain also depicted in green. D) Soluble form of mouse Bid.

micelles have shown that the presence of lipids induces large structural changes and an overall increase of helicity Losonczi et al. (2000). These results suggest that the tertiary organisation in micelles in different from that in water, where helices $\alpha 1$ and $\alpha 6$ interact with the hydrophobic core of the micelle (the resonances of $\alpha 5$ are not well resolved, but probably behaves similarly). In the case of tBid, EPR and NMR experiments in lipid media have been performed Oh et al. (2005). These experiments show that tBid adopts an unfolded structure upon interaction with the membrane, characterised by a unique conformation and orientation. The EPR results indicate that the helix $\alpha 6$ is inserted in the membrane with a calculated tilt of 26^{o}, while $\alpha 7$ lays parallel, embedded in the polar head-group region of the bilayer. In contrast, NMR spectra indicate that all the helices of tBid organise parallel to the bilayer, even in the case of $\alpha 6$.

2.3.2. Bcl-xL, Bax and Bid form ion channels in lipid bilayers

By analogy with the colicins, for which the mechanism of action has been studied in more detail Cramer et al. (1995); Stroud et al. (1998), it was immediately proposed that the two central α-helices might be responsible of the formation of TM pores Muchmore et al. (1996), and this idea was indeed supported by measurements of ion channel activity in synthetic lipid membranes for Bcl-xL, Bcl-2, Bax and Bid Minn et al. (1997); Schendel et al. (1999, 1997); Schlesinger et al. (1997).

Addition of Bcl-xLΔC-t to planar lipid membranes at neutral pH rapidly promotes current fluctuations that accumulate over time and individual step-like channels can be observed Minn et al. (1997). This activity is higher at acidic pH. The predominant conductance state corresponds to 276$\pm$28 pS, while other states of lower conductance are also observed. Moreover, the I/V characteristics shows simple ohmic dependence, and the channel is cation selective in PS:PC (4:6) bilayers. The behaviour displayed by full-length Bcl-xL was similar to the truncated protein Basanez et al. (1999).

BaxΔC-t exhibits a similar channel activity in planar lipid membranes (see figure 2.6) Antonsson et al. (1997). However, it has a higher activity at neutral than at acidic pH. At pH 7, Bax induces early channels of 5.6$\pm$0.2 pS and larger fluctuations of 250$\pm$25 pS. Later abrupt changes of about 450 pS are observed, which give conductances up to 2 nS. These channel activity is also voltage independent and selective for cations in DPhPC membranes at pH 7. Moreover, experiments with full length Bax and the truncated version showed that the protein induces monotonic increases in the conductance that eventually lead to membrane destabilisation and rupture (figure 2.6, B) Basanez et al. (1999). In fact, Bax provokes a decrease in the membrane line tension in a dose dependent fashion, which has been related to the promotion of intrinsic monolayer curvature and the formation of a partially lipidic pore. A comparable behaviour was observed for the cleaved ΔN76Bcl-xL, which has been shown to have a proapoptotic action.

In the case of Bid, only tBid showed channel activity at neutral pH Schendel et al. (1999). This activity was observed only when positive potentials were applied, and showed no voltage dependence. Several conductance steps were observed, ranging from 7.4 to 100 pS, as shown in figure 2.7.

These results are in agreement with a mode of action similar to that of colicins, the diphtheria toxin or the δ-endotoxin. Supporting this model, deletion of the α5-α6 hairpin of Bax abrogated its ability to form ion conducting channels and to release cytochrome c from mitochondria Heimlich et al. (2004). Also, the hairpin α6-α7 of tBid has been found to be important for mitochondrial targeting Hu

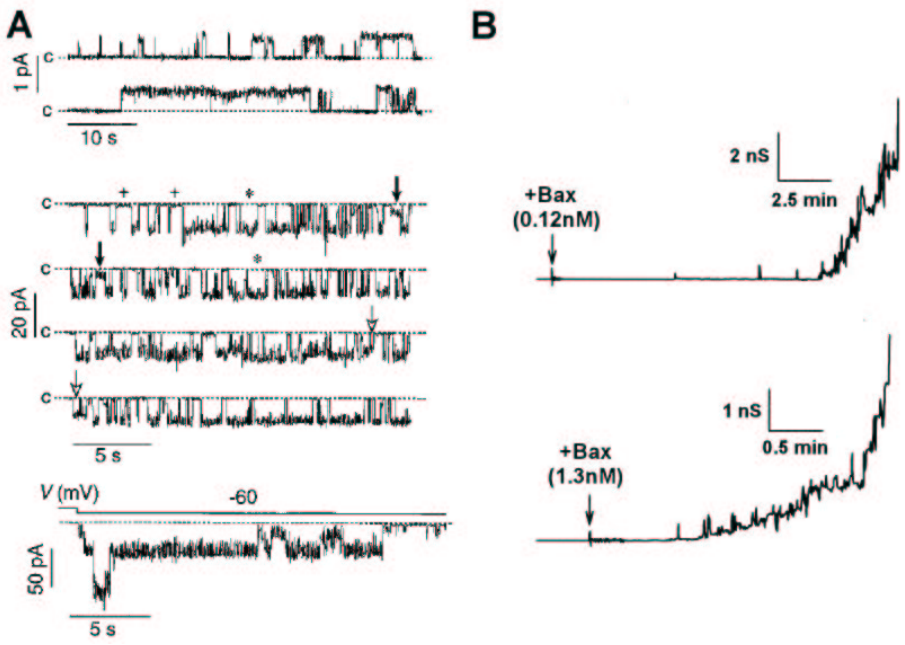

Figure 2.6.: Bax channel activity. A, channel events induced by BaxΔC-t in DPhPC bilayers at +100 mV, -50 mV and -60 mV. The channel conductance varies from around 5 pS to 1.6 nS (adapted from Antonsson et al. (1997)). B shows the conductance changes induced by full length Bax in a DOPC:DOPE:DOPS (1:1:1) bilayer at 40 mV (from Basanez et al. (1999)).

et al. (2003). However, the structural similarity of pro and antiapoptotic Bcl-2 proteins and the capacity of members of the two categories to form ion channels are not easily conciliable with their opposed functions Lazebnik (2001).

2.3.3. Roles of BH3-only proteins

Among the proapoptotic Bcl-2 proteins, two groups can be functionally and structurally distinguished. The group represented by Bax and Bak is involved on directly mediating the release of mitochondrial apoptogenic factors Bouillet and Strasser (2002a)(see section 2.3.4). A second group of proapoptotic proteins that contain only domain BH3, like Bid and Bim, assist the former proteins in their function by a still unresolved mechanism, of which only some general guide lines appear to be clear.

It has been suggested that these proteins are essential initiators of apoptosis that have evolved to recognise distinct forms of cell stress, and thus, cell knock outs for individual BH3-only proteins are resistant to apoptosis induced by selective signals. BH3-only proteins are activated by transcriptional upregulation and by post-translational modifications in response to apoptotic stimuli Bouillet and Strasser (2002b). For example, under normal conditions Bid exists as an inactive form in the cytosol (see figure 2.8). Proteolytic cleavage by caspase 8 within an unstructured loop releases an inhibitory p7 N-terminal fragment and a proapoptotic p15 C-terminal fragment, known as tBid, which remain associated in an inactive complex. Myristoylation at the new N-terminal glycine of tBid acts as a molecular switch, and then it relocalises and inserts into the OMM, where it is able to induce cytochrome c release Gross et al. (1999); Zha et al. (2000). Another BH3-only protein, Bim, exists in its inactive form bound to the microtubule-associated dinein motor complex, and under apoptotic stimuli, it is released and exerts its proapoptotic action O'Connor et al. (1998).

tBid, and other BH3-only proteins, may neutralize antiapoptotic Bcl-2 proteins through BH3 dependent heterodimerisations Bouillet and Strasser (2002b). Additionally, they may activate Bax-type proteins by direct binding via their BH3 domain. A conformational change, that involves exposure of hydrophobic groups, followed by mitochondrial targeting, insertion in the MOM and oligomerisation, is known to be necessary for the permeabilising activity of Bax Desagher et al. (1999) (see section 2.3.4). The change in conformation can occur upon interaction with lipid vesicles Yethon et al. (2003), while membrane insertion, oligomerisation, and pore formation need the presence of tBid and probably other, yet unknown, proteins Eskes et al. (2000).

During apoptosis, a process of CL distribution in the mitochondrial membranes associated to cristae remodeling takes place, which enlarges the available pool of cytochrome c to be released Scorrano et al. (2002). Specific interactions with CL have been connected to the targeting of tBid to the OMM, mainly to the contact sites, which are enriched in this lipid Lutter et al. (2000). Recent studies have suggested that tBid has an active role in these morphological reorganisation of mitochondria, likely through interaction with CL. Moreover, Petit and colleagues have observed that tBid, and a peptide encompassing the helix $\alpha 6$ are able to affect the mitochondrial metabolism and to induce CL segregation in lipid monolayers F. Gonzalvez and Petit (2005) [personal communication].

Although tBid needs in vivo the presence of Bax-type proteins to induce release of cytochrome c, in vitro it displays, by itself, a characteristic poration activity: tBid promotes leakage of fluorescent probes from LUVs Epand et al. (2002a), and forms ion channels in planar lipid bilayers accompanied by destabilization

of the membrane Kudla et al. (2000). Interestingly, it has been shown recently that tBid collaborates with Bax in the formation of large lipidic pores, which are enhanced by positive curvature-inducing lipids and characterized by transbilayer lipid movement Terrones et al. (2004). Additional data also suggest that lipids play important roles in the apoptotic permeabilisation of mitochondria. Thus, targeting of tBid to membranes is increased by N-myristoylation of a glycine residue and the presence of negatively charged lipids Zha et al. (2000), and the specific mitochondrial lipid cardiolipin has been involved in tBid addressing to the MOM Lutter et al. (2000) and in the enhancement of membrane permeabilisation in an in vitro system containing this latter protein and Bax Kuwana et al. (2002).

2.3.4. Mechanisms of Bax activity

Activation of typical proapoptotic type-II Bcl-2 proteins, like Bax, is accompanied by a change in their subcellular localisation and an extensive structural reorganisation, which facilitates membrane targeting and insertion to the MOM Desagher et al. (1999); Hsu et al. (1997); Goping et al. (1998); Nechushtan et al. (1999); Yethon et al. (2003). This latter process is promoted by activated type-III Bcl-2 proteins Desagher et al. (1999); Eskes et al. (2000); Wei et al. (2001); Roucou et al. (2002); Luo et al. (1998) (see section 2.3.3), which may in turn activate Bax-like proteins through BH3 dependent interactions (although additional interactions, independent of BH3, seem to be involved Terrones et al. (2004)). Once in the mitochondrial membrane, the type II Bcl-2 proteins form oligomers, which may selectively permeabilise the MOM by means of direct pore formation or regulation of other existing pores (figure 2.8).

Careful biophysical investigations have shown that Bax can promote the release of fluorescent probes and cytochrome c from large unilamellar lipid vesicles (LUVs) Saito et al. (2000), being this permeabilising activity connected to the ability of Bax to multimerise. As shown in section 2.3.2, in planar phospholipid bilayers, truncated Bax (lacking its C-terminal hydrophobic tail) induces channel-like fluctuations with multiconductance states Antonsson et al. (1997). This complex behavior is accompanied by marked decreases of voltage dependent lifetime and linear tension of the membrane, which are largely enhanced in the case of full-length Bax Basanez et al. (1999). Basañez, et al. interpreted these results as due to Bax induced changes in the intrinsic monolayer curvature, promoting the formation of an, at least, partially lipidic pore. Recently, formation of a toroidal pore has been also proposed to explain the mode of action of colicins. This idea introduced a novelty as to the nature of the apoptotic pore Zimmerberg and Chernomordik (1999) that has been subsequently supported by the depen-

dence of the activity of Bax-type proteins on intrinsic monolayer curvature. Thus, Bax induced membrane permeabilisation is promoted by non-lamellar lipids with positive intrinsic curvature, but inhibited by lipids with negative intrinsic curvature Basanez et al. (2002); Terrones et al. (2004). In agreement with these observations, Bax-type proteins have been found during apoptosis at outer mitochondrial scission sites Karbowski et al. (2002), a likely location for non-bilayer lipid structures. Additionally, Bax pore-like structures, claimed to be toroidal, have been recently observed by atomic force microscopy Epand et al. (2002b).

2.3.5. Bcl-xL and Bcl-2, how do the inhibitors work?

With respect to the molecular mechanism of inhibition of apoptosis by type I Bcl-2 proteins, it is also a matter of debate and various schemes, apart from the already mentioned BH3 dependent hetero-dimerisation (see figure 2.8), have been proposed Minn et al. (1999). These include inhibition of mitochondrial pores through direct protein-protein interaction Shimizu et al. (1999, 2000a), countering the effect of Bax channels Minn et al. (1999) and control of Ca2+ homeostasis at the level of the ER Smaili et al. (2000); Pinton et al. (2002). Type I Bcl-2 proteins are C-terminal anchored to the cellular membranes, but conformational arrangements and extensive insertion in the OMM and ER membrane have been reported for Bcl-2 and may be implied in their antiapoptotic functionKim et al. (2004a).

In the case of Bcl-xL, it is constitutively anchored to the OMM through its C-terminal helix, but a small fraction of the protein is soluble in the cytosol forming homodimers in normal conditions, and translocates to the OMM during apoptosis Jeong et al. (2004). Mitochondrial targeting specificity is achieved thanks to two basic amino acids at both ends of the C-terminal anchoring domain Kaufmann et al. (2003).

Different inhibitory effects of apoptosis have been described for Bcl-xL: i) Interactions between the C-terminal domain of one molecule and the hydrophobic cleft of the partner have been implicated in both dimer formation and the heterodimerisation-dependent mechanism of Bax inhibition Jeong et al. (2004). In addition, a mutant unable to interact with Bax can still inhibit it. ii) Bcl-xL decreases DISC formation in the plasma membrane and thus caspase 8 activation in TRAIL induced apoptosis **?**, iii) it protects apoptosis even after cytochrome c release and **?** iv) blocks the contact site increase in mitochondria. v) It has been shown to interact with VDAC Shimizu et al. (2000b), vi) to inhibit tBid insertion and Bax/Bak oligomerisation and insertion in the OMM Gross et al. (1999), and to block the release of cytochrome c and SMAC/DIABLO **?**.

In addition, Bcl-xL has been shown to form channels in planar lipid membranes, which are pH sensitive, cation selective for $Na^+$and inhibitable by Ca^{2+} (see section 2.3.2), and this channel activity has been also observed in the outer membrane of presynaptic mitochondria **?**. Interestingly, a mutant with a deletion in the α5-α6 hydrophobic hairpin, proposed to be the putative pore forming domain, is unable to block apoptosis. However, it is difficult to conciliate this ion channel activity with its inhibitory function.

Regulation of Bcl-xL is carried out through a number of mechanisms and has different consequences on its activity. Phosphorylation at Ser62 Basu and Haldar (2003) and deamidation of two asparagines in the unstructured loop inactivate its antiapoptotic action Deverman et al. (2002), whereas proteolytic cleavage of the N-terminal domain, between BH3 and BH4, turns it into a proapoptotic protein. ΔN-Bcl-xL induces cytochrome c release from mitochondria and apoptosis Basanez et al. (2001). It has been shown to form larger channels in the OMM which are dependent on the BH3 domain and to interact with VDAC. *In vitro* studies with model membranes have shown that ΔN-Bcl-xL alone is able to permeabilise liposomes to cytochrome c and dextrans of high molecular weight, and to destabilise planar lipid membranes and decrease the membrane line tension Basanez et al. (2001).

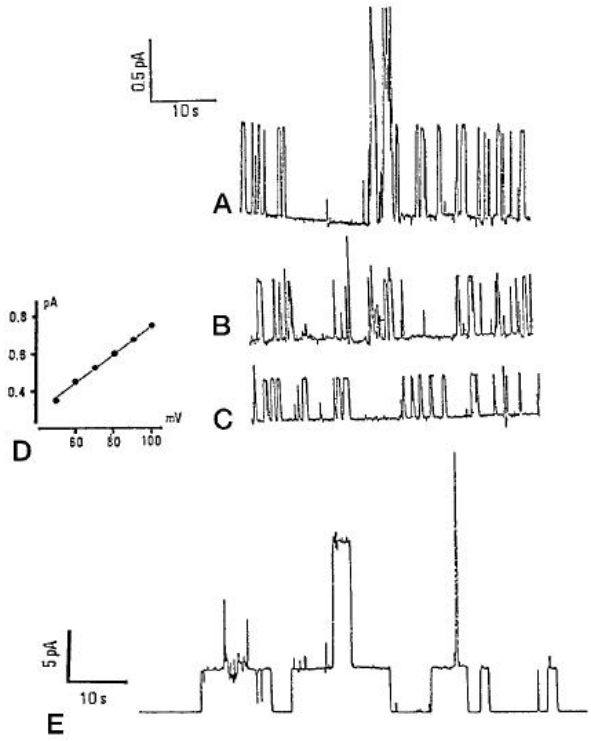

Figure 2.7.: tBid ion channel activity. Traces in A, B and C represent the current versus time induced by tBid at voltages of +100 mV, +70 mV and +50 mV, respectively. The single channel conductance is of about 8 pS, with a lifetime of around 0.5 s. D shows the I/V plot for open channels at positive potentials. Larger channels observed at +100 mV and higher protein concentrations are shown in E. In all cases membranes were made of POPE:POPG (1:1), at pH 7.3. (From Schendel et al. (1999)).

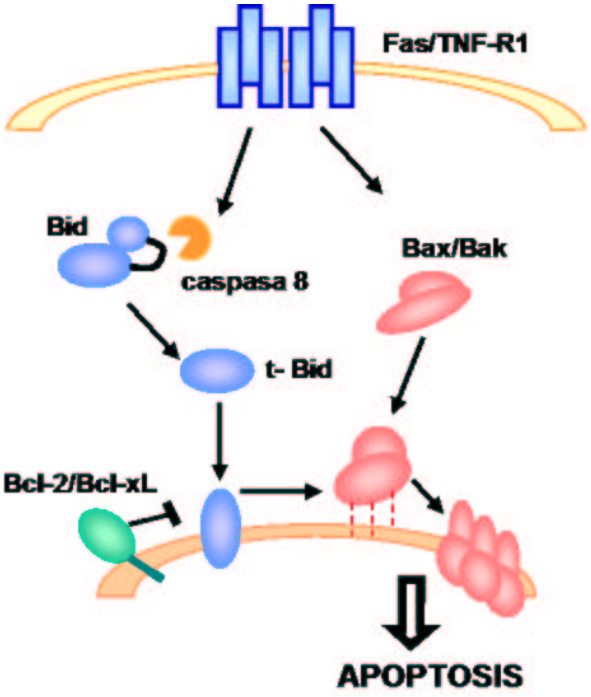

Figure 2.8.: Functions and relationships between some Bcl-2 members.

3. Objectives

The generally assumed colicin-like model implies TM spanning insertion of both the $\alpha 5$ and $\alpha 6$ fragments, of which there is only indirect or incomplete evidence Nouraini et al. (2000); Heimlich et al. (2004); Kim et al. (2004a); Franzin et al. (2004). This is specially important since the above segments contain a significant number of (potentially) charged residues, which should in principle impose restrictions to a membrane inserted state Nouraini et al. (2000). Is is also unknown whether these and/or other fragments participate in the formation of the channel. Undoubtedly, a better knowledge of the interaction of the Bcl-2 proteins with biological membranes is needed in order to define consistent models of the functional structures of these proteins.

In this thesis, we have tackled the characterisation of the interactions with membranes of the proteins of the Bcl-2 family. For this purpose we have chosen a representative member of each of the groups constituting the family, concretely Bcl-xL, Bax and Bid, and the following objectives were proposed:

- Prediction analysis of the TM fragments in the sequences of Bax, Bid and Bcl-xL by using the programs TopPred II and DAS.

- Evaluation of the propensity to insert in the membrane that the hydrophobic domains of the proteins Bax, Bid and Bcl-xL show. With this aim, we have constructed chimeric proteins based on the Lep protein, where the different hydrophobic fragments have been inserted, and we have studied their insertion in the membrane through *in vitro* transcription/translation/glycosylation assays.

- Chemical synthesis and purification of the peptides corresponding to each of the α-helices that form the putative pore forming hairpin. Concretely, the peptides Bax-$\alpha 5^K$, Bax-$\alpha 5$, Bax-$\alpha 6$, derived from the putative pore forming domain from Bax; Bid-$\alpha 6$ and Bid-$\alpha 7$, derived from the homologous domain from Bid; and Bcl-xL-$\alpha 5$ and Bcl-xL-$\alpha 6$ derived from the corresponding hairpin from Bcl-xL.

- Characterisation of the pore forming activity of the different peptides, by means of assays of release of calcein and fluorescent dextrans of different sizes from LUVs of different lipidic compositions, assays of lipid transbilayer redistribution between both leaflets in asymmetric LUVs, and ion channel formation in PLM.

- Structural characterisation of the peptides in aqueous environment, in lipid-mimetic media and in presence of LUVs, by means of experiments of circular dichroism (CD) and infrared spectroscopy (ATR-FTIR).

4. The experimental approach

In addition to the problems generally associated to the handling of membrane proteins, the difficulties to study proteins of the Bcl-2 family in a lipid membranes arise from their complex folding properties. As the pore-forming toxins, Bcl-2 proteins can adopt stable structures both in water and lipidic environments. The water soluble fold is known for Bax, Bcl-xL, Bid and Bcl-2; yet it says little about the active structures of these proteins in the membrane. In addition, the change from the globular, water soluble fold to a membrane bound structures appears to be a complex, regulated process, that include protein-protein and protein-lipid interactions, and covalent modifications such as phosphorylation and proteolysis. In order to overcome some of these difficulties, we have employed a reductionist approach that consists on the identification and characterisation of the fragments involved in the interactions with membranes, both from structural and functional points of view. This strategy has been previously used with success in the study of similar systems, like the δ-endotoxin Gazit and Shai (1993); Gazit et al. (1994) and other membrane proteins, such as bacteriorhodopsin Popot et al. (1986), the lactate permease Bibi and Kaback (1990) or the potassium channel Ben-Efraim and Shai (1997).

4.1. Prediction of transmembrane fragments

About one fourth of the open reading frames (ORFs) encoded in sequenced genomes correspond to integral membrane proteins. In spite of this, the number of structures of membrane proteins in the Protein Data Bank (PDB) is less than 1% of the total. This is a consequence of the difficulties still encountered for the structural studies of these systems. In the absence of high resolution structural data, establishing the number of possible TM fragments and their topology results of great value, allowing the construction of low resolution models. Theoretical methods that predict the number of transmembrane fragments, their position within the polypeptide chain, and their topology in the membrane are generally a good starting point before more laborious experimental studies. Currently,

these methods explode mainly the information accumulated about helix-bundle membrane proteins of known structure and topology, to evaluate the potential of segments of a target sequence to contain a putative TM fragment.

The prediction of membrane spanning helices is based on the fact that TM segments contain mostly non-polar residues. To evaluate the hydrophobic nature of the different amino acids, several hydrophobicity scales have been proposed. Some of the best known are the Kyte-Doolittle scale, which combines the statistical analysis of resolved crystallographic structures and partitioning equilibria between an aqueous and an organic solvent, the Goldman-Engelman-Steiz scale, based on the analysis of the solvent interaction with the different residues in a polyalanine helix context, and the Whimley-White scale, which uses values of the free energy cost associated to the transfer of small peptides from water to a POPC bilayer and to octanol Scarlata (2004). Based on these scales, simple analysis of target protein sequences generate hydropathy plots, which represent a hydrophobicity score within a window of typically 20 residues (enough to span the 30Å thickness of the hydrocarbon core of the bilayer) against the first amino acid of the window. A peak in the hydrophobicity plot above a defined threshold predicts the presence of a transmembrane helix. However these simple methods tend to overpredict transmembrane helices, as they do not discriminate true TM fragments from hydrophobic regions within the core of globular water soluble proteins.

A second generation of advanced prediction methods incorporate new parameters, like the statistical representation of amino acids in known TM fragments, sequence alignments, characteristics of flanking residues normally found at the interface, and topological rules, like the positive inside rule [1]. Parallelly, they incorporate more complex calculations in their algorithms. In general, these methods predict correctly 55-60% of the membrane protein topologies in whole genomes. Some examples are the TMHMM and the HMMTOP methods, both based on hidden Markov models.

An analysis of the reliability and accuracy of the different TM prediction methods reveals that those based on alignment information are more accurate than the ones based on single sequences Chen et al. (2002). Most common errors in advanced methods include the overprediction or underprediction of one TM helix,

[1] According to the positive inside rule, the regions flanking the TM segments of polytopic membrane proteins have a biased distribution of positively charged amino acids. Those facing the cytosol are enriched in arginyl and lysyl residues, while those translocated barely contain these residues. This implies that the distribution of positively charged amino acids is a key determinant of the transmembrane topology of integral membrane proteins von Heijne (1989).

the underprediction of membrane helices which are too short or contain charged residues, and the prediction of signal peptides as membrane helices. In addition, the percentage of correct predictions for multi-spanning membrane proteins with more than five helices decreases abruptly. It should be noted that the reliability of the advanced methods is most likely overestimated, as in many cases cross-validation data are not available. Moreover, their result may also be biased, as the methods have been trained using the structure of the limited number of membrane proteins available to date.

Recently Hessa et al. have proposed a biological hydrophobicity scale using a system based on membrane insertion of a reporter protein through the translocon Hessa et al. (2005). They show that the free energy of insertion depends on the position of the amino acids within the helix, the contribution of charged flanking residues and the influence of helix-helix interactions during the insertion of multispanning membrane proteins. Additionally, protein-lipid interactions seem to be essential for the recognition of transmembrane helices by the translocon. However, these effects still need to be better quantified to elaborate a reliable scale.

In this work, we have employed the DAS (Dense Alignment Surface) and the TopPred methods. The DAS method was first developed in an attempt to improve sequence alignment for the family of transmembrane proteins known as the G-protein-coupled receptors Cserzo et al. (1997). Later, it was extended to predict transmembrane segments in any integral membrane protein. DAS performs low-stringency dot-plots of the sequence of interest and compares them with a compilation of non-homologous membrane proteins using a previously derived, special scoring matrix. It generates a hydrophobicity profile with high and low cut-offs values for membrane insertion. Comparison with other existing methods has revealed that the DAS method has essentially the same predicting power as the best programs, which need multiple sequence alignments. On the other hand, the TopPred performs a hydrophobicity analysis combined with the positive inside rule Claros and von Heijne (1994); Melen et al. (2003). Initially, it calculates a standard hydropathy profile, with an upper and a lower cut-off, for "certain" and "putative" transmembrane helices respectively. Among the possible topologies that then arise, the best is that with the highest difference in positively charged residues between both membrane sides.

4.2. Model membrane systems

To study both the structural and functional properties of membrane proteins, a number of model membrane systems, which provide a controlled environment to perform experiments, have been developed. This section describes briefly the model membrane systems used in this work.

4.2.1. Microsomes

Microsomes are lipidic vesicles derived from the ER. Both the lipid and membrane protein components of the ER are contained in the microsomal membranes, and the lumen of the ER and the microsomal lumen are topologically equivalent spaces. As a consequence, microsomes are good models of natural membranes and have been extensively used to study the processes that take place in the ER.

The most important feature in our experiments is the fact that the microsomes contain the translocon complex and the machinery for post-translational modification normally found at the ER, thus providing glycosylation competent membranes to study the insertion of Lep chimeras (see 4.3).

4.2.2. Micelles and Liposomes

In an aqueous environment, amphipatic molecules tend to associate excluding their hydrophobic regions from the polar water molecules, whereas the polar groups are exposed to and interact with the solvent. Depending on their geometry, the association of amphipatic molecules leads to different structures.

Fatty acids, detergents and lysolipids, which have the shape of an inverted cone (see figure 1.4) tend to organise forming spherical structures, known as *micelles* (figure 4.1).

In contrast, most phospholipids are nearly cylindrically shaped molecules (see figure 1.4), and form spherical water-filled compartments enclosed by lipid bilayers, known as *liposomes* or *lipid vesicles* (figure 4.1). They constitute a very useful model system. They are easily prepared with a variety of compositions and sizes, which enable the control of membrane properties such as fluidity, temperature of phase transition, charge or intrinsic curvature. In addition, they can be prepared with the desired membrane proteins or fluorescent lipids, and a number of substrates can be encapsulated inside. This allows the study of several membrane processes, such as membrane permeabilisation, membrane fusion and transbilayer diffusion of lipids.

Depending on their size and the number of lamellae they contain, liposomes can be classified as follows:

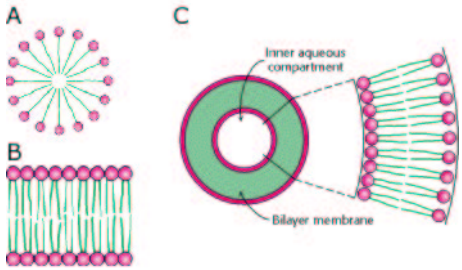

Figure 4.1.: Model systems of lipid membranes. The representation of the organisation of a micelle is depicted in A. In B and C, a planar lipid bilayer and a lipid vesicle, respectively, are schematically shown.

Multilamellar large vesicles (MLV), which have many lamellae and a heterogeneous size, that varies from 100 to 1000 nm. They are prepared by directly resuspending a dried film of lipids in an aqueous solvent.

Giant Unilamellar Vesicles (GUV), which contain a single lamella and can reach dimensions up to 300 μm. They can be prepared using a variety of methods, including electroformation and controlled hydration.

Large Unilamellar Vesicles (LUV), have also one lamella and dimensions varying from 100 to 600 nm. They are prepared from a suspension of MLVs followed by freezing and thawing cycles, and extrusion through a polycarbonate membrane with pores of controlled size.

Small Unilamellar Vesicles (SUV), which contain a single lamella and have a smaller size than LUVs, ranging from 30-50 nm. They are usually formed after sonication of a suspension of MLVs. The membranes of LUVs, GUVs and MLVs are considered to have a curvature similar to that of cells. The lipid distribution between the leaflets has been calculated to be almost symmetrical, with 50-55% of phospholipids in the outer, and 45-50% in the inner monolayers. SUVs, however, have a higher membrane curvature and an asymmetric distribution of lipids, with 60-70% of them in the external leaflet.

When liposomes are deposited on a flat surface, such as a germanium crystal, and gently dried with a N_2 flux, capillary forces flatten the membranes, which spontaneously organise into *oriented multibilayer systems.* As a result, several

thousands of aligned multibilayers, with a dispersion of a few degrees, are formed. This systems are useful to study the orientation of peptides and proteins in membranes by solid NMR or ATR-FTIR (see 4.5.2 on page 66) Goormaghtigh et al. (1999).

4.2.3. Planar membranes

Planar membranes are lipid bilayers with a diameter of approximately 100 nm, which are held at a small hole in a Teflon film, separating two bathing solutions of aqueous buffer. As with liposomes, planar membranes constitute highly controlled systems, and the lipid composition can be varied almost at will. If two electrodes are inserted at both sides of the membrane, the electrical conduction properties of the membranes, as well as proteins or peptides inserted in them, can be characterised (see 4.4.3).

Planar membranes can be prepared using the Black Lipid Membrane technique or the Montal-Müller technique, which generates solvent-free lipid bilayers Serra and Menestrina (2000). In the latter case, the lipids are dissolved in pentane and deposited on two water solutions at both sides of the Teflon film. After some minutes, the organic solvent is evaporated and the lipid molecules are organised in a monolayer on the buffer surface. When the level of one of the water solutions reaches the hole in the Teflon film, the lipid molecules cover it and form an oriented monolayer. Then, the level of the second bathing solution is slowly increased and the lipids on the surface interact with the preexisting monolayer to form a lipid bilayer (see figure 4.1).

4.3. Characterisation of the membrane insertion domains: Glycosylation mapping

N-glycosylation is a usual post-translational modification of eukaryotic membrane proteins which adds topological information. It is performed in the lumen of the ER of eukaryotic cells, by the oligosaccharyl transferase (OST), activity associated to the translocon machinery, and links oligosaccharide molecules to the amine group of asparagine in the consensus site Asn-X-Thr/Ser van Geest and Lolkema (2000).

The level of glycosylation of a protein can be evaluated *in vitro* in a cell-free system using a reticulocyte lysate, or white germ lysate, which provide the translation machinery, in the presence of ER microsomes, providing the membrane insertion and post-translational modification machinery. In a SDS-PAGE, the presence

of the oligosaccharide molecule produces a band shift equivalent to an increase in molecular mass of ~2.5 kDa with respect to the non-glycosylated protein. Control treatments like glycosydases, inhibitors of glycosylation or competitive acceptor peptides can be employed, allowing one to ensure that the glycosylated protein was indeed formed.

Several glycosylation strategies, collectively named as glycosylation mapping, have been used to study the topology and insertion properties of membrane proteins in the ER membrane. These include approaches like glycosylation scanning mutagenesis, glycosylation fusions or insertion vehicles with a glycosylation reporter van Geest and Lolkema (2000). Among the latter, systems based on the H^+/K^+-ATPase, prolactin and the *E. coli* inner membrane protein leader peptidase (Lep), have been most widely used.

The Lep system

Lep is involved in the processing of targeting sequences from proteins destined to be exported. It is inserted in the cytoplasmic membrane of *E. coli* through two N-terminal hydrophobic helices, H1 and H2, that are connected by a cytosolic loop called P1. The C-terminal domain, P2, is periplasmic and responsible of the catalytic activity. The insertion of Lep in microsomal membranes has been extensively studied. The H1 domain drives the insertion and orientation of the protein in the membrane. The N-terminus is located in the lumen, while the P1 loop, which is highly positively charged, remains in the cytosol, in good agreement with the *positive inside rule*. Insertion of the H2 fragment, leaves the P2 domain oriented to the lumen.

The Lep insertion vehicle contains an engineered glycosylation sequence in the P2 domain that is efficiently glycosylated upon correct insertion into the microsomal membrane. To test the insertion of individual hydrophobic segments, the H2 domain is replaced by the putative transmembrane segments under study. After an *in vitro* translation/insertion assay, the glycosylation state of the P2 domain is a reporter of the ability to insert of the fragment of interest (see figure 4.2). This system analyses the intrinsic ability of the assayed segments to insert into the microsomal membranes, since the targeting and topology into the membrane are determined by H1 and the P1 loop, respectively.

4.4. Activity studies

Bcl-2 proteins of different types, including pro and antiapoptotic members, display characteristic ion channel activities in vitro. It is thus of interest, to evaluate

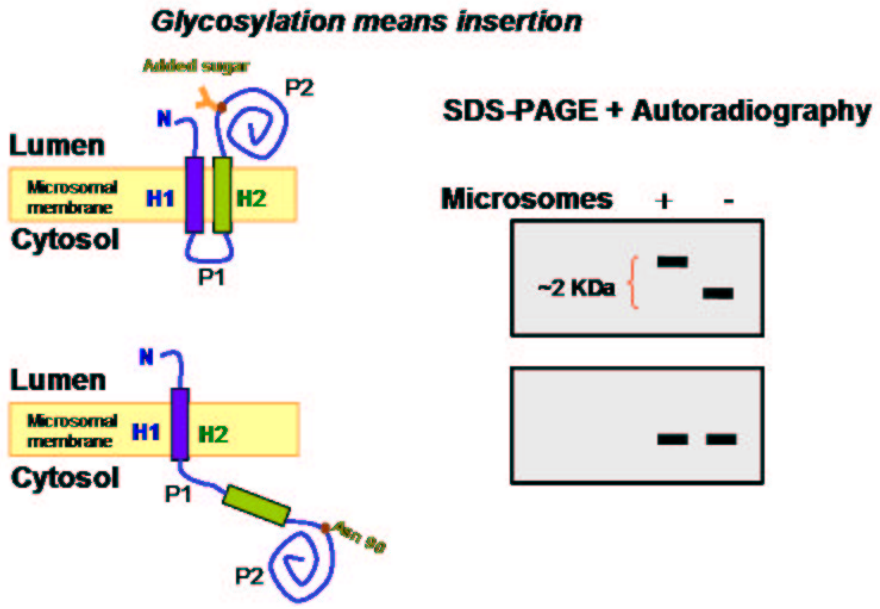

Figure 4.2.: Glycosylation mapping. Possible topologies and glycosylation patterns in a chimeric Lep system. A band delay is observed between glycosylated and non-glycosylated ^{32}S-Met labeled Lep chimera in a SDS-PAGE.

the ability of fragments from these proteins to permeabilise lipid membranes, as well as to characterise the possible mechanisms involved. With this aim, we have used assays of content release from LUVs and ion channel formation in PLM. Mechanistic studies were complemented by experiments of lipid transbilayer diffusion in LUVs.

4.4.1. Release of vesicular contents

The pore forming activity of a given molecule can be studied by analysing the release of encapsulated markers from lipidic vesicles as a consequence of the presence of this molecule. These experiments can be adapted to a 96-well-plate format, thus permitting the systematic analysis of the permeabilising activity of the molecules of interest at different conditions in parallel. The same molecule can then be studied simultaneously at different concentrations and in several lipidic compositions. The use of fluorescent markers of different sizes allows also the estimation of the pore diameter.

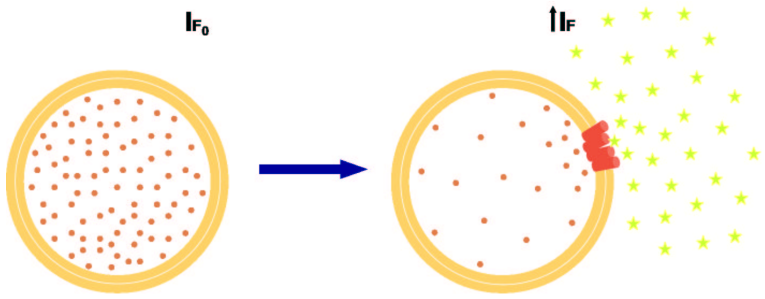

Figure 4.3.: Schematic representation of an experiment of content release.

As a fluorescent probe, we have used calcein (fluorescein-bis-methyliminodiacetic acid) or dextrans of different size marked with fluorescein isothiocyanate. If the probe is entrapped in lipid vesicles at a self-quenching concentration, its release in the external medium is accompanied by dilution and an increase of the intensity of fluorescence, as schematically shown in figure 4.3. From the time dependence of the increase of fluorescence, the kinetics of the release of the probe can be studied.

The percentage of release R is calculated from the expression:

$$R = \frac{F_{ss} - F_0}{F_{max} - F_0} 100 \tag{4.1}$$

where F_0 is the initial fluorescence of LUVs, F_{max} is the maximum fluorescence, obtained after the complete release of the probe by the addition of Triton X-100, and F_{ss} is the equilibrium fluorescence emitted in the presence of the molecule of interest. The permeabilising activity of a particular molecule can be characterised in terms of the concentration needed to induce 50% of content release, C_{50}, or more directly by the inverse of this quantity, $1/C_{50}$.

4.4.2. Lipid transbilayer diffusion

Under normal conditions, the diffusion of lipids across pure lipid bilayers is very slow. The alteration of the membrane structure through the formation of toroidal pores connects the two leaflets and allows the rapid redistribution of lipids between the monolayers through lateral diffusion. Thus, the ability of polypeptides to promote lipid transbilayer redistribution can be used as a test experiment to help discriminate between different models of pores.

We use a lipid transbilayer diffusion assay based on the change of the intrinsic properties of a fluorescent probe upon redistribution between the membrane monolayers Muller et al. (2000). This strategy allows the continuous monitoring of transbilayer distribution, which can be useful for rapid kinetics measurements, as in the case of Bax and membrane active peptides like melittin and magainin.

As a fluorescent probe, we used pyrene-PC (py-PC), a fluorescent analogue of PC. py-PC contains a long chain fatty acid, lauroyl, at the sn-1 position and a short chain fatty acid, butyroyl, carrying the fluorescent moiety pyrene at the sn-2 position. The presence of a short fatty acid chain improves the translocation of the analogue from the aqueous phase to the membrane, and the probe can be simply added externally to the suspension of lipid vesicles Muller et al. (2000).

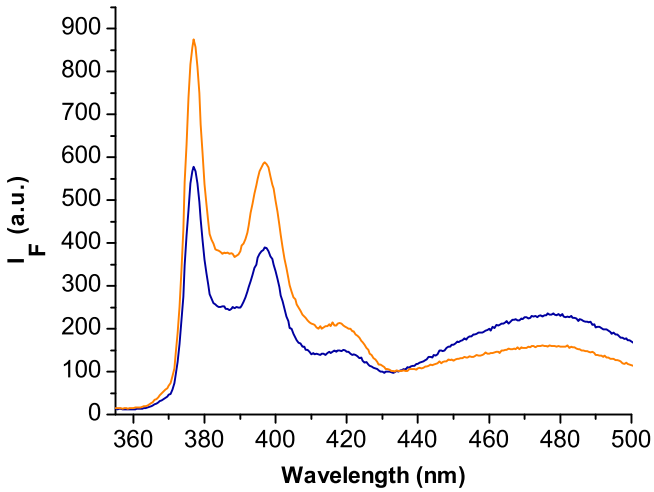

Figure 4.4.: Fluorescence spectra of pyPC. The peak at 395 nm is due to the emission of the monomer form of pyPC, while the emission band around 470 nm is originated by the excimer. The spectrum of asymmetric vesicles with the probe in the external leaflet is shown in blue. After transbilayer diffusion, the probe redistributes also to the inner leaflet and gives rise to the spectrum in orange. The excitation wavelength was set at 345 nm, with band slits of 4 nm.

Detection is based on the dilution of the probe initially bound to the outer leaflet as a consequence of its redistribution in the inner leaflet by lateral diffusion in the wall of the pore, which causes a change of the fluorescence spectrum. The

spectrum of py-PC presents two maxima of emission characteristic of the excited monomer and the excited dimer (excimer) molecules, as shown in figure 4.4. The concentration of excimer in the membrane depends on the collision frequency between pyrene-labeled homologues, which is determined by their concentration and their lateral diffusion. As depicted in figure 4.5, once incorporated to the outer leaflet, redistribution of py-PC to the inner leaflet provokes a change in the concentration of the analogue in both monolayers and then, a change in the concentration of excimers and monomers, which alters the intensity ratio between the excimer and the monomer maxima (I_E/I_M). Thus, the transbilayer diffusion of py-PC in LUVs can be measured by monitoring the time dependent decrease of I_E/I_M Muller et al. (2000).

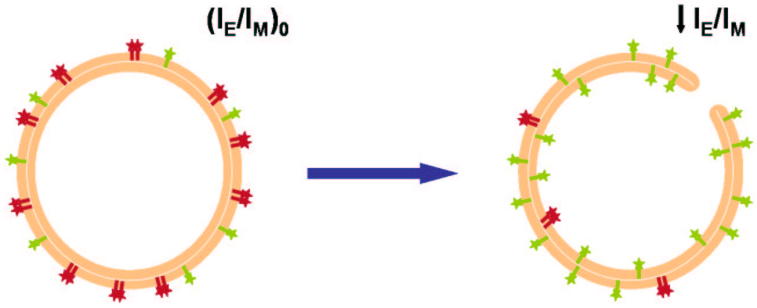

Figure 4.5.: Schematic representation of lipid transbilayer diffusion assay. The relative ratio between the emission of the monomer and excimer varies upon py-PC redistribution to the inner leaflet. The emission of monomer molecules is depicted in green, and that of excimers is shown in red.

4.4.3. Electrophysiology studies in Planar Lipid Bilayers

The measurement of ionic fluxes across a membrane is of special interest for the study of pore forming proteins. Several properties, such as the size of the pore, its ionic selectivity (preference for cations or anions), the voltage dependence of ion current, or the permeability to different ions based on their size, can be studied at the molecular level.

The use of Planar Lipid Membranes (PLMs) for such studies offers many advantages Serra and Menestrina (2000). PLMs are small fragments of lipid bilayers, usually made of pure lipids, and held on a hole in a Teflon septum between two aqueous solutions. This constitutes a simple model membrane system

to study channel formation by single molecules. Physicochemical parameters, like temperature and chemical composition, both of the membrane and the water phases, can be easily controlled. The detection of single-channel events is possible due to the current resolution, and the transmembrane voltage is fully controllable. However, it is necessary that the channel self-incorporates into the lipid bilayer from the bathing solution, and the efficiency of this process is normally low. Special care must be taken of the presence of small impurities, which may alter the permeability properties of the PLM.

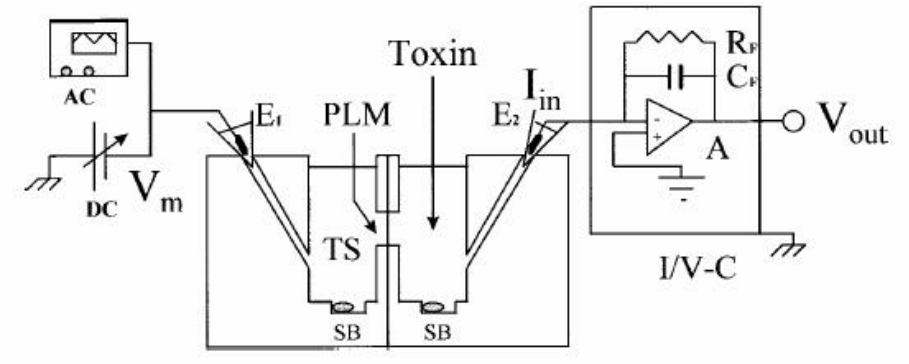

Figure 4.6.: Schematic representation of the setup used in the experiments with PLMs. The added pore-forming protein or peptide is written as Toxin. The various elements are not drawn to scale.

The setup used for the experiments described in this work is shown schematically in figure 4.6. The planar bilayer is prepared by apposing two lipid monolayers onto a small hole of 0.1-0.2 mm made on a Teflon septum (TS), using the Montal-Müller technique (see also 4.2.3 on page 54). This system separates two cells containing two aqueous solutions and two Ag-AgCl electrodes ($E_1$and E_2), which are immersed in agarose bridges. Using a DC battery supply, which generates a steady voltage, or a waveform generator (AC), which generates a periodic signal, the voltage (V_m) is applied to the membrane through one of the electrodes. The current that passes through the membrane (I_m) is driven by the other electrode to the current/voltage converter ($I/V - C$). The output voltage (V_{out}) is then driven to an oscilloscope, a chart recorder and a digital recorder, were the data are saved. In such a system, the pore forming protein is added to the *cis* (by convention) cell and stirred with magnetic spin-bars (SB).

In this system, the planar bilayer acts as an isolator and the conductivity is

very low, G $< 10\ pS$. If the added protein is able to insert into the membrane and form a pore, ions can pass through it and a higher conductivity state is reached. Each channel formation is observed as a stepwise increase on the membrane current. Usually one or a few typical amplitudes can be estimated. The pore conductance G is calculated by dividing the current value by the applied voltage. Varying the experimental conditions allows the study of several pore properties, such as the effect of the lipid composition, the presence of water or fixed charges on the lumen of the pore, the size and the geometry of the channel, or the influence of the voltage (gating) Serra and Menestrina (2000).

The selectivity of the pore can be estimated using different salt gradients between the two cells in the chamber. If a gradient of a monovalent salt is generated and a current can be measured in the absence of an applied voltage, there is ionic selectivity. In turn, this informs about the type of charges that are exposed to the lumen of the pore. Under these circumstances, the value of the applied voltage that makes the current zero is called the reversal voltage, V_{rev}. The Goldman-Hodgkin-Katz equation relates the V_{rev} to the ionic selectivity of the pore Serra and Menestrina (2000) as:

$$V_{rev} = \frac{RT}{zF} \ln \frac{P_+ C_+^{I\,I} + P_- C_-^{I}}{P_+ C_+^{I} + P_- C_-^{I\,I}} \tag{4.2}$$

or

$$\frac{P_+}{P_-} = \frac{C^{I\,I}/C^{I}\, e^{\frac{zFV_{rev}}{RT}} - 1}{C^{I\,I}/C^{I} - e^{\frac{zFV_{rev}}{RT}}} \tag{4.3}$$

where R is the gas constant, T is the absolute temperature, F is the Faraday constant, z the valence (at 23°C, RT/zF equals $25mV$), C^{I} and $C^{I\,I}$ are the salt concentrations on the *cis* and *trans* sides, and P_+ and P_- are the permeability of the cation and anion, respectively. A P_+/P_- ratio higher than 1 indicates that the channel is cation selective.

PLMs are stable enough to perform multichannel experiments, that is, to study the membrane permeability in the presence of several thousand pores. In this case, the information obtained is similar to that of single channel experiments, but averaging the many individual contributions. Properties like ion selectivity, molecularity, conductance and life time can be estimated.

4.5. Structural studies

Among the several techniques that provide structural information of peptides, undoubtedly x-ray crystallography and NMR spectroscopy are the most powerful,

as they can generate a high resolution model of the peptide or protein structure. However, in the case of membrane proteins, the above techniques can encounter serious difficulties that prevent obtaining high-resolution structures. Electron crystallography and cryo-electron microscopy are other low-resolution alternatives. Additionally, other techniques such as circular dichroism (CD) and Fourier Transform Infrared (FTIR) spectroscopy, are becoming increasingly useful tools for structural studies of peptides and proteins in lipidic environments. Despite their lower resolution, these techniques provide valuable data of secondary structure. Additionally, they can yield relatively accurate orientation constraints that allow positioning secondary structure elements with respect to the reference plane of the membrane.

4.5.1. Circular Dichroism

Circular dichroism (CD) results from the interaction between asymmetrical molecules and plane polarised light. Asymmetric molecules are those which lack a center, a plane or an n fold axis of symmetry, or those whose arrangement in space is asymmetric. Plane polarised light can be parallel or perpendicular. In a plane, it can be visualised as an oscillating sine wave, which is the sum of two vectors of circularly polarised light, one going rightwards and the other leftwards (figure 4.7).

Asymmetric molecules are optically active, i.e., they absorb right-handed and left-handed circularly polarised light to different extents. As a result, the two forms of light have a different refractive index, and the plane of polarisation of light rotates. This effect is dependent on the wavelength, and is known as optical rotatory dispersion (ORD). The combination of CD and ORD in the region of absorbance gives right to a transmitted light which is elliptically polarised, as schematically shown in figure 4.8. The CD spectrum shows the difference in left and right-handed absorbance as a function of the wavelength. The intensity of the CD bands is called ellipticity, Θ, units given in millidegrees, which is usually converted to molar ellipticity, $[\Theta] = \Theta/(10 \cdot c \cdot l)$, where c is the concentration of the chromophor and l is the path length. In the case of peptides and proteins, the mean residue molar ellipticity is frequently given, where c refers to the concentration of peptide bonds.

Theoretical background

The absorption of light in a CD experiment generates a movement of charges in the molecule, which is associated to an electronic and a magnetic transition,

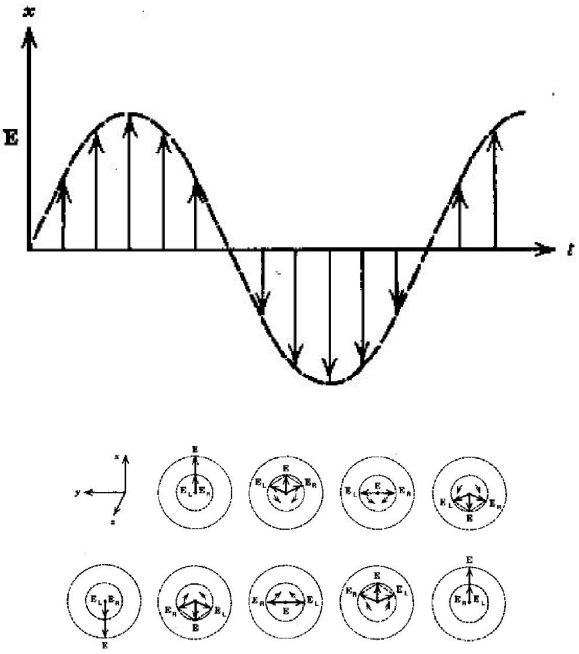

Figure 4.7.: Plane polarised light. *Top*, Electric component (E) as a function of time in a linearly polarised light. *Bottom*, Schematic representation of the separation of light into left and right circularly polarised light. The sum of the vectors traces the sine wave shown on top (from Moscowitz (1960)).

that are perpendicular to each other. The energy of the transition depends on the electric and magnetic dipole moments induced by the action of light on the electrons of the molecule. The rotational strength of a transition, R_K, is the imaginary part of the dot product of the electric and magnetic induced dipoles (the product of the two vectors and the cosine of the angle between them). In symmetric molecules, the sum of all the magnetic and electric induced dipoles is zero, or the angle between them is 90^o, then annulling R_K and optical activity.

However, there are many cases in which the product R_K is not zero. The $n \rightarrow \pi*$ transition is electrically forbidden but magnetically allowed, so they are no longer perpendicular to each other. In an asymmetric molecule, such a transition gives rise to little total absorption of light, but high optical activity, and is present in the case of helical polypeptides and proteins. Most of the optical activity in helices is the result of the interaction of groups with simple electric

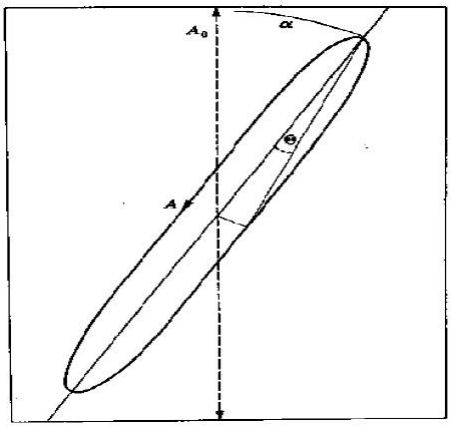

Figure 4.8.: A schematic representation of circular dichroism, Θ, and optical rotation, α, of polarized light. The dashed line A_o represents the planepolarised monochromatic ray striking the sample. The transmitted ray A is elliptically polarized. (From Tinoco and Cantor (1970))

transitions, which interact to generate a magnetic moment. Another possibility is the coupling between a magnetic and an electric transition arising from different chromophores within the same molecule Cantor and Shimmel (1980).

CD spectroscopy has many biological applications. It is used to determine the conformation of proteins and nucleic acids, the conformational changes produced by the interaction of asymmetric molecules, the thermodynamics and kinetics of folding and unfolding of proteins and nucleic acids, and the estimation of binding constants.

The chromophore responsible of light absorption in CD of peptides is the amide bond. According to the simplified theory of molecular orbitals, the $2p_x$ atomic orbitals of N, C and O in the amide bonding are combined to form three molecular orbitals of π symmetry, π^+, π^o and π^-, which are bonding, non-bonding and antibonding, respectively. The four π electrons of the HOMO (highest occupied molecular orbital) distribute in the π^+ and π^o orbitals, and the remaining two electrons are in the nonbonding $2p_y$ atomic orbitals of the O atom. The transitions observed in CD spectra are: i) the $n \rightarrow \pi*$ transition, which promotes one electron to the π^- orbital, and is electrically forbidden, but magnetically permitted, thus giving rise to large bands; ii) the $\pi \rightarrow \pi*$ transition, which promotes one electron from the nonbonding to the antibonding orbital, and has a high extinction coefficient Adler et al. (1973).

These transitions are affected by the solvent and the environment. As a consequence, the spectra of peptides observed depend on their conformation. In biopolymers, the chromophores are in ordered arrays and the electrons interact during the excitation process. This results in an exchange of excitation, and affects the energy of the transition.

The interaction between the transitions originates two new transitions, one of higher and one of lower energy with respect to the transitions of two isolated non-interacting chromophores. The interactions of the N chromophores in a polypeptide would give rise to N splitted transitions, however, most of them are equivalent due to the symmetry of the ordered structures in peptides. As a consequence, determination of the symmetry elements in the permitted polypeptide conformations and then, of their space groups, allows the prediction of whether a transition will be allowed and what the polarisation of a transition will be Greenfield and Fasman (1969).

The CD spectrum of a random peptide is similar to that of a simple amide, but with more intense bands. It has a large negative band of a $\pi \rightarrow \pi*$ transition at 195 nm, and a small positive $n \rightarrow \pi*$ at approximately 230 nm. An α-helix originates a spectrum with a large negative $n \rightarrow \pi*$ transition at 222 nm, and a $\pi \rightarrow \pi*$ transition which splits into two due to transition coupling. This generates two intense bands, one negative at approximately 208 nm, and one positive at 192 nm. The $\pi \rightarrow \pi*$ transition in an β-sheet is also splitted into a negative band at 218 nm and a positive band at 195 nm Adler et al. (1973).

Estimation of secondary structures from CD spectra

Initially, to estimate the secondary structure of peptides and proteins from CD spectra, the x-ray structure of many proteins were compared to their CD spectra and the method of least squares was used to determine the components of the different conformations. Then, these values were used to calculate the structure of unknown proteins Saxena and Wetlaufer (1971).

The methods used currently include the deconvolution of the spectra to the basis curves corresponding to α-helix, β-sheet and turn. However, the set of reference protein CD spectra used for the deconvolution considerably affect the basis curves obtained. This is due to the unusual spectra that some proteins display, as a result of aromatic amino acids, disulfide bridges and rare conformations. To solve these problems, some methods select reference sets of proteins which are spectrally similar to the proteins to be evaluated.

The methods to analyse CD spectra interpret the spectrum of a protein as a linear combination of the spectra of its constituting secondary structural elements,

and a noise contribution which considers the effect of aromatic chromophores:

$$\Theta_\lambda = \Sigma \varepsilon_i S_1 + noise \tag{4.4}$$

where Θ_λ is the CD of the protein as a function of the wavelength, ε_i is the fraction of each element of secondary structure, and S_1 is the ellipticity at each wavelength of each element of secondary structureGreenfield (2004).

To analyse the CD spectra, we have used the CDPro pack, which contains the CDSSTR, SELCON3 and CONTIN/LL programs Sreerama and Woody (2000, 2004). The final solution of each program is the average of the solutions that satisfy four selection rules: i) the sum of fractions of components of secondary structure is between 0.95 and 1.05; ii) each fraction is larger than -0.03; iii) the RMS deviation between the constructed and the measured CD spectra is smaller than 0.25 $\Delta\epsilon$; iv) the helical content, determined from the helix fraction in the full reference data set, must coincide with the helix fraction of the accepted solutions.

The CDSSTR program needs a minimum number of reference proteins to perform a good analysis. These are randomly selected from the data set and give rise to a large number of combinations. This method is very flexible and the solutions are obtained using the self-consistent formalism with the singular value decomposition (SVD) algorithm. The SELCON3 is the latest version of a self consistent method, where the CD spectrum of the protein is included in a matrix of CD data initially assuming the structure of the reference protein with the most similar CD spectrum. The solution obtained replaces the initial estimation and the process is iterated until convergence is reached. The matrix equation is solved by the SVD algorithm and variable selection in the locally linearised model. The CONTIN/LL program is a modification of the CONTIN method and uses the rigde regression procedure, which fits the CD spectrum of the studied protein to a linear combination of the CD spectra of a set of proteins. The proteins in the data set are organised in order of increasing RMS distance in the CD spectra, and those that differ most are systematically deleted to construct smaller sets of proteins.

4.5.2. ATR-FTIR

The energy involved in the vibrational transitions of matter corresponds to the energy of the infrared light in the spectrum of electromagnetic radiation. The diverse vibration modes, such us stretching, bending or scissoring, have different energies, which depend also on the nature of the chemical bonds, and give rise to the absorption bands in the infrared (IR) spectrum. A net dipolar moment must exist in the molecule for absorption to occur.

Table 4.1.: Amide bands of polypeptides. (From Tamm and Tatulian (1997))

Band of amide absorption	Wavenumber range (cm^{-1})
Amide A	~3300
Amide B	~3100
Amide I	1600-1700
Amide II	1510-1580
Amide III	1200-1400
Amide V	610-710

Despite the complexity of IR spectra, the absorption bands of some functional groups in proteins and lipids can be assigned. The vibrational transitions of amide bonds in the protein backbone give rise to different absorption bands (see table 4.1) and the amide I band, which occurs between 1600-1700 cm^{-1}, is the most widely used to analyse protein and peptide conformations. Both theoretical calculations and experimental studies, have established correlations between standard secondary structures of peptides and amide I frequency ranges, as shown in table 4.2 Tamm and Tatulian (1997). There are, however, proteins and peptides which show a different behavior, like alamethicin Haris and Chapman (1988) or bacteriorhodopsin Rothschild and Clark (1979).

Table 4.2.: Correlations between standard elements of secondary structure and the wavenumber of the absorption band in the amide I region.(From Tamm and Tatulian (1997))

Secondary structure	Amide I wavenumber (cm^{-1})
Aggregated strands	1610-1628
β-sheet	1625-1640
Unordered	1652-1660 (deuterated: 1640-1648)
α-helix	1648-1660
3_{10}-helix	1660-1670
Turns	1660-1685
Antiparallel β-sheet/ aggregated strands	1675-1695

Lipids show many absorption bands in the IR spectrum. The $C = O$ stretching

absorbs near the amide I region at 1730 cm^{-1}, while the stretching of CH_2 and CH_3 groups gives rise to strong bands above 2850 cm^{-1}. It is important to note that the NH_3^+-stretching of PE and PS, and the antisymmetric carboxylate stretching of PS overlap with the amide I region. Similarly, the CH_2 scissoring and wagging bands overlap with the amide II and amide III regions respectivelyTamm and Tatulian (1997).

The IR spectra of biomolecules are usually complex, with overlapping broad bands. It is then of interest, to identify the component bands of the spectrum in order to extract the structural information Goormaghtigh et al. (1991). The first step consists in carefully subtracting the peaks due to residual water vapor. Absorptions of buffer, lipids or other molecules present in the sample and different from the molecule of interest may also be subtracted. Eliminating of noise, zapping and/or smoothing of the spectra can also be performed. Next, the spectrum is Fourier deconvoluted in a set of narrower bands. After component analysis, the original corrected spectrum is curve-fitted with the component bands using Lorentzian or Gaussian curves at the identified band positions. When this processing is applied to the amide I band, the percentages of secondary structure elements that are present in the sample and that contribute to the observed band, can be calculated.

FTIR has several advantages that make it an interesting technique to study the structure of peptides:

- Spectra can be obtained in a wide range of conditions, thus allowing the analysis of conformational changes of peptides as a function of the environment.
- Membrane peptides can be studied in their native environment, as the presence of lipid bilayers does not decrease the spectroscopic resolution or sensitivity.
- There is no need of external probes.
- Being the time scale in the order of $10^{-12}s$, and then anisotropic motions do not complicate data interpretation.
- Both data measurement and analysis are rather fast.

Attenuated Total Reflection geometry

Attenuated Total Reflection Fourier Transform Infrared spectroscopy (ATR-FTIR) is one of the most powerful methods for collecting infrared spectra of biological

membranes. It allows the characterisation of the orientation of molecules related to the membranes, and it is very sensitive, yet micrograms of sample give a strong signal. Moreover, environmental conditions, such as pH, pressure, temperature, solvent or the presence of ligands, can be varied *in situ*. Another advantage respect to transmission infrared spectroscopy is that absorption of water and other molecules in the bulk solution is highly reduced.

The most usual set-up in ATR-FTIR consists in a trapezoidal plate through which the infrared beam is directed. This plate, known as Internal Reflection Element (IRE) is transparent to the IR radiation of interest and has a high refractive index. Above a critical angle, which depends on the refractive indexes of the IRE and the external medium, n_1 and n_2, the radiation is completely reflected at the surface of the IRE, as shown in figure 4.9, and several total internal reflections occur inside the IRE before the beam exits the plate Goormaghtigh et al. (1991).

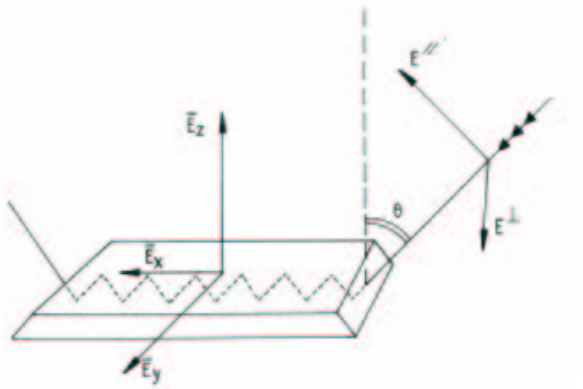

Figure 4.9.: Schematic representation of the internal reflection element (IRE) and the light pathway. As the edges are inclined, the light enters the perpendicular to the crystal, but with an angle θ with respect to the normal of the IRE surface. Two possible planes of polarisation of the incident beam are shown by E$\perp$ (polarisation perpendicular to the incident plane) and by E$\parallel$ (polarisation parallel to the incident plane). The cartesian components of the electric field, $\vec{E_x}$, $\vec{E_y}$ and $\vec{E_z}$ are also shown. (From Goormaghtigh et al. (1991))

The superimposition of the incoming and reflected waves generates a standing wave (see figure 4.10) inside the IRE and perpendicular to its surface, according to the Maxwell's equations, and that can be described by

$$E = 2\cos(\frac{2\pi z}{\lambda_e} + \phi) \tag{4.5}$$

where z is the coordinate perpendicular to the IRE surface, $\phi$is a phase shift, and $\lambda_e = \lambda_1/\cos\theta$, being λ_1 the wavelength within the IRE, $\lambda_1 = \lambda/n_1$ and θ the incidence angle of the beam. As a result, an electromagnetic perturbation is generated in the rarer medium beyond the reflecting interface, which is called the evanescent wave (see figure 4.10), and that decays exponentially with the distance to the interface, as described in

$$E = E_0 \cdot e^{-z/d_p} \tag{4.6}$$

where E_0 is the time averaged electric field intensity at the interface in the rarer medium, and E is the time averaged intensity of the electric field at a distance z from the interface. d_p is the penetration depth of the electric field,

$$d_p = \frac{\lambda_1}{2\pi(\sin^2\theta - n_{21}^2)^{1/2}} \tag{4.7}$$

where $n_{21} = n_2/n_1$. Thus, the penetration depth depends on λ and θ, and a typical decay of the evanescent field intensity is in the μm range for total reflection. As it is shown schematically in figure 4.10, a displacement of the totally reflected beam is produced. Thanks to the presence of the evanescent wave, the interaction between the infrared radiation and the sample, which is deposited on the surface of the IRE, takes place within the penetration depth, so that the light is absorbed and gives rise to the infrared spectrum Goormaghtigh et al. (1991).

Determining molecular orientations by ATR-FTIR

The analysis of the orientation of lipids and the different secondary structures of peptides in the sample by ATR-FTIR is based on the fact that the IR absorption is maximal if the dipole transition moment is parallel to the electric field component of the incident radiation. All the molecules, and then their dipole moments, in an ordered membrane deposited on the IRE have the same orientation with respect to the normal of the IRE surface. As a result, it is possible to obtain information on the orientation of the dipoles if the intensity of the absorption bands is measured at different orientations of the incident light electric field, using a polariser Goormaghtigh et al. (1991).

The parameter used for optical orientation measurements, the dichroic ratio R, is defined as:

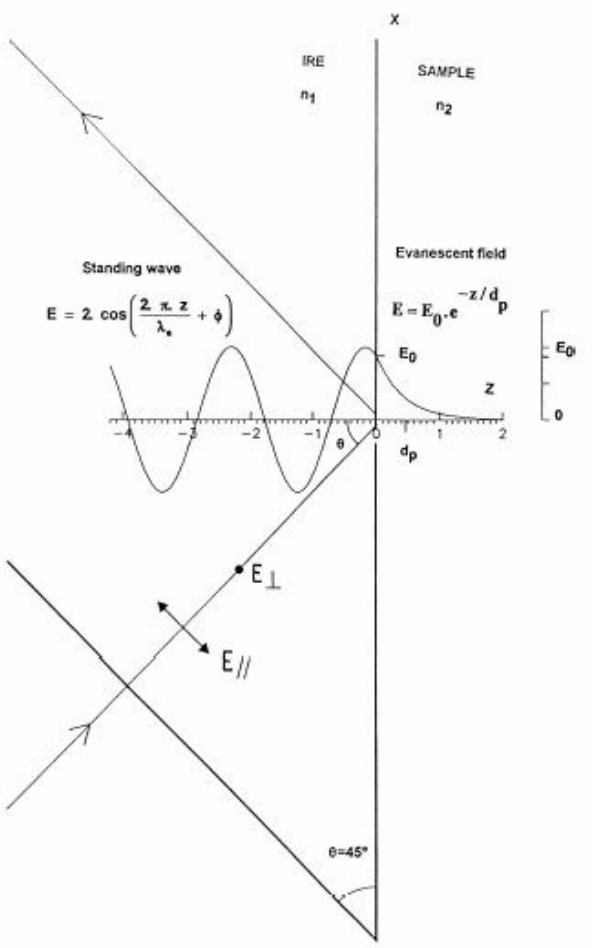

Figure 4.10.: Side view of the IRE in figure 4.9. The propagation of the electric field of the electromagnetic radiation at one point of reflection and the parallel and perpendicular planes of polarisation are indicated. The generated evanescent wave decays exponentially outside the IRE, while a standing wave exist inside the IRE. (From Goormaghtigh et al. (1991)).

$$R = \frac{A_{\parallel}}{A_{\perp}} \tag{4.8}$$

where $A_{\parallel}$ and $A_{\perp}$ are the integrated absorbances of a band measured with parallel and perpendicular, respectively, polarisations of the incident radiation. Due to the fluctuations of the orientations of the molecules in lipid bilayers, a distribution of molecular orientations contribute to R. A uniaxial symmetry with respect to the IRE normal is assumed for the orientational distribution around this normal. However, the distribution of the orientations with respect to the normal around the mean value and other sources of disordering must be considered. The dichroic ratio R is related to an orientational order parameter S, by:

$$R = \frac{E_x^2}{E_y^2} + \frac{E_z^2}{E_y^2}(1 + \frac{3S}{1-S}) \tag{4.9}$$

where E_x^2, E_y^2 and E_z^2 are the time averaged square electric field amplitudes of the evanescent wave in the film at the IRE/film interface.

In the case of an α-helix, which has uniaxial symmetry, the measured order parameter $S_{experimental}$, obtained from R through 4.8, can be expressed as a set of uniaxial symmetric distributions

$$S_{experimental} = S_{membrane} \cdot S_{helix} \cdot S_{dipole} \tag{4.10}$$

as schematically shown in figure 4.11. Where $S_{membrane}$ is the distribution of orientations of the lipid bilayers to the IRE normal, S_{helix} is the orientation of the helices with respect to the membrane, and S_{dipole} is the dipole orientation of amide I or II with respect to the helix axis. If S_{dipole}, which is characteristic of the secondary structure, and $S_{membrane}$, which can be measured, are known, we can calculate S_{helix}, and then the angle of the helix axis with respect to the membrane normal β, using the expression:

$$\beta = \arccos \frac{2S_{helix} + 1}{3} \tag{4.11}$$

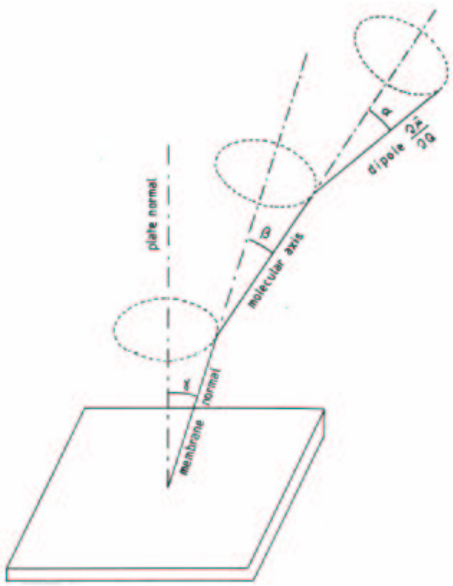

Figure 4.11.: Set of nested axially symmetric distributions. The membrane normal is distributed with an angle γ with respect to the IRE normal, the molecular axis is distributed with an angle β to the membrane normal, and the transition dipole moment of the molecule is distributed with respect to the molecular axis with an angle α.(From Goormaghtigh et al. (1991)).

Part II.

Materials and Methods

5. Materials and methods

5.1. *Escherichia coli* strains

The *E. coli* strains used in this study and some of their properties are described next:

DH5α DNA amplification

XL1Blue DNA amplification; used in transformations with the site-directed mutagenesis QuickChange kit

JM110 DNA amplification; contains the dam$^-$ mutation and is used to produce non-methylated plasmidic DNA (needed to digest with BclI restriction enzyme)

5.2. Growing and transformation conditions

The *E. coli* cells were grown at 37°C in liquid LB medium (1% w/v triptone (Pronadisa, Madrid, Spain), 0.5% w/v yeast extract (Pronadisa), 1% w/v NaCl) or solid (liquid medium with 1.5% bacteriologic agar (Pronadisa). All media were sterilised in an autoclave for 20 min at 121°C. 100 μg/mL ampicillin (Roche Molecular Biochemicals, Mannheim, Germany) was added to LB media when used with transformed cells.

Competent DH5α and JM110 cells were prepared using the one-step method-Chung et al. (1989). A fresh overnight culture of bacteria was diluted 1:100 in LB and incubated at 37°C until cells reached an O.D. of 0.3-0.4. Cells were pelleted, resuspended in a volume of ice-cold 1x TSS (10% w/v sterilised polyethylene glycol (PEG), 50 mM MgCl2, and 5% v/v DMSO in LB at pH 6.5) and gently mixed on ice. 200μL aliquots were stored at -80°C. Transformations of DH5α with plasmidic DNA (approximately 50 ng) were done according to Hanahan's protocol, consisting on a thermal shock at 42°C for 1.5 min Hanahan (1983). Supercompetent XL1Blue strains were purchased from Stratagene and transformed according to the manufacturers protocol.

5.3. Isolation and analysis of DNA

A commercial kit of DNA extraction (Qiagen, Hilden, Germany) was used for small scale isolations of *E. coli* plasmids.

Polymerase chain reactions (PCR) were performed in a thermocycler device (Eppendorf Mastercycler Personal, Upsala, Sweden). The Taq polymerase employed was from Bioline (London, UK). Oligonucleotides were from Isogen (Mannheim, Germany). PCR reactions were carried out in a final volume of 50 μL, containing 0.1-1 ng of DNA template, 2 μM of primer oligonucleotides (Isogen Bioscience, Maarsen, The Netherlands), 0.5 mM dNTPs, 1x commercial PCR buffer, 3 mM MgCl2, and 5 units of Taq polymerase. After a initial denaturing step of 30 s at 95°C, 30 amplification cycles (30 s at 94°C, 30 s at 55°C, 30 s at 72°C) and a final extension step of 10 min at 72°C were performed. Amplified DNA was purified and digested with the corresponding restriction enzymes.

Site-directed mutagenesis reactions contained 5-50 ng of DNA template, 125 ng of each primer, 25 mM of the dNTPs mixture and 1 unit of Pfu Turbo DNA Polymerase (Stratagene, La Jolla, CA). They were made according to the manufacturer's protocols of the Quick Change kit (Stratagene), which consisted on 15-18 amplification cycles (1 min at 95°C, 1 min at 50°C, 2 min per kb of plasmid at 68°C). Amplified DNA was digested with DpnI at 37°C for 1 hour and used in transformation of supercompetent *E. coli* bacteria, strain XL1Blue, according to the kit's handbook.

The oligonucleotides used in PCR and mutagenesis reactions are collected in table 5.1.

Digestions of amplified inserts for Lep chimeras were done with BclI and NdeI (both from Roche, Basel, Switzerland) in appropriate buffers and temperatures. All constructs were sequenced at the Servei de Seqüenciació of the Univeristat de Valencia.

Analytical and preparative electrophoresis were carried out in agarose gels 0.8-1.8 % (w/v), prepared with TAE 1x buffer (40 nM Tris, 20 mM EDTA, 1.14 mL/L glacial acetic acid) with 10 μg/mL of ethidium bromide. As a sample buffer, a mixture of 50% glycerol, 0.05% bromophenol blue and 100 mM EDTA was used. Fragments of DNA were cut and purified with a DNA extraction kit from agarose bands (Qiagen).

5.4. Vector and construction schemes

The vectors used in this study were derivatives of pGem-1Lep (kindly provided by Prof. von Heijne, University of Stockholm, Sweden) described by Nilsson et

Table 5.1.: Oligonucleotides used.

Chimera	Name	Sequence
LEP/Bcl-xL-α1	BclxL1	5'-CTTCTGTTGATCAAAATGTCTCAGAGCAACCGGGAGCTG-3'
	NdexL28	5'-CGTGGATTCATATGGACTAAACTGACTCCAGCTGTATCC-3'
LEP/Bcl-xL-α5	BclxL135	5'-CTTGACTTGATCAAAGTAAACTGGGGTCGCATT-3'
	NdexL157	5'-CGTGGATTCATATGGCTTGTCTACGCTTTCCACGC-3'
LEP/Bcl-xL-α5α6	BclxL157	5'-CTTGACTTGATCAAGGAGATGCAGGTATTGGTG-3'
	NdexL185	5'-CGTGGATTCATATGGGTTCTCCTGGATCCAAGG-3'
LEP/Bcl-xL-α5α6	BclxL135	see above
	NdexL185	see above
LEPΔH1/Bcl-xL-α5α6	BclxL135	see above
	NdexL185	see above
LEP/Bcl-xL-Ct	BclxL209	5'-CTTGACTTGATCAAATTCAACCGCTGGTTCCTGACGGGC-3'
	NdexL233	5'-CGTGGATTCATATGGTTTCCGACTGAAGAGTGAGCCCAG-3'
LEP/Bcl-xL-α5α6[EEE]	XL166EEE	5'-GCAGGTATTGGTGAGTCGGGAGGAAGAGTGGATGGCCACTTACC-3'
	XL166EEEr	5'-CAGGTAAGTGGCCATCCACTCTTCCTCCCGACTCACCAATCAC-3'
LEP/Bcl-xL-α5C79W	XLC79W	5'-CCTTCGGCGGGGCACTGTGGGTGGAAAGCGTAGAC-3'
	XLC79Wr	5'-GGCTTGTCTACGCTTTCCACCCACAGTGCCCCGCCG-3'
LEP/Bcl-xL-α5α6C79W[EEE]	XLC79W	see above
	XLC79Wr	see above

Table 5.2.: Oligonucleotides used (continued)

LEP/Bax-α1	BclBax14	5'-CTTGACTTGATCAAAACCAGCTCTGAACAGATCATGAAG-3'
	NdeBax40	5'-CGTGGATTCATATGGCCCAGCCATCCTCCCTGCTCGATC-3'
LEP/Bax-α5	BclBax110	5'-CTTGACTTGATCAAAGTGGTTGCCCTCTTCTACTTTGCT-3'
	NdeBax133	5'-CGTGGATTCATATGGGATCAGCTCGGGCACTTTAGTGCA-3'
LEP/Bax-α6	BclBax131	5'-CTTGACTTGATCAAAGAGCTGATCAGAACCATCATGGGC-3'
	NdeBax154	5'-CGTGGATTCATATGGGTCTTGGATCCAGACAAGCAGCCG-3'
LEP/Bax-α5α6	BclBax110	see above
	NdeBax154	see above
LEPΔH1/Bax-α5α6	BclBax110	see above
	NdeBax154	see above
LEP/Bax-C-t	BclBax160	5'-CTTGACTTGATCAAAGGGACCCCCACATGGCAGACAGAT-3'
	NdeBax188	5'-CGTGGATTCATATGCCCAGATGGTGAGCGAGGCGGTGAG-3'
LEP/Bid-N-t	BclBid12	5'-CTTGACTTGATCAAAAGGGATGAGTGCATCACAAACCTA-3'
	NdeBid33	5'-CGTGGATTCATATGGGAAGCTGTTGTCAGAACAGCTTTG-3'
LEP/Bid-α4	BclBid98	5'-CTTGACTTGATCAAAGACGCTAGCATCCCTCCGGGCCTG-3'
	NdeBid122	5'-CGTGGATTCATATGGGTCCTCCTCCGACCGGCTGGTGTT-3'
LEP/Bid-α6	BclBid144	5-'CTTGACTTGATCAAAAAGGAGAAGACCATGCTGGTGCTG-3'
	NdeBid165	5-'CGTGGATTCATATGGGGACGGCGTGTGACTGGCCACCTT-3'
LEP/Bid-α6α7	BclBid144	see above
	NdeBid183	5'-CGTGGATTCATATGGGCGTAGGTTCTGGTTAATAAAATTCAC-3'

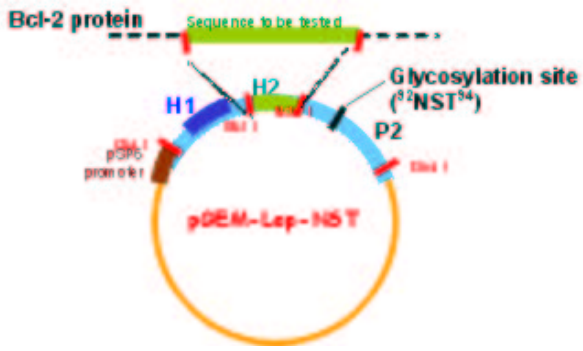

Figure 5.1.: Scheme of the vector used in the construct of Lep chimeras.
The SP6 promoter, the restriction sites introduced, the Lep domains and the glycosylation sequence are indicated.

al. Nilsson et al. (1994). In this construct, the Lep gene has been engineered: the natural glycosylation site of Lep 214N-E-T216 has been mutated to 214Q-Q-T216 and a new glycosylation site has been introduced in position 90N-S-T92 to produce the vector pGEM-Lep-NST. Moreover, restriction sites for BclI and NdeI have been introduced before and after the transmembrane H2 fragment of Lep respectively. The vector pGEM-LepΔ1 has also a deletion of the H1 natural transmembrane of Lep, and an additional glycosylation site introduced at the N-terminal segment. The DNA sequences encoding human Bcl-xL and mouse Bax were obtained from G. Nuñez (University of Michigan Medical School) and a construct of human Bid was provided by X. Wang (University of Texas Southwestern Medical Centre).

Lep chimeras containing the putative transmembrane segments of the different Bcl-2 proteins instead of the H2 natural fragment of Lep (amino acids 59-81), were prepared. For this purpose, the corresponding Bcl-xL, Bax and Bid fragments were amplified by PCR with primers containing BclI and NdeI restriction sites and were digested with these enzymes. After purification, these inserts were introduced in the pGEM-Lep-NST vector, previously digested with BclI and NdeI. Ligation reactions were carried out in 1x commercial ligase buffer and 3 units of T4 DNA ligase (Promega, Madison, WI), in a final volume of 10 μL containing appropriate quantities of both insert and vector. Lep/Bcl-xL-α5α6[EEE], Lep/Bcl-xL-α5α6C79W[EEE] and Lep/Bcl-xL-α5C79W constructions were produced from Lep/Bcl-xL-α5α6 and Lep/Bcl-xL-α5, respectively, by site-directed mutagenesis as described in section 5.3. For the Lep/Bcl-xL-α5α6[EEE] con-

struct, the nucleotide codons for residues 166Ile-Ala-Ala168 (numbering from the full length human Bcl-xL) were changed to Glu codons. For the Lep/Bcl-xL-α5α6C79W[EEE] and Lep/Bcl-xL-α5C79W fragments, the codon corresponding to C151 was replaced by a Trp codon.

5.5. Glycosylation mapping assays

5.5.1. Obtaining mRNA by *in vitro* transcription

The plasmids used for the *in vitro* RNA synthesis contained the SP6 promoter and were isolated with a miniprep kit (Qiagen). Transcription reactions were performed for 2 h at 37°C in a final volume of 50 μL containing 10 μL of transcription buffer 5x, 5 μL rNTPs mixture (25 mM rATP, rCTP, rUTP and rGTP), approximately 1 μg of DNA and 5 μL of a enzyme mixture provided by the Ribomax Large Scale RNA production System-SP6 (Promega). Obtained RNAs were purified with the RNeasy RNA purification kit (Qiagen), according to the manufacturer instructions.

5.5.2. *In vitro* translation

The RNAs of the Lep chimeras obtained as described in the preceding section were translated *in vitro* using a reticulocyte lysate system (Promega). The translation reactions were carried out for 2 h at 30°C and contained 10 μL of reticulocyte lysate, 0.5 μL of an amino acids mixture of 100 mM, 1 μL 35S-Met 100mM (Amersham Biosciences) and 1 μL RNA approximately 150 ng/μL in a final volume of 15 μL. 1 μL pancreatic canine microsomes (Promega) was added to the appropriate reactions.

As a control of glycosylation, a tripeptide codifying for the glycosylation acceptor site Ac-N-Y-T-NH_2 was added to the corresponding translation reactions in a final concentration of 100 μM. This acceptor peptide (AP) acts as a competitive inhibitor of the glycosyl transferase attached to the microsome membrane. In order to corroborate that the competition for glycosylation was sequence specific, and not an artifact, a non-acceptor peptide with the sequence Ac-Q-Y-T-NH_2 was added to the corresponding reactions in the same concentration.

N-methoxysuccinyl-Ala-Ala-Pro-Val-Chloromethyl ketone (Sigma Chemical, St. Louis, USA) was added to the corresponding reactions in a final concentrations of 2 mM. This molecule acts as a specific signal peptidase (SPase) inhibitor (SPI) and was used as a control for processing van Geest et al. (1999).

5.5.3. Analysis of association with membranes

Alkaline extractions were performed according to Whitley et al. (1996), and urea treatments according to Schaad et al. (1997). Briefly, after translation, mixtures containing microsomes were added 4 volumes of either 100 mM Na_2CO_3 (pH 11.5) or 4 M urea (in 35 mM Tris-HCl, pH 7.4, 140 mM NaCl buffer). The Na_2CO_3 and urea samples were clarified by centrifugation at 3,000 × g and 4°C for 10 min, and membranes were collected by layering the supernatant onto a 50 μl sucrose cushion and centrifugation at 100,000 × g for 20 min at 4°C. Finally, pellet and supernatant were analysed by 10% (Na_2CO_3 treated samples) or 12% (urea treated samples) SDS-PAGE.

The Triton-X114 partitioning experiments were performed according to Schaad et al. (1997). 15 μl of hydrated Triton-X114 were added to 15 μl of the translation reactions containing microsomes and the mixtures were incubated for 30 min on ice. The incubated Triton-X114 samples were equilibrated at 37°C for 10 min to allow development of aqueous and organic phases Bordier (1981). These phases were then separated by centrifugation at 10,000 × g at 37°C. Subsequently, the lower, detergent-rich fraction was washed two times by addition of ten volumes of fresh detergent-free buffer, followed by vortexing, incubation on ice for 30 min, and phase separation as before. The proteins present in the aqueous and detergent-rich fractions were precipitated in acetone. Eight volumes of acetone were added to one volume of protein sample and precipitated for 2 hours at -20°C. The samples were centrifuged 5 min at 10.000 rpm and washed twice with 20 volumes of acetone. They were dried in the speed-vac, resuspended in sample buffer and analysed by 12% SDS-PAGE.

5.5.4. Protein electrophoresis

To analyse the glycosylation pattern of the *in vitro* translation insertion reactions, 10 % SDS-PAGE gels were prepared using the Mini-Protean system (Bio-Rad) and run at 12 mA in SDS-PAGE buffer (125 mM Tris, 1 M glycine, 0.5% w/v SDS). They were charged with 10 μL of the protein samples, prepared by adding 25 μL H2O and 25 μL of 5x SDS-PAGE sample buffer (composition of 1x: 625 mM Tris-HCl pH 6.8, 10% v/v glycerol, 2% w/v SDS, 4% v/v β-mercaptoethanol, 0.025% w/v bromophenol blue) to 15 μL of the *in vitro* translation reaction and heating the mixture at 95°C for 5 min. The ^{35}S-Met and ^{14}C-methylated molecular weight marker were from Amersham Pharmacia Biotech (Upsala, Sweden).

The pellets resulting from the alkaline extraction were dried and resuspended in 25 μL 1x SDS-PAGE sample buffer. Samples were heated at 95°C for 5 min and analyzed by SDS-PAGE. Samples were also prepared with the supernatants

by adding the corresponding 5x SDS-PAGE sample buffer and heating at 95°C for 5 min.

The protein samples were fixed in the polyacrylamide gels with a solution of 20% methanol and 5% acetic acid, softly shaking for 30 min. The gels were dried in a Slab Gel Drier model SGD5040 (ThermoSavant, Holbrook, NY) at 80°C for 1 h and exposed overnight with a intensifier screen (Fujifilm, Fuji Photo Film, Tokyo, Japan). The screen was revealed with a Phosphorimager PLA-3000 from Fujifilm.

5.6. Prediction programs

The sequences of Bcl-xL, Bax and Bid were analysed for possible transmembrane segments with the help of the programs TopPred II Claros and von Heijne (1994) and DAS Cserzo et al. (1997) (see section 4.1 on page 49). TopPred II predicts the topology of bacterial inner membrane proteins using a strategy based on hydrophobicity analysis, that generates a set of possible topologies which are ordered according to the positive inside rule. The DAS program generated a hydrophobic score for each amino acid and provided a hydrophobicity profile with high and low cut-offs for membrane insertion.

Search for possible signal peptidase cleavage sites was made with the help of SignalIP Nielsen et al. (1997). This program uses a training data set from the SWISS-PROT, which is divided intro eukaryotic, and Gram-positive and negative prokaryotic signal peptides. These share a common structure, with a positively charged region, which is followed by a hydrophobic region and a polar neutral region. The residues in the cleavage site are found to be small and neutral. This method of prediction is based on an artificial neural network extended with a Hidden Markov Model, and was evaluated by five-fold cross-validation.

These programs were used via the Internet through available servers and using standard parameters. The URL localisation of prediction methods used for this study are:

TopPredII, http://bioweb.pasteur.fr/seqanal/interfaces/toppred.html.

DAS, http://www.sbc.su.se/~miklos/DAS/maindas.html.

SignalIP, http://www.cbs.dtu.dk/services/SignalP/

5.7. Peptide Synthesis and purification

The peptides showed in table 5.3 were synthesized chemically according to previously reported protocols Vilar et al. (2001). Two peptides corresponding to the sequence of the alpha helix 5 from Bax were synthesised. Initially, Bax-α5K was extended by one lysine on each side, with respect to the natural sequence, to improve water solubility and facilitate peptide purification and handling. This approach has been previously used with success and no observable functional interference Orzaez et al. (2004); Melnyk et al. (2001). A second peptide, Bax-α5 was synthesised with no lysines added and with a longer sequence that could be perfectly aligned with the sequence of the peptide Bcl-xL-α5. A mutation of threonine to tyrosine was introduced in Bid-α6 to allow determination of peptide concentration (see below). Cysteine residues in the natural sequences were mutated to serine in the peptides to avoid oxidation and aggregation during manipulation.

Solid phase synthesis of the peptides was performed on an Applied Biosystems 433A Peptide synthesizer using Fmoc chemistry and Tentagel S-RAM resin (0.24 meq/g substitution) as a solid support. A 6-fold molar excess of amino acids (Senn Chemicals) was used and double and triple couplings were applied on difficult residues Fisher and Engelman (2001). All peptides were N-terminal acetylated and C-terminal amidated. Deprotection and cleavage reactions were carried out in a mixture of 70% trifluoroacetic acid (TFA), 20% dichloromethane, 5% water, 2.5% triisobutylsilane (TIBS), 2.5% ethanedithiol (v/v), all from Merck. Cleaved peptides were precipitated in ice-cold t-butyl-methyl ether and centrifuged. Pellets were dried, redissolved in water:acetonitrile (90:10), and lyophilized. Peptides were purified using a C18 preparative reversed-phase column, by high performance liquid chromatography (RP-HPLC), to a purity of about 95% as determined by analytical RP-HPLC. Purified peptides were analyzed by mass spectrometry to confirm their molecular mass. Unless otherwise indicated, all reagents and solvents used in the solid phase synthesis of peptides were from Applied Biosystems.

All peptide concentrations were determined from UV spectra using a Jasco spectrophotometer and the molar extinction coefficient used for each one is indicated in table 5.3.

Table 5.3.: Peptides synthesised.

Name	Sequence*	aa's	MW (Da)	$\epsilon(\mathrm{cm^{-1}M^{-1}})$
Bax-$\alpha 5^K$	Ac-*K*GR**V**VA**LFYF**ASK**LVL**KA**L*S*T**RVPELIRT*K*-NH_2	30	3418,22	1450
Bax-$\alpha 5$	Ac-**DGNFNW**GR**VV**A**LFYF**ASK**LVL**KA**L*S*T**KV**PELIRT-NH_2	34	3895,61	6970
Bax-$\alpha 6$	Ac-E**LI**R**TI**MG**WT**LD**FL**RER**LLVWI**QD-NH_2	24	3058,64	11380
Bid-$\alpha 6$	Ac-EKE**KT**M**LVLALLL**AKKVASH*Y*PS-NH_2	23	2611,19	1450
Bid-$\alpha 7$	Ac-**SLLRDVFHTTVNFI**NQNLRTYVR-NH_2	23	2848,26	1280
Bcl-xL-$\alpha 5$	Ac-**RDGVNWGRIVAFFSFGGAL*S*V**ESVDKEM**QVLV**SR-NH_2	34	3798,34	5690
Bcl-xL-$\alpha 6$	Ac-**VLV**SR**IAAWMAT**YLNDHLEPWIQE-NH_2	24	2897,35	12660

*Multiple couplings are indicated in bold, modifications of the natural sequences are in italics, and couplings with capping are shown underlined.

5.8. Preparation and Size Measurement of Lipid Vesicles

All lipids used were from Avanti Polar Lipids (Alabaster, AL), except for asolectin, which was from Sigma and purified according to Kagawa et al. (1973). Large unilamellar vesicles (LUVs) were prepared as described previously Dalla Serra and Menestrina (2003). Lipids were dissolved in chloroform, mixed to desired molar composition and vacuum-dried to a film on the bottom of a round glass flask. Further drying was accomplished with 30 min under strong vacuum. To prepare calcein containing LUVs, lipids were resuspended to a concentration of 4 mg/mL in a solution containing 80 mM calcein, neutralized with NaOH. After six cycles of freezing and thawing, they were passed 31 times through two stacked polycarbonate filters of 100 nm pore size, using a two-syringes extruder from Avestin (Ottawa, Canada). To remove external non encapsulated dye, LUVs were washed with Sephadex-G50 (Sigma-Aldrich) minicolumns, previously equilibrated in 140 mM NaCl, 20 mM Hepes, 1 mM EDTA pH 7 (buffer A). In the case of LUVs encapsulated with fluorescent dextrans, the lipid films were resuspended to a concentration of 10 mg/mL in a 100 mg/mL solution of dextrans in buffer A. The vesicles were subjected to 20 cycles of freezing and thawing and extruded as described above, but using 200 nm polycarbonate filters. Non-encapsulated dextrans were removed by gel filtration. Chromatographies were carried out in an ÄKTA system (Amersham) with a column of 35x1,6 cm, containing Sephacryl HS-500 (Amersham) equilibrated with buffer A, and at at flux of 0.5 mL/min. The fractions corresponding to the LUVs peaks were collected and used in experiments of content release.

Vesicle size was measured by Quasielastic Light Scattering (QLS) at a fixed angle (90°) and room temperature, using a laser particle sizer (Malvern Z-sizer 3) upgraded with a 30 mW laser diode emitting at 675 nm. Measurements were done adding 500 μL of buffer A and 1.5 μL of vesicles to a cylindrical cell in a water solution in the laser light path. Fluctuations in the scattered light are due to the Brownian movements of the particles. This is analysed with the autocorrelation function, which allows the estimation of the diffusion coefficient of the particles through Laplace inversion, and then their hydrodynamic radius, using the using the cumulant method Santos and Castanho (1996) and the Stokes-Einstein equation.

Lipid concentration was estimated with the Phospholipids B kit (WAKO, Japan), following the supplier's protocol. It is an enzymatic colorimetric method based on the hydrolysis of choline containing phospholipids by phospholipase D. The free choline is then oxidised to betaine by the choline oxidase, and hydrogen

peroxide is quantitatively produced during the reaction, which couples 4-amino-antipyrine and phenol to give a red quinone pigment with a maximum absorption at 505 nm.

5.9. CD Spectroscopy

Samples for CD spectroscopy were prepared at a 30 μM concentration of peptide in 10 mM phosphate buffer at pH 7. Several percentages of trifluoroethanol (TFE), or different concentrations of sodium dodecylsulfate (SDS), under and above the critic micellar concentration, were added to the corresponding samples. Spectra were measured at 20 °C on a Jasco J-810 CD spectropolarimeter, using a cell of 1mm path-length. The data were collected every 0.2 nm at 100 nm/min from 250 to 185 nm, with a band width of 1nm, and results were averaged from 10 scans.

Data analysis was performed with the help of the CDPro software package, which contains three commonly used programs: SELCON3, CONTIN/LL and CDSSTR Sreerama and Woody (2000, 2004). This software allows the use of different reference sets of proteins, increasing the reliability of the analysis.

5.10. Fourier-transformed Infrared Spectroscopy (FTIR) experiments

FTIR spectroscopy was used to assess the secondary structure of peptides either in solvent (TFE) or in buffer, or adsorbed to the lipid phase. Analysis of peptide orientation with respect to the lipid phase and binding to LUVs were also performed. This was done by analysis of the amide I' band as described previously Menestrina et al. (1999). LUVs composed of either egg phosphatidylcholine (PC) or of PC and phosphatidic acid (PA) in a 1:1 molar ratio were prepared with the procedure described in 5.8, except that lipids were resuspended in buffer A. Each peptide was incubated for 1 hour at room temperature with LUVs, at a 1:50 mol/mol protein/lipid ratio, in buffer A. The mixtures were centrifuged, together with controls, in an Optima TL ultracentrifuge (Beckman, U.S.A), using a fixed-angle rotor (TLA-100.2) at 350 000 g, for 3 h at 4°C. After centrifugation, the pellet was resuspended in 100 μl of 10 mM HEPES, pH 7.0 (buffer B). Samples were deposited on 10-reflection germanium crystals (45° cut) and gently dried by nitrogen flushing. To obtain the spectra of the peptides in aqueous solution, these were dissolved in buffer A and directly applied to the germanium crystals. The samples were redissolved in TFE on the crystal surface and dried again to collect spectra in TFE.

5.10. Fourier-transformed Infrared Spectroscopy (FTIR) experiments

Spectra of hydrated and deuterated films were collected, in an ATR geometry, using a FTS 185 spectrometer (Bio-Rad, U.S.A), with MCT-detector. For the polarization experiments, a rotating KRS5 wire-grid polarizer was interposed and set either at 0° or 90° (with respect to the plane of internal reflections). Raw spectra were pretreated prior to analysis to optimise the signal. This pretreatment consisted on subtraction of the water peaks digitally with a file containing the water signal in the IR spectrum, manually zapping the noise and peaks out of phase, and line smoothing with the Saavs-Golay method. These modifications and the subsequent analysis were carried out with the program GRAMS (Galactic Industries Co.).

The orientation of a structural element was calculated from the dichroic ratio $R = A_{0^o}/A_{90^o}$, where A_{0^o} and A_{90^o} are the absorption bands pertaining to the functional group of that element, in the parallel and perpendicular configuration, respectively Tamm and Tatulian (1997); Goormaghtigh et al. (1999). From R we derived the form factor, S, which was then used to calculate the average tilt angle β as in Axelsen et al. (1995), described in section 4.5.2 on page 66 and Goormaghtigh et al. (1999).

To estimate the secondary structure content of Bax-$\alpha 5^K$ and Bid-$\alpha 6$, the amide I' band in the region 1700-1600 cm^{-1} was deconvoluted into a set of Lorentzian components, whose frequencies were assigned to different structural elements in the standard way Menestrina et al. (1999). In particular we used the following assignments: band at 1680±3 cm^{-1}, ß-turn; bands in the region 1656-1646 cm^{-1}, α-helix; band at 1640±5 cm^{-1}, random coil; band around 1610±5 cm^{-1}, side chains contribution. In addition we observed two bands, a major one around 1624 cm^{-1} and a minor one at 1692 cm-1, which are typical of aggregated peptide in an extended configuration and correspond to strong interstrand and intrastrand interactions Tamm and Tatulian (1997); Gordon et al. (2002). This set of Lorentzians was used to best fit the original spectrum and the resulting relative areas were taken as the proportion of the related structure present. The small side chain band was excluded from the normalization. In some cases, a single band at 1672 cm^{-1} was present, indicating the presence of some TFA remaining from the synthesis. Such minor band was digitally removed before analysis.

The curve fit was used to calculate the percentage of peptide aggregation. The aggregated peptide is represented by the bands around 1624 and 1692 cm^{-1}, and the non aggregated by all the remaining amide I' components in the region 1630 to 1690 cm^{-1}. Due to the centrifugation procedure used for sample preparation, in the peptide-lipid samples the non aggregated part represents lipid-bound peptide only, whereas the aggregated part may be formed by both lipid-attached aggregates and other aggregates present in the aqueous phase that might co-precipitate

or form during sample drying.

The secondary structure content in the remaining peptides was analysed qualitatively, determining the major wavelength contributions to the amide I' peak and the elements of secondary structure associated to them (see table 4.2 on page 67). In addition, the difference spectra were obtained subtracting the normalised amide I' peak in the spectrum in buffer A from the normalised amide I' peak in the spectrum in TFE or in lipid vesicles. In the absence of secondary structure rearrangements, a straight horizontal line is expected. Positive deviations indicate an increase in the element of secondary structure which absorbs at the corresponding wavelength, while negative deviations indicate the decrease of the secondary structure element associated to that wavelength. This is a good approximation to the changes in secondary structure suffered by the peptides in response to changes in the environmental conditions Goormaghtigh et al. (1999).

For the peptide-lipid samples, the spectrum of the peptide was obtained after subtracting the contribution of the lipid alone, with a weight that minimizes the band remaining at 1738 cm^{-1} (stretching of the carbonyl groups in phospholipids). This was necessary in view of the high lipid/peptide ratio. On the other hand, and for the same reason, it was not necessary to subtract the peptide spectrum from the lipid-peptide one, in order to calculate the lipid contribution in the methylene C-H stretching region (from 3000 to 2800 cm^{-1}).

The lipid to peptide ratio (L/P) in the pellet, was calculated by the following algorithm Rodionova et al. (1995); Tamm and Tatulian (1993):

$$L/P = 0.208(n_{res} - 1)\frac{(1 - S_{amideI'})}{(1 + S_L/2)}\frac{\int_{2800}^{2980} A_{90^o}(\nu_L)d\nu}{\int_{1600}^{1690} A_{90^o}(\nu_{amideI'})d\nu} \qquad (5.1)$$

where: n_{res} is the number of residues of the peptide (i.e. 23 and 31 in Bid-α6 and Bax-α5, respectively), A_{90^o} is the absorption with the 90° polarizer and S_L, $S_{amideI'}$are order parameters calculated from the ratio of the parallel and perpendicular absorption bands. S_L corresponds to the lipid chains, and is derived either from the symmetric and asymmetric CH_2 stretching (bands centred at 2853 and 2923 cm^{-1}) or from the symmetric CH_3 stretching at 2872 cm^{-1}, using θ (the angle between the direction of the dipole moment change and that of the long axis of the molecule) set at 90° or 0° respectively. $S_{amideI'}$is the order parameter for the amide I' band (with $\theta = 0°$). The integral with suffix L was calculated from the spectrum of the lipid-alone, and that with suffix amide I' from the one of the non-aggregated peptide alone (i.e. after subtracting the lipid and the aggregated peptide). The order parameter for the α-helix, S_α, was obtained using the Lorentzian components at 1651±5 cm^{-1} with θ=30° Axelsen et al. (1995);

Frey and Tamm (1991); Menikh et al. (1997).

5.11. Permeabilisation of Unilamellar Lipid Vesicles

The permeabilising activity of the peptides was assayed by measuring the release of calcein or fluorescein labeled dextrans from LUVs. Calcein release experiments were performed using a 96-well microtiter plate that was filled with 100 μL of buffer A containing the desired amount of peptide. To avoid unspecific interactions of the peptides and vesicles with the plastic walls, microplates were pretreated with a 0.1 mg/mL Prionex (Pentapharm, Basel, Switzerland) solution for 30 min. All experiments were done at room temperature. After adding 100 μL of LUVs, at a final lipid concentration between 2 and 5 μg/mL, the time-course of calcein release was measured as the increase in fluorescence emission at 520 nm with the excitation set at 495 nm, using a fluorescence microplate reader (Fluostar, BMG, Germany). Experiments of fluorescent dextrans release were carried out using a cell of 1 cm path-length in a LS-50B luminescence spectrometer (Perkin Elmer, USA). The desired amount of peptide was added to the reaction mixture containing 1 mL of buffer A and 100 μL of LUVs (final concentration of lipid 45 μM) . The increase in fluorescence intensity at 520 nm (excitation wavelength set at 490 nm, excitation and emission band slits 2 nm) due to the release kinetics was monitored until the stationary state was reached.

The percentage of peptide-induced fluorescent dye release (%R) was calculated by:

$$R = \frac{(F_{ss} - F_{i)}}{(F_m - F_i)} 100 \tag{5.2}$$

where F_{ss} is the value of fluorescence measured at the stationary state (after 1 hour of reaction in the case of calcein experiments and 12.5 min in dextrans experiments), F_i is the initial fluorescence before adding the peptides, and F_m is the maximal value after addition of 1 mM Triton X-100. Spontaneous release of calcein or dextrans was negligible in all cases.

5.12. Lipid transbilayer diffusion in LUVs

Asymmetrically labeled vesicles were prepared as described in Muller et al. (2000). The desired amount of py-PC from a chloroform stock was dried on a glass tube with a nitrogen flux and solved in ethanol at the desired concentration. The fluorescent probe in ethanolic solution was added with a final concentration of 1μM to a solution of buffer A. Then LUVs prepared as described above, but rehydrated

in buffer A, were added to a final concentration of 20 μM (lipid). The labeled lipid was incorporated only into the external leaflet of LUVs after incubation of 20 minutes to ensure the stability of the I_E/I_Mratio. The fluorescence spectra between 355 and 500 nm were recorded at room temperature using a LS-50B luminescence spectrometer (Perkin Elmer) and a 1cm path-length cell with constant stirring. The excitation wavelength was 345 nm, the excitation and emission slits were set to 4 nm and the scan speed was 250. During the experiments, emission spectra were measured at several times after peptide addition and the emission intensities of the excimers ($I_E$at 465 nm) and the monomers ($I_M$at 395 nm) were taken from the spectra to represent the I_E/I_Mratio versus time.

5.13. Electrical Recordings of Ion Channel Activity

Electrical properties of Bax-$\alpha 5^K$ and Bid-$\alpha 6$ were measured on planar lipid membranes (PLM) as reported in **?**. Experiments were done at room temperature with solvent-free bilayers composed of asolectin, or 1,2 diphytanoyl-sn-glycerophosphocholine (DPhPC), or DPhPC:PA in a 4:1 molar ratio. Membranes were bathed symmetrically by 2 mL of buffer A. Peptides were added always on the *cys* side to stable preformed membranes with typical capacitance of 100 pF. Macroscopic currents were measured with a patch clamp amplifier (Axon Instruments). The current traces were filtered at 100 Hz and directly acquired by a computer using Axoscope 8 software (Axon Instruments). Same traces were also acquired at higher frequency and stored on a magnetic DAT tape for allowing re-analysis of the fast events, eventually present. To obtain the I/V characteristics, the current intensities going through the pore at several applied voltages, both positive and negative, were recorded. The measured intensity versus the applied voltage was plotted. For selectivity determination, reversal voltages were measured in a increasing NaCl gradient (with the higher salt concentration on the trans side), and translated into a permeability ratio P_+/P_-(where P_+ and P_- refer to cation and anion permeability, respectively) by the Goldmann-Hodgkin-Katz equation **?**, as described in section 4.4.3 on page 59.

Part III.

Results

6. Membrane insertion fragments of Bcl-xL Bax and Bid

Apoptosis regulators of the Bcl-2 family associate with intracellular membranes from mitochondria and the endoplasmic reticulum where they perform their function. The activity of these proteins is related to the release of apoptogenic factors, sequestered in the mitochondria , to the cytoplasm, probably through the formation of ion and/or protein transport channels. Most of these proteins contain a C-terminal putative transmembrane fragment and a pair of hydrophobic α-helices ($\alpha 5\alpha 6$) similar to the membrane insertion fragments of the ion channel domain of diphtheria toxin and colicins. Here we report on the membrane insertion properties of different segments from antiapoptotic Bcl-xL and proapoptotic Bax and Bid, that correspond to defined α-helices in the structure of their soluble forms. According to prediction methods, there are only two putative transmembrane fragments in Bcl-xL and Bax (the C-terminal α-helix and α-helix 5), and one in activated tBid (α-helix 6). The rest of their sequence, including the second helix of the pore forming domain, displays only weak hydrophobic peaks which are below the prediction threshold. However, subsequent analysis by glycosylation mapping in a model chimeric system allows finding three membrane inserted fragments for Bcl-xL (helices C-terminal, $\alpha 5$ and $\alpha 6$), four in the case of Bax ($\alpha 1$, $\alpha 5$, $\alpha 6$ and $\alpha 9$) and two in the case of Bid ($\alpha 6$ and $\alpha 7$). Among them, the second helix of the pore forming domains ($\alpha 6$ of Bcl-xL and Bax, and $\alpha 7$ of Bid) insert only as part of the $\alpha 5$-$\alpha 6$ ($\alpha 6$-$\alpha 7$ of Bid) hairpin. These behaviour suggests a synergistic insertion and folding of the two helices of the hairpin, that could be due to charge complementarity and additional stability provided by turn-inducing residues at the interhelical region.

Although these data come from chimeric systems, they show direct potentiality for acquiring a membrane inserted state. Thus, the above fragments should be considered for the definition of plausible models of the active, membrane bound species of Bcl-2 proteins.

6.1. Prediction of TM fragments of Bcl-xL, Bax and Bid

Interaction of proteins of the Bcl-2 family with lipid membranes most likely involves insertion of hydrophobic protein segments, apart from the already well characterised C-terminal tail of Bcl-xL and the analogous C-terminal segment from Bax. In order to localise all possible TM fragments, the sequences of Bcl-xL, Bax and Bid were analysed by using two prediction methods based on different principles (6.1 on the facing page). TopPred Claros and von Heijne (1994); von Heijne (1992) performs essentially a hydropathy plot and requires no statistical parametrization. DAS Cserzo et al. (1997), on the other hand, is based on the comparison of the query sequence with a set of known, non homologous membrane proteins and relies on the principle that the amino acid composition of TM fragments is more conservative than their sequence itself. The results of the predictions made with these two methods for the three Bcl-2 proteins studied in this work are shown in figure 6.1.

Using the standard cutoff values of TopPred and the Kyte-Doolittle hydrophobicity scale Kyte and Doolittle (1982), this program predicts two certain TM segments in the case of Bcl-xL (residues 136-156 and 212-232, figure 6.1, A), two certain TM segments in the case of Bax (residues 107-127 and 170-190, figure 6.1, B), and one certain (residues 145-165) and one putative (residues 10-30) TM segments in the case of Bid (figure 6.1, C). The qualifications as *certain* or *putative* correspond to the standard output of TopPred and depend on the default cutoff hydrophobicity values of the program Claros and von Heijne (1994) (see Materials and Methods 5.6 on page 84 and figure 6.1).

When predictions were made with DAS (figure 6.1, D-F), most probable TM segments were found to include residues 140-150 and 216-229 for Bcl-xL, residues 110-122 and 172-185 for Bax and residues 16-25 and 148-157 for Bid, which basically coincide with the TopPred prediction. The DAS profile is better resolved and shows an additional peak with significant TM propensity for a segment centred around residue 170 in the case of Bcl-xL. Additionally, there are five peaks with DAS score values below the lower cutoff, although probably still significant. These are centred around residue 12 for Bcl-xL, residues 27 and 139 for Bax and residues 106 and 174 for Bid.

Interestingly, all hydrophobic fragments mentioned above almost coincide with defined α-helices in the structures of soluble forms of Bcl-xL, Bax, and Bid (figure 6.2). Thus, the hydrophobic C-terminal segment of Bax corresponds to α-helix 9 in the structure of this protein. Bcl-xL has an analogous C-terminal fragment which was absent in the modified form of this protein used for the structure

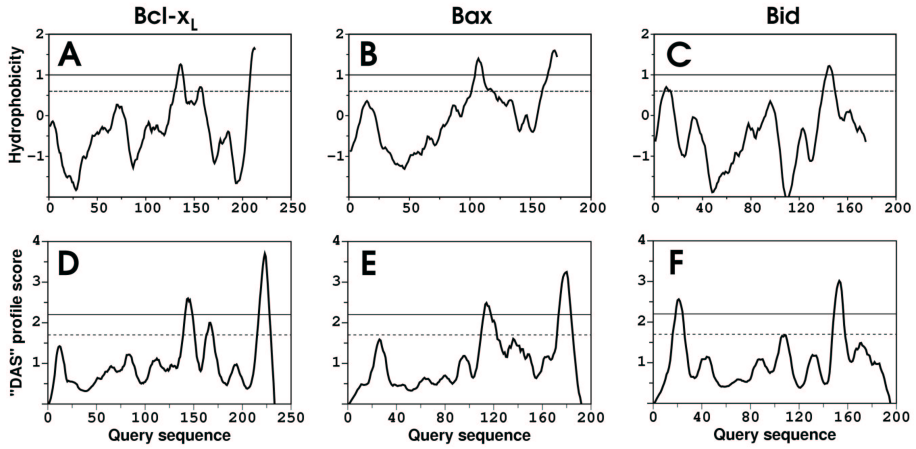

Figure 6.1.: Transmembrane potency of the sequences of Bcl-xL, Bax, and Bid as determined by two prediction methods. Graphs A (Bcl-xL), B (Bax) and C (Bid) are hydrophobicity plots made by using TopPred II Claros and von Heijne (1994) with default parameter settings. The horizontal lines indicate cutoff values for certain (continuous line) and putative (dashed line) TM fragments. Graphs D (Bcl-xL), E (Bax) and F (Bid) are DAS Cserzo et al. (1997) score profiles. Horizontal lines in this case correspond to score values of 2.0 (continuous line) and 1.7 (dashed line) which indicate high and low potential, respectively, to be TM segments.

determination Muchmore et al. (1996). This C-terminal tail is considered to form a membrane anchor that, together with flanking basic amino acids, direct specific association of Bcl-xL to the OMM Kaufmann et al. (2003). The second probable TM segment of Bax and Bcl-xL corresponds to the central hydrophobic α-helix 5, found in the structure of both proteins. Adjacent to it, α-helix 6 is much less hydrophobic, specially in the case of Bax, due to the abundance of charged residues which gives these segments an amphipatic character. With respect to Bid, the first hydrophobic segment of this protein is the first α-helix found in its structure, and the second corresponds to α-helix 6, which is analogous to α-helix 5 from Bcl-xL and Bax. Each of these two segments belongs to a different fragment among the two formed after processing of Bid by caspase-8. Finally, we will consider four additional fragments that show low, but probably significant, DAS TM propensity. These roughly coincide with α-helix 1 from both Bcl-xL and Bax, and α-helices 4 and 7 from Bid.

6.2. Testing membrane insertion of Bcl-xL fragments

6.2.1. Membrane insertion of single helix fragments of Bcl-xL

Glycosylation mapping in a transcription/translation/insertion assay has been employed before to study insertion and topology of putative TM fragments in ER microsomal membranes van Geest and Lolkema (2000) (see also chapter 4.3 on page 54). It consists on the use of a model, engineered TM protein derived from the leader peptidase of *E. coli* (Lep), with an N-terminal TM fragment (H1) followed by a highly positively charged loop (P1), a second TM segment (H2) and a soluble C-terminal domain (P2) with an engineered glycosylation acceptor site (figure 6.3, A). The flanking regions of the H1 fragment direct the insertion of the protein according to the positive inside rule von Heijne (1989) (see 50), with the N-terminus oriented towards the lumenal side of the microsomes. Thus, the protein will be glycosylated only when the fragment H2 inserts in the membrane, exposing the P2 glycosylation domain towards the lumen (figure 6.3, A). In such a system, the potential of a sequence to function as a TM segment can be tested by using it in place of the H2 fragment of Lep, in vitro transcribing and translating the corresponding chimera in presence of ER microsomes and finally checking for possible glycosylation through the observation of approximately 2 kDa increase of expected molecular weight by SDS-PAGE (figure 6.3, B).

Based on the predictions made by TopPred and DAS, different peptide segments from Bcl-xL Bax and Bid were selected for their analysis of membrane insertion using Lep chimeras (see figure 6.1 and 6.2). The C-terminal hydropho-

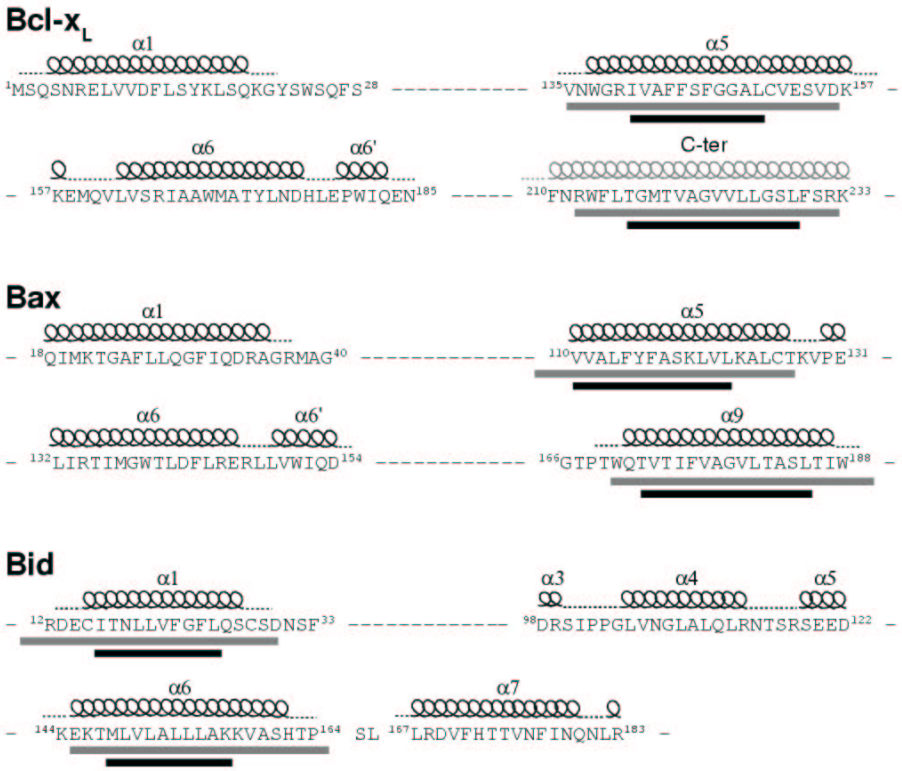

Figure 6.2.: Schematic representation of the sequences of α-helical segments from Bcl-xL, Bax and Bid. Only the segments studied in this work are represented, with numbers in superscript indicating the first and last residue of assayed fragments (numbering corresponds to the full-length proteins). Positions of α-helices are as reported for the structures of water soluble forms of these proteins Muchmore et al. (1996); Suzuki et al. (2000); McDonnell et al. (1999). In the case of the C-terminal tail of Bcl-xL, the α-helix structure is hypothetical, since this fragment was deleted in the protein used for the structure determination Muchmore et al. (1996). Possible TM segments, according to the TopPred II Claros and von Heijne (1994) and DAS Cserzo et al. (1997) predictions, are indicated below the corresponding sequences as gray (TopPred) and black (DAS) horizontal bars.

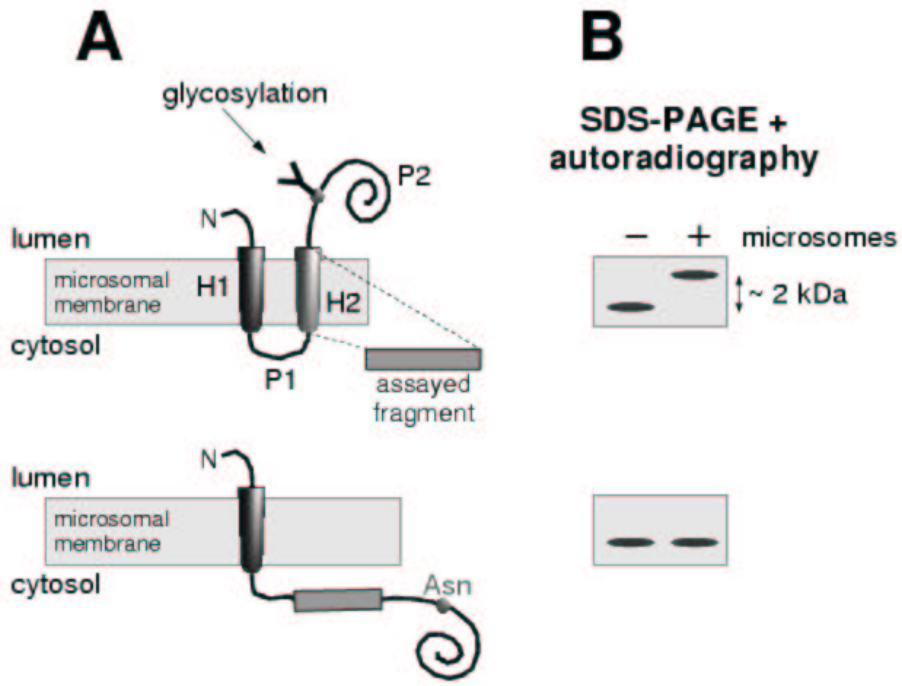

Figure 6.3.: Topology of Lep and scheme of a glycosylation mapping experiment. A) TM fragment H1 inserts with the N-terminus towards the lumen of microsomes. Assayed putative TM fragments are introduced in place of H2. Membrane insertion of the assayed H2 fragments places domain P2 in the lumenal side, where it can be glycosylated at an engineered acceptor site (Asn90 residue). B) Observation of approximately 2 kDa band shift to higher molecular weight means that P2 has been glycosylated and informs of membrane insertion of the H2 replacement fragment.

bic segment of type I Bcl2s has been previously shown to function as an anchoring tail that attaches this protein to the ER and outer mitochondrial membranes Janiak et al. (1994); Kaufmann et al. (2003). As expected, when we assay the C-terminal putative TM segment from Bcl-xL (Lep/Bcl-xL-Ct construct) in the presence of ER microsomes, we observe the appearance a new SDS-PAGE band corresponding to an increased molecular weight of the protein (figure 6.4, A, lane 2). This band shift is due to glycosylation of Lep P2 at the lumenal side, as it attenuates with the use of a specific inhibitor of the microsomal glycosyl transferase (acceptor peptide, AP, figure 6.4, A lane 3), demonstrating TM insertion of the assayed Bcl-xL-Ct sequence in the context of the Lep/Bcl-xL-Ct chimera. Notably, modification of the fusion protein was not quantitative, which we attribute to incomplete or heterogeneous efficiency of the translocation/glycosylation machinery. No quantitative modifications are often observed in these type of experiments for putative TM fragments Nilsson et al. (1994); Nilsson and von Heijne (1998, 1993); Vilar et al. (2002); Nilsson et al. (2002); van Geest et al. (1999). We should also bear in mind that physiological membrane insertion of Bcl-2 proteins occurs post-translationally through a hitherto unknown mechanism independent of the ER translocon Borgese et al. (2003), which can be an additional reason for incomplete modification in this case. Nevertheless, because the TM character of this fragment offers no doubt Janiak et al. (1994); Kaufmann et al. (2003), the results of figure 6.4A can be considered as an internal positive control throughout this work.

When a fusion containing the α-helix 5 from Bcl-xL (Bcl-xL-α5) was assayed, a band corresponding to slightly lower molecular weight was obtained in the presence of microsomes (figure 6.4B, lane 2). This behaviour suggest that digestion of the Lep/Bcl-xL-α5 chimera is taking place. Treatment with AP allows the observation of an even lower molecular weight band, demonstrating that the processed protein was also glycosylated (figure 6.4B, lane 3) and indicating that the domain P2 was translocated to the lumen of the microsomes through insertion of the Bcl-xL-α5 segment across the membrane.

Observation of cleaved Lep chimeras in a similar assay has been previously reported, and it has been attributed to the activity of the microsomal signal peptidase Nilsson et al. (2002); van Geest et al. (1999). In agreement with this possibility, using an inhibitor of the mammalian signal peptidase (N-methoxysuccinyl-Ala-Ala-Pro-Val-chloromethyl ketone, ISP) abolished digestion of Lep/Bcl-xL-α5 and a faint band corresponding to full length glycosylated Lep/Bcl-xL-α5 is now observed (figure 6.4, B, lanes 5 and 7). Interestingly, glycosylation is much more efficient after protein cleavage, as it has been observed before for a similar case van Geest et al. (1999). Although processing sites for signal peptidases usually con-

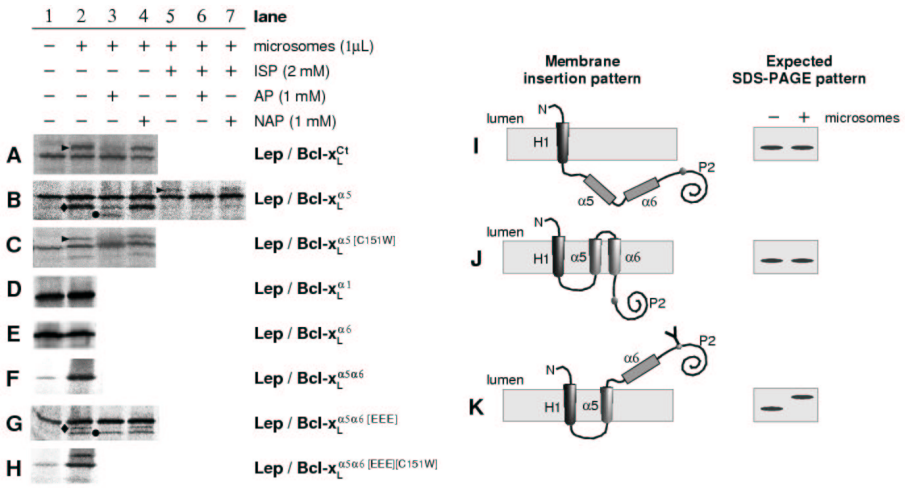

Figure 6.4.: SDS-PAGE analysis of Lep/Bcl-xL constructs. Fusions were expressed and ^{35}S-methionine-labeled in vitro in reticulocyte lysate in the absence (lane 1) and presence (lanes 2-7) of dog pancreas microsomes. Glycosylation gives rise to a higher molecular weight band (black triangle), which intensity is substantially reduced in presence of a glycosylation acceptor tripeptide (AP, lanes 3 and 6). A glycosylation non-acceptor tripeptide (NAP) is used as a control (lanes 4 and 7). In B and G, the black diamond indicates a processed and glycosylated product and black circle a processed and non-glycosylated product. Processing is prevented in presence of an inhibitor of the signal peptidase, ISP (B, lanes 5-7), or by mutating residue C151 into a tryptophan (C, H). Schemes I-J represent possible membrane insertion and expected SDS-PAGE patterns for the assays of wild-type and mutant double helix Bcl-xL-α5α6 fragments.

tain low stringent sequences, the program SignalIP Nielsen et al. (1997) allowed us finding a possible cleavage motif within the Bcl-xL-α5 segment, consisting on the sequence ALC^{151}VE (numbering corresponding to full-length Bcl-xL). Involvement of this motif in the processing of Lep/Bcl-xL-α5 was tested by site directed mutagenesis. As shown in figure 6.4, C, replacement of C151 by a tryptophan allows the observation of a normal length glycosylation band, while processing is now almost completely impaired. All together, these data indicate that Bcl-xL-α5 can act as a TM fragment, at least in the context of the Lep/Bcl-xL-α5 chimera.

The sequences corresponding to the α-helices 1 and 6 from Bcl-xL (figure 6.2) were also tested for insertion in the Lep/Bcl-xL-α1 and Lep/Bcl-xL-α6 fusions. However, in these two latter cases neither glycosylation nor cleavage was observed (figure 6.4, D, E), indicating that none of the corresponding assayed fragments inserts across the microsomal membrane. This result is specially significant in the case of Bcl-xL-α6, since, according to the colicin-like model, it is part of the proposed membrane insertion domain.

6.2.2. Membrane insertion of the α5-α6 hairpin from Bcl-xL.

Although the absence of insertion for Bcl-xL-α6 is in agreement with the predicted low TM propensity (see figure 6.1), it prompted us the question whether the surrounding protein context had an influence in the insertion tendency of this sequence. In order to test this possibility, a fragment corresponding to the α5-α6 hairpin (Bcl-xL-α5α6) was assayed. As shown in figure 6.4, F, no glycosylation is observed for the Lep/Bcl-xL-α5α6 chimera. This result is ambiguous, since both the simultaneous absence of insertion (figure 6.4, I) and the simultaneous insertion (figure 6.4, J) of the two helices of the hairpin can give rise to the observed pattern. The second possibility was challenged by assaying a mutant of Lep/Bcl-xL-α5α6, where three hydrophobic residues from the centre of α-helix 6 were replaced by glutamates (Lep/Bcl-xL-α5α6[EEE]). Such a mutation should avoid insertion of α-helix 6, without affecting insertion of α-helix 5 Vilar et al. (2002). In this case, a pattern similar to the one obtained for Lep/Bcl-xL-α5 is observed (figure 6.4, G), consisting of lower molecular weight bands due to cleavage and glycosylation of the translocated C-terminal domain. Again, a C151W mutant of the latter construct (figure 6.4, H) proves that cleavage occurs at the ALC^{151}VE motive of α-helix 5, most likely by the microsomal signal peptidase, and the pattern represented in figure 6.4, K, is observed. These data indicate that the absence of glycosylation in the case of the Lep/Bcl-xL-α5α6 chimera was due to the simultaneous insertion of α-helices 5 and 6 (figure 6.4, J). Although with this topology the ALC151VE motive could be accessible for processing, the different

protein context, with respect to the single-fragment construct or the Lep/Bcl-xL-α5α6[EEE] mutant, or structural restrictions imposed by a tight turn in the hairpin might render this case unfavorable for signal peptidase cleavage.

Additional support for the capacity of the Bcl-xL-α5α6 hairpin to insert into microsomal membranes came from the use of a modified version of Lep, where the H1 TM fragment has been deleted and a second glycosylation site has been added in the P1 loop (LepΔH1, figure 6.5, A) Nilsson and von Heijne (1998). In this case, when H2 is replaced by a hairpin of two potential TM fragments, the insertion of only one of them can be clearly distinguished from the insertion of the two (figure 6.5, B-D). The transcription of the LepΔH1/Bcl-xL-α5α6 fusion gave no glycosylation (not shown), indicating that neither the P1 nor the P2 glycosylation sites were accessible at the inside of the microsomes. To rule out the possibility that the LepΔH1/Bcl-xL-α5α6 fusion does not bind at all to the membranes, the microsomes were pelleted after a sodium carbonate wash. Under these conditions, the non-glycosylated protein was retained in the membrane fraction (figure 6.5, E, lanes 1 and 2), suggesting that it binds tightly to the microsomal membranes through the Bcl-xL-α5α6 hairpin.

Binding of LepΔH1/Bcl-xL-α5α6 as an integral membrane protein was further supported by treating the microsomes with urea and Triton-X114 Schaad et al. (1997); Bordier (1981). Incubation of the microsomal samples with 4M urea, followed by ultracentrifugation, shows again that the protein appears mostly associated with the membrane fraction (figure 6.5, F, lanes 1 and 4), as it corresponds to an integral membrane protein. The non-ionic detergent Triton-X114 separates in aqueous and detergent-rich phases above the so called cloud point temperature (20 ^{o}C) Bordier (1981). It has been shown that membrane lipids and hydrophobic proteins partition to the detergent-rich phase, and this has been used to specifically isolate integral membrane proteins Schaad et al. (1997); Bordier (1981); **?**. Preincubation of microsomal samples with 1% Triton-X114 at 0 ^{o}C, followed by incubation at 37 ^{o}C and centrifugation allows detection of LepΔH1/Bcl-xL-α5α6 mostly in the hydrophobic fraction (figure 6.5, G, lanes 1 and 4). The latter three stringent treatments of the microsomes are consistent with tight binding of the chimera to the lipid membranes, as it corresponds to membrane insertion. Additionally, the absence of glycosylation of the membrane-associated protein means that insertion involves both helices of the α5-α6 hairpin.

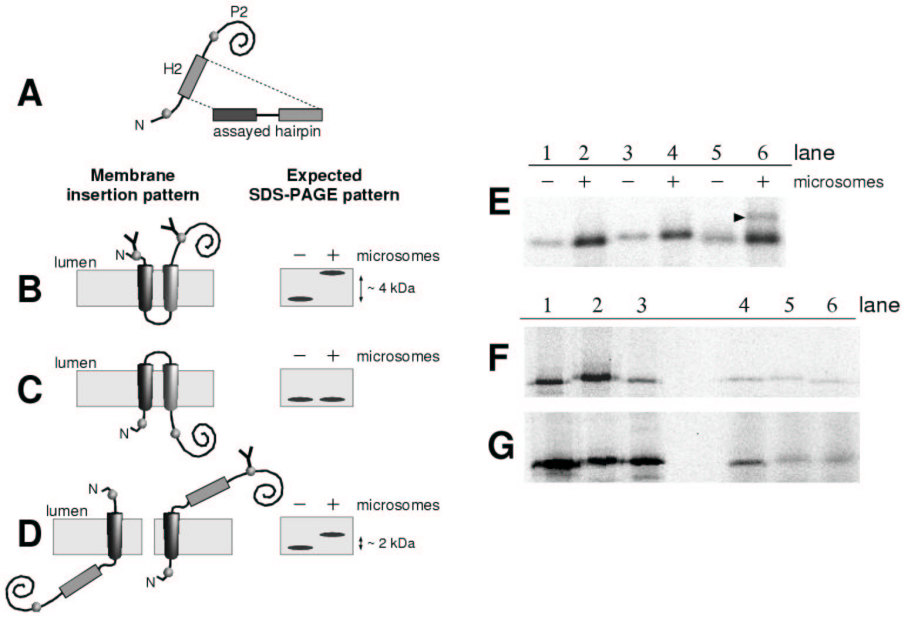

Figure 6.5.: Schemes of possible membrane insertion patterns and results of SDS-PAGE analysis of double-helix hairpins inserted in LepΔH1. Two glycosylation sites are present in this construct, placed N-terminal and C-terminal with respect to the assayed double helix (A). Simultaneous insertion of both α-helices should give rise to a doubly glycosylated product with around 4 kDa molecular weight increase (B), or to a normal size non-glycosylated product (C). A band shift corresponding to about 2 kDa mass increase is due to the insertion of only one α-helical segment (D). E shows the results of in vitro expressions of ^{35}S-methionine-labeled LepΔH1/Bcl-xL-α5α6 (lanes 1 and 2), LepΔH1/Bax-α5α6 (lanes 3 and 4) and LepΔH1/Bid-α6α7 (lanes 5 and 6) in reticulocyte lysate in the absence (lanes 1, 3 and 5) or presence (lanes 2, 4 and 6) of dog pancreas microsomes. All samples were alkaline washed and pelleted before loaded in the gel. The band of glycosylated protein in lane 6 is marked with the black triangle. In F, the pellet and supernatant after treatment of the microsomal samples with 4 M urea are shown for the LepΔH1/Bcl-xL-α5α6 (lanes 1 and 4), LepΔH1/Bax-α5α6 (lanes 2 and 5) and LepΔH1/Bid-α6α7 (lanes 3 and 6). The SDS-PAGE analysis of hydrophobic (lanes 1-3) and aqueous (lanes 4-6) phases after Triton X-114 treatment is shown in G, for LepΔH1/Bcl-xL-α5α6 (lanes 1 and 4), LepΔH1/Bax-α5α6 (lanes 2 and 5) and LepΔH1/Bid-α6α7 (lanes 3 and 6).

6.3. Membrane insertion of Bax fragments.

According to the predictions made above, the sequence of Bax contains various hydrophobic segments which are analogous to similar fragments from Bcl-xL (see figure 6.1). Among them, the C-terminal tail corresponding to the α-helix 9 in the structure of soluble Bax (Bax-α9) shows important hydrophobicity and DAS score peaks and is expected to function as TM. When the sequence of this fragment (figure 6.2) replaces Lep H2, the Lep/Bax-α9 fusion is glycosylated in the presence of microsomes (figure 6.6, A, lanes 1-4), which agrees with membrane insertion of the assayed Bax-α9 fragment. With respect to the hydrophobic α-helix 5 from Bax (Bax-α5, figure 6.2) it behaves as its analogous fragment from Bcl-xL. Thus, the Lep/Bax-α5 chimera gives a processed and glycosylated protein when translated in the presence of microsomes (figure 6.6, B), which indicates that Bax-α5 can insert into the microsomal membrane. A possible cleavage site made of the sequence ALC^{126} TK can also be found in the fragment Bax-α5, and processing can be prevented in the presence of an inhibitor of the microsomal signal peptidase (figure 6.6, B). Additionally, as we have seen before, the full-length Lep/Bax-α5 protein is barely glycosylated.

As a difference with respect to Bcl-xL, the N-terminal α-helix 1 of Bax (Bax-α1), which showed modest hydrophobicity and DAS score (figure 6.1), can adopt a TM position, as we deduce from the band of glycosylated protein that appeared when the Lep/Bax-α1 chimera was assayed (figure 6.6, C).

With respect to α-helix 6 of Bax, when assayed alone in the corresponding Lep fusion (Lep/Bax-α6), it did not insert across the membrane, since no glycosylation was observed (figure 6.6, D).

Also in this case, we investigated the insertion behaviour of the double helix fragment Bax-α5α6. As shown in Figure 6E, the Lep/Bax-α5α6 chimera is neither glycosylated nor processed when translated in the presence of microsomes. Since, again, this result is ambiguous (see figure 6.6, I, J), we prepared and analysed a LepΔH1/Bax-α5α6 chimera. After translated in the presence of microsomes, the pellet of alkaline washed membranes shows only non-glycosylated LepΔH1/Bax-α5α6 protein (figure 6.5, E, lanes 3 and 4). Similar to the case of LepΔH1/Bcl-xL-α5α6 (see above), the urea and Triton-X114 treatments also agrees with tight association of the Bax chimera with the membrane (figure 6.5, F, G, lanes 2 and 5), which supports the simultaneous insertion of the two helices of the Bax-α5α6 hairpin.

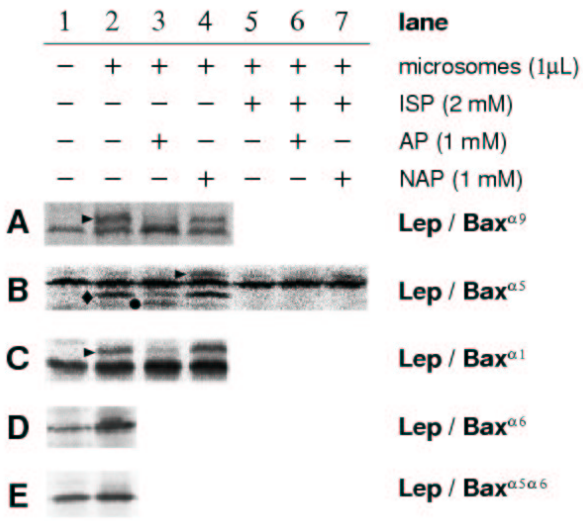

Figure 6.6.: SDS-PAGE analysis of Lep/Bax constructs. ^{35}S-methionine-labeled in vitro translation products in the absence (lane 1) and presence (lanes 2-7) of dog pancreas microsomes. For lanes 3 and 6 a glycosylation acceptor tripeptide (AP) was added in the reaction mixture, and for lanes 4 and 7 this was substituted by a non-acceptor peptide (NAP). lanes 7 are from translation reactions containing an inhibitor of the signal peptidase (ISP). Marks indicate glycosylated products (triangle), processed and glycosylated products (diamond), and processed and non-glycosylated products (circle).

6.4. Membrane insertion of Bid fragments.

The hydropathy profile of this BH3 only protein is clearly different from those of Bcl-xL and Bax (see figure 6.1). Here, two possible TM segments can be found, made of α-helices 1 (Bid-α1) and 6 (Bid-α6) of the structure of the soluble protein (figure 6.2), although only the second of them belongs to the active fragment tBid. Additionally, α-helix 4 (Bid-α4) displays also appreciable hydrophobicity (figure 6.1).

When the Lep/Bid-α1 chimera is assayed, a faint higher molecular weight band is observed in the presence of microsomes (figure 6.7, A). This is due to glycosylation of the protein, as it is not observed in the presence of AP, and indicates a weak tendency of the Bid-α1 fragment to insert into the membrane. The weakly hydrophobic Bid-α4 fragment does not act as TM (figure 6.7, B). With respect to the Bid-α6, assaying the corresponding Lep chimera resulted in a pattern similar to the one found for Bcl-xL-α5 and Bax-α5 (see above), although the amount of full-length glycosylated chimera is somewhat higher. Thus, in this case, both lower and a higher molecular weight bands were observed in the presence of microsomes (figure 6.7, C, lane 2). Treatment with the AP inhibitor shows that the two new bands correspond to glycosylated proteins (figure 6.7, C, lane 3). Additionally, treatment with the signal peptidase inhibitor shows that the lower molecular weight band was a processed chimeric protein (figure 6.7, C, lane 5). A possible cleavage site (VAS^{161} HT) was also found in the sequence of Bid-α6 with the help of SignalIP Nielsen et al. (1997).

Finally, we assayed the hairpin α6-α7 from Bid, which despite the low hydrophobicity of the fragment α7 is also considered as a colicin-like insertion domain. A Lep fusion containing this sequence (Lep/Bid-α6α7) gave rise to a higher molecular weight glycosylation band (figure 6.7, D), indicating insertion of only α-helix 6. As it happened in the previous cases, the modification was not quantitative, which we attribute to incomplete efficiency of the translocation process. However, because here we are assaying a double helix fragment chances are that the pool of unmodified protein contains species where both helices were successfully inserted (see figure 6.4, J). To test this possibility a chimera of the LepΔH1 model protein was assayed. The result is shown in figure 6.5, E, lanes 5 and 6. Part of the protein appears as a band corresponding to glycosylation of one site, which is due to the TM insertion of just one fragment (figure 6.5, D), most likely the more hydrophobic α-helix 6. However, most of the LepΔH1/Bid-α6α7 fusion retained after alkaline wash is not glycosylated, corresponding to insertion of both α-helix 6 and 7. The urea and Triton-X114 treatments (figure 6.7, F ,G, lanes 3 and 6) support that the LepΔH1/Bid-α6α7 chimera is an integral membrane

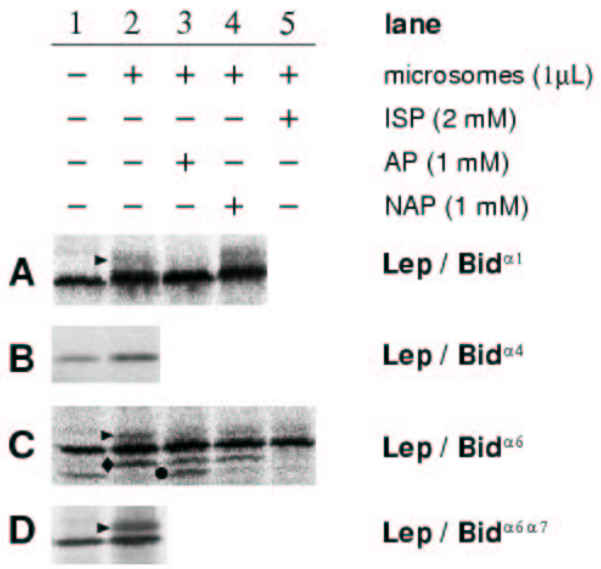

Figure 6.7.: SDS-PAGE analysis of Lep/Bid constructs. Lep chimeras containing Bid hydrophobic fragments in place of TM domain H2 were translated in vitro using reticulocyte lysate and ^{35}S-methionine in the absence (lane 1) and presence (lanes 2-5) of dog pancreas microsomes. Glycosylation acceptor (AP) and non-acceptor (NAP) tripeptides were added in the reactions corresponding to lanes 3 and 4, respectively. Lane 5 is from translation reactions containing an inhibitor of the signal peptidase (ISP). Marks indicate glycosylated products (black triangle), processed and glycosylated products (black diamond), and processed and non-glycosylated products (black circle).

protein.

6.5. Short discussion and conclusion of this chapter

Although the results are widely and globally discussed in Part III of this thesis, we record here the main ideas that can already be extracted from the results presented in this chapter. We make also a summary of main conclusions, as well as open questions to be addressed in the following chapters.

7. Activity studies

The function of many Bcl-2 proteins has been related to their ability to permeabilise membranes, and the double-helix hairpins buried in the core of the soluble structures of Bax, Bid and Bcl-xL, are considered to be the pore-forming domains in these proteins. Although these domains have a significant amphipatic character, they are predominantly hydrophobic. As we have shown in the previous chapter for chimeric model systems, the hairpins associate tightly to biological membranes, although only the first helix of these domains is found to act independently as TM.

In this chapter we focus on the permeabilising activity of peptides encompassing the individual helices[1] of the hairpin domain. The peptides are obtained by chemical synthesis and assayed on lipid vesicles of different composition and planar lipid bilayers. Poration activity is found, which resembles the activity of the full-length proteins. Moreover, the properties of the characterised pores and channels allow proposing a model for their mechanism of action.

7.1. Ability to induce the release of contents from LUVs

Permeabilisation of model membranes at a macroscopic level was studied by measuring the release of calcein from LUVs made of different lipid compositions. Interestingly, not all the peptides were able to permeabilise the vesicles at relatively low concentrations. In all cases, Bax-α5 and Bax-α6 induced efflux of the fluorescent dyes at nanomolar concentrations, although the Bax-α5 peptide

[1] The peptides used for this study contain the segments that in the full-length, water soluble parent proteins make the fifth and sixth α-helices of Bax and Bcl-xL, and the sixth and seventh α-helices in the case of Bid. These are part of a characteristic hairpin that is taken as a signature domain of this type of proteins. Fragments of these proteins encompassing any of the original helices are normally named with the word "helix" followed by the corresponding order number, and we just follow this use. Thus, this way of naming the fragments should not be taken as a priori assumption of their structure, nor as a qualitative structural description.

displayed higher poration activity (figure 7.1). In the case of Bax-α5, two versions of the peptide were synthesised and analysed[2]. In the case of Bax-α5 In the case of the peptides derived from Bid, Bid-α6 provoked calcein outflow at two order of magnitude higher concentrations, while Bid-α7 shows permeabilising activity at concentrations in the micromolar range. On the other hand, Bcl-xL-α5 and Bcl-xL-α6 only released calcein at micromolar concentrations. Additionally, the activities of the different peptides displayed markedly distinct responses to changes of lipid properties. To better understand the influence of the lipidic environment, the effect of the lipid composition of the LUVs was systematically analyzed.

7.1.1. Activity of Bax peptides

Influence of lipid charge

Because the peptides derived from the helix α5 from Bax present a net positive charge at neutral pH, an effect of net lipid charge on the activity of these peptides was expected. Thus, release of calcein was measured for LUVs made of pure PC (neutral), mixtures of PC and the negatively charged PA, PS and CL, and pure PA in the case of Bax-$\alpha5^K$. Similar experiments were carried out with Bax-α5 using LUVs composed of PC and mixtures of PC and PS or CL. Interestingly, the presence of negatively charged lipids reduced the activity of both peptides, that exhibited a similar pattern of activities (see table 7.1). This inhibiting effect is somewhat smaller in the case of PS than in the presence of PA or CL. A similar result was obtained with Bax-α6, which has a net neutral charge. In this latter case, the presence of CL or increasing concentrations of the negative PS results in a decrease of activity too. These results may indicate a negative effect of electrostatic forces on the activity of the Bax peptides (see Discussion, 7.1 on the facing page).

[2]Due to the high hydrophobicity of the sequence, we initially synthesised the peptide corresponding to the helix α5 of Bax with two flanking lysines in order to improve its solubility and hence its purification and handling (Bax-$\alpha5^K$, see 7.1 on the next page). For a second series of experiments, we were successful synthesising an extended version of the peptide, Bax-α5, containing exclusively the natural sequence. Moreover this second version encompasses a conserved region which is highly homologous with the helix α5 of Bcl-xL. Unexpectedly, Bax-α5 was soluble enough and exhibited a higher activity than Bax-$\alpha5^K$, but conserving the same activity pattern with the different lipidic compositions. The experiments carried out with both peptides indicate they behave comparably on lipid membranes, thus promoting much the same effects.

Table 7.1.: Effect of the lipidic composition on the release of calcein.

Lipid composition*	$1/C_{50}(\mu M^{-1})^{\$}$						
	Bax-α5	Bax-$\alpha5^K$	Bax-α6	Bcl-xL-α5	Bcl-xL-α6	Bid-α6	Bid-α7
Effect of lipid net charge							
PC	158.7	46.5	35.2	<0.5	0.56	<0.5	<0.5
PC:PS(75:25)	59.3	43.0	15.8	<0.5	0.56	2.85	0.73
PC:PS(50:50)	37.6	28.0	13.8	<0.5	0.88	6.07	1.4
PC:PS(25:75)		21.3				7.69	
PA		5.2				5.05	
PC:PA(50:50)		13.3				1.93	
PC:CL(90:10)	35.3	10.9	5.7	<0.5	<0.5	0.80	0.9
Effect of intrinsic monolayer curvature							
PC:LPC(95:5)	215.1	185.2	53.1	<0.5	0.88	<0.5	<0.5
PC:LPC(90:10)	238.1	238.1	69.4	<0.5	1.4	<0.5	<0.5
PC:LPC(80:20)		285.7				2.5	
PC:PE(95:5)		52.1				<0.5	
PC:PE(75:25)	198.0	56.4	28.3	<0.5	<0.5	<0.5	0.61
PC:PE(50:50)	175.4	63.5	16.3	<0.5	<0.5	<0.5	1.7
PC:PE:LPC(4:4:2)		158.7				0.64	
Others							
Asolectin		28.6				2.05	
DPhPC		0.42				<0.5	

*Lipid mixtures are reported on a molar base.

$^{\$}C_{50}$is defined as the micromolar concentration of the particular peptide causing 50% of calcein release. Typical standard deviations of the reported $1/C_{50}$ values were 8-12%.

Effect of intrinsic monolayer curvature

The poration activity of full-length Bax and Bax-type proteins is greatly influenced by the intrinsic monolayer curvature of membrane lipids. The presence of lipids with a positive intrinsic curvature, like lysophospholipids, enhances Bax activity, while the opposite is observed for lipids with a negative intrinsic curvature Basanez et al. (1999). To investigate the role of intrinsic lipid curvature in the pores induced by Bax-α5 and Bax-α6, we carried out experiments of release of

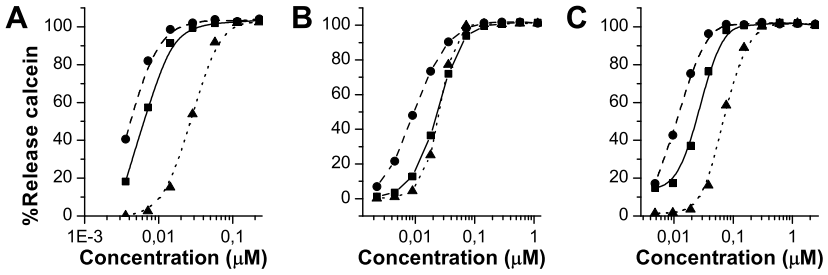

Figure 7.1.: Calcein release from LUVs induced by peptides derived from Bax. The percentage of calcein release calculated with equation 7.1 on the preceding page is represented as a function of the concentration of added peptide. A) shows the effect of Bax-α5, B) corresponds to Bax-$\alpha 5^K$ and C) to Bax-α6. Vesicles were prepared with the following compositions: (square) PC, (circle) PC:LPC (90:10) and (triangle) PC:PS (50:50).

calcein from PC LUVs containing increasing concentrations of lysophosphocholine (LPC), positively curved, or phosphatidylethanolamine (PE), negatively curved.

As shown in figure 7.1, a large increase (near 6 fold) of the permeabilising activity of the Bax-$\alpha 5^K$ peptide was observed in the presence of LPC. This marked effect was seen already at a 5% molar ratio of the lysophospholipid, with a much smaller increase between this ratio and 20% (table 7.1). Also an increase of activity is observed for Bax-α5, although the enhancing effect is smaller in this case, probably because Bax-α5 has already a high base activity in pure PC LUVs. In the case of Bax-α6, the presence of LPC also enhances the activity of the peptide, which doubles the observed calcein release at 10% LPC, compared to pure PC LUVs.

The effect of PE is summarised in table 7.1. The activity of Baxα6 is reduced significantly to about half of the base value in the presence of 50% PE. However, for Bax-α5 or Bax-$\alpha 5^K$, a small increase of activity was found in the presence of PE, up to a 50% molar ratio. Interestingly, in ternary lipid mixtures of PC:LPC:PE (40:40:20) , the enhancing effect induced by LPC appears to be attenuated by the presence of PE (table 7.1, Bax-$\alpha 5^K$). These results show that spontaneous lipid curvature greatly affects the permeabilizing activity of the Bax peptides, being principally enhanced by positive intrinsic curvature.

7.1.2. Activity of Bid peptides

Influence of the lipid charge

Both peptides, Bid-α6 and Bid-α7, contain a net positive charge and exhibited an enhanced calcein release in vesicles containing negatively charged lipids with respect to the neutral PC liposomes (see table 7.1). The Bid-α6 peptide displayed permeabilising activity in the nanomolar range only in LUVs with a net negative charge, and the effect of PS is stronger than that of PA or CL. This clearly indicates an influence of electrostatic forces in the activity of this peptide. However, the increase of activity for Bid-α7 due to the presence of negative charges was much less pronounced (figure 7.2).

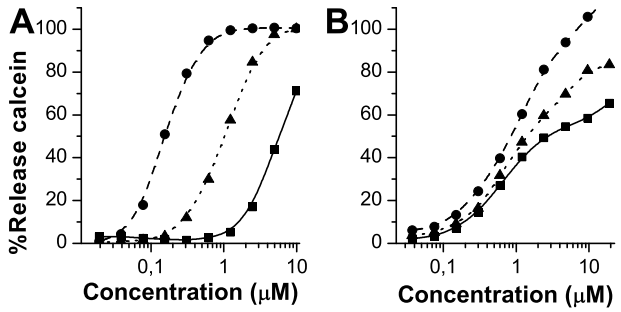

Figure 7.2.: Calcein release from LUVs induced by peptides derived from Bid. The percentage of calcein release calculated with equation 12.1 on page 193 is represented as a function of the concentration of added peptide. A) shows the effect of Bid-α6, and B) corresponds to Bid-α7. Vesicles were prepared with the following compositions: (square) PC, (circle) PC:PS (50:50) and (triangle) PC:CL (90:10).

Effect of the intrinsic monolayer curvature

In contrast to the behaviour observed for the peptides derived from Bax, when vesicles containing LPC or PE were assayed for the activity of Bid-α6 and Bid-α7 only small increments of the calcein release were observed (table 7.1). These results suggest that the intrinsic monolayer curvature of lipids is not a key parameter affecting the permeabilising activity of the Bid peptides.

7.1.3. Activity of Bcl-xL peptides

The helices $\alpha 5$ and $\alpha 6$ of Bcl-xL show an important level of sequence homology with the corresponding fragments of Bax (figure 9.5 on page 174). However, the peptides derived from the Bcl-xL helices exhibit a weak permeabiling activity in LUVs (approximately three orders of magnitude lower) compared to the activity of the Bax peptides (figure **??** and table 7.1). In the case of Bcl-xL-$\alpha 5$, release of calcein is observed for concentrations of the peptide well above 1 μM for any of the lipidic compositions employed. On the other hand, Bcl-xL-$\alpha 6$ displayed a slightly higher activity, in the micromolar concentration range, which was increased to some extent in the presence of LPC or PS when compared with pure PC LUVs (see table 7.1).

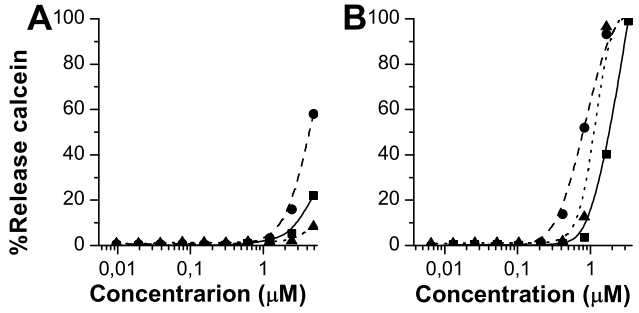

Figure 7.3.: Release of calcein from LUVs induced by Bcl-xL peptides. The percentage of calcein release calculated as in equation 12.1 on page 193 is represented as a function of the concentration of added peptide. A) shows the effect of Bcl-xL-$\alpha 5$, and B) corresponds to Bcl-xL-$\alpha 6$. Vesicles were prepared with the following compositions: (square) PC, (circle) PC:LPC (90:10) and (triangle) PC:PS (50:50).

7.2. Study of the pore size: Release of high molecular weight dextrans

Because the functional role of apoptotic Bcl-2 proteins is releasing proteins from the mitochondrial intermembrane space, we want to have a estimate of the size

of the pores formed by our fragment peptides. With this aim, we evaluated the induced release of partners larger than calcein (MW 622.55), like 20 kDa and 70 kDa dextrans labeled with fluorescein (FD-20 and FD-70, respectively) from LUVs. Exit of entrapped dextrans at self-quenching concentrations, was monitored as an increase in the fluorescence intensity with time, due to the dilution of the fluorescent probe, as is released to the external solution, figure 7.4.

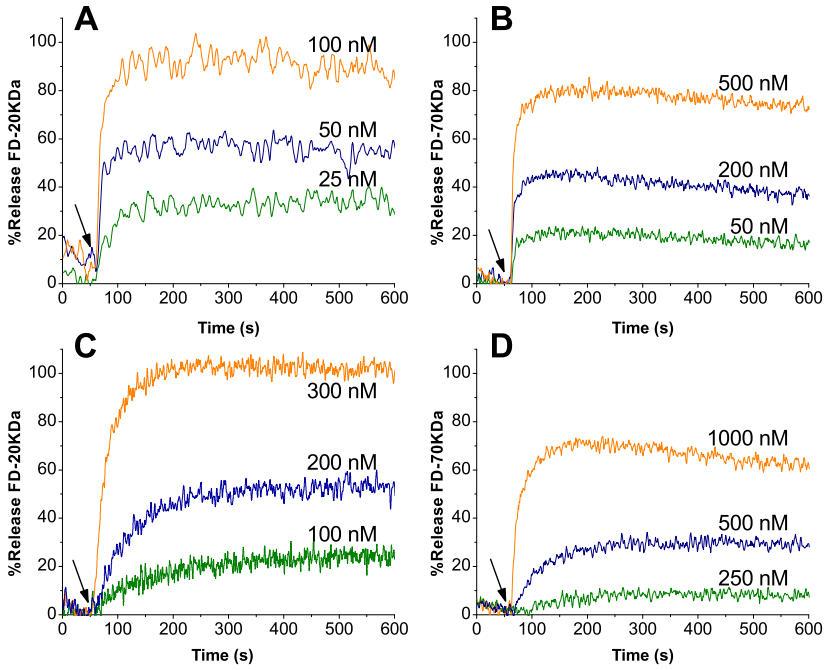

Figure 7.4.: Release of fluorescein-labeled dextrans. A) and B) show the time dependent percentage of release of FD-20 and FD-70 from egg PC LUVs induced by Bax-α5, at the concentrations indicated. C) and D) show similar experiments performed with Bax-α6 at the concentrations indicated in the graph. The arrow indicates the time of addition of the corresponding peptides to the vesicle suspension.

We observed that both Baxα5 and Baxα6 provoked the release of dextrans at nanomolar concentrations. In the case of Baxα5, release of FD-20 is produced at peptide concentrations similar to those observed for the concerted action of Bax

and tBid, but higher concentrations were needed to release equivalent percentages of FD-70. As observed previously in the calcein experiments, the membrane permeabilising activity of Baxα6 was lower, and it needed twice the concentration of Baxα5 to promote a similar release of FD-20. Again, the Baxα6 peptide required higher concentrations to release FD-70 to a similar extent. In contrast, none of the peptides from Bcl-xL and Bid, assayed at concentrations up to 10 μM were able to induce the release of FD-20 from egg PC LUVs.

These results indicate that only the peptides derived from Bax form large pores in lipidic vesicles, enough to allow the exit of molecules with sizes comparable to those of proteins.

However the possibility existed that the permeabilising activity was due to micellisation of the LUVs membrane. In fact, such a "detergent-like" mechanism has been described for some antimicrobial peptides, such as melittin at micromolar concentrations, which solubilise the membranes into small fragments or disk-like structures Dufourcq et al. (1986). To address this question, we measured the changes in the size distribution of egg PC LUVs after treatment with the peptides using quasi-elastic light scattering. The results obtained in one representative experiment are collected in table 7.2.

Table 7.2.: Effects of Baxα5, Baxα6 and Triton X-100 on the LUV size and on the release of FD-20 from LUVs.

Additive*	%Release of FD-20	LUV size (nm)	Polydispersity	Intensity (kc/s)
None	0	154.4	0.064	15.9
Baxα5	99.5	176.8	0.158	15.7
Baxα6	56.5	174.8	0.173	15.4
Triton X-100	100	172.1	1	3.6

* Baxα5 concentration was 50 nM, Baxα6 concentration was 120 nM and concentration of Triton X-100 was 1 mM.

As a control of vesicle solubilisation, we added 1 mM Triton X-100, which is the detergent used in the release experiments to accomplish 100% of release. The detergent effect of Triton X-100 dramatically decreased the intensity of the signal and increased the polydispersity of the measure. This indicates that most of the vesicles were destroyed, while those still remaining exhibited an unchanged size. When the peptides, Baxα5 or Baxα6, were added at concentrations which provoked the release of substantial amounts of FD-20 kDa, neither the size dis-

tribution of LUVs nor the intensity of the scattered light were affected.

7.3. Ion channel activity in PLM

To study the characteristics of the pore formed by Bax and Bid peptides at a microscopic level, we performed experiments using planar lipid bilayers. This technique allows the characterization of single channel properties, as voltage dependence and ionic selectivity **?**. We performed these studies with peptides Bax-$\alpha 5^K$ and Bid-$\alpha 6$.

With planar bilayers made of DPhPC, which easily forms stable membranes, the number of channel events induced Bax-$\alpha 5^K$ was very low, and negligible in the case of Bid-$\alpha 6$ (not shown). In agreement with this behavior, both peptides displayed a reduced release of calcein from LUVs containing DPhPC, compared to LUVs made of PC alone (table 7.1). However, when bilayers made of PC:PA (4:1 molar ratio) or asolectin (a natural mixture of plant lipids) were assayed, the two peptides exhibited channel activity. We had previously tested asolectin membranes for calcein release from LUVs (table 7.1).

Just upon addition of Bax-$\alpha 5^K$ to asolectin planar bilayers, it demonstrated interaction with the membranes at low positive potentials. Yet, from +10 mV on, a continuous increase in the current was observed. This behavior was maintained at higher voltages and the slope current/time increased also with the potential applied. However, such an effect was absent at negative potentials, for which no currents were seen, while the same level of currents was recovered when we changed again to positive voltages (figure 7.5, A). These results suggest that positive voltages induce adsorption of Bax-$\alpha 5^K$ to the lipid bilayer and formation of microchannels. In this state, the peptide remains attached to the membrane at negative potentials, although no discrete channel activity occurs at these latter conditions. The current/voltage plot of such a conductance state revealed some voltage dependence, as shown in figure 7.6.

At a certain point, probably when the concentration of Bax-$\alpha 5^K$ attached to the membrane achieved a critical level, very high conductance pores were observed (figure 7.5, B), which varied between 0.3 and 5 nS. The current/voltage characteristics obtained for this second state are given in figure 7.6, which shows no voltage dependence of the single channel conductance. This channel kept open during a long time at both positive and negative voltages, revealing a different behavior from the fluctuations seen before, and eventually provoked membrane disruption.

The permeabilising effect of Bax-$\alpha 5^K$ on planar lipid membranes was unex-

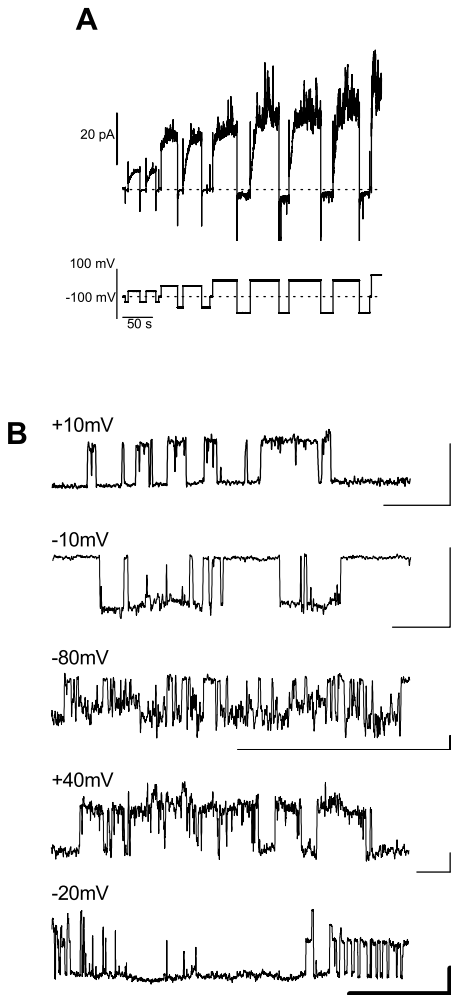

Figure 7.5.: Formation of ion channels by Bax-$\alpha 5^K$ in planar lipid membranes. Addition of Bax-$\alpha 5^K$ to the buffer bathing the *cis* side of asolectin planar lipid membranes increases the ion flux across the bilayer. A) Just upon addition of the peptide, a microchannel-like increase in the ion current was observed at positive potentials. B) Step-like current increases corresponding to the opening of one large single channel (0.3-5 nS) were observed at several voltages, as indicated in the traces. The reference scales on the right bottom of the traces indicate 5 pA on the Y-axis and 2 s on the X-axis, except in the last trace, where the thicker scale refers to 50 pA on the Y-axis and 20 s on the X-axis.

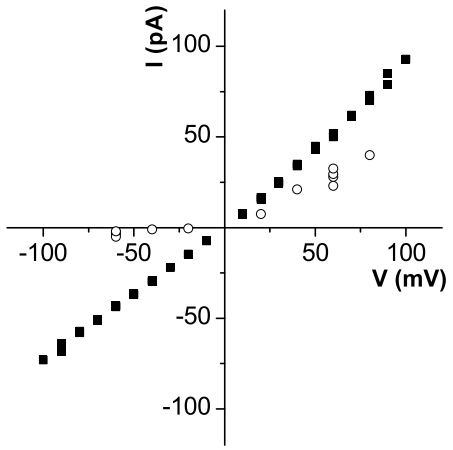

Figure 7.6.: Current/voltage representation of the different permeabilising activities displayed by Bax-$\alpha 5^K$ corresponding to figure 7.5 A (white circle) and B (black square).

pected for typical ion channels, which usually show more discrete and reproducible conductance states and do not affect membrane stability, at least at low concentrations. A likely possibility is that toroidal pores are being formed, in which both, the peptide and membrane lipids, are involved Basanez et al. (1999). If this is indeed the case, the ionic selectivity of the pores should depend on the electrical charge of the membrane lipids. To test this hypothesis we measured the ionic selectivity in neutral and negatively charged membranes Anderluh et al. (2003). We found that pores were cation selective in asolectin membranes (negatively charged), but showed no selectivity on DPhPC membranes (neutral) (see table 7.3). This effect strongly suggests that the pore lumen is lined by both, peptide molecules and lipid head groups.

In the case of Bid-$\alpha 6$, different channel characteristics were again observed as compared to Bax-$\alpha 5^K$. Addition of the peptide to the solution bathing a PC:PA (4:1 molar ratio) planar bilayer produced the opening and closure of different discrete channels of small conductance. Up to eight step current-like transitions, representative of ion channel formation, were observed simultaneously open (figure 7.7). The statistical analysis of these transitions led to an estimation of the conductivity comprised between 13 and 15 pS. These channels opened equally at both, positive and negative potentials, in a voltage-independent channel gating

Table 7.3.: Ion selectivity of Bax-α5^K in planar lipid membranes.

	P+/P-[2]	
[NaCl](M)[1]	Asolectin[3]	DPhPC[3]
0.27	6.5	-
0.43	5.9	1.0
0.57	6.2	1.0
0.70	6.2	1.1
0.82	6.3	1.4
0.93	-	1.8

[1] Saline concentration on the trans side. On the cis side, [NaCl] was always 0.140 M.
[2] Ratio between the permeability cations (P+) and to anions (P-) that expresses the ionic selectivity. Values above 1 indicate a cation selective channel. Values below 1 indicate that the channel is selective for anions. A ratio of 1 indicates no selectivity for cations or anions.
[3] Membrane composition.

manner.

7.4. Lipid transbilayer diffusion

Permeabilisation of membranes through formation of partially lipidic pores, as suggested by the results above for the Bax derived peptides, implies the contact between the two leaflets of the bilayer by means of non-lamellar structures created by the pore lining lipids. As a consequence of this structure, the movement of lipids from one monolayer to the other is allowed. If a peptide molecule is able to induce such structures, it should also promote lipid transbilayer diffusion. To test this possibility, we used the assay developed by Muller et al. Muller et al. (2000) and described in section 7.1 on page 113. Briefly, it is based on the spectral changes observed upon redistribution of pyPC from the external leaflets to both of them. Incorporation of pyPC to LUV composed of egg PC was fast, and the ratio I_E/I_M remained practically constant during a time-course of 20 min in the absence of peptides, indicating that the spontaneous transbilayer movement of the fluorescent analogue is negligible (not shown). As shown in figure 7.8, addition of the peptides derived from Bid or those derived from Bcl-xL, up to a concentration of 2 μM, showed no effect on the redistribution of pyPC between the two monolayers. In contrast, addition Bax-α5 or Bax-α6 at nanomolar concentrations induced a rapid decrease of the I_E/I_M ratio, and thus,

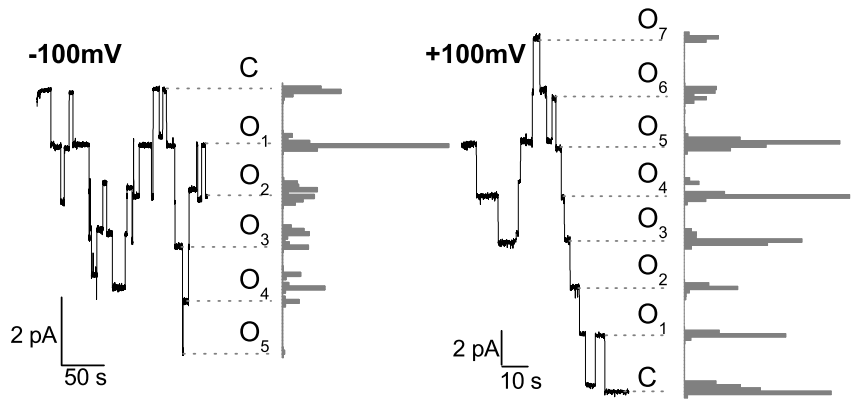

Figure 7.7.: Ion channel activity displayed by Bid-α6 in planar lipid membranes. When a solution containing Bid-α6 was added to the buffer bathing the cis side of the membrane, discrete increases of the ionic current through the bilayer were observed. Each step-like current increase corresponded to the opening of one single channel with an average conductance of 13-15 pS. The closed state (C) and the different open levels (O_i) are marked with dotted lines, where i is the number of single channels simultaneously open at the indicated voltages. On the right hand side, the occupation histogram of each level is reported. The membrane composition was PC:PA (1:1).

a rapid transbilayer lipid distribution.

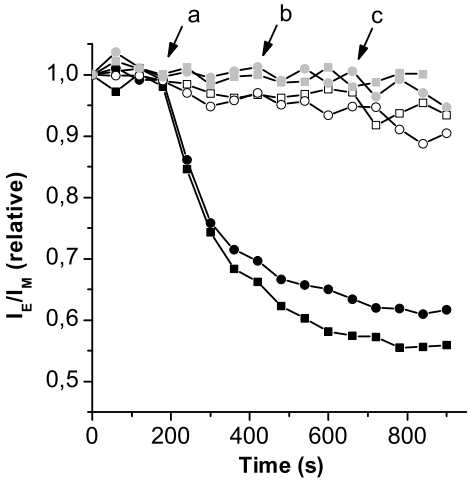

Figure 7.8.: Time dependent induction of lipid transbilayer diffusion exerted by the peptides derived from Bax, Bid and Bcl-xL. The decrease with the time of the I_E/I_M fraction upon addition of Bax-α5 at 20 nM (black squares) and Bax-α6 at 40 nM (black circles) is shown. The peptides derived from Bid, Bid-α6 (white squares) and Bidα7 (white circles), and those derived from Bcl-xL, Bcl-xL-α5 (gray squares) and Bcl-xL-α6 (gray circles), did not affect significantly I_E/I_M . In the case of these latter peptides, three consecutive additions of peptide were performed: final concentration of 500 nM was added at the time indicated by the first arrow, while the second and third arrows indicate addition of up to 1 μM and 2 μM of peptide, respectively.

Figure 7.9 shows the redistribution of the fluorescent lipid analog to the inner leaflet as a function of concentration of Bax-α5 or Bax-α6. For both peptides, maximum activity was observed at concentrations of the same order as for the activity of full length Bax and mixtures of Bax and tBid Terrones et al. (2004). However, this activity is more pronounced in the case of Bax-α5, as Bax-α6 needed twice the concentration of Bax-α5 to achieve a comparable decrease of I_E/I_M.

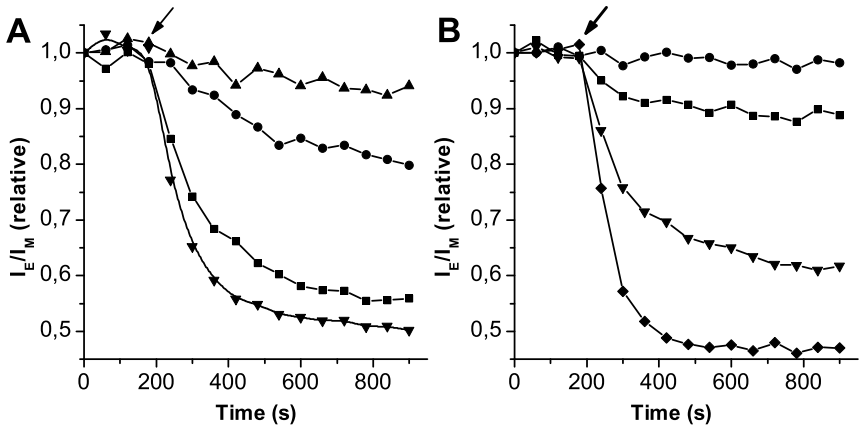

Figure 7.9.: Concentration dependent induction of lipid transbilayer diffusion displayed in the presence of Bax-α5 and Bax-α6. The time dependent decrease of I_E/I_M induced at different concentration of the peptides was analysed: 100 nM (diamond), 40 nM (triangle down), 20 nM (square), 10 nM (circle) and 5 nM (triangle up). The arrow indicates the moment of addition of peptide.

8. Structural studies

To better understand the activity observed for the different peptides, we performed a structural characterisation of these molecules using CD and ATR-FTIR. These techniques allow the rapid qualitative analysis of the content in secondary structure of the peptides, and the study of the effects of different environmental conditions. The CD spectra were analysed using the CDpro package, which combines analysis with the CDSSTR, the CONTINLL and the SELCON3 programs (see 4.5.1). In the case of Bax-$\alpha 5^K$ and Bid-$\alpha 6$, we performed also a quantitative analysis of the FTIR spectra, thus obtaining the percentages of the different elements of secondary structure present in the samples, and a estimation of the orientation of the peptides with respect to the membrane plane.

8.1. Peptides derived from Bax

Bax-$\alpha 5^K$

The secondary structure of Bax-$\alpha 5^K$ was analyzed by CD in aqueous media (figure 8.1, dotted lines) and in the presence of different concentrations of TFE (figure 8.1, A) or SDS (figure 8.1, B). Both lipid-mimetic environments induced a large change in the conformation of the peptide, with respect to the spectra in water, which was globally consistent with an increase of the α-helical structure.

To obtain a more detailed structural description, the CD spectra were analyzed by using the CDPro suite of programs (SELCON3, CONTIN/LL and CDSSTR) (Sreerama and Woody, 2000, 2004). Similar results were obtained with the three programs and using the reference set of proteins SMP50, which includes 37 soluble and 13 membrane proteins, therefore supporting the reliability of the structure estimation. The results obtained from the use of the different methods were finally averaged for each peptide and the dispersion of the results was estimated calculating the standard deviation (see table 8.1).

In aqueous media, Bax-$\alpha 5^K$ contained less than 10% helical structure, being predominantly in a disordered state. However, the presence of TFE (up to 60%, figure 8.1, A) induced over 60% helical conformation, of which around 20%

Table 8.1.: Secondary structure of the peptides derived from Bax, after analysis of the CD spectra using the CDPro package.

		% Secondary structure[c]											
		H(r)		*H(d)*		*S(r)*		*S(d)*		*Trn*		*Unrd*	
Peptide[a]	**Medium**[b]	*Av*	*s*	*Av*	*s*	*Av*	*s*	*Av*	*s*	*Av*	*s*	*Av*	*s*
	buffer	2	2	5	1	22	3	12	1	23	1	36	1
	20% TFE	34	1	18	0,4	5	1	5	0,1	15	1	23	1
Bax-$\alpha 5^K$	60% TFE	37	2	21	1	3	1	4	1	14	1	21	1
	0.5mM SDS	29	3	15	0,3	9	0,4	5	1	18	1	24	2
	4mM SDS	34	1	18	1	5	1	4	0,3	16	1	23	6
	buffer	23	6	15	2	10	2	7	1	19	4	26	3
	20% TFE	62	5	26	2	0	1	0	1	3	1	9	6
Bax-$\alpha 5$	60% TFE	61	5	27	2	0	1	0	2	1	1	11	5
	0.5mM SDS	63	6	19	3	1	2	0	1	4	4	13	4
	4mM SDS	61	4	25	3	0	1	0	1	4	2	10	6
	buffer	13	1	10	1	20	4	9	1	20	2	28	3
	20% TFE	27	4	15	0,2	8	1	6	0,2	18	2	26	2
Bax-$\alpha 6$	40% TFE	40	4	22	2	2	1	3	1	12	3	21	2
	0.5mM SDS	33	3	16	0,2	8	1	5	0,3	15	2	23	3
	4mM SDS	42	1	19	0,3	3	1	2	0,3	11	1	22	1

[a] All measurements were performed at 30 μM concentration of the corresponding peptide.

[b] Buffer medium was 10 mM NaH_2PO_4 at pH7. TFE or SDS were added at the concentrations indicated, over a 10 mM NaH_2PO_4 solution.

[c] H: helix, S: strand, Trn: turn, Unrd: unordered, (r): regular and (d): distorted, as defined by the standard output of CDPro. *Av* is the average of the results obtained with CDSSTR, CONTINLL and SELCON3, and *s* is the standard deviation.

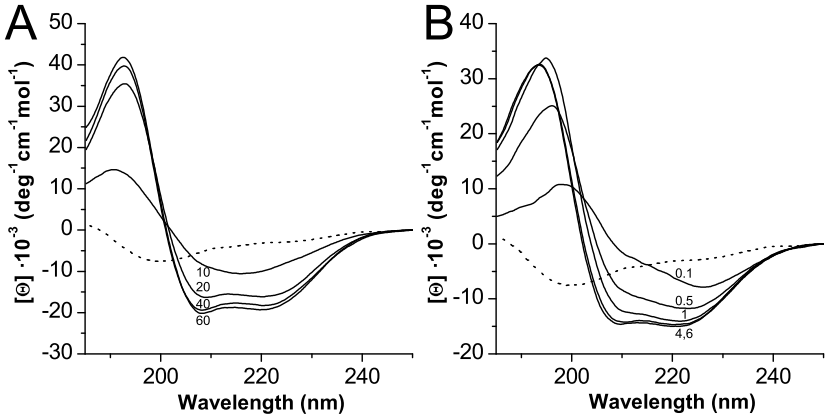

Figure 8.1.: CD spectra of Bax-$\alpha 5^K$ in lipid-mimetic media. A and B show the spectra of Bax-$\alpha 5^K$ in the pure aqueous buffer (dotted lines) or titrated with increasing amounts of TFE or SDS, respectively (solid lines). In all samples the peptide was at a 30 μM concentration, and the aqueous buffer was 10 mM sodium phosphate, pH 7.0. The amounts of added TFE (in percentage) or SDS (in mmol/L) are indicated in the graphs.

corresponded to a distorted α-helix. A similar effect was observed for samples containing up to 6 mM SDS (figure 8.1, B), where more than 50% of the peptide conformation was α-helical, even below the critical micellar concentration (table 8.1). Interestingly, almost all the helical structure was already induced at low concentrations of TFE (20%) or SDS (5 nM).

The FTIR-spectra obtained for Bax-$\alpha 5^K$, either in aqueous buffer or TFE solvent, and in the presence of lipid vesicles, are shown in figure 8.3, A. Structural changes were already evident when comparing the spectra in TFE with respect to aqueous media. The secondary structure composition was estimated by deconvolution and curve fitting with a set of single Lorentzian components, which were then attributed to different structural elements (figure 8.3, A, and table 8.2). The main difference was a significant decrease of the β-sheet aggregates in TFE, as compared to the aqueous buffer (from 40% to 20%), while the distribution of secondary structures in the non-aggregated part remained almost the same, i.e. 13% β-turn, 60% α-helix and 27% random coil. Interestingly, in the case of the

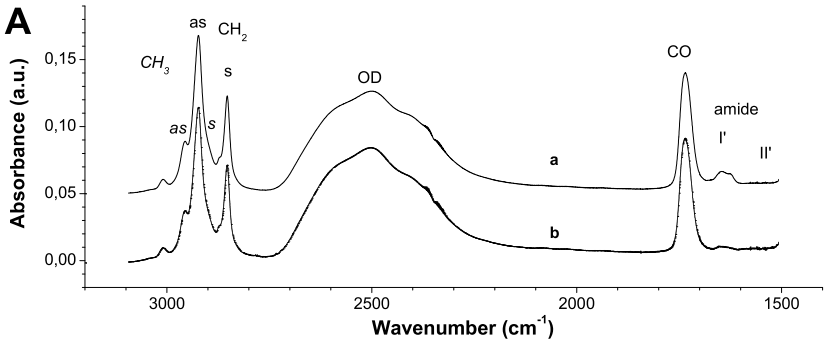

Figure 8.2.: Infrared attenuated total reflection spectra of Bax-$\alpha 5^K$ in PC vesicles. Deuterated films of Bax-$\alpha 5^K$ bound to PC vesicles (a, solid line) and PC vesicles alone (b, dotted line). Indicated are the bands corresponding to: CH_3 stretching (asymmetric, *as*, and symmetric, *s*, at 2956 cm^{-1} and 2872 cm^{-1}, respectively); CH_2 stretching (asymmetric, *as*, and symmetric, *s*, at 2923 cm^{-1} and 2853 cm^{-1}, respectively); OD stretching of deuterated water; CO stretching of the phospholipid carbonyl groups; amide I' and II' bands.

Bax-$\alpha 5^K$ peptide, the α-helical structure was represented by two bands, one at around 1656 cm^{-1} (α_1) and the other at 1646 cm^{-1} (α_2). While the former exhibited a frequency in the typical range for α-helices, the latter had an unusually low frequency, which however had been previously observed in other membrane binding peptides, like in the case of melittin (Sharon et al., 1999).

Bax-$\alpha 5^K$ co-sedimented with LUVs of PC or PC:PA (1:1) was next analysed. The relative amounts of peptide bound to the lipid vesicles for the two lipid compositions is shown in table 8.2. A high portion of the peptide appeared bound to PC:PA LUVs, with a lipid/peptide (L/P) ratio of 80, quite near of the pre-centrifugation ratio of 50. In contrast, the amount of Bax-$\alpha 5^K$ bound to pure PC LUVs decayed to a half, with a L/P value of 160. Compared to the situation in aqueous buffer, we observed a significant decrease of the aggregated portion upon binding to PC:PA and PC LUVs, suggesting that the peptide bound to the membranes in the non-aggregated form. In this non aggregated portion, an increase in α-helical composition was also evident, at the expenses of β-turn and random structures (figure 8.3 and table 8.2).

The large amounts of β-type aggregates observed by FTIR for this and the

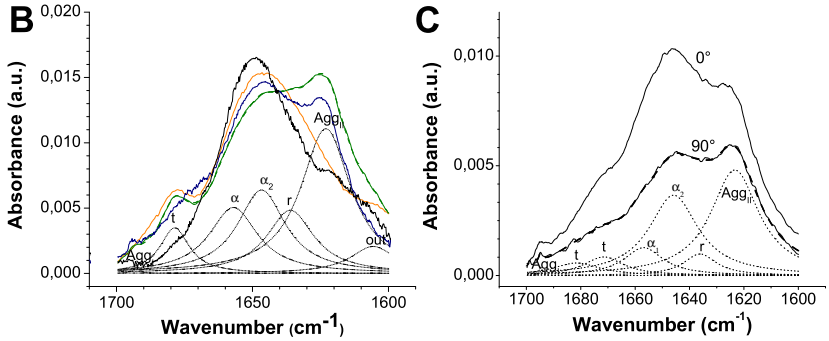

Figure 8.3.: Analysis of the amide I' band of deuterated films of Bax-$\alpha 5^K$ samples. B, Samples deposited from buffer (green solid line), from a TFE solution (orange line) and from a suspension of LUVs composed by PC (blue line) or PC:PA (1:1) (black line) are overlayed. The original spectrum (green line) was deconvoluted and curve fitted to resolve the component frequencies. The corresponding Lorentzian bands are reported as dotted lines and their sum (thick dashed green line) was superimposed to the original spectrum. Bands labeled as Agg_I and Agg_{II} derive from aggregated peptide and were excluded from the secondary structure calculation. The other bands are: t (β-turn); α_1 and α_2 (α-helix); r (random coil). The evaluated percentages of secondary structures are reported in 8.2. C, Spectra were taken with either parallel (0°) or perpendicular (90°) polarization. The amide I' region of Bax-$\alpha 5^K$ bound to PC vesicles was reported after subtraction of the lipid contribution. The best curve fit with Lorentzian components (dotted lines) was superimposed as a thick dashed line to the 90° polarized trace (solid line). The absorption bands in the parallel and perpendicular configuration were used to calculate the orientation of the corresponding structural element as reported in 8.3. Bands are: α_1 and α_2 (α-helix); t (turn); r (random coil) and $Agg_I$and Agg_{II} (aggregated peptide).

Table 8.2.: FTIR spectroscopic determination of the secondary structure of Bax-$\alpha 5^K$ in aqueous buffer, with and without lipids, and in TFE solvent.

Medium	**%Secondary structure**[a]					
	t	α_1	α_2	r	**%βAgg**[b]	**L/P**[c]
Wavenumber (cm^{-1})	1680±2	1656±1	1646±1	1636±1		
buffer	12	28	34	26	37	
TFE	13	27	33	27	17	
LUVs PC	5	38	47	10	34	160
LUVs PC:PA (1:1)	-	32	43	25	9	80

[a] t: β-turn, $\alpha_1$and α_2: α-helix, r: random coil. Percentages refer to the non-aggregated peptide.
[b] βAgg: total aggregated peptide calculated from the relative areas of the corresponding Lorentzian bands (Agg_I and Agg_{II} in 8.3).

[c] L/P: lipid to peptide molar ratio.

other peptides studied (see below), as compared to CD, may be explained by the different sample conditions used for each case. Thus, while samples for CD measurements were of low concentration and completely dissolved, in the case of FTIR measurements, aggregates may have build up while drying the samples during the preparation of the films over the germanium crystals.

From the 0° and 90° polarized spectra of the inserted peptide, it was possible to calculate the dichroic ratio of the helices and the orientation of their main axis with respect to the perpendicular to the plane of the membrane (Menestrina, 2000) (figure 8.3, B). With PC:PA LUVs, we obtained an average tilt angle ($\gamma_\perp$) of 55° and 83° for α_1 and α_2, respectively, of Bax-$\alpha 5^K$ (table 8.3). When we considered the average orientation of the lipid chains, their tilt angle was found to be 34° in the absence of peptide, and increased to 41° in the presence of Bax-$\alpha 5^K$. This finding means that the binding of the peptide increased lipid disorder. The tilt angles of the lipid chains were used to recalculate the relative orientation of the helices with respect to the axis of the lipid chains (Menestrina, 2000), providing an angle (γ_L) of around 59° and 90° for α_1 and α_2, respectively, of Bax-$\alpha 5^K$ (table 8.3).

In the case of the PC LUVs, the lipid chains had already an average tilt of about 42°, with respect to the normal of the membrane plane, and this did not change appreciably upon binding of the peptides, which was consistent with the lower binding observed. The orientation of the α-helical structures of Bax-$\alpha 5^K$, with respect to the lipid chains, was around 0° and 90° for α_1 and α_2, respectively.

This suggested that the distorted α-helix, α_2, seemed to be oriented parallel to the membrane surface independently of the lipid composition, while the regular α-helix, α_1, appeared fully immersed into the lipid matrix and its tilt decreased when negatively charged lipids were present.

Bax-α5

As shown in chapter 7, the two versions, Bax-$\alpha5^K$ and Bax-α5, exhibits a comparable permeabilising activity, in agreement with a common mechanism of action. In fact, the peptide with the flanking lysines displayed a slightly lower ability to release calcein. To assess the possible effects of the sequence differences on the structure of these molecules, we also measured the spectra of Bax-α5 by CD and ATR-FTIR in similar media and conditions as for Bax-$\alpha5^K$.

As shown in the CD spectra of figure 8.4, A and B, large conformational changes were induced by the presence of TFE or SDS, with respect to the peptide in pure aqueous buffer. However, and in contrast to Bax-$\alpha5^K$, Bax-α5 exhibited a significant proportion of α-helix structure already in aqueous media. The presence of this intrinsic helical structure, that reached nearly 40%, was corroborated in the calculations with the CDPro program (see table 8.1). Again, the addition of low amounts of SDS or TFE were enough to promote the maximum proportion of α-helix observed, which in this case reached the outstanding value of 90%, if we sum up the percentages of regular and distorted α-helix. Most of the helix induction took place at expenses of the β-strand structure, which completely disappeared in the presence of the lipid-mimetic reagents (table 8.1).

These results were in agreement with the ATR-FTIR spectra obtained for Bax-α5 in the different environments. The normalised amide I' region of the different spectra are depicted in figure 8.4, C. In samples made of Bax-α5 deposited onto the Ge crystal from an aqueous solution (figure 8.4, C, green line), the major contribution to the amide I' band aroused from β-aggregates, but a significant contribution of helical structure with an overall vibration around 1652 cm^{-1} also existed. The spectra corresponding to samples prepared in TFE, PC LUVs or PC:PA (1:1) LUVs are represented overlayed (figure 8.4). The structural changes induced by these media with respect to aqueous buffer are better appreciated in difference spectra, as represented in figure 8.4, D. The latter reveal that the conformational changes consisted mainly on the induction of helical structure, while the β-aggregate components at 1622-1626 cm^{-1} decreased. In contrast to Bax-$\alpha5^K$, the major conformational change was stimulated by the PC vesicles (blue line), followed by the PC:PA liposomes (black line) and the TFE solvent (orange line). Interestingly, the presence of PC LUVs induced the appearance of a

Table 8.3.: Orientation of the helical elements of Bax-$\alpha 5^K$ and Bid-α6 bound to PC and PC:PA membranes. Also reported is the assignment and dichroic ratio of some relevant IR bands.

Wave number (cm^{-1})	**Vibration**[a]	$(\Theta)^b$	**PC** Dichroic Ratio	Form Factor (S)	Angle $(\gamma_\perp)^c$	Angle $(\gamma_L)^d$	**PC:PA (1:1)** Dichroic Ratio	Form Factor	Angle $(\gamma_\perp)^c$	Angle $(\gamma_L)^d$
	Lipid alone									
2920	*as* CH_2 stret.	90°	1.59±0.01	0.31±0.01	43°±1°	-	1.36±0.01	0.51±0.01	34°±1°	-
2850	*s* CH_2 stret.	90°	1.56±0.01	0.33±0.01	42°±1°	-	1.34±0.01	0.53±0.01	34°±1°	-
2870	*s* CH_3stret.	0°	3.20±0.70	0.25±0.13	45°±5°	-	4.50±0.90	0.42±0.09	38±4°	-
	Bid-α6									
2920	*as* CH_2 stret.	90°	1.53±0.01	0.35±0.01	41°±1°	-	1.46±0.01	0.42±0.01	38°±1°	-
2850	*s* CH_2 stret.	90°	1.49±0.01	0.39±0.01	40°±1°	-	1.42±0.01	0.45±0.01	37°±1°	-
2870	*s* CH_3 stret.	0°	3.90±0.70	0.36±0.08	40°±4°	-	3.80±0.60	0.34±0.11	41°±4°	-
1655	Amide I' α	30°	2.10±0.10	0.04±0.05	53°±2°	50°±5°	2.58±0.03	0.24±0.01	46°±1°	34°±2°
	Bax-$\alpha 5^K$									
2920	*s* CH_2 stret.	90°	1.51±0.01	0.36±0.01	40°±1°	-	1.53±0.01	0.35±0.01	41°±1°	-
2850	*as* CH_2 stret.	90°	1.48±0.01	0.40±0.01	39°±1°		1.50±0.01	0.38±0.01	40°±1°	-
2870	*s* CH_3 stret.	0°	3.40±0.80	0.27±0.13	44°±4°		3.50±0.80	0.29±0.18	43°±4°	-
1656	Amide I' α_1	30°	3.64±0.22	0.52±0.04	34°±2°	0°±2°	1.92±0.01	-0.04±0.01	55°±2°	59°±2°
1646	Amide I' α_2	30°	1.30±0.10	-0.40±0.10	80°±10°	90°±2°	1.22±0.01	-0.46±0.01	83°±2°	90°±2°

[a] *s*, symmetric; *as*, asymmetric

[b] Direction of the variation of the dipole moment associated to the vibration with respect to the direction of the main molecular axis (aliphatic chain or α-helix axis).

[c] Average angle between the direction of the molecular axis and the perpendicular to the crystal plane (i.e. the membrane plane).

[d] Average angle between the directions of the α-helix and the lipid chain axis.

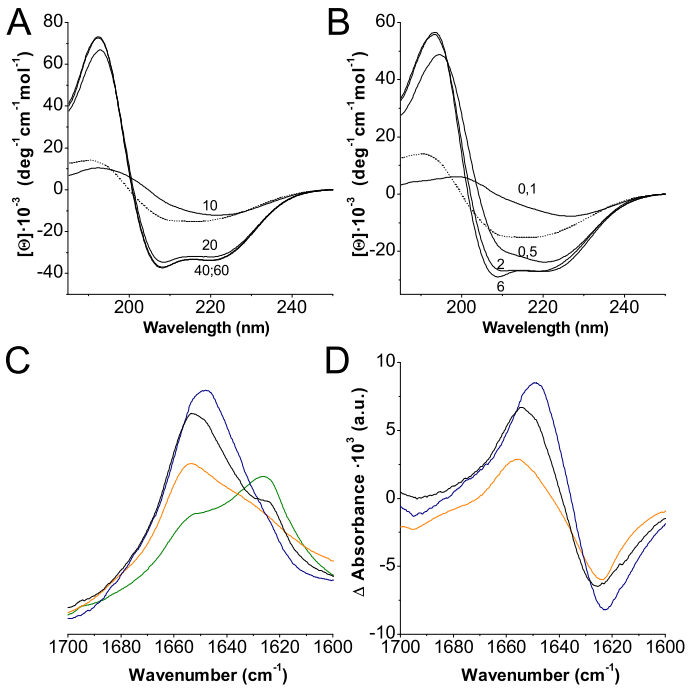

Figure 8.4.: CD and FTIR spectra of Bax-α5 in different media. A and B show the spectra of Bax-α5 in the pure aqueous buffer (dotted lines) or titrated with increasing amounts of TFE or SDS, respectively (solid lines). In all samples the peptide was at a 30 μM concentration, and the aqueous buffer was 10 mM sodium phosphate, pH 7.0. The amounts of added TFE (in percentage) or SDS (in mmol/L) are indicated in the graphs. C, amide I' band of Bax-α5 in lipid bilayers deposited from aqueous buffer (green), TFE (orange), and suspensions of LUVs made of PC (blue) and PC:PA (1:1) (black). Spectra have been normalised to the amide I' region for comparison. D, difference spectra of the amide I' region obtained by subtraction of the normalised spectra of Bax-α5 deposited from TFE (orange) and suspensions of PC LUVs (blue) or PC:PA (1:1) LUVs (black), from the normalised spectra of the same peptide in aqueous buffer.

maximum of absorption at 1648 cm^{-1}, which was comparable to the α_2 component observed for Bax-$\alpha 5^K$, while the maxima of the peaks induced by PC:PA vesicles or TFE were in the range of more typical α-helices, at 1652-1654 cm^{-1}.

Bax-α6

The permeabilising activity displayed by the fragment corresponding to the second helix of the hydrophobic hairpin in Bax, Bax-α6, was very similar to that observed for the peptide corresponding to the first helix of the hairpin, Bax-α5. However, the CD and ATR-FTIR experiments performed with Bax-α6 reveal some differences.

The CD spectra indicated that Bax-α6 presented around 20% helical structure in water, as observed in figure 8.5, A and B (see also8.1). The titrations with TFE or SDS induced an increase of the α-helical content, as expected. However in contrast to the behaviour of Bax-α5, Bax-α6 experimented a gradual increase in α-helix structure as the concentration of lipid-mimetic agents increased, which reached up to around 60% in 4 mM SDS or 60% TFE. This increment in α-helix was parallel to the decrease in the β-strand and turn contributions, while the percentage of unordered peptide remained practically the same (table 8.1).

The qualitative analysis of the ATR-FTIR spectra revealed that the major contributors to the amide I' band in Bax-α6 deposited from aqueous solution were β- type aggregates coming from unstructured peptide, and a distorted α-helix with a characteristic vibration at 1647 cm^{-1}(figure 8.5, C). Unexpectedly, the spectra obtained from a suspension of Bax-α6 with PC LUVs did not exhibit large conformational changes, although the helical component at 1647cm^{-1} was then more evident, as observed in figure 8.5, C and D. In contrast, the presence of TFE or PC:PA vesicles promoted considerable conformational rearrangements, which consisted on the decrease of the aggregated structures (bands at 1624-1628 cm^{-1}) and the appearance of a major helical element, with a canonical absorption at 1654 cm^{-1}.

8.2. Peptides derived from Bid

Bid-α6

When we analysed the CD spectra obtained for Bid-α6, we observed that about 30% of the peptide presented a random-coil structure in aqueous buffer, while the helical fraction reached approximately 20% (table 8.5). The addition of TFE again induced a rapid increase of the helical content, which reached values above

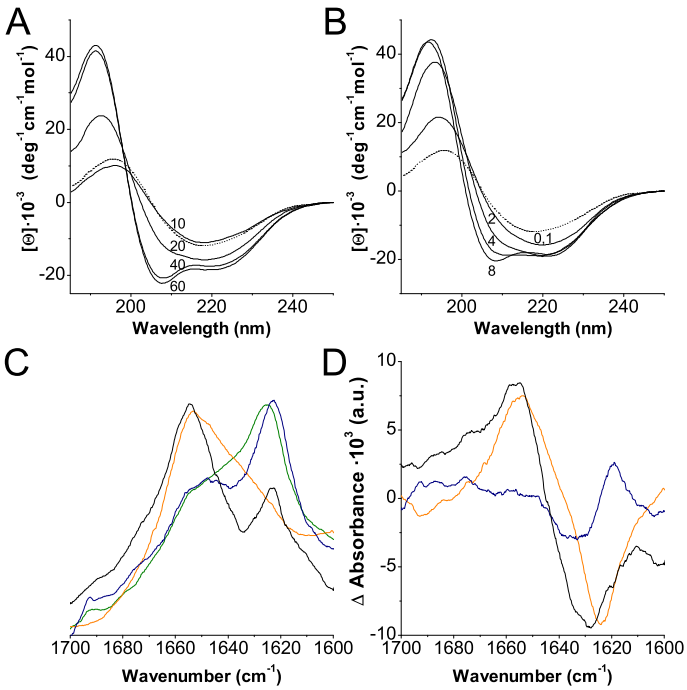

Figure 8.5.: CD and FTIR spectra of Bax-α6 in different media. A and B show the spectra of Bax-α6 in the pure aqueous buffer (dotted lines) or titrated with increasing amounts of TFE or SDS, respectively (solid lines). In all samples the peptide was at a 30 μM concentration, and the aqueous buffer was 10 mM sodium phosphate, pH 7.0. The amounts of added TFE (in percentage) or SDS (in mmol/L) are indicated in the graphs. C, amide I' band of Bax-α6 in lipid bilayers deposited from aqueous buffer (green), TFE (orange), and suspensions of LUVs made of PC (blue) and PC:PA (1:1) (black). Spectra have been normalised to the amide I' region for comparison. D, difference spectra of the amide I' region obtained by subtraction of the normalised spectra of Bax-α6 deposited from TFE (orange) and suspensions of PC LUVs (blue) or PC:PA (1:1) LUVs (black), from the normalised spectra of the same peptide in aqueous buffer.

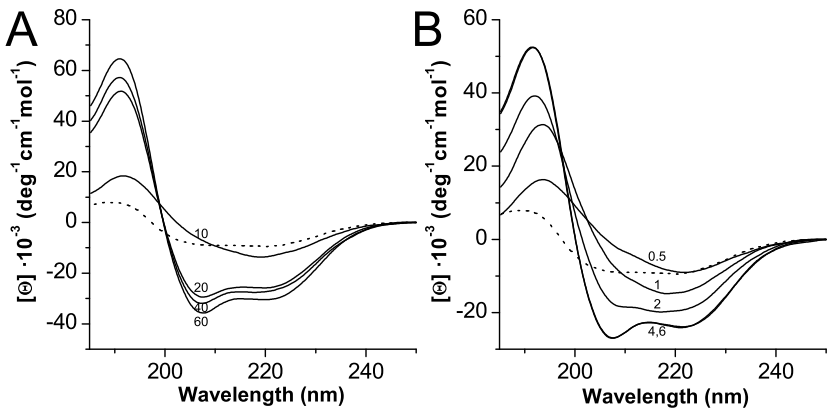

Figure 8.6.: CD spectra of Bid-α6 in lipid-mimetic media. A and B show the spectra of Bid-α6 in pure aqueous buffer (dotted lines) or titrated with increasing amounts of TFE or SDS, respectively (solid lines). In all samples the peptide was at a 30 μM concentration, and the buffer was 10 mM sodium phosphate, at pH 7.0. The amounts of added TFE (in percentage) or SDS (in mmol/L) are indicated in the graphs.

75%, with nearly 25% of it corresponding to a distorted α-helix (figure 8.6, A, and table 8.5). In the titration with SDS, high levels of helical structure also appeared, amounting to about 70% at 4 mM SDS. However, in this case, the induction of structure was more gradual and needed higher concentrations of detergent than in the case of the Bax peptides, as shown in figure 8.6, B.

Figure 8.7 shows the FTIR spectra obtained for Bid-α6 bound to PC:PA (1:1) LUVs and for PC:PA (1:1) LUVs in the absence of peptide. When we analysed quantitatively the amide I' region, we observed the presence of a large aggregated β-sheet component , as in the case of Bax-$\alpha 5^K$, which was resistant to TFE and constituted about 40% of the peptide (see figure 8.8, A and table 8.4). Passing from water to TFE, or to a suspension of lipid vesicles, the non-aggregated portion showed a strong increase in the α-helix content, from 30% to $>$ 70%, and a corresponding decrease of the random coil component. In contrast to Bax-$\alpha 5^K$, there was a single helical component in the case of Bid-α6, represented by a band at 1655$\pm$2 cm^{-1}, typical for α-helix.

When the spectra of Bid-α6 bound to vesicles were analysed, a significant

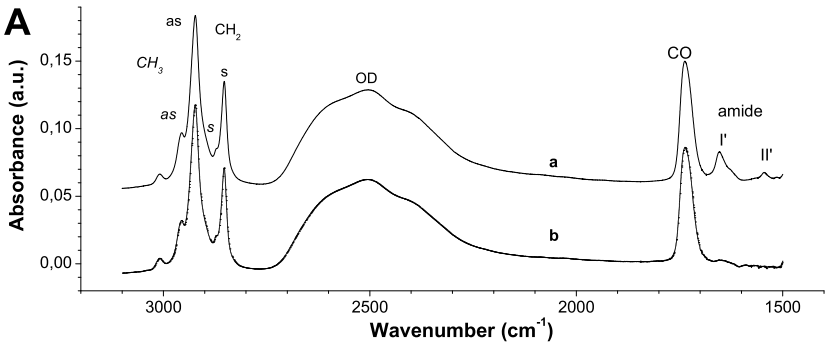

Figure 8.7.: Infrared attenuated total reflection spectra of Bid-α6 in PC vesicles. Deuterated films of Bid-α6 bound to PC vesicles (a, solid line) and PC vesicles alone (b, dotted line). Indicated are the bands corresponding to: CH_3 stretching (asymmetric, *as*, and symmetric, *s*, at 2956 cm^{-1} and 2872 cm^{-1}, respectively); CH_2 stretching (asymmetric, *as*, and symmetric, *s*, at 2923 cm^{-1} and 2853 cm^{-1}, respectively); OD stretching of deuterated water; CO stretching of the phospholipid carbonyl groups; amide I' and II' bands.

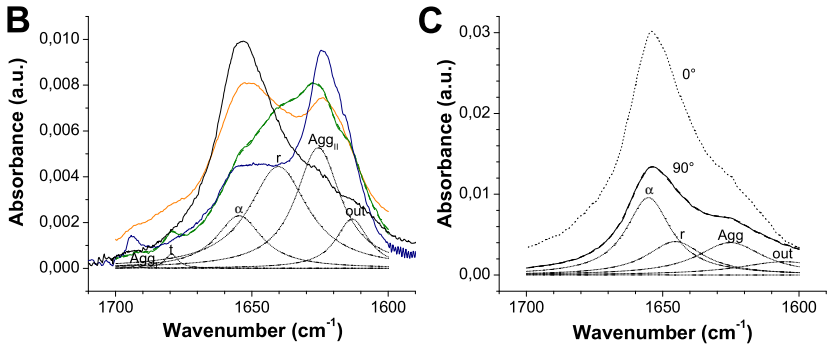

Figure 8.8.: Analysis of the amide I' band of deuterated films of Bid-α6 samples. Samples deposited from buffer (green solid line), from a TFE solution (orange line) and from a suspension of LUVs composed by PC (blue line) or PC:PA (1:1) (black line) are overlayed. The original spectrum (green line) was deconvoluted and curve fitted to resolve the component frequencies. The corresponding Lorentzian bands are reported as dotted lines and their sum (thick dashed green line) was superimposed to the original spectrum. Bands labeled as Agg_I and Agg_{II} derive from aggregated peptide and were excluded from the secondary structure calculation. The other bands are: t (β-turn); α (α-helix); r (random coil). The evaluated percentages of secondary structures are reported in table 8.4. C, spectra were taken with either parallel (0°) or perpendicular (90°) polarization, as indicated. The amide I' region of Bid-α6 bound to PC:PA (1:1) vesicles was reported after subtraction of the lipid contribution. The best curve fit with Lorentzian components (dotted lines) was superimposed as a thick dashed line to the 90° polarized trace (solid line). The absorption bands in the parallel and perpendicular configuration were used to calculate the orientation of the corresponding structural element as reported in table 8.3. Bands are labeled as: α (α-helix); t (turn); r (random coil) and Agg (aggregated peptide).

Table 8.4.: FTIR spectroscopic determination of the secondary structure of Bid-α6 in aqueous buffer, with and without lipids, and in TFE solvent.

Medium	% Secondary Structure[a]				
	t	α	r	%βAgg[b]	L/P[c]
Wavenumber (cm^{-1})	1681±1	1655±2	1642±3		
Buffer	2	29	69	39	
TFE	7	74	28	42	
LUVs PC	-	72	28	49	110
LUVs PC:PA (1:1)	-	60	40	21	56

[a] t: β-turn, α: α-helix, r: random coil. Percentages refer to the non-aggregated peptide.
[b] βAgg: total aggregated peptide calculated from the relative areas of the corresponding Lorentzian bands (AggI and AggII in ...).
[c] L/P: lipid to peptide molar ratio.

association of the peptide to PC:PA LUVs was observed. The L/P molar ratio in the pellet, estimated by using equation 5.10 on page 90, was around 55. This value is very similar to the pre-centrifugation ratio of 50 (see Materials and Methods, 5.10 on page 88), suggesting that virtually all the peptide was associated to the vesicles. With PC LUVs, instead, the estimated L/P was around 110, indicating a two-fold lower association. The relative affinity of Bid-α6 for the two lipid compositions showed the same trend observed for Bax-$\alpha5^K$, but in both cases it was about 1.5 times higher for Bid-α6 (table 8.4). This is in agreement with the fact that the presence of PC:PA (1:1) LUVs solubilise of an important part of the aggregated peptide, which decreased from ~40% to around 20% (table 8.4 and figure 8.8, A).

From the 0° and 90° polarized spectra of the membrane-bound Bid-α6 peptide, the dichroic ratio of the helices and the orientation of their main axis with respect to the perpendicular to the plane of the membrane were calculated Menestrina (2000) (see figure 8.8, B). With PC:PA LUVs we obtained an average tilt angle ($\gamma_\perp$) of 46° for Bid-α6 (table 8.3). When we considered the average orientation of the lipid chains, their tilt angle was found to be 38°. This value was larger than the 34° obtained for vesicles alone, and indicated that the binding of the peptide increased lipid disorder, like in the case of Bax-$\alpha5^K$. The relative orientation of the helices with respect to the axis of the lipid chains (γ_L) was calculated from these values Menestrina (2000), and an angle of around 34° was obtained for Bid-α6 (table 8.3).

Bid-α7

Titration of Bid-α7 with increasing concentrations of TFE and SDS gave rise to the CD spectra showed in figure 8.9. This peptide was also mainly unstructured in water solution, with circa 20% α-helix, and, as observed for the previous peptides, it adopted a prevailing helical conformation upon addition of the lipid-mimetic agents. In the case of Bid-α7, low amounts of TFE or SDS scarcely affected the overall structure, and concentrations of at least 40% TFE or 2 mM SDS were needed to induce significantly the helical component, which reached near 60% in the first, and almost 50% in the presence of 4 mM SDS (see table 8.5). The increase in helical structure was accompanied by a decrease in the β-strand and turn components, while the unordered structure remained practically the same.

Figure 8.9, C, shows the superposition of the normalised amide I' bands obtained from ATR-FTIR measurements of Bid-α7 deposited from aqueous buffer, TFE solvent or suspensions of PC or PC:PA (1:1) vesicles. In all cases, the major component of the amide I' region corresponded to β-aggregates with absorbances in the range of 1624-1629 cm^{-1}, which were resistant to TFE and lipid vesicles. Absorbances of other secondary structure components were present in the spectra, and corresponded to α-helix and turn structures, with vibrations in the range of 1649-1652 $cm^{-1}$and 1670 cm^{-1}, respectively. The difference spectra displayed in figure 8.9, D, illustrate the conformational changes induced by TFE or lipid vesicles with respect to the aqueous solution. Similar to the case of Bax-α6, the presence of PC vesicles barely affected the FTIR spectrum (blue line). The major change was produced by the PC:PA liposomes (black lines), which significantly increased the percentage of α-helix, while the presence of TFE (orange line) had a similar, but lower impact.

8.3. Peptides derived from Bcl-xL

Bcl-xL-α5

In spite of the high level of sequence homology between the α5 region of Bax and Bcl-xL, the permeabilising activity of the Bcl-L-α5 peptide is at least three orders of magnitude lower than the activity of the Bax counterpart. The structural studies carried out with the former peptide revealed other differences.

The CD spectra acquired for Bcl-xL-α5 in aqueous buffer, and in the presence of several amounts of TFE or SDS, are depicted in figure 8.10, A and B, respectively. The peptide was practically unordered in water, with only around 10% helical content. The addition of lipid-mimetic agents induced conformational ar-

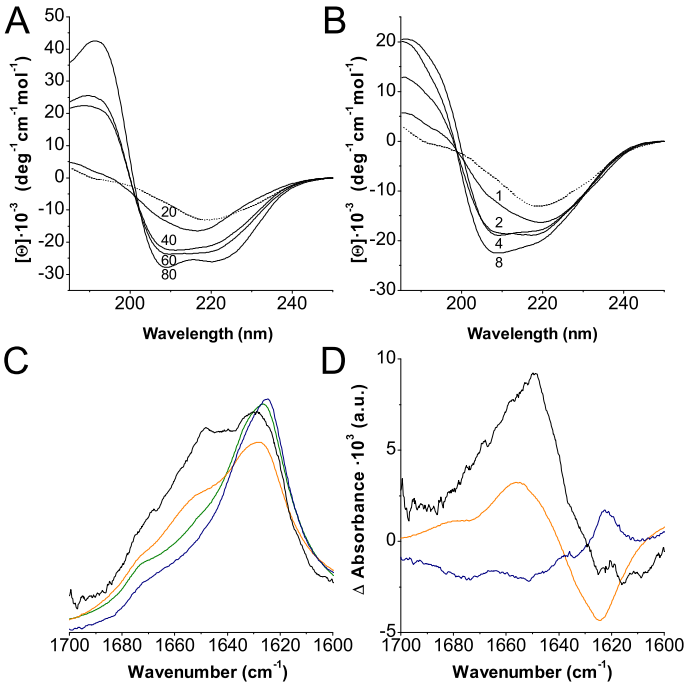

Figure 8.9.: CD and FTIR spectra of Bid-α7 in different media. A and B show the spectra of Bid-α7 in the pure aqueous buffer (dotted lines) or titrated with increasing amounts of TFE or SDS, respectively (solid lines). In all samples the peptide was at a 30 μM concentration, and the aqueous buffer was 10 mM sodium phosphate, pH 7.0. The amounts of added TFE (in percentage) or SDS (in mmol/L) are indicated in the graphs. C, amide I' band of Bid-α7 in lipid bilayers deposited from aqueous buffer (green), TFE (orange), and suspensions of LUVs made of PC (blue) and PC:PA (1:1) (black). Spectra have been normalised to the amide I' region for comparison. D, difference spectra of the amide I' region obtained by subtraction of the normalised spectra of Bid-α7 deposited from TFE (orange) and suspensions of PC LUVs (blue) or PC:PA (1:1) LUVs (black), from the normalised spectra of the same peptide in aqueous buffer.

Table 8.5.: Secondary structure of the peptides derived from Bid, after analysis of the CD spectra using the CDPro package.

		%Secondary structure[c]											
		H (r)		*H(d)*		*S(r)*		*S(d)*		*Trn*		*Unrd*	
Peptide[a]	**Medium**[b]	*Av*	*s*	*Av*	*s*	*Av*	*s*	*Av*	*s*	*Av*	*s*	*Av*	*s*
	buffer	10	2	11	0,3	15	2	10	1	21	1	33	1
	20% TFE	41	7	23	5	2	2	4	1	9	5	21	8
Bid-α6	60% TFE	52	5	25	3	0	2	2	2	4	3	17	7
	0.5mM SDS	12	1	10	0,4	19	1	9	1	23	1	27	1
	4mM SDS	45	6	25	4	2	1	2	1	7	3	19	7
	buffer	9	2	9	1	21	4	10	0,4	20	3	31	1
	20% TFE	11	4	11	2	18	4	10	2	20	2	30	4
Bid-α7	60% TFE	38	4	19	3	4	1	4	2	14	3	21	6
	0.5mM SDS	11	1	11	0,4	17	2	10	1	20	1	31	1
	4mM SDS	31	8	17	2	6	3	5	2	16	5	25	6

[a] All measurements were performed at 30 μM concentration of the corresponding peptide.

[b] Buffer medium was 10 mM NaH_2PO_4 at pH7. TFE or SDS were added at the concentrations indicated, over a 10 mM NaH_2PO_4 solution.

[c] *H*: helix, *S*: strand, *Trn*: turn, *Unrd*: unordered, *r*: regular and *d*: distorted, as defined by the standard output of CDPro. *Av* is the average of the results obtained with CDSSTR, CONTINLL and SELCON3, and *s* is the standard deviation.

rangements to different extents. On one hand, the analysis performed with CDPro indicated that the addition of increasing proportions of TFE induced the gradual adoption of α-helical structure, and 60% TFE was needed to reach 50% helix conformation. In contrast, the presence of SDS promoted a weak induction of α-helix, which did not surpass 30% even at concentrations above the critical micellar concentration of the detergent (see table 8.6).

The amide I' band of the ATR-FTIR spectra obtained for Bcl-xL-α5 evidences that most of the peptide existed in an aggregated form during the measurements, with vibrations centered at 1622 and1637 cm^{-1} (figure 8.10, C), typical of aggregated and β-strand structures, respectively. The presence of TFE or lipid vesicles reduced the absorbance of the aggregate at 1622 cm^{-1}, suggesting a solubilising effect. These agents also increased the absorbance at around 1656 cm^{-1}, indicative of the appearance of some helical structure, at expenses of the β-structure. As shown in the difference spectra in figure 8.10, D, these conformational changes were small, compared to the previously studied peptides, and followed the trend PC:PA>PC>TFE.

Bcl-xLα6

In the case of Bcl-xL-α6, the expected conformational change induced by the presence of TFE or SDS was also observed in the CD spectra, as represented in figure 8.11, A and B. TFE produced a sharp induction of helical structure when increasing its concentration from 20% to 40%. More than 50% of the peptide was arranged into an α-helix in these latter conditions. In contrast, SDS induced the same percentage of α-helix at concentrations as low as 0.5 mM. Further increase of the SDS concentration caused a gradual enhancement of the helical content, up to around 65%, which was mostly achieved at expenses of the β-strand component.

ATR-FTIR spectra were also recorded for Bcl-xL-α6 deposited on the Ge crystals from aqueous buffer, TFE and suspensions of lipid vesicles made of PC or PC:PA (1:1). The amide I' region of the FTIR spectra is represented in figure 8.11, C. The peptide from aqueous environment presented a maximum of absorbance in the region between 1620 and 1640 cm^{-1} which indicated the presence of β-strand structure, and also of an extended, aggregated form. A smaller contribution in the region of 1651 cm^{-1} denoted the presence of helical structure. Addition of TFE had a slight solubilising effect and induced the decrease of the absorbance due predominantly to the β-structure, but also to the aggregated state, while enhancing the helical contribution, as observed in figure 8.11, D. This trend was stronger when lipid vesicles were present, and in the case of PC:PA vesicles, the amide I' region showed a well-defined peak centered at around 1651 cm^{-1}, thus

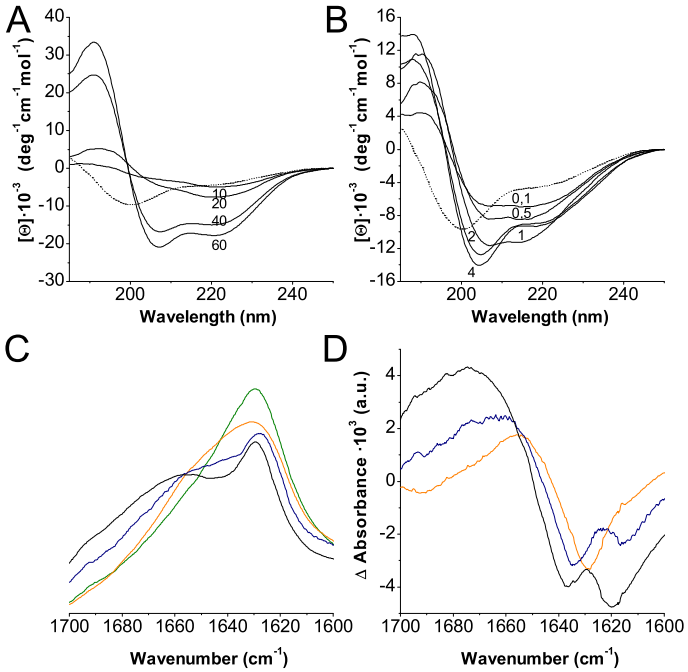

Figure 8.10.: CD and FTIR spectra of Bcl-xL-α5 in different media. A and B show the spectra of Bcl-xL-α5 in the pure aqueous buffer (dotted lines) or titrated with increasing amounts of TFE or SDS, respectively (solid lines). In all samples the peptide was at a 30 μM concentration, and the aqueous buffer was 10 mM sodium phosphate, pH 7.0. The amounts of added TFE (in percentage) or SDS (in mmol/L) are indicated in the graphs. C, amide I' band of Bcl-xL-α5 in lipid bilayers deposited from aqueous buffer (green), TFE (orange), and suspensions of LUVs made of PC (blue) and PC:PA (1:1) (black). Spectra have been normalised to the amide I' region for comparison. D, difference spectra of the amide I' region obtained by subtraction of the normalised spectra of Bcl-xL-α5 deposited from TFE (orange) and suspensions of PC LUVs (blue) or PC:PA (1:1) LUVs (black), from the normalised spectra of the same peptide in aqueous buffer.

Table 8.6.: Secondary structure of the peptides derived from Bcl-xL, after analysis of the CD spectra using the CDPro package.

		%Secondary structure[c]											
		H(r)		*H(d)*		*S(r)*		*S(d)*		*Trn*		*Unrd*	
Peptide[a]	**Medium[b]**	*Av*	*s*	*Av*	*s*	*Av*	*s*	*Av*	*s*	*Av*	*s*	*Av*	*s*
	buffer	3	3	6	1	19	5	11	1	23	1	38	3
	20% TFE	8	4	7	2	22	3	11	1	22	2	30	1
Bcl-xL-α5	60% TFE	34	3	20	2	3	1	4	1	15	3	24	2
	0.5mM SDS	10	1	10	0.3	18	1	10	0.2	22	0,3	30	1
	4mM SDS	15	2	13	2	10	3	8	1	22	1	32	2
	buffer	8	0,4	11	0,4	14	2	10	0,3	23	1	34	0,2
	20% TFE	20	1	15	0,3	9	1	7	0,1	21	2	28	1
Bcl-xL-α6	60% TFE	37	3	20	0.4	1	2	4	1	14	3	24	2
	0.5mM SDS	35	2	19	1	1	1	4	0,3	15	2	26	2
	4mM SDS	46	8	22	3	1	1	2	1	9	5	20	6

[a] All measurements were performed at 30 μM concentration of the corresponding peptide.

[b] Buffer medium was 10 mM NaH_2PO_4 at pH7. TFE or SDS were added at the concentrations indicated, over a 10 mM NaH_2PO_4 solution.

[c] *H*: helix, *S*: strand, *Trn*: turn, *Unrd*: unordered, *r*: regular and *d*: distorted, as defined by the standard output of CDPro. *Av* is the average of the results obtained with CDSSTR, CONTINLL and SELCON3, and *s* is the standard deviation.

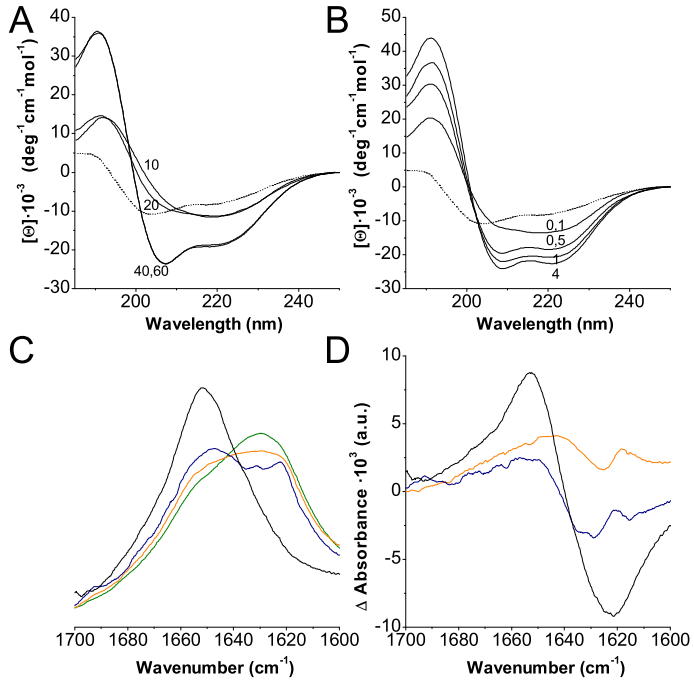

Figure 8.11.: CD and FTIR spectra of Bcl-xL-α6 in different media. A and B show the spectra of Bcl-xL-α6 in the pure aqueous buffer (dotted lines) or titrated with increasing amounts of TFE or SDS, respectively (solid lines). In all samples the peptide was at a 30 μM concentration, and the aqueous buffer was 10 mM sodium phosphate, pH 7.0. The amounts of added TFE (in percentage) or SDS (in mmol/L) are indicated in the graphs. C, amide I' band of Bcl-xL-α6 in lipid bilayers deposited from aqueous buffer (green), TFE (orange), and suspensions of LUVs made of PC (blue) and PC:PA (1:1) (black). Spectra have been normalised to the amide I' region for comparison. D, difference spectra of the amide I' region obtained by subtraction of the normalised spectra of Bcl-xL-α6 deposited from TFE (orange) and suspensions of PC LUVs (blue) or PC:PA (1:1) LUVs (black), from the normalised spectra of the same peptide in aqueous buffer.

suggesting that Bax-α6 was mainly in a helical conformation while the aggregated component was practically disappeared (see figure 8.11, C).

Part IV.

Discussion

9. Discussion

9.1. Membrane insertion fragments in Bcl-xL, Bax and Bid

Although the association of Bcl-2 proteins with intracellular lipid membranes is crucial for their function, little is known about the characteristics of this interaction. Activation of Bax is accompanied by translocation to the mitochondrial outer membrane, an extensive structural change, membrane insertion and oligomerisation Antonsson et al. (2000); Desagher et al. (1999); Goping et al. (1998); Nechushtan et al. (1999). This is facilitated by tBid Wei et al. (2000), which also translocates and interacts with the MOM Desagher et al. (1999); Gross et al. (1999). With respect to antiapoptotic Bcl-xL, it constitutively resides at the MOM, anchored through a C-terminal tail Kaufmann et al. (2003). But also in this latter case, a more extensive membrane insertion should be hypothesised in order to explain the ion channel activity observed in vitro Minn et al. (1997) and the heterodimerisation-independent regulation of cell survival reported in vivo Minn et al. (1999). Indeed, a change of membrane topology that implies insertion of α-helix 5 has been recently observed in the case of Bcl-2 as a consequence of apoptosis induction Kim et al. (2004a). One way to gain knowledge about the structures of the active, membrane-bound species of Bcl-2 proteins is by defining those segments which can be directly involved in membrane insertion.

Prediction of TM fragments of possible membrane proteins can be performed by using a number of different algorithms. In the absence of known membrane proteins which are homologous to the query sequence, the choice is restricted to methods that use single sequence information. In this study we have used two of such methods, based on different principles. TopPred takes into account a priori principles, like hydrophobicity of the target sequence, and extra information in the form of the distribution of positively charged residues (the positive inside rule) von Heijne (1992). On the other hand, the analysis of DAS is of statistical nature, because it involves indirect comparison of the query sequence with a collection of non homologous, known TM proteins Cserzo et al. (1997). The good

agreement that we find in the output of both methods is significant and suggest a possible TM character, of different degrees, for various segments of Bcl-xL, Bax and Bid, corresponding to defined α-helices of their soluble structures (figures 6.1 on page 97 and 6.2 on page 99). These predictions are tested through glycosylation mapping experiments, revealing that some weakly hydrophobic segments (below the threshold of prediction) can also act as TM. Notably, among these latter fragments are those corresponding to the second α-helix of the proposed pore forming domains, which appear to insert in the membrane only as part of a double-helix hairpin.

9.1.1. TM insertion of C-terminal and N-terminal helices

The C-terminal part of most type I and type II Bcl-2 proteins contain a canonical TM fragment. In the case of Bcl-xL this has been reported to form a TM anchoring tail, where specific targeting to the MOM depends on the presence of, at least, two basic residues in the flanking ends Kaufmann et al. (2003). Here we confirm the TM character of this sequence, since it is able to insert across the ER microsomal membrane in a Lep chimera.

The C-terminal region of Bax, that includes α-helix 9 and the upstream connecting loop, has been shown to be necessary and sufficient for this protein to target the MOM during apoptosis Schinzel et al. (2004). The loop residue Pro168 controls the conformational change that is necessary to release the α-helix 9 from its firmly stabilised position in a hydrophobic cleft of the inactive soluble structure of the protein. We find that Bax-α9, including the residues of the preceding loop, can function as a TM spanning fragment, at least in a Lep chimera.

At the N-terminal part of the three Bcl-2 proteins studied here, the most hydrophobic fragment corresponds to α-helix 1 of Bid (figure 6.1 on page 97), which does not belong to the active fragment, tBid, formed after caspase 8 cleavage. Nevertheless, glycosylation mapping shows that TM propensity of Bid-α1 is very weak (figure 6.7 on page 109A). In agreement with this result, no membrane binding has been reported for the N-terminal piece of caspase 8 processed Bid. The function of the Bid-α1 hydrophobic fragment is most probably controlling accessibility of the hydrophobic surfaces of the domain BH3 and the membrane binding fragment Bid-α6 McDonnell et al. (1999).

On the other hand, the main difference between the membrane insertion properties of Bax and Bcl-xL is the behavior of the first α-helix of these two proteins. From an NMR structural study of Bcl-xL in detergent micelles, Bcl-xL-α1 was proposed to be able to interact with lipid membranes Losonczi et al. (2000). However, we found no evidence of membrane insertion from the analysis of the

Lep/Bcl-xL-α1 chimera. Conversely, fragment Bax-α1 is found to insert across the membrane. The reason for the different behavior of the Bcl-xL-α1 and Bax-α1 fragments might be the larger number of charged residues and the shorter stretch of consecutive hydrophobic residues in the first one (see figure 6.2 on page 99).

The sequence of α-helix 1 from the structure of the water soluble Bax and the Bax-α1 fragment analysed here (figure 6.2) overlap with a proposed N-terminal mitochondrial targeting region (residues 20 to 37) Cartron et al. (2003). Association of chimeric proteins containing this N-terminal segment with mitochondria was found to be alkaline sensitive, suggesting that this sequence does not function as a TM domain, but rather as a targeting sequence that interacts peripherally with the MOM Cartron et al. (2003, 2004). However, it starts to become clear Yethon et al. (2003) that the activation/membrane-insertion of Bax is a multi-step process where both peripherally bound and membrane inserted forms may be intermediate species (see Discussion, in 9.1.3 on page 161).

9.1.2. Hairpins of Bcl-xL, Bax and Bid: Synergistic insertion of the two helices?

Because of structural analogy with the ion channel forming domains of diphtheria toxin and bacterial colicins (see 2.3.1 on page 35 and 2.3.2 on page 38), the α5-α6 helical hairpin (α6-α7 of Bid) is regarded as a pore-forming domain. Site directed mutagenesis and deletion studies support this idea and show that the α5-α6 hairpin of Bcl-xL (or its homologous Bcl-2) is important for the ion channel activity of this protein in vitro Schendel et al. (1999) and for its cytoprotective and antiapoptotic activities, independent of BH3 binding, in vivo Matsuyama et al. (1998); Minn et al. (1999). In the case of Bax, similar studies have shown the importance of this domain for the mitochondrial localisation of this protein ans its interaction with Bcl-xL Nouraini et al. (2000), as well as for its insertion into the mitochondrial membrane and the release of cytochrome c Heimlich et al. (2004).

The first helix of the hairpin can insert across ER membranes

The colicin-like model involves membrane insertion of the central α-helical hairpin, which apart from hydrophobic residues, contains also a significant number of acidic and basic residues (figure 9.1). Here we find that the first helices of the hairpin: α5 from Bcl-xL and Bax, and its analogous α6 from Bid, can be predicted as clear TM fragments. But, if we were to consider sequence data alone, the accompanying α-helix from the proposed pore-forming domain (α6 of Bcl-xL and Bax and α7 of

Bid) would only qualify as potential TM (although mildly) in the case of Bcl-xL (see figure 6.1 on page 97). The analysis of Lep chimeras shows that Bcl-xL-α5, Bax-α5 and Bid-α6 can act as TM fragments. In these cases, glycosylation occurs together with processing by the microsomal signal peptidase. Nevertheless, this latter modification is most likely a coincidence of no physiological significance, similar to that observed in other glycosylation mapping experiments van Geest et al. (1999), that anyhow implies membrane insertion.

In agreement with membrane insertion of Bcl-xL-α5, it has been recently reported that Cys158 of Bcl-2, which belongs to the α-helix 5 of this tail-anchored antiapoptotic protein, is protected from chemical modification upon induction of apoptosis and in response to BH3 peptides Kim et al. (2004a). These data strongly indicate that Bcl-2 is activated through a topology change that involves TM insertion of α5.

Insertion of the two helices of the hairpin: Possible sources of stability

Accepting insertion of helix α5 of Bcl-2 *in vivo*, as just discussed, while the protein remains anchored through the C-terminal tail Kim et al. (2004a), leads one to admit insertion of α-helix 6, just due to topological reasons[1]. This is in line with a preliminary solid-state NMR investigation on Bcl-xL, which suggests that α-helices 5 and 6 insert in the membrane Franzin et al. (2004), although with an angle of 45°.

In our study, support for insertion of the second helices of the hairpins of Bcl-xL, Bax and Bid, was only found when fragments containing the complete hairpins were assayed. A rough comparison of the amounts of inserted protein in the Lep chimeras of Bcl-xL-α5, Bax-α5 and Bid-α6, with respect to the LepΔH1 fusions of their corresponding hairpins, indicates an increased insertion efficiency in favor of the hairpins. In addition, in the LepΔH1 fusions, the absence of glycosylation bands indicates that the hairpins insert in the membrane as a whole, with no independent insertion of any of the helices conforming the hairpin. These results suggest the existence of complementarity, or a synergistic insertion, between the two α-helix fragments of each hairpin. One possible source for such a complementarity might be favorable electrostatic interactions between charged residues from each of the two α-helices of the the hairpin, which would help stabilising both fragments in a membrane inserted state. Looking at the structures

[1] Keeping both helices α5 and α9 simultaneously inserted across the membrane implies that another segment between them should also cross the membrane. Helix α6 is the most obvious candidate. In fact, in their model, Kim et al. Kim et al. (2004a) assume insertion of helix α6, of which they do not have direct experimental evidence.

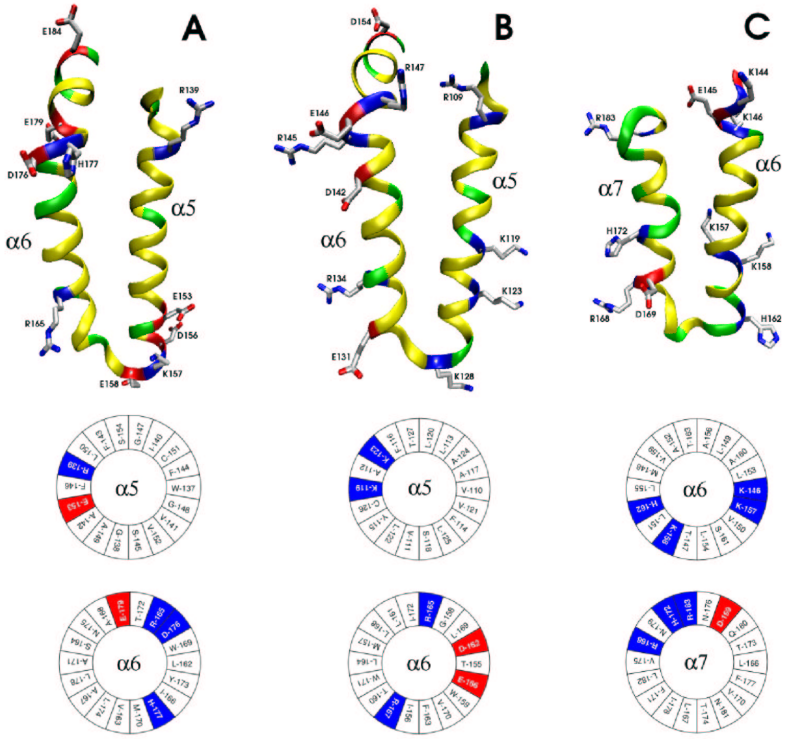

Figure 9.1.: Ribbon structures and helix wheel representations of hairpins from Bcl-xL, Bax and Bid. The hairpin structures are part of the experimental 3D structures of soluble forms of human Bcl-xL (PDB ID: 1MAZMuchmore et al. (1996)), human Bax (PDB ID: 1F16 Suzuki et al. (2000)) and human Bid (PDB ID: 2BID Chou et al. (1999)). The α5-α6 hairpin sequence of mouse Bax, used by us in this study, differs from that of human Bax by only Val150 to Gly replacement. Colors red, blue, green and yellow in the ribbon figures correspond to acidic, basic, polar and hydrophobic residues, respectively. The side chains of acidic and basic residues are represented as bonds, with colors red, blue and gray used for oxygen, nitrogen and carbon, respectively. For the helix wheels, only the 18 most central residues are represented. Potentially charged residues, both acidic and basic, are written with bold white characters over a red (acidic) or blue (basic) background. Residues are numbered according to the corresponding full-length proteins.

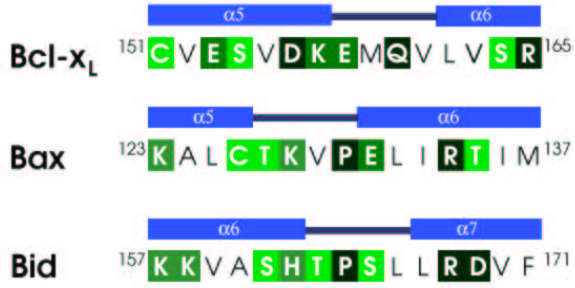

Figure 9.2.: Turn-inducing propensity at the interhelical regions of hairpins Bcl-xL-α5α6, Bax-α5α6 and Bid-α6α7. The scale of von Heijne and coworkers Monne et al. (1999b) is used for the turn-propensity analysis. Stretches of 15 residues are shown, with numbers for the first and last residue as a superscript (numbering corresponds to the full length proteins). Residues written in plain black characters are nonturn-inducers (normalised turn potential < 1). Residues written in bold white characters are turn-inducers. They are highlighted according to their turn potential as follows: cyan for a potential between 1.1 and 1.6 (Trp, Ser, Tyr, Thr, Cys), green for a potential between 2.1 and 2.3 (His, Gln, Lys and Glu) and red for a potential between 2.5 and 2.7 (Pro, Asn, Arg, Asp). Glycine (potential=1.9), normally abundant in turns of water soluble and membrane proteins, is not present in these sequences. The blue bars on top of the sequences represent their secondary structure as determined for the full length proteins in solution: the thick light-blue bar corresponds to α-helix and the thin dark-blue bar corresponds to the connecting turn.

represented in figure 9.1, one can find that charge complementarity may indeed exist. This can be more clearly envisioned in the cases of Bcl-xL (figure 9.1, A) and Bax (figure 9.1, B), although it does not seem to be obvious in the case of Bid (figure 9.1, C).

A second source of stability of the inserted hairpin can be the turn between the two helices. It has been shown that charged and polar residues plus Pro and Gly display turn induction in a poly(Leu) stretch Monne et al. (1999b,a). In our case, we do not know exactly which are the amino acid residues that make the turn in the membrane bound hairpins, although to a good approximation we may assume that such turns are placed at positions similar to the ones found in solution. In figure 9.2 we show a 15 residues extract of the interhelical region

of Bcl-xL, Bax and Bid, where the residues are highlighted according to their turn-inducing propensities Monne et al. (1999b). The dominance of turn-inducing residues (normalised turn potential > 1) over non-inducing ones (turn potential < 1) is clearly noticeable. Among them, more than half have a high turn potential (> 2), and there are at least two residues in each region of the group of highest turn-inducers (Pro, Asn, Arg and Asp, with potential > 2.5). In essence, the highest turn promoters concentrate close to the actual turn of the hairpins found in the structures of the soluble proteins, although we can predict slight shifts towards groups of consecutive highly turn-inducers. Thus, in the membrane bound form we can expect the turn of Bcl-xL-$\alpha 5\alpha 6$ to be centred around 156DKE158, while in the Bax-$\alpha 5\alpha 6$ and Bid-$\alpha 6\alpha 7$ hairpins the turn is expected to leave the Pro residue at the N-terminus of the second α-helix Monne et al. (1999b).

As a third source of stability for inserted hairpins configurations, we will consider the interaction of charged residues at both ends of the α-helices with the polar head regions of the membrane. Particularly, there exists a large number of charged groups in the loop connecting the two helices of the hairpins (figure 9.2). Thus, in our experiments, once inserted by the translocon, the hairpin might be locked at a TM fashion, where electrostatic interactions at both sides of the membrane might compensate an opposing hydrophobic mismatch effect due to the relatively short hydrophobic stretch of these helices.

Are the hairpins true TM domains?

A recent EPR investigation of Cys-labeled tBid mutants shows that in this protein, the first helix of the $\alpha 6\alpha 7$ hairpin inserts up to the hydrophobic region of the membrane with a small tilt angle, while $\alpha 7$ lays essentially flat in the polar interface and exhibits weak interactions with the hydrophobic core Oh et al. (2005). Additionally, solid-state 2D ^{15}N NMR measurements indicate that none of the helices of tBid deviate from an approximately parallel orientation with respect to the membrane plane (gong04). This appears to contradict our results and raises the question of whether the membrane inserted hairpin of tBid, and Bcl-2 proteins in general, are indeed TM spanning domains.

Although we could argue that the protein context (tBid versus the chimeric LepΔH1 construct) and/or experimental differences (spontaneous insertion in synthetic membranes, versus translocon dependent insertion) might justify the differences, we start by critically discussing our own results.

Indeed, because the results from the experiments based on the LepΔH1 construct stand on the absence of glycosylation, a TM insertion of the hairpins can not be directly concluded. The alkaline wash, urea treatment and Triton-X114

partitioning experiments demonstrate a strong association of the hairpins with the membrane (figure 6.5 on page 105). Such a tight binding is characteristic of integral membrane proteins and implies hydrophobic interactions between the protein and the acyl chains of the lipids. On this basis, we conclude that the hairpins must be inserted.

It must be also pointed out that a peripheral arrangement of tBid, as proposed by the EPR and NMR structural studies, is not easily conciliable with the membrane permeabilising and lipid reorganisation activities described for this protein Degli Esposti (2002); Epand et al. (2002a); Kim et al. (2004b); Schendel et al. (1999). These apparent contradictions coud be explained if we consider the presence of membrane inserted species that might have escaped observation by the NMR or EPR methods. Additionally, the existence of induced non-lamellar structures increasingly seems to be implicated in the activity of Bcl-2 proteins Basanez et al. (2001, 2002, 1999); Epand et al. (2002a); Terrones et al. (2004). As we discuss later in this work, our own findings of membrane permeabilisation exerted by a peptide encompassing helix $\alpha 6$ of Bid, and the structural characterisation of this molecule in lipid membranes by ATR-FTIR again supports membrane insertion of tBid.

In the case of Bcl-xL, a TM insertion of the hairpin domain finds indirect support from other literature data. As we have mentioned above, an structural study by 1D ^{15}N solid-state NMR is in agreement with tilted insertion of some of the helices Franzin et al. (2004). Additionally, the antiapoptotic protein Bcl-2, which is similar to Bcl-xL, has been shown to protect part of the sequence of helix $\alpha 5$ by inserting in the membrane Kim et al. (2004a). Membrane insertion of the $\alpha 5\alpha 6$ domain agrees also with the ion channel activity observed for this protein Basanez et al. (2001); Minn et al. (1997), although we find very weak poration activity associated to peptides containing the sequence of the single helix (see below).

The case of Bax: TM spanning at the edge of a pore

Finally, the case of Bax seems to be special. The ability of this protein to form partially lipidic pores has been reported in a series of papers by Basañez and coworkers Basanez et al. (2002, 1999); Terrones et al. (2004), and we have found that this activity resides on sequences included in the hydrophobic$\alpha 5\alpha 6$ hairpin (see chapter 9.1 on page 157). But, can these observations be related to a TM insertion of the hairpin? The interaction of Bax with lipid membranes may be accompanied by formation of non-bilayer structures, as proposed in the toroidal pore model for the activity of some antimicrobial peptides and bacterial toxins Ander-

luh et al. (2003); Zakharov et al. (2004); Huang et al. (2004); Sobko et al. (2004). In such a configuration, the Bax hairpin may indeed span the bilayer, although in a different arrangement with respect to a regular TM fragment. Moreover, binding at a toroidal pore rim would solve apparent contradictions, like the presence of Lys polar residues within the membrane spanning region, as they can be exposed to the lipid head-groups region while the rest of the peptide keeps immersed in the hydrophobic core. Similarly, the short length of the hydrophobic region, as we find in the Bax hairpin domain, can be better stabilised close to the edge of the toroidal pore, where the hydrophobic thickness is reduced. In fact, hydrophobic mismatch could be an important factor in the mechanism of pore formation, as membrane thinning can be a source for membrane tension that destabilises the lamellar phase and favours the pore. In addition, hydrophobic mismatch can as well stabilise the pore, once formed, by reducing line tension Huang et al. (2004).

9.1.3. Models for membrane insertion

Based on the above results and data from the literature we propose schematic membrane insertion models for the three proteins studied in this work (figure 9.3). The models start with constitutive inactive forms, found in the absence of apoptotic signals (figure 9.3, 1), and assume the existence of intermediate species, peripherally bound to the membrane (figure 9.3, 2), previous to active membrane inserted forms (figure 9.3, 3). Stepwise mechanisms of insertion have been proposed before in the cases of Bax and Bcl-2 to explain different degrees of membrane/protein interaction and to provide multiple levels of regulation Yethon et al. (2003); Schinzel et al. (2004); Kim et al. (2004a).

In healthy cells, Bcl-xL exists constitutively bound to the OMM through the C-terminal anchoring tail, but a small water soluble fraction has been also found. Interestingly, in the soluble fraction Bcl-xL forms homodimers, and the C-terminal domain seems to be involved in the dimerisation Jeong et al. (2004). Solid-state NMR data indicate that the interaction of Bcl-xL (depleted of its C-terminal hydrophobic tail) with synthetic lipid membranes involves insertion of the $\alpha 5$-$\alpha 6$ hairpin, while the rest of the protein lays parallel to the bilayers Franzin et al. (2004). This umbrella-like model (figure 9.3, A3) agrees with the data reported here and with cysteine modification studies of Bcl-2 Kim et al. (2004a). In this latter case, interaction with a BH3 domain might work as a trigger for the change of topology from the tail-anchored form (figure 9.3, A1). However, insertion of helix $\alpha 5$ appears to require additional proteins, as it is not observed in liposome membranes Kim et al. (2004a). This suggest the existence of an intermediate state, similar to the case of the pore forming domain of colicin E1 Zakharov and

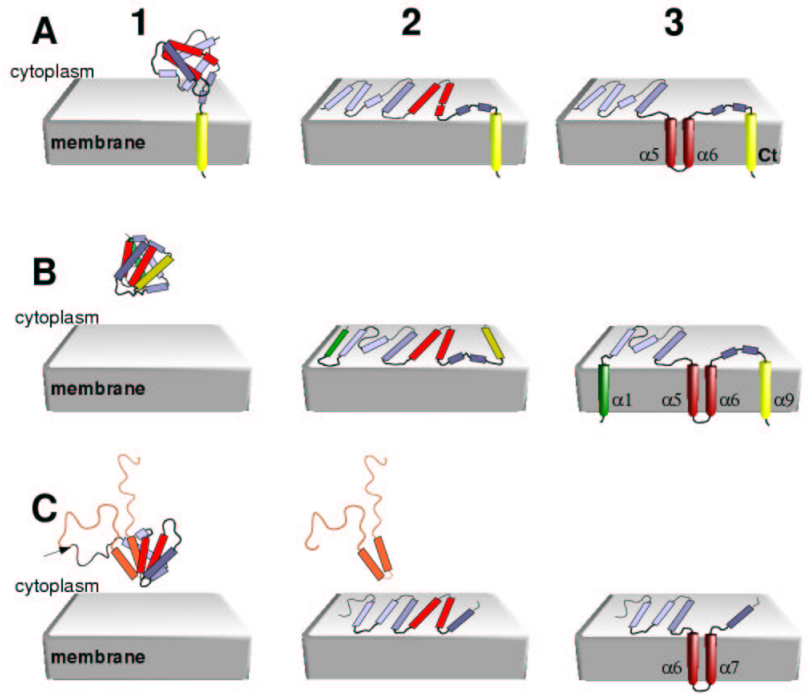

Figure 9.3.: Models of membrane insertion as a simplified two step process. Bcl-xL is represented in A, with the C-terminal hydrophobic tail coloured in yellow and α-helices 5 and 6 in red. Bax is represented in B, with helices α1 in green, α5 and α6 in red and α9 in yellow. Bid is drawn in C, where the caspase-8 cleavage site is indicated with an arrow, the N-terminal fragment is coloured in orange and helices α6 and α7 in red. Column 1 corresponds to the constitutive inactive species, in the absence of apoptotic stimuli. Upon apoptotic signal triggering, the latter evolves into a membrane inserted species, represented in column 3, passing through a hypothetical intermediate represented in column 2. The models in 1 are based on the experimental structures of water soluble forms of these proteins Muchmore et al. (1996); Suzuki et al. (2000); McDonnell et al. (1999). The models in 3 are based on data from this work, in agreement with literature data in the case of Bcl-xL Kim et al. (2004a)Franzin et al. (2004). The models in 2 are proposed by analogy with the mechanism of insertion of the pore-forming domain of colicin E1 Zakharov and Cramer (2002), taking also into account data from references Yethon et al. (2003); Kim et al. (2004a)(gong04). The transitions 1→2 and 2→3 are most likely regulated processes, with the expected interplay of other proteins not shown in the figure (see the text).

Cramer (2002), where it has been proposed that, prior to the integral membrane state, the protein arranges in the membrane interfacial layer as an extended mobile helical array (figure 9.3, A2).

A multistep mode of insertion may also apply to Bax. As a consequence of activation of apoptosis, cytoplasmic Bax (figure 9.3, B1) relocalises at the MOM. Targeting to mitochondria is accompanied by structural changes and strong association to the lipid membrane, followed by oligomerisation and formation of a pore. In this sequence of events, a change in conformation of the inactive, water soluble form, would act as a preliminary step that releases the C-terminal (α9) and N-terminal (α1) hydrophobic helices, and the central hydrophobic hairpin. It has been suggested that the conformational change is controlled at the level of two Pro residues: Pro13, that controls exposition of α-helix 1, and Pro168, that controls disclosure of the α5α6 hairpin through a displacement of α-helix 9 Cartron et al. (2004); Schinzel et al. (2004). Additionally a salt bridge between Asp33 (from α-helix 1) and Lys64 (from the BH3 domain) might also be involved in the mitochondrial addressing of Bax. The partially open intermediate would be capable of targeting to the mitochondrial membrane, where the structural transition proceeds to give a membrane associated, though neither inserted nor oligomerised species (figure 9.3, B2). Evidence for a peripherally bound intermediate is provided in a recent in vitro study Yethon et al. (2003). In a subsequent step, probably mediated by tBid, TM insertion of fragments Bax-α1, Bax-α9 and the Bax-α5α6 hairpin may happen (figure 9.3, B3). This latter state would be prompted to formation of a toroidal pore, due to the surface tension generated by a strong membrane-protein interaction. In the final pore state, Bax would be stabilised as an oligomer, as it has been reported Antonsson et al. (2000); Eskes et al. (2000).

In a recent study, Vallette and colleagues report that the N-terminal and C-terminal helices of Bax are involved in targeting to the OMM and exposure of the α5α6 hairpin, respectively, without acting as TM insertion domains Cartron et al. (2004), and thus leaving the hairpin as the only TM fragment. However, from their data one cannot conclude that the membrane inserted state of Bax involves only the two hairpin helices. Accepting that α1 and α9 have a preliminary role in controlling membrane targeting and change in conformation, once the protein gets close to the membrane, these two helices may as well insert. As we have shown here, both α1 and α9 exhibit a sufficient TM potential for them to acquire an inserted state in their natural context.

With respect to Bid, membrane targeting must be preceded by an apoptosis activation signal, provided by the caspase-8 digestion of the inactive cytoplasmic full-length protein Luo et al. (1998); Li et al. (1998) (figure 9.3, C1). Interaction

of the active C-terminal fragment, tBid, with synthetic lipid membranes has been recently studied by solid-state 1H/15N NMR and by EPR experiments on cysteine mutants. In the NMR studyGong et al. (2004), all α-helices appear to interact with the membrane in a parallel fashion. On the other hand, in the EPR analysis Oh et al. (2003), the authors report the tight binding of the $\alpha 6\alpha 7$ hairpin of tBid to membranes, which is considered as inserted through the $\alpha 6$ helix, although not in a TM fashion. As we have dicussed above, this does not completely agree with our data and previous reports claiming that tBid behaves as an integral membrane protein Gross et al. (1999). However, the possibility exists that the structures observed by NMR and EPR correspond to an intermediate membrane bound state (figure 9.3, C2), previous to an inserted state (figure 9.3, C3), for which the activity of additional specific elements might be required. Indeed, the insertion of tBid in the membrane may need the presence of specific mitochondrial lipids, like cardiolipin Lutter et al. (2000), or the assistance of proteins present in the MOM, as we have also discussed above for Bcl-xL and Bax.

9.2. Activity and structure of peptides derived from the putative pore forming hairpins

The regulation of release of apoptotic factors from the mitochondria involves alteration of the permeability properties of the outer membrane of this organelle, which is believed to be performed by proteins of the Bcl-2 family. Members of this clan, like Bax, Bid and Bcl-xL, can form ion channels, and in some cases, permeabilise lipid vesicles to large molecules, in a way that is, however, still not well understood at the molecular level. Similar to the pore forming domain of colicins and other bacterial toxins, there exists in most Bcl-2 proteins a hairpin of two hydrophobic α-helices that are considered to be responsible of membrane-insertion and pore formation. As we have just seen, our glycosylation experiments show that the first fragment of the hairpin of Bax, Bcl-xL and Bid, namely α-helices 5, and 6 in the case of Bid, has the capacity to insert across natural lipid bilayers in the absence of the rest of the protein. Additionally, the complete hydrophobic hairpins interact strongly with lipid membranes (see chapter 9.1 on page 157). Continuing with such a reductionist approach, we now discuss the poration activity of peptides including the helices[2] $\alpha 5$ and $\alpha 6$ of Bax and Bcl-xL,

[2]The word helices means no assumption of the structure of these molecules. It refers only to the structure found for these fragments in the corresponding soluble species of the protein from which they are derived. The actual structure in relevant lipid-mimetic and lipidic media is discussed below in this section.

and α6 and α7 of Bid, are reported here.

We have found that both peptides derived from Bax, namely Bax-α5 and Bax-α6, and the peptide Bid-α6, induce the release of calcein from lipidic vesicles at a physiological pH and at concentrations close to those reported for the full-length proteins. Additionally, we show that the Bax peptides release dextrans of high molecular weight through a pore structure that allows also lipid transbilayer diffusion. The peptides Bax-$\alpha5^K$ and Bid-α6 also show the ability to form ion conducting channels in planar lipid bilayers, but exhibit a different pattern of channel formation. Moreover, the peptides derived from Bax distinguish from those of Bid-α6 by their behavior when we study the effect of the lipid composition in LUVs. These facts, together with their distinct pattern of orientation with respect to the membrane plane, indicate that they follow different permeabilisation mechanisms.

In contrast, the peptide fragments derived from Bcl-xL, namely Bcl-xL-α5 and Bcl-xL-α6, as well as Bid-α7, were unable to permeabilise lipid vesicles at concentrations below micromolar. Here we discuss the biophysical characterisation of the peptides derived from the putative pore forming helices of Bax, Bid and Bcl-xL and their interaction with membranes.

9.2.1. Bax-α5 and Bax-α6 independently exhibit a pore forming activity similar to that of full length Bax

Two peptides were synthesised with the sequence corresponding to the helix α5 of Bax (see footnote on page 111), namely Bax-α5 (containing residues 102 to135) and Bax-$\alpha5^K$ (containing residues 108 to135 and one extra Lys on each side) (see sequences on table 5.3 on page 86). Both peptides displayed a very similar membrane permeabilisation activity on LUVs loaded with calcein, with also similar dependence on the lipid composition. The major difference observed between them is the slightly higher activity displayed by Bax-α5, probably related to its higher α-helical content in lipid vesicles and lipid-mimetic environments (see figures 8.1 and 8.4 and table 8.1). Although both peptides have a net positive charge, this is higher in the case of Bax-$\alpha5^K$ ($+6$ in this latter case versus $+3$ in the case of Bax-α5). This may explain the different solubilisation observed for these two peptides in the presence of negatively charged PC:PA LUVs. Thus, bax-α5 adopts a predominantly helical structure in PC LUVs, with a small residual β-aggregate fraction, while the solubilisation of aggregates is lower in the presence of PC:PA LUVs, as observed in the FTIR spectra (figures 8.3 on page 131 and 8.4 on page 135). The opposite behaviour is observed in Bax-$\alpha5^K$ (higher solubilisation of β-aggregates in PC:PA LUVs than in PC LUVs), presumably due

to enhanced interactions between the negative charges of PA head-groups and the higher net positive charge.

The quantitative analysis of the amide I' frequencies was performed with more detail in the case of Bax-$\alpha 5^K$. A deconvolution of the Lorentzian bands reveals the existence of two types of helices for this peptide, one with a typical absorbance at around 1656 $cm^{-1}$and a second one with an absorbance in the region of 1646 cm^{-1}, being both of them also distinguished by their relative orientation in PC and PC:PA LUVs (table 8.3 on page 134). These two types of helices may also be found in Bax-$\alpha 5$. Although no deconvoluted, the spectrum of this peptide in PC LUVs shows a peak of absorbance at around 1648 cm^{-1}, which could be a combination of the two α-helix components.

The structural analysis of Bax-$\alpha 6$ revealed a similar arrangement into an α-helix when passing from an aqueous environment to lipidic or lipid-mimetic conditions. In spite of the net neutral charge of the Bax-$\alpha 6$ peptide, incubation with PC:PA vesicles had a higher solubilising effect than PC vesicles, as observed in figure 8.5 on page 137. Interestingly, the presence of a component absorbing at around 1647 cm^{-1} can also be deduced from the FTIR spectra and, comparably to Bax-$\alpha 5$, be attributed to the presence of a distorted α-helix. The similar features of the permeabilising activity of both peptides agree with this interpretation.

The data obtained with the peptides derived from the helices 5 and 6 of Bax indicate that these peptides induce, independently, the formation of lipidic (or partially lipidic) pores of toroidal-like structure.

Toroidal pores formed by Bax peptides

The release of calcein from lipid vesicles by the Bax-$\alpha 5$ and Bax-$\alpha 6$ peptides is markedly enhanced by the positively curved LPC. In the case of Bax-$\alpha 6$, the calcein release is reduced in the presence of PE, but the same lipid produces a small enhancement of the activity of Bax-$\alpha 5$. Additionally, for this latter peptide, PE appears to exert some attenuation over the enhancing activity of LPC (table 9.1 on page 157). As we have explained in the introductory part, the spontaneous curvature of lipids has a direct effect in the stabilisation of non-lamellar structures, which is related to the formation of pores of toroidal structure.

Because of its geometry, a toroidal pore is characterised by possessing positive curvature, at the place of monolayer fusion, as well as negative curvature, all around the pore rim (figure 9.4 on page 170) Valcarcel et al. (2001). However, the negative curvature is large only for very small pores, and decreases rapidly as the pore radius increases. In contrast, positive curvature stress will increase with the pore radius, being normally the dominant effect. Thus, while lipids with intrinsic

positive curvature should generally favor pore formation, negatively curved lipids are expected to favor small sized pores but oppose large pores. For example, small amounts of negatively curved cone-shaped lipids have been shown to favor the small pore formed by sticholysins (around 1 nm radius), which is proposed to be of toroidal nature Valcarcel et al. (2001). In contrast, the much larger proteo-lipidic pores formed by full-length Bax, allowing passage of at least 70 kDa dextrans (approximately 5.9 nm Stocks radius), are inhibited by lipids with intrinsic negative curvature Terrones et al. (2004); Basanez et al. (2002). In line with these ideas, the increased activity of the Bax-α5 and Bax-α6 peptides in the presence of LPC, as observed here, suggests a reduction of the positive curvature stress of toroidal pores formed by these peptides. Additionally, the moderate but different effects of the PE, depending on the analysed peptides, could in principle be related to the stabilisation of pores of moderate size, which may be smaller in the case of Bax-α5 than in the case of Bax-α6. These effects have been characterised from the release of calcein, which is a 0.6 kDa molecule that can exit the vesicles through small pores. Thus, the weak enhancing effect of PE observed for Bax-α5 could be explained in terms of the stabilisation of pores of small size. To test this possibility, the effect of PE should be reevaluated through the study of the release of high molecular weight dextrans.

Pore size and lipid transbilayer diffusion

In concerted action with tBid, Bax has been reported to release fluorescent dextrans of high molecular weight form lipidic vesicles Kuwana et al. (2002); Terrones et al. (2004). Our experiments with Bax-α5 and Bax-α6, show that these peptides, independently and at concentrations similar to those used for full-length Bax, are able to promote the release of 20 and 70 kDa dextrans from PC LUVs. This indicates hata Bax-α5 and Bax-α6 can both induce the formation of pores of at least 6 nm radius[3]. Interestingly, higher peptide concentrations were needed in both cases to release similar amounts of FD-70 compared to FD-20. This shows an effect of peptide concentration on the pore size that has not been reported in the case of tBid+Bax Terrones et al. (2004). From this latter effect we can conclude that the pores formed by Bax fragments are of smaller size than the pores formed by the full-length protein, since in the first case a size exclusion limit of the pore, dependent on the concentration of the pore-inducer peptide molecules, is observed. This latter conclusion is in agreement with the effect of PE on the release of calcein (see above).

[3]It is estimated that a 70 kDa dextran has a Stock-radius of 569 nm.

Additionally, the pore forming activity of Bax-α5 and Bax-α6 was accompanied by a redistribution of lipids between the two monolayers. The process of lipid transbilayer diffusion was induced at comparable concentrations to those needed for dextran release and also exhibited a similar time-course, which indicates a mechanistic connection between the two observations. Both, the release of high molecular dextrans and the lipid transbilayer redistribution, occurred without significantly affecting the size of the vesicles, thus excluding the possibility of a detergent-like action. Such a behaviour is expected if a mixed lipidic/peptidic pore with toroidal structure is being formed, and has also been reported for the concerted action of Bax and tBid by Terrones et al. Terrones et al. (2004).

Bax-α6 exhibits lower permeabilising and lipid redistribution activities than Bax-α5. This could be attributed to a lower ability to alter the integrity of the bilayer, or to a lower binding of this peptide to vesicles. Additional studies need to be performed in order to clarify this point.

Mechanism of pore formation by Bax peptides

The characteristics of the ion channel activity observed on planar lipid bilayers add further important information about the type of pores formed by the Bax peptides. We have measured these channels only for Bax-$\alpha5^K$, for which we have also a more complete structural analysis by ATR-FTIR, including orientation information in ordered multibilayers. Here we discuss together the electrical recordings and FTIR structural data and we propose a model for the pore formed by the Bax-$\alpha5^K$ peptide. A similar model of pore formation can be proposed for the Bax-α5 peptide, and possibly for the Bax-α6 peptide[4].

The main observations from the ion channel activity of Bax-$\alpha5^K$ are the formation of a large conductance pore through a two stage process and, specially, the dependence of the ionic selectivity of this pore on net lipid charge (table 7.3). Both characteristics are strong indications in favor of lipidic pores. A general mechanism of formation of toroidal lipidic/peptidic pores by amphipatic, positively charged peptides has been recently formulated by H. W. Huang Huang et al. (2004). According to this model, the stability of pores depends on a fine balance between two opposite forces: A membrane tension, σ, representing a stress on the surface of the membrane, which favours pore formation, and a line

[4]Ion channel recordings have not yet been acquired for the Bax-α5 and Bax-α6 peptides, also a detailed deconvolution analysis of the FTIR spectra of these peptides has still to be performed. However, at least in the case of Bax-α5, the similarity of this molecule with Bax-$\alpha5^K$ and a qualitative interpretation of the spectroscopic data allows proposing a similar model of pore formation.

tension, γ, related to the curvature stress at the place of monolayer fusion, that opposes the pore. Each of them contributes a term, that is a function of the pore radius, R, to the energy of the pore, given by

$$E_R^0 = 2\pi R\gamma - \pi R^2\sigma$$

In the process of pore formation, the peptide can act by affecting both stability terms in two stages. In a first stage (see column 2 in figure 9.4), the interaction of the peptide at the lipid head-group region generates a stress (or internal membrane tension) that, passed a critical P/L value, ends up inducing the opening of a lipidic pore. Once the pore is open, some peptide molecules change orientation to occupy a membrane inserted position at (or close to) the rim of the pore (column 3 of figure 9.4). In this new state, the peptide would interact favorably with the pore edge, stabilizing it by diminishing the line tension term, probably through a reduction of the curvature stress at the place of monolayer fusion Lee et al. (2004).

Our data fit well in the framework of Huang's mechanism. Thus, measurements of Bax-$\alpha 5^K$ channels in planar lipid membranes show a two-step behaviour, suggesting that the peptide attaches initially to the membrane (and presses it in the presence of a positive potential), and only when it reaches a critical concentration on the surface of the bilayer, it inserts to form the large conductance channel observed. The effect of lipids with intrinsic curvature would be affecting the membrane line tension, being decreased (and the pore favored) by the positively curved LPC (see above).

The existence of two types of α-helix described in the case of Bax-$\alpha 5^K$, one canonical (α_1) and one distorted (α_2), and their distinct orientation in lipid bilayers, being α_1 tilted (with an angle dependent on lipid composition) and α_2 parallel with respect to the membrane plane (table 9.1 on page 153), can also be discussed in the context of the above mechanism. The two helices can be interpreted as either, an equilibrium of two populations of differently structured peptides (figure 9.4, A), or two α-helical stretches of different structure within the same peptide molecule (figure 9.4, B). Because only helix α_1 is found to be tilted in the lipid samples, the first option would mean that α_1 and α_2 represent membrane inserted and non-inserted states, respectively, of the Bax-$\alpha 5^K$ peptide. This, in turn, implies that the two peptide forms interact differently with the membrane, and we would expect that the relative proportion of α_1 with respect to α_2 (α_1/α_2 ratio) changes in the presence of lipid vesicles. However, the α_1/α_2 ratio keeps almost constant (around 0.8) regardless the presence of lipids (table 8.2 on page 132), which makes this first option unlikely. Considering the second option, the percentages of α_1 and α_2 can now be related to the average

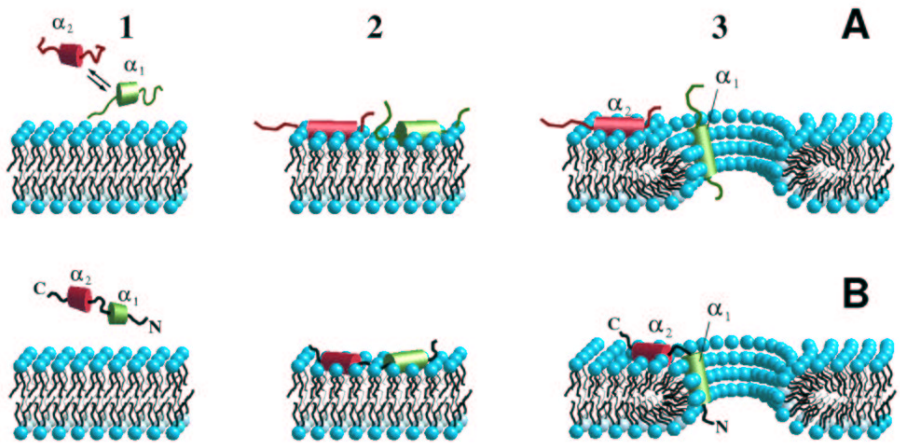

Figure 9.4.: Model representing the interaction of Bax-$\alpha 5^K$ with lipid membranes and formation of toroidal pores. A, the two helices, α_1 and α_2, observed by FTIR can be envisioned as an equilibrium between two structural states (column 1). Both states can interact with membranes (column 2), creating a tension that induces the opening of a lipidic pore. In column 3, the state α_1, acquiring a tilted orientation, interacts with the pore edge, which reduces the curvature stress and stabilises the pore. The state α_2 remains oriented flat at the membrane interface. B, alternatively, α_1 and α_2, are two stretches of the same peptide molecule with slightly different α-helical structure. The pore is formed through the same mechanism as above, but the membrane inserted state is represented by a kinked peptide, where the part encompassing α_2 remains flat with respect to the membrane plane while the stretch corresponding to α_1 is tilted over the rim of the pore. Helix α_1 can be ascribed to the more hydrophobic, N-terminal half of the peptide (see the text). The tilted stretch is represented interacting with the head-group region, but it may as well inmerse deeper into the hydrocarbon core. We have no data about the depth of inmersion.

length of two helical fragments in the 30 residues Bax-$\alpha 5^K$ peptide. We can estimate that the regular α-helix, α_1, is about 8 residues long in TFE, while the distorted helix, α_2, would corresponds to approximately 10 residues. Both helices increase in a similar proportion as the peptide binds to lipid membranes, up to about 11 and 14 residues for PC LUVs or 10 and 13 residues for PC:PA LUVs, respectively. In the membrane inserted state, only the stretch encompassing helix α_1 would stick into the bilayer, while the stretch α_2 remains flat at the surface. Thus, the species responsible of the stabilization of the pores would be a kinked helical rod (figure 9.4, B, column 3). Since the most hydrophobic part of the peptide is at the N-terminal half, comprising α-helix 5 of parent Bax (residues Gly108 to Cys/Ser126) it is likely that the tilted helix α_1 is at this side. Helix α_2 is most likely at the C-terminal half of the assayed peptide, where residues correspond to the turn between helices 5 and 6 of the Bax hairpin. This latter region contains various charged residues and could be organized as an amphipatic structure. The above model may also explain the apparent contradiction between the reduction of the Bax-$\alpha 5^K$ induced calcein release in the presence of negatively charged lipids, like PS, PA and CL (table 7.1 on page 113), and the increased binding of this peptide to negatively charged membranes (PC:PA), determined from the FTIR experiments (table 8.2). Thus, a stronger binding to a negatively charged membrane surface may impair pore formation by stabilizing a state with the complete peptide (both helical stretches) aligned flat on the membrane (figure 9.4, state 2). The smaller average tilt angle determined for helix $\alpha 1$ when bound to PC LUVs, as compared to PC:PA LUVs, is in agreement with this idea. It is also interesting to note that the two types of α-helices are already present in the Bax-$\alpha 5$ samples in the absence of lipids (although at a lower proportion), suggesting that the structural properties of this peptide are intrinsically prompted to pore formation.

In summary, our data demonstrate that the helices conforming the pore forming domain of Bax can independently reproduce the activity displayed by full length Bax, and in the absence of tBid. In addition, these results suggest that Bax has the intrinsic ability to form large pores and to induce the lipid transbilayer redistribution associated to toroidal pores. Thus, the need of the concerted action of Bax with tBid and specific lipids that has been reported, may rely on an upstream regulating event related with the priming of Bax to form the pores.

9.2.2. Poration activity of Bid peptides

Although Bid is a BH3-only protein and shares less sequence homology with other proteins of the Bcl-2 family, the structure of its soluble form shows important

similarities with structures of other Bcl-2 proteins, like Bax and Bcl-xL. Thus, Bid posses also a hairpin of hydrophobic helices in the core of its globular structure, which, by analogy, has been proposed to be a colicin-like pore forming domain. However, the data presented here and other emerging evidences do not completely agree with this role Degli Esposti (2002); Kim et al. (2004b); Liu et al. (2004).

The permeabilising activity and poration pattern of Bid-α6 and Bid-α7, measured in this work, is clearly different from that observed for the similar peptides derived from Bax. In the case of Bid-α6, only small effects of intrinsic lipid curvature were observed. However, electrostatic interactions with the membrane seem determining for the action of the peptide, which exhibits calcein release activity in the submicromolar range, as observed for tBid, only in the presence of negatively charged lipids. Moreover, Bid-α6 was unable to release fluorescent dextrans of 20 or 70 kDa and to induce lipid transbilayer diffusion in LUVs at concentrations which effectively released calcein. These facts are also important, as they show that the ability to permeate membranes is not necessarily linked with the capacity to promote the release of large dextrans or to facilitate the redistribution of lipids between the leaflets of the bilayer, and thus serve as a negative control for those experiments.

Additionally, in contrast to the Bax peptides, Bid-α6 formed step-like ion channels of small size in planar bilayers, gave rise to a sigle type of α-helix, and inserted in PC:PA membranes with an average angle of ~34º (~50º for pure PC membranes) with respect to the lipid chains, as deduced from FTIR experiments (table 9.1 on page 157). In this case, the peptide exhibited a larger solubility in PC:PA LUVs than in PC LUVs. Altogether, these observations indicate that Bid-α6 does not form lipidic pores when interacting with lipid membranes, but rather suggest that it may permeabilise the membranes through the organisation of barrel-stave channels.

The experiments performed with Bid-α7 show a weak permeabilising activity, compared to the previous peptides. Moreover, in the FTIR experiments this molecule is mainly aggregated in all cases studied, with little solubilisation in the presence of PC:PA LUVs, and even smaller in TFE solvent or PC vesicles. This results indicate that Bid-α7 interacts poorly with the membranes, or that the interaction is unspecific and preferentially in the aggregated form. We may then conclude that this fragment alone is unable to account for any of the functional features of tBid, in agreement with previous results showing that helix α7 is dispensable for tBid activity Hu et al. (2003); Liu et al. (2004).

According to our results, Bid-α6 would be responsible of the membrane insertion and permeabilisation processes exhibited by tBid. Nevertheless, the physiological importance of such a permeability to ions and small molecules, of the size

of calcein, is not clear. For example, the outer mitochondrial membrane is normally permeable to molecules of size <1.5 kDa Halestrap et al. (2002). Thus, the membrane poration activity of Bid-α6, and probably that of tBid, might be a non-specific consequence of its tight association with membranes. Related to this, we recall that the way of binding of Bid to membranes remains highly controversial (see section 9.1).

Among other possible roles of Bid, in which α-helix 6 might be involved, we cite the capacity of tBid to interact with specific mitochondrial lipids, like cardiolipin, through a so called cardiolipin binding domain (CBD), which contains α-helices 4, 5 and 6 Liu et al. (2004). Interestingly, the presence of CL does not seem to exert any special effect, other than a small increase of activity that can be attributed to its net negative charge (table 7.1). However tBid has been shown to interact with lipid monolayers containing CL and to induce segregation of CL into lipid domains with a time-course comparable to the release of cytochrome c from mitochondria (gonzalvez). This interaction and reorganisation of CL containing monolayers have been further reproduced with a peptide similar to Bid-α6 (Petit, personal communication).

Additionally, tBid participates in a BH3 independent fashion, in the remodeling of mitochondrial cristae during apoptosis, and, as a consequence, in the mobilisation of the cytochrome c stores Scorrano et al. (2002). Moreover, a Bid-CL interaction at the mitochondrial contact sites has been reported to contribute to this cristae reorganisation and cytochrome c release Kim et al. (2004b). These and our results suggest that CL is not required for the membrane permeabilising activity, but may be rather involved in targeting of tBid to mitochondria and subsequent activation of Bax and/or in the events associated with the reorganisation of the cristae and the contact sites, likely through interactions with the helix 6.

9.2.3. The peptides derived from Bcl-xL exhibit no significant pore activity

As far as the apoptotic function is concerned, Bcl-xL and Bax have antagonistic roles, and the first one is mostly considered an inhibitor of the pores formed by the second. However, the putative pore forming domain of these two proteins shares a high level of sequence homology (figure 9.5). This domain has been claimed to be responsible of the ion channel activity displayed by both Bcl-xL and Bax. Further studies have manifested a high tendency of Bax to form pores, which are large and of lipidic nature Terrones et al. (2004). In the case of Bcl-xL, additional experimental evidence of poration activity has been reported only for the processed forms of Bcl-xL (ΔN61Bcl-xL and ΔN76Bcl-xL), which become

Figure 9.5.: Sequence alignment of the hydrophobic hairpin of Bax and Bcl-xL. In light yellow are indicated the fragments that correspond to the helices 5, 6a and 6b in the solved structures of the soluble forms of both proteins. Blue letters indicate identical amino acids, green letters correspond to residues with similar properties and red letters show amino acids with opposing characteristics (polar/non-polar or opposite charge). The dark blue bars indicate the sequences of the peptides Bax-α5, Bax-$\alpha 5^K$ and Bcl-xL-α5, while the dark red bars mark the fragments corresponding to Bax-α6 and Bcl-xL-α6.

proapoptotic and seem to display a Bax-like behaviour Basanez et al. (2001). These processed proapoptotic forms of Bcl-xL contain the central $\alpha 5\alpha 6$ hairpin, which is supposed to be responsible of the Bax-like activity.

However, our data show that the peptides consisting on α-helices 5 and 6 of Bcl-xL do not exhibit a significant pore forming activity, at least in the conditions assayed, which try to reproduce physiological conditions. This is in clear contrast to the high activity displayed by the homologue peptides derived from Bax. In the case of Bcl-xL-α5, the small activity could be related to the low level of helical structure induced in lipid-mimetic and lipidic media, which is indicative of the low affinity of this peptide for lipid membranes. This is, however, not the case of Bcl-xL-α6, which shows a helical content similar to, or even higher than Bax-α6 in lipidic environments.

One possibility is that the pore forming activity of the peptides derived from Bcl-xL depends on pH, as it has been reported for full length Bcl-xL Minn et al. (1997). However, it is also possible that these peptides are responsible of the BH3-independent inhibitory activity that has been suggested for the antiapoptotic Bcl-2 proteins Minn et al. (1999). Both possibilities should be tested in additional experiments.

If we look close to the sequences of Bcl-xL and Bax peptides, we find striking similarities between the two homologous molecules. For the α5 helices, the homology is higher at the N-terminal half. The major differences arise from the presence of charged residues at positions i and i+4 in the C-terminal region, which in the Bax peptide originate an amphipatic surface with net positive charge, while in the case of Bcl-xL exhibits a net negative charge. In the case of the peptides

corresponding to the helices $\alpha 6$ of the hairpins, the homology is also significant. Here the main differences are the presence of some charged residues on Bcl-xL-$\alpha 6$ at the positions corresponding to non-polar residues in Bax-$\alpha 6$, and vice versa. These differences do not follow a similar pattern to those observed for the $\alpha 5$ helices, but are dispersed all over the sequence of the peptides. Experiments with mutant peptides should help to clarify the interesting differences found between the Bcl-xL and Bax peptides.

9.2.4. Final comments about the activity of the full length proteins

Finally, some comments should be added about the implications of our findings for the general understanding of the functional mechanism of the full-length proteins Bax, Bid and Bcl-xL. In these three cases, putative pore forming domains with a high level of sequence and structure homology have been proposed. Such similarity was difficult to conciliate with the diverse functions of these three proteins. Our results with individual peptides illustrate the important differences found between the full length proteins, both at the level of their pore forming activity and their mechanism of action, and evidence the possibility that very similar sequences display very diverse functions.

As already mentioned, formation of lipidic pores has been reported for Bax and other Bax-like Bcl-2 proteins. These latter pores are accompanied by decreases of bilayer lifetime and membrane line tension Basanez et al. (2001, 2002, 1999); Terrones et al. (2004), strongly suggesting that full length Bax and the fragments corresponding to helices $\alpha 5$ and $\alpha 6$ porate membrane bilayers by analogous mechanisms. Similarly, the pores formed by Bid$\alpha 6$ have some parallel with the channel activity of its parent protein Schendel et al. (1999). This raises the idea that a short peptide encompassing 20-30 residues may carry in its sequence enough structural information to reproduce crucial aspects of the function of a much larger parent protein. It may be particularly so for functions like membrane poration, where the requirements can be provided by only a few residues. From this we can conclude that mechanistic links may exist between simple pore-forming peptides, like antibiotics, and more complex pore forming proteins, like bacterial toxins and Bcl-2 type apoptotic regulators.

For the cases studied here, synergistic and antagonistic effects should be studied to complete the sketched activity demonstrated by the Bax-$\alpha 5$, Bax-$\alpha 6$ and Bid-$\alpha 6$ fragments. These fragments and other missing parts are essential to give Bax and Bid the complex regulatory faculties that single fragments lack. Nevertheless, the study of the small fragments is important to help understanding the functioning of the whole, having also the potential to open new ways of exploring

possible therapeutic uses.

Although our reductionist approach has allowed us to sketch some important aspects of the structure and function of Bcl-2 proteins. Additional work is needed to complete our understanding of the complex behavior of these systems. We realise that unexpected new features may emerge form the synergistic action of different parts, as it has also become evident in this work. Thus, the new studies should include other fragments, like helix $\alpha 1$ of Bax, but they should also be directed to larger protein domains, like the double helix hairpins and even complete proteins.

Part V.

Conclusions

10. Conclussions

In this work, we have analysed the individual propensity of the hydrophobic fragments of Bcl-xL, Bax and Bid, to insert in the membrane. In the context of Lep chimeras, we have shown that the C-terminal fragments of Bcl-xL and Bax, together with helix α1 of Bax, and the first helix of the putative pore forming hairpin of these proteins (α5 of Bcl-xL and Bax, and α6 in Bid), can adopt a TM organisation in ER microsomes. The second helix of the putative pore forming hairpin, α6 in Bcl-xL and Bax, and α7 in the case of Bid, is able to insert in the membrane only when accompanied by the the first one. In addition, the central hairpins contain the sufficient information to target lipid membranes and insert into them in a fashion which is resistant to alkaline and urea extractions, and which stays in the detergent fraction after Triton X-114 partition.

Continuing with a reductionist strategy, we have also performed structural and activity studies with peptides derived from the individual helices of the putative pore forming domains of Bcl-xL, Bax and Bid. We have observed that Bax-α5, Bax-α6 and Bid-α6 reproduce, at least partially, the membrane permeabilising activity of the parent full-length proteins. In contrast, the peptides derived from Bcl-xL and Bid-α7 exhibit pore activity only at higher concentrations, which do not account for the permeabilising activity reported for the parent full-length proteins.

In particular, the Bax peptides are unstructured in water solution, but adopt a helical conformation in lipid-mimetic and lipidic media. They can porate membranes at nanomolar concentrations, through a mechanism which is sensitive to the intrinsic monolayer curvature of the lipid membranes. The pores formed induce lipid transbilayer redistribution and are large enough to allow the passage of dextrans of at least 70 kDa. The electrophysiological studies with Bax-$\alpha5^K$ reveal a two-step process of channel formation with a conductance of about 0.3-5 nS, whose ion selectivity depends on the net charge of the membrane lipids. Moreover, the structure of this peptide is represented by two types of α-helices, one of them oriented parallel to the membrane plane, and the other nearly perpendicular to it. These results lead us to propose a model of lipidic or partially lipidic pore

formation for the activity of these peptides, as also suggested for full-length Bax.

In the case of Bid-α6, the presence of negatively charged lipids strongly affects its membrane permeabilising activity. This peptide is able to release calcein at submicromolar concentrations, but not high molecular weight dextrans nor to induce lipid transbilayer diffusion. Bid-α6 forms discrete ion channels of 13-15 pS in PLM, and adopts a structure which is represented by one single type of tilted α-helix when associated with lipid membranes. This results show that the permeabilising activity of Bid-α6 is different from that of the Bax peptides, and suggest that it affects membrane permeability likely by means of barrel-stave pore formation.

Part VI.

Resumen en Español

11. Introducción y objetivos

11.1. Apoptosis

La apoptosis es un proceso de muerte celular programada altamente conservado y regulado, que juega un papel central en la muerte celular fisiológica de los organismos pluricelulares. Está implicada en procesos clave para el organismo, como el mantenimiento de la homeostasis de los tejidos, el desarrollo embrionario o el correcto funcionamiento del sistema inmunitario. Fallos en la regulación de la apoptosis pueden conducir a una proliferación celular excesiva, relacionada con los procesos cancerosos, o una muerte celular desproporcionada, implicada en enfermedades neurodegenerativas.

Inicialmente se describió como un tipo de muerte celular caracterizada por una serie de cambios morfológicos concretos, que producen un desmantelamiento celular ordenado, dando lugar a unas vesículas llamadas cuerpos apoptóticos, que encierran los contenidos celulares y que son fagocitadas por macrófagos vecinos. De modo que tras la apoptosis, la célula desaparece sin verter sus contenidos al medio, en contraposición a la muerte por necrosis.

Los principales ejecutores de la muerte celular son una familia de proteasas llamadas caspasas, que cortan selectivamente un conjunto concreto de proteínas diana de un modo coordinado, que conduce a la muerte por apoptosis. Las caspasas se sintetizan como proenzimas inactivos y, en respuesta a estímulos apoptóticos, se procesan y activan en una cascada de autoamplificación, ya que también son sustratos de ellas mismas. La activación de las caspasas supone un punto de no retorno para la muerte celular.

Dadas las dramáticas consecuencias de la acción de las caspasas, tanto su activación como su actividad están altamente reguladas. Por un lado, existen inhibidores de caspasas, o IAPs, que a su vez pueden ser contrarrestados por proteínas inhibidoras de IAPs, como SMAC/DIABLO (second mitochondrial activator of caspases/ direct IAP binding protein with low pI).

Por otro lado, el procesamiento y la activación de las caspasas se regula principalmente a través de dos rutas, conocidas como la ruta extrínseca y la ruta

intrínseca o mitocondrial. La ruta extrínseca responde a estímulos extracelulares a través de la oligomerización de receptores de la familia TNF-α, que a su vez activan a la caspasa 8, del grupo de las iniciadoras.

La ruta mitocondrial se activa en respuesta a la mayoría de los estímulos apoptóticos, y todos los intracelulares. Durante la apoptosis, la mitocondria experimenta un proceso de reestructuración y permeabilización específica de la membrana externa mitocondrial (OMM), que da lugar a la liberación de los llamados factores apoptóticos al citosol. Estos factores incluyen proteínas como citocromo c, AIF (Apoptosis Inducing Factor), SMAC/DIABLO, Omi/HtrA2, procaspasa-9 y Endonucleasa G. Las proteínas de la familia Bcl-2, que están formadas por miembros proapoptóticos y antiapoptóticos, controlan estos procesos al nivel de la OMM. La principal consecuencia de la liberación de los factores apoptóticos es la activación de un gran holoenzima llamado apoptosoma, que inicia la activación de las caspasas

A su vez, las rutas intrínseca y mitocondrial están interconectadas. En ciertos casos, caspasa-8 puede inducir la ruta mitocondrial a través de la activación de Bid, una proteína proapoptótica de la familia Bcl-2.

11.2. Las proteínas de la familia Bcl-2

Las familia de proteínas Bcl-2 controla la liberación de los factores apoptóticos de la mitocondria, y por tanto, los efectos apoptóticos de estos, como el ensamblaje del apoptosoma y la consiguiente activación de las caspasas. Las proteínas de esta familia, pese a su alto nivel de homología, presentan funciones opuestas, ya que algunas de ellas son proapoptóticas, e inducen la muerte celular por apoptosis, mientras que otras son antiapoptóticas y contrarrestan los efectos de las primeras.

Las proteínas de la familia Bcl-2 se clasifican además por el número de dominios de homología BH (se han definido hasta cuatro) que presentan. Así, los miembros antiapoptóticos, como Bcl-2 o Bcl-xL, forman el tipo I y se caracterizan por presentar los cuatros dominios BH. Los miembros proapoptóticos pueden ser de dos tipos: proteínas Bcl-2 de tipo II, como Bax o Bak, que contienen los dominios BH1, BH2 y BH3, y proteínas Bcl-2 de tipo III, o BH3-only, como Bid o Bim, que presentan sólo el dominio BH3. Los dominios BH1, BH2 y BH3 forman un hueco hidrofóbico, propio de los grupos I y II, que forma un sitio de unión para dominios BH3 de otras Bcl-2s, y posibilita las interacciones que dan lugar a los distintos patrones de homo- y heterodimerización descritos entre proteínas de la familia.

Varias líneas de evidencia relacionan la función de estas proteínas con su lo-

calización intracelular y su interacción con las membranas. Algunas de ellas se encuentran constitutivamente ancladas a las membranas celulares a través de un fragmento hidrofóbico en C-terminal, como Bcl-2, Bcl-xL o Bak. En cambio, otras son solubles en el citosol, como Bax, Bid o Bcl-w, y se translocan a las membranas celulares en respuesta a estímulos apoptóticos.

Se han resuelto las estructuras de las formas solubles de algunas proteínas de la familia, como Bcl-xL, Bax o Bid. Pese a sus funciones opuestas, todas son muy similares y presentan una horquilla de hélices hidrofóbicas ($\alpha 5\alpha 6$ en Bax y Bcl-xL, y $\alpha 6\alpha 7$ en Bid) rodeada por hélices anfipáticas, en una organización que recuerda a la de toxinas bacterianas como las colicinas o la δ-endotoxina. De acuerdo con esta analogía, se comprobó que Bax, Bid, Bcl-2 y Bcl-xL son capaces de formar canales iónicos en bicapas planas, y se propuso que la horquilla hidrofóbica central constituye el dominio formador de poros. Sin embargo, existe muy poca información sobre las estructuras de las formas activas e insertadas en la membrana de estas proteínas.

El mecanismo molecular de acción las proteínas Bcl-2 todavía se desconoce. En el caso de las proteínas antiapoptóticas, se ha descrito que la dimerización con miembros proapoptóticos a través del dominio BH3 es la responsable de la inhibición de estos últimos, de acuerdo con la idea de que el balance entre proteínas pro- y antiapoptóticas es esencial para el desencadenamiento final de la apoptosis. Sin embargo, se han propuesto otros mecanismos de inhibición independientes de BH3, todavía por esclarecer. Bcl-xL es un miembro representativo de esta familia que se encuentra constitutivamente anclado a la OMM a través de su dominio hidrofóbico C-terminal. Bcl-xL es capaz de inhibir la acción de Bax y de tBid mediante mecanismos dependientes e independientes de dimerización directa a través del dominio BH3. Se ha descrito que durante la apoptosis se genera una variante truncada de Bcl-xL, llamada ΔN-Bcl-xL que es proapoptótica y que es capaz de permeabilizar liposomas a citocromo c y a dextranos de alto peso molecular, y de desestabilizar bicapas planas mediante disminución de su tensión lineal.

Las proteínas BH3-only son las que presentan mayor divergencia estructural y de secuencia en la familia. Se ha propuesto que los componentes de este grupo son iniciadores esenciales de la apoptosis, que han evolucionado para reconocer las distintas formas de stress celular. Así, en respuesta a estímulos apoptóticos, las proteínas BH3-only se activan y se relocalizan a la OMM, donde inducen la liberación de citocromo c. Actúan a dos niveles: por una lado inhiben a las proteínas antiapoptóticas, y por otro activan a las proteínas de tipo Bax. El caso de Bid es uno de los más estudiados. Durante la apoptosis, Bid es procesada por caspasa-8 dando lugar a una forma truncada C-terminal activa llamada tBid.

Posteriormente, tBid es N-miristoilado y se transloca a la mitocondria, donde induce la liberación de citocromo c dependiente de la presencia de Bax o Bak. En sistemas *in vitro*, se ha descrito que tBid es capaz de liberar moléculas fluorescentes de LUVs y de formar canales iónicos en bicapas planas, además de colaborar con Bax y con cardiolipina para formar poros lipídicos de gran tamaño y de estructura toroidal (ver abajo).

En cuanto a las proteínas proapoptóticas del grupo II, se encuentran constitutivamente inactivas, bien solubles en el citosol, como Bax, o ancladas a la membrana por un dominio C-terminal, como en el caso de Bak. Estas proteínas son activadas por las BH3-only, de modo que se translocan a la mitocondria (en el caso de las citosólicas), y sufren un cambio conformacional que va acompañado de un proceso de oligomerización e inserción en la membrana, directamente relacionado con la liberación de los factores proapoptóticos al citosol. En el caso de Bax, la horquilla de hélices $\alpha 5\alpha 6$ parece ser esencial para su actividad. Estudios biofísicos han demostrado que Bax induce la liberación de citocromo c de LUVs en un mecanismo que depende de su estado de oligomerización, y que es capaz de disminuir el tiempo de vida media de bicapas planas. Además, en colaboración con tBid, Bax forma poros permeables a dextranos de alto peso molecular mediante un mecanismo que es sensible a la curvatura intrínseca de la membrana y que está relacionado con la redistribución de lípidos entre las monocapas de la membrana. Estas observaciones apoyan el modelo de acción propuesto para Bax, que se basa en la inducción de la liberación de los factores apoptóticos de la mitocondria mediante la formación de poros parcialmente lipídicos.

Aunque algunas evidencias están de acuerdo con el modelo de inserción análogo al de las colicinas que se ha propuesto para las Bcl-2s, este no es suficiente para explicar las grandes diferencias funcionales entre las proteínas de la misma familia. Por tanto, es necesario un mayor conocimiento de la interacción de estas proteínas con la membrana, en aspectos tales como la inserción de la horquilla central o su papel en la formación de poros, para definir modelos consistentes con su estructura funcional.

11.3. Objetivos

En este trabajo hemos abordado la caracterización de la interacción con membranas de las proteínas de la familia Bcl-2. Para ello hemos escogido un miembro representativo de cada uno de los grupos que constituyen la familia, en concreto, Bcl-xL, Bax y Bid, y nos hemos propuesto los siguientes objetivos:

- Análisis de predicción de fragmentos transmembrana en las secuencias de

Bax, Bid y Bcl-xL mediante el uso de los programas TopPredII y DAS.

- Evaluación de la tendencia a insertarse en la membrana que presentan los dominios hidrofóbicos de las proteínas Bax, Bid y Bcl-xL. Para ello, se han construido quimeras basadas en la proteína Lep, en las que se han insertado los distintos fragmentos hidrofóbicos, y se ha estudiado su inserción en la membrana mediante ensayos *in vitro* de transcripción/traducción/glicosilación.

- Síntesis química y purificación de los péptidos correspondientes a cada una de las hélices que forman la horquilla putativa formadora de poros. En concreto, los péptidos Bax$\alpha 5^K$, Baxα5, Baxα6, derivados del dominio putativo de formación de poros de Bax; Bidα6, Bidα7, derivados del dominio homólogo Bid; y Bcl-xlα5 y Bcl-xLα6 derivados de la horquilla correspondiente de Bcl-xL.

- Caracterización de la actividad formadora de poros de los distintos péptidos, mediante ensayos de liberación de calceína y dextranos fluorescentes de diversos tamaños de vesículas unilamelares grandes (LUVs) de diversas composiciones lipídicas, ensayos de redistribución lipídica entre las monocapas de LUVs asimétricas, y formación de canales iónicos en bicapas planas.

- Caracterización estructural de los péptidos en entorno acuoso, en medios miméticos de membrana y en presencia de LUVs, mediante experimentos de dicroísmo circular (CD) y espectroscopia de infrarrojo de transformada de Fourier (FTIR).

12. Materiales y métodos

12.1. Preparación de quimeras de Lep

En las preparaciones de plásmidos de E. coli (cepas DH5α, XL1Blue y JM110) a pequeña escala se utilizó el kit de comercial de extracción de DNA de Qiagen, según las instrucciones del fabricante. Las reacciones en cadena de la polimerasa (PCR) se llevaron a cabo en un volumen final de 50 μL, con 0.1-1 ng de DNA molde, 2 μM de oligonucleótidos cebadores (Isogen), 0.5 mM de dNTPs, 1x de tampón de PCR comercial, 3 mM $MgCl_2$ y 5 unidades de Taq polimerasa (Bioline). Tras una desnaturalización inicial de 30 s a 95°C, se realizaron 30 ciclos de amplificación (30 s a 94°C, 30 s a 55°C, 30 s a 72°C) y un paso de extensión final de 10 min a 72°C. El DNA amplificado fue purificado (PCR Purification Kit de Qiagen) y digerido con los enzimas de restricción BclI y NdeI (Roche). En las reacciones de mutagénesis dirigida se empleó el Quick Change Kit (Stratagene), de acuerdo con las instrucciones del fabricante, y el DNA amplificado se transformó en células supercompetentes comerciales XL1Blue, según el manual de instrucciones.

Los vectores usados en este estudio derivan de pGem-1Lep (proporcionado amablemente por el Prof. von Heijne, Universidad de Estocolmo), descrito en (39). En la variante pGEM-Lep-NST, el gen Lep se ha mutado en 214N-E-T216 a 214Q-Q-T216, se han introducido un sitio de glicosilación en 90N-S-T92, y sitios de restricción para BclI y NdeI antes y después del fragmento H2, respectivamente. El vector pGEM-LepΔH1 tiene además una deleción en el fragmento H1 y un sitio de glicosilación adicional en N-terminal. Las secuencias de DNA que codifican para Bcl-xL y Bax fueron proporcionadas por G. Nuñez (Universidad de Michigan) y la de Bid por X. Wang (Universidad de Texas).

Las quimeras de Lep con los fragmentos putativos transmembrana de las distintas proteínas Bcl-2 en lugar del fragmento H2 natural se prepararon de la siguiente manera: los fragmentos de interés de Bcl-xL, Bax y Bid fueron amplificados por PCR conteniendo sitios de restricción para BclI y NdeI, y digeridos con estos enzimas. Tras su purificación, los insertos fueron introducidos en el vector corre-

spondiente previamente digerido con BclI y NdeI mediante reacciones de ligación de 10 μL conteniendo 3 unidades de ligasa de DNA T4 (Promega). Las construcciones Lep(+)α5α6Bcl-xL-EEE, Lep(+)α5α6Bcl-xL-EEE-C79W y Lep(+)α5Bcl-xLC79W se produjeron por mutagénesis dirigida a partir de Lep(+)α5α6Bcl-xL y Lep(+)α5Bcl-xL respectivamente. En la primera, los codones 166I-A-A168 (numeración de Bcl-xL humana) se cambiaron a codones de E, y en la siguientes, el codón C151 se reemplazaron por un codón de W.

12.2. Ensayos de glicosilación y asociación con microsomas

La transcripción de las quimeras derivadas de Lep se llevó a cabo utilizando el Ribomax Large Scale RNA Production System-SP6 (Promega), durante 2 h a 37°C, en reacciones de 50 μL que contenían: 10 μL de tampón de traducción, 5 μL de rNTPs 25 mM, aproximadamente 1 μg de DNA molde y 5 μL de mezcla enzimática. Los RNAs obtenidos se purificaron con el RNeasy RNA Purification Kit (Qiagen), según las instrucciones del fabricante.

Los RNAs se tradujeron con el Reticulocyte Lysate System (Promega), durante 2 h a 30°C, en reacciones de 15 μL que contenían: 10 μL de lisado de reticulocitos, 0.5 μL de una mezcla de aminoácidos 100 mM, 1 μL ^{35}S-Met 100 mM (Amersham Biosciences) y aproximadamente 150 ng de RNA. En las reacciones adecuadas se añadió 1 μL de microsomas de páncreas de perro (Promega). Como control de glicosilación, se añadió a las reacciones correspondientes un péptido aceptor de glicosilación Ac-NYT-NH_2con una concentración final de 100 μM, que actúa como un inhibidor competitivo de la glicosil transferasa de los microsomas. Para comprobar que esta inhibición era específica de secuencia, se utilizó en las reacciones adecuadas un péptido no aceptor con la secuencia Ac-QYT-NH_2. Como control de procesamiento, se añadió a las reacciones correspondientes un inhibidor (SPI) específico de la peptidasa señal (SPase), N-metoxisuccinil-A-A-P-V-clorometilcetona, a concentración final de 2mM. Las muestras se sometieron a SDS-PAGE 10 % y se fijaron en los geles con una disolución de 20 % metanol y 5 % ácido acético. Los geles fueron secados y expuestos toda la noche a una pantalla intensificadora (Fujifilm) que fue revelada con un Phosphorimager PLA-3000 de Fujifilm.

Las extracciones alcalinas y los tratamientos con urea se realizaron de acuerdo a (75) y (76) respectivamente. Tras la traducción, se añadió 4 volúmenes de 100 mM Na_2CO_3 pH 11.5 o 4 M urea (en tampón 35 mM Tris-HCl, pH 7.4, 140 mM NaCl) a las mezclas con microsomas y se centrifugó a 3000 g a 4°C durante

10°C. Las muestras clarificadas se depositaron sobre 50 μL de colchón de sacarosa y se ultracentrifugaron a 100000 g a 4°C durante 20 min. Los sobrenadantes y precipitados se analizaron por SDS-PAGE 10 % (extracciones alcalinas) o 12 % (extracciones con urea) como arriba.

Los experimentos de partición con Tritón-X114 se realizaron según (76). Se añadieron 15 μL de Tritón-X114 hidratado a las muestras de reacción con microsomas y se incubó 30 min en hielo. Las mezclas se equilibraron después 10 min a 37°C para desarrollar las fases acuosa y orgánica, que se separaron por centrifugación a 10000g y 37°C. La fracción inferior, enriquecida en detergente, se lavó 2 veces con 10 volúmenes de tampón sin detergente, con agitación, incubación de 30 min en hielo y separación de fases como anteriormente. Las proteínas presentes en las fases acuosa y orgánica fueron precipitadas en acetona y analizadas por SDS-PAGE 12 % como arriba.

12.3. Programas de predicción

Las secuencias de Bcl-xL, Bax y Bid fueron analizadas en busca de posibles fragmentos transmembrana con los programas TopPredII (67) y DAS (68). La búsqueda de posibles sitios de corte de la peptidasa señal se realizó con el programa SignalIP (69). Estos programas fueron usados vía internet y utilizando los parámetros estándar. Su localización URL es: TopPredII, http://bioweb.pasteur.fr/seqanal/interfaces/toppred.html; DAS, http://www.sbc.su.se/~miklos/DAS/maindas.html, SignalIP, http://www.cbs.dtu.dk/services/SignalP/ .

12.4. Síntesis y purificación de péptidos

Los péptidos de la tabla ... se sintetizaron químicamente de acuerdo a Villar2001. Se sintetizaron dos péptidos correspondientes a la hélice $\alpha 5$ de Bax. Inicialmente se añadió una lisina en cada extremo, Bax$\alpha 5^K$, para mejorar su solubilidad y manejo (Orzáez2004), y después se sintetizó un segundo péptido sin las lisinas, Bax$\alpha 5$, y con una secuencia homologa a la de Bcl-xl$\alpha 5$. En Bid se mutó una Thr por Tyr para permitir su cuantificación espectrofotométrica, y las Cys de las secuencias naturales se mutaron a Ser en los péptidos para evitar problemas de oxidación y agregación.

La síntesis en fase sólida de los péptidos se realizó en un sintetizador Applied Biosystems 433A utilizando química Fmoc y resina Tentagel S-RAM (sustitución 0.24 meq/g). Se utilizaron 6 excesos (molar) de aminoácidos (Senn Chemicals) y acoples dobles y triples en las posiciones difíciles (fisher2001). Todos los pép-

tidos fueron amidados en C-terminal y acetilados en N-terminal. La reacción final de corte y desprotección se realizaron en 70 % ácido trifluoroacético, 20 % diclorometano, 5 % agua, 2.5 % triisobutilsilano, 2.5 % etanoditiol (v/v). Los péptidos cortados se precipitaron en t-butilmetil éter frío y se centrifugaron. Los precipitados fueron secados y redisueltos en agua:acetonitrilo (90:10), y liofilizados. Los péptidos fueron purificados hasta una pureza aproximada del 95 %, por cromatografía de alta resolución en fase reversa (RP-HPLC) con una columna C18. Los péptidos purificados fueron liofilizados y su masa molecular fue confirmada por espectrometría de masas. La concentración de los péptidos en los experimentos se calculó por espectroscopia UV-Visible, utilizando los coeficientes de extinción de la tabla ... .

12.5. Ensayos de permeabilización y de redistribución lipídica en LUVs

Todos los lípidos usados eran de Avanti Polar Lipids, excepto la asolectina, que era de Sigma, y purificada según (Kagawa1971). Los lípidos disueltos en cloroformo se mezclaron en la composición molar deseada y se secaron en vacío en un matraz de fondo redondo. En el caso de los LUVs con calceína, la película lipídica se resuspendió a una concentración de 4 mg/mL de 80 mM calceína. Tras seis ciclos de congelación/descongelación, se pasaron 31 veces a través de dos filtros de policarbonato de 100 nm de tamaño de poro, utilizando un extrusor de Avestin. Para eliminar la calceína no encapsulada, los LUVs se lavaron con minicolumnas de Sephadex-G50 preequilibradas con 140 mM NaCl, 20 mM HEPES, 1 mM EDTA pH 7 (tampón A). Los LUVs con dextranos fluorescentes encapsulados de 20 (FD-20) o 70 kDa (FD-70) se prepararon por resuspensión de la película lipídica en 100 mg/mL de los dextranos correspondientes en tampón A. Las vesículas se congelaron y descongelaron 20 veces y fueron pasadas a través de filtros de policarbonato de 200 nm de diámetro de poro, como se ha descrito arriba. Los dextranos no encapsulados se eliminaron por cromatografía de filtración en gel con una columna de 35x1.6 cm, empaquetada con Sephacryl HS-500 (Amersham Biosciences) y equilibrada con tampón A. El tamaño de las vesículas se midió por dispersión cuasielástica de la luz (QLS) utilizando un Malvern Z-Sizer 3, como se describe en ... . La concentración lipídica se determinó con el kit comercial Phospholipids B (WAKO), según las instrucciones del fabricante.

La actividad permeabilizadora de los lípidos se determinó a temperatura ambiente midiendo la liberación de calceína o dextranos marcados fluorescentemente de LUVs. Los experimentos de liberación de calceína se realizaron en placas de

96 pocillos pretratadas con 0.1 mg/mL Prionex (Pentapharm). Tras la adición de 100 μL de LUVs, a una concentración final entre 2 y 5 μg(mL), se midió la liberación de calceína en un lector de placas Fluostar (BMG) como el aumento de la fluorescencia a 520 nm con el tiempo, excitando a 495 nm. Los experimentos de liberación de dextranos se realizaron en cubetas de 1cm de camino óptico a una concentración de LUVs de 45 μM en tampón A. La cinética se liberación se midió como el aumento de fluorescencia a 520 nm con el tiempo, excitando a 490 nm y con anchura de banda de 2 nm. El porcentaje de liberación de sonda fluorescente se calculó con la siguiente expresión:

$$R = \frac{(F_{ss} - F_{i)}}{(F_m - F_i)} 100 \tag{12.1}$$

donde F_{ss} es la fluorescencia en el estado estacionario, F_i es la fluorescencia inicial antes de añadir los péptidos, y F_m es la fluorescencia máxima tras la adición de 1 mM Tritón X-100. La liberación espontánea de las sondas fue despreciable en todos los casos.

Los experimentos de difusión lipídica entre monocapas se realizaron con LUVs asimétricos preparados como en ... . El lípido fluorescente pireno-fosfatidilcolina (pyPC) disuelto en etanol, se añadió a una disolución de tampón A a una concentración final de 1 μM, sobre la que se añadieron los LUVs a una concentración final de 20 μM. La pyPC se incorporó espontáneamente a la monocapa externa de los LUVs tras una incubación de 20 min. Los espectros de emisión entre 355 y 500 nm se midieron a temperatura ambiente utilizando un fluorímetro ... con una cubeta de 1 cm de camino óptico y agitación constante. La excitación se realizó a 345 nm, con anchuras de banda de 4 nm. Durante los experimentos, los espectros de fluorescencia se midieron a varios tiempos tras la adición del péptido correspondiente. La relación entre el lípido monomérico (I_Ma 395 nm) y la forma de excímero (I_Ea 465 nm) medida a partir de los espectros, se representó como I_E/I_M frente al tiempo.

12.6. Formación de canales iónicos

Las propiedades eléctricas de Bax$\alpha 5^K$ y Bidα6 en bicapas planas (PLM) se midieron como en DallaSerra2000. Los experimentos se hicieron a temperatura ambiente en membranas de 1,2-diftanoil-sn-glicerofosfocolina (DPhPC), asolectina, o PC:PA (4:1, razón molar). Los péptidos se añadieron al lado *cis* de membranas estables con una capacitancia de 100 pF, bañadas por tampón A. Las corrientes macroscópicas se midieron con un amplificador de "patch-clamp" (Axon Instru-

ments) y se filtraron a 100 Hz con el programa Axoscope 8. Para calcular la relación I/V, se midió la intensidad de corriente a distintos potenciales . En los experimentos de selectividad, se midieron los voltajes de anulación en un gradiente de NaCl en el lado *trans*, y la razón P_+/P_-(P_+ y P_-se refieren a la permeabilidad a cationes y aniones, respectivamente) se calculó mediante la ecuación Goldman-Hodgkin-Katz (DallaSerra2000).

12.7. Experimentos de dicroísmo circular

Los experimentos de dicroísmo circular (CD) se realizaron a 30 μM de péptido en 10 mM de tampón fosfato a pH 7. Varios porcentajes de trifluoroetanol (TFE) o dodecilsulfato de sodio (SDS) se añadieron a las muestras correspondientes. Los espectros fueron medidos a 20^{o}C en un espectropolarímetro Jasco J-810, con una cubeta de 1 mm de camino óptico. Para cada espectro, se tomaron puntos cada 0.2 nm a 100 nm/min desde 250 a 185 nm, y se promediaron 10 medidas. El análisis de los datos se realizó con el programa CDPro (Sreerama2000).

12.8. Medidas de ATR-FTIR

Las muestras peptídicas para los experimentos de espectroscopia de infrarrojo de transformada de Fourier, con reflexión total atenuada (ATR-FTIR), se incubaron 1 h con LUVs de fosfatidilcolina (PC) o PC y ácido fosfatídico (PA) (1:1 razón molar) a una relación 1:50 mol/mol proteína/lípido en tampón A. Las muestras se centrifugaron (Optima TL, Beckman) a 350000g durante 3 h a 4^{o}C. Tras la centrifugación, el sedimentos se resuspendió en 100 μL de 10 mM HEPES pH 7. Las muestras se depositaron sobre cristales de Ge de 10 reflexiones y ángulo de corte de 45^o, y se secaron con flujo de N_2. Los péptidos en disolución acuosa se secaron directamente sobre el cristal desde tampón A, y luego fueron redisueltos en TFE y secados de nuevo para tomar nuevos espectros. Los espectros se midieron en un espectrofotómetro FTS 185 (BioRad) con detector MCT. En los experimentos de polarización se usó un polarímetro rotatorio KRS5 a 0 y 90^o respecto al plano de reflexión. Los espectros obtenidos se analizaron con el programa GRAMS (Galactic Indutries).

La orientación de los elementos estructurales se calculó a partir de la razón dicroica $R = A_{0^o}/A_{90^o}$, donde A_{0^o} y A_{90^o} son las absorciones del grupo funcional de ese elemento en configuraciones paralela y perpendicular respectivamente (Tamm1997,Goormaghtigh1999). A partir de R se calculó el factor de forma S, que se usó ara calcular el ángulo promedio de inclinación β como en Axelsen1995.

Para estimar cuantitativamente el contenido en estructura secundaria de los péptidos, la banda amida (1700-1600 cm^{-1}) se descompuso en un conjunto de Lorencianas, cuyas frecuencias se asignaron a los distintos elementos estructurales de forma estándar (Menestrina1999). El conjunto de Lonrencianas se ajustó al espectro original y las áreas relativas resultantes se interpretaron como porcentajes de estructura asociada. La banda de las cadenas laterales fue excluida de la normalización. La presencia de TFA a 1672 cm^{-1} en algunos casos se eliminó digitalmente. Las absorciones a 1624 y 1692 cm^{-1} corresponden a formas agregadas del péptido formadas durante la preparación de la muestra, y fueron excluidas de los cálculos de estructura secundaria. El análisis cualitativo de la estructura secundaria se basó en las componentes de absorción principales en la región amida I del espectro. Se obtuvieron los espectros diferencia por substracción de la banda amida I normalizada del espectro en tampón A a las bandas amida I normalizadas de los espectros en TFE o en presencia de LUVs.

La relación lípido/péptido (L/P) en el sedimento se calculó mediante la ecuación (TAmm19993,Rodionova1995):

$$L/P = 0{,}208(n_{res}-1)\frac{(1-S_{amideI'})}{(1+S_L/2)}\frac{\int_{2800}^{2980} A_{90^o}(\nu_L)d\nu}{\int_{1600}^{1690} A_{90^o}(\nu_{amideI'})d\nu} \qquad (12.2)$$

Donde n_{res} es el número de residuos del péptido, A_{90^o} es la absorción con el polarímetro a 90°, y S_L y $S_{amideI'}$ son los parámetros de orden de las cadenas lipídicas y de la banda amida I' respectivamente. La integral con el sufijo L se calculó a partir del espectro del lípido solo, y la del sufijo amideI' a partir del espectro no agregado del péptido (menos la contribución del lípido). El parámetro de orden de la hélice α, S_α, se calculó a partir de la componente Lorenciana a 1651±5 cm^{-1} con θ=30° (frey1991,Axelsen1995,Menikh1997).

13. Resultados

13.1. Inserción en membrana de Bax, Bcl-xL y Bid

La interacción de las proteínas de la familia Bcl-2 probablemente implica la inserción de otros segmentos hidrofóbicos, además de los dominios de anclaje C-terminal de Bcl-xL y Bax, ya caracterizados. Con el objetivo de localizar posibles fragmentos transmembrana (TM), realizamos un análisis de las secuencias de Bcl-xL, Bax y Bid con los programas TopPredII (67) y DAS (68). Utilizando sus valores estándar, el TopPredII y el DAS detectaron dos fragmentos TM en Bcl-xL y dos en Bax, que en ambos casos corresponden a sus fragmentos C-terminal y hélice $\alpha 5$. En el caso de Bid, sólo la hélice $\alpha 6$ se predijo como TM, y el segmento N-terminal (residuos 10-30) se predijo como putativo TM. Además, el DAS detectó también un fragmento putativo de membrana en la hélice $\alpha 5$ de Bcl-xL, y varios picos de hidrofobicidad notable, pero no suficiente, que correspondían a las hélices $\alpha 1$ de Bax y Bcl-xL, la hélice $\alpha 6$ de Bax y las $\alpha 4$ y $\alpha 7$ de Bid.

13.1.1. Fragmentos de Bcl-xL que se insertan en membrana

Los experimentos de marcaje con glicosilación en ensayos de transcripción/traducción/inserción han sido utilizados previamente para estudiar la topología de fragmentos TM putativos en membranas de microsomas (vesículas derivadas del RE) (80). Estos estudios se basan en quimeras de la proteína Lep (ver 12.2), que presenta un fragmento TM en N-terminal (H1), que dirige la proteína a la membrana y determina su topología, seguido de un lazo cargado positivamente (P1) y un segundo fragmento que en Lep original es TM (H2). Por último, en C-terminal presenta un dominio soluble P2 con un sitio de glicosilación. En las quimeras de Lep, H2 se sustituye por el fragmento que se desea estudiar. Si el fragmento introducido en H2 es capaz de insertarse en la membrana, P2 queda orientado al lúmen del microsoma y el sitio de glicosilación es accesible a la glicosil transferasa, que lo glicosila. Si el fragmento introducido no se inserta en la membrana, P2 queda orientado al exterior del microsoma y no se glicosila. Se puede distinguir entre estas dos situaciones porque la proteína glicosilada sufre un retardo en SDS-PAGE

equivalente a unos 2 kDa con respecto a la proteína sin glicosilar.

De acuerdo con las predicciones de TopPredII y DAS, los fragmentos correspondientes a las hélices $\alpha 1$, $\alpha 5$ y $\alpha 6$ y el fragmento C-terminal de Bcl-xL fueron introducidos en quimeras de Lep, sustituyendo a H2. Los ensayos de glicosilación se muestran en la figura .... En ellos se observa que el fragmento C-terminal da lugar a una banda glicosilada, que indica que se inserta en la membrana, de acuerdo con otros estudios previos. En los casos de las hélices $\alpha 1$ y $\alpha 6$ no se observa banda de glicosilación, lo que indica que estos fragmentos no se insertan en la membrana, al menos en el contexto de la quimera de Lep. En el caso de la construcción con la hélice $\alpha 5$, se observa una banda de peso molecular menor, que corresponde a una banda de procesamiento. Esto se demuestra al añadir un inhibidor específico de la peptidasa señal, que disminuye la intensidad de la banda, y al hacer un mutante de no procesamiento C79W (basado en los resultados de secuencias señal obtenidos con el programa SignalIP), que da lugar a una banda que corresponde a la proteína no procesada y glicosilada. Además, la banda de procesamiento está glicosilada, como se observa al añadir un péptido aceptor que actúa como inhibidor competitivo de la glicosil transferasa. En este caso, tanto la glicosilación como el procesamiento, son modificaciones post-traduccionales indicativas de la inserción del fragmento $\alpha 5$ en la membrana de los microsomas.

Aunque la ausencia de inserción de la hélice $\alpha 6$ está de acuerdo con su baja tendencia TM según los programas de predicción, esta hélice forma parte del putativo dominio de formación de poros de Bcl-xL y existía la posibilidad que el contexto de la proteína afectase a su inserción en membrana. Para estudiar este asunto, se construyó una quimera de Lep que contenía la horquilla $\alpha 5\alpha 6$ en lugar de H2. Como se muestra en la figura ... , esta quimera no se glicosilaba, lo que se podía interpretar como inserción simultánea de ambas hélices o no inserción de ninguna de ellas. Para esclarecer este asunto, se creó un mutante en el que se introdujeron tres glutámicos en la hélice $\alpha 6$ que eliminaban totalmente su tendencia a insertarse. Este mutante daba lugar a una banda de procesamiento, que a su vez estaba glicosilada, y que desaparece al mutar C79W. Estos resultados indican que la ausencia de glicosilación en la quimera de $\alpha 5\alpha 6$ se debe a una inserción simultánea de las dos hélices.

En experimentos con una versión de la quimera de Lep en la que se ha delecionado el fragmento TM H1 y se ha añadido un sitio de glicosilación en N-terminal (LepΔH1) (ver figura ...), se obtuvieron evidencias adicionales a favor de la inserción de la horquilla de Bcl-xL. La construcción LepΔH1/Bcl-xL$\alpha 5\alpha 6$ no daba lugar a banda de glicosilación, pero permanecía asociada a membranas tras ensayos de sedimentación de microsomas y de extracción alcalina y con urea. Estos resultados indican que la quimera se encuentra insertada en la membrana, pero

que ninguno de los sitios de glicosilación son accesibles a la glicosil tranferasa, de acuerdo con una topología en la que ambas hélices se encuentran insertadas en la membrana y los extremos N y C-terminal se encuentran orientados al exterior de los microsomas. La inserción de la quimera en la membrana se demostró además con experimentos de partición a Tritón X-114, en los que la proteína se repartía a la fase orgánica junto con la fracción de membranas.

13.1.2. Fragmentos de Bax que se insertan en la membrana

Cuando se ensayaron los fragmentos hidrofóbicos de Bax en experimentos de marcaje por glicosilación (ver figura ...), se obtuvo que la hélices α9, que corresponde al fragmento C-terminal, y α5, daban patrones de modificación post-traduccional análogos a los de Bcl-xL, indicando la inserción de estos fragmentos. Del mismo modo, la hélice α6 tampoco mostraba glicosilación ni, por tanto, inserción. Sin embargo, a diferencia de Bcl-xL, en este caso la quimera Lep/Baxα1 sí que daba lugar a una banda de glicosilación indicativa de inserción en la membrana microsomal.

También en este caso se estudió la inserción de la horquilla Baxα5α6 en el contexto de las quimeras Lep(+)NST y LepΔH1. Como se muestra en las figuras ..., las quimeras de Bax no se glicosilan ni procesan al traducirse en presencia de microsomas. En el caso de LepΔH1/Baxα5α6, al igual que la correspondiente a Bcl-xL, la proteína permanece asociada a las membranas en los ensayos de sedimentación, extracción alcalina y con urea, y partición con Tritón X-114, lo que sugiere la inserción simultánea de las hélices α5α6 de Bax, con los fragmentos N y C-terminal orientados al exterior de las vesículas.

13.1.3. Fragmentos de Bid que se insertan en la membrana

El perfil de hidropatía de Bid es distinto al de Bax y Bcl-xL. En este caso, la hélice α1 de Bid, en el contexto de la quimera de Lep, no se glicosila ni, por tanto, se inserta, tal y como se muestra en la figura ..., de acuerdo con los datos existentes en la bibliografía. Tampoco la hélice α4 daba un patrón de inserción en la membrana. Únicamente la hélice α6, que es homóloga a las hélices α5 de Bcl-xL y Bax, daba bandas de procesamiento y glicosilación indicativas de inserción en la membrana.

Finalmente, estudiamos la inserción de la horquilla α6α7, que a pesar de la baja hidrofobicidad de α7, se considera también un dominio de inserción tipo colicinas. La quimera Lep/Bidα6α7 dio lugar a una banda de glicosilación que indicaba la inserción sólo de la hélice α6. La fracción sin glicosilar podía sin

embargo deberse, como en casos anteriores, a la inserción de ambas hélices o de ninguna de ellas. Los ensayos con LepΔH1/Bidα6α7 se muestran en la figura ..., indican que la horquilla es capaz de insertarse integralmente en la membrana, ya que la quimera permanece asociada a la membrana tras los experimentos de sedimentación, extracción alcalina y con urea, y partición con Tritón X-114.

13.2. Estudios funcionales

La función de muchas proteínas de la familia Bcl-2 se ha relacionado con su capacidad para permeabilizar membranas, y las horquillas de hélices hidrofóbicas en el núcleo de las estructuras de las formas solubles de Bax, Bid y Bcl-xL son consideradas como los dominios formadores de poros de estas proteínas. Estas hélices son predominantemente hidrofóbicas y son capaces de insertarse en la membrana en sistemas quiméricos (ver 13.1). Con el objetivo de estudiar su interacción con vesículas lipídicas, sintetizamos péptidos que incluyen la secuencia de las hélices individuales que forman las horquillas hidrofóbicas (ver 12.4): Baxα5 y Baxα6 en el caso de Bax, Bidα6 y Bidα7 para Bid, y en el caso de Bcl-xL, los péptidos Bcl-xLα5 y Bcl-xLα6.

13.2.1. Liberación de contenidos de LUV

La permeabilización de las membranas a nivel macroscópico se estudió en experimentos de liberación de calceína y de dextranos marcados fluorescentemente (FD-20 y FD-70) de LUVs de diversas composiciones lipídicas. No todos los péptidos fueron capaces de permeabilizar las vesículas a concentraciones relativamente bajas.

Péptidos derivados de Bax

Como se observa en las figuras ... y ..., los péptidos Baxα5 y Baxα6, se mostraron capaces de permeabilizar los LUVs a calceína y a dextranos de alto peso molecular a concentraciones del orden de nanomolar. Baxα6 necesitaba aproximadamente el doble de concentración para producir efectos comparables a Baxα5, pero en ambos casos su actividad se encuentra en el rango de concentraciones descrito para la proteína completa Bax. La posibilidad de permeabilización a través de un efecto tipo detergente, fue descartada tras comprobar por QLS que estos péptidos no afectaban significativamente al tamaño de las vesículas en concentraciones que inducían liberación significativa de dextranos.

El efecto de la composición lipídica se estudió sistemáticamente mediante experimentos de liberación de calceína (ver tabla ...). A pesar de que ambos péptidos presentan una carga neta positiva, la presencia de lípidos cargados negativamente disminuye la actividad de Baxα5 y Baxα6. En cambio, la presencia de lípidos con curvatura positiva, como la lisofosfatidilcolina (LPC), induce un aumento notable de su actividad, de acuerdo con los experimentos descritos con Bax. En el caso de lípidos con curvatura intrínseca negativa, como la fosfatidiletanolamina (PE), que tiene un efecto inhibidor sobre la proteína Bax, los resultados obtenidos muestran un comportamiento análogo para Baxα6. Sin embargo, la presencia de PE produce un pequeño aumento de la actividad de Baxα5.

Péptidos derivados de Bid

En el caso de los péptidos derivados de Bid, sólo Bidα6 era capaz de liberar calceína de LUVs en el rango nanomolar de concentraciones (figura ...). Sin embargo, este péptido era incapaz de liberar dextranos de alto peso molecular. Estas observaciones son análogas al comportamiento descrito para la proteína tBid. En cambio, de Bidα7, sólo era capaz de liberar calceína a concentraciones en el rango micromolar.

En ambos casos, los péptidos presentan una carga neta positiva, y como era de esperar, la presencia de lípidos con carga negativa induce un aumento de su actividad con respecto a LUVs neutros (ver tabla ...). La cardiolipina (CL), que según la bibliografía dirige a tBid a la OMM, no produjo ningún aumento en la actividad que no fuese explicable por su carga negativa. Además, y a diferencia de lo observado con los péptidos de Bax, la presencia de lípidos con curvatura intrínseca positiva apenas afecta su capacidad de permeabilización.

Péptidos derivados de Bcl-xL

A pesar del alto nivel de homología con los péptidos de Bax, tanto Bcl-xLα5 como Bcl-xLα6 presentan una actividad mil veces menor que la observada en los péptidos de Bax (ver figura ... y tabla ...). Bcl-xLα5 no llegó a liberar el 50 % de calceína en las condiciones ensayadas. La actividad de Bcl-xLα6 era algo mayor, siempre en la zona micromolar de concentraciones, y aumentaba ligeramente en presencia de LPC o fosfatidilserina (PS) en comparación con las vesículas de PC.

13.2.2. Formación de canales en bicapas planas

Los experimentos de formación de canales en bicapas planas con Bax$\alpha5^K$ y Bidα6 nos permitieron estudiar la formación de canales individuales a nivel microscópico,

además de caracterizar su dependencia con el voltaje aplicado y la selectividad iónica (DallaSerra2003). En ambos casos, los péptidos afectaban muy poco a la permeabilidad de membranas de DPhPC, pero en membranas de asolectina o PC:PA (4:1), ambos inducían conductividad iónica.

Nada más ser añadido a bicapas de asolectina, Bax$\alpha 5^K$ mostraba ya interacción con la membrana a potenciales positivos bajos (ver figura ...). A partir de +10 mV se observó un incremento continuo en la corriente. Sin embargo este efecto no ocurría a potenciales negativos, y la conductividad se recuperaba al volver a potenciales positivos. En cierto punto, probablemente cuando la concentración de péptido en la membrana había alcanzado un nivel crítico, se formaban un poro de conductividad muy alta, entre 0.3 y 5 nS, de intensidad independiente del potencial aplicado. Este canal permanecía abierto largo tiempo, tanto a potenciales positivos como negativos, y finalmente provocaba la ruptura de la bicapa. Este comportamiento se ha relacionado con la formación de poros toroidales, en cuyo caso los grupos polares forman parte del borde del poro y afectan a su selectividad iónica. Para comprobar esta hipótesis, se midió la selectividad iónica en membranas neutras y cargadas negativamente. Los poros formados resultaron ser selectivos para cationes en membranas de asolectina, con una carga neta negativa, y no selectivos en membranas neutras de DPhPC, de acuerdo con la hipótesis de partida.

En el caso de Bid$\alpha 6$, el péptido era capaz de formar canales únicamente en membranas con carga neta negativa. En distintos experimentos se llegó a observar al apertura y el cierre de hasta 8 canales discretos de baja conductividad, entre 13-15 pS, que se abrían igualmente a potenciales positivos y negativos independientemente del potencial aplicado (figura ...).

13.2.3. Difusión lipídica entre monocapas

El modelo de poro toroidal implica el contacto entre las monocapas en estructuras no lamelares que se crean en la pared del poro. Como consecuencia, los lípidos pueden difundir libremente entre la monocapas. Para comprobar si los péptidos derivados de las Bcl-2s formaban este tipo de poros, se prepararon LUVs asimétricos con un lípido fluorescente (pyPC) en la monocapa externa. La difusión de la pyPC a la monocapa interna tras la adición de los péptidos se midió como la disminución de la relación I_E/I_M, como consecuencia de la dilución de la sonda (ver 12.5). Sólo tras la adición de Bax$\alpha 5$ y Bax$\alpha 6$ se observó redistribución de pyPC a la monocapa interna, de acuerdo con el modelo de poro lipídico (figura ...).

13.3. Estudios estructurales

Con objeto de establecer relaciones entre la actividad observada en los distintos péptidos y su estructura en diversos medios, llevamos a cabo su caracterización por CD y ATR-FTIR. Los espectros de CD fueron evaluados con el paquete CDPro, que combina análisis de los programas CDSSTR, CONTINLL y SELCON3. En el caso de Bax$\alpha 5^K$ y Bid$\alpha 6$, se realizó un análisis cuantitativo de los espectros de FTIR, y obtuvimos los porcentajes de estructura secundaria y una estimación de la orientación de los péptidos respecto al plano de l membrana.

Péptidos de Bax

En el caso de Bax$\alpha 5^K$, en los espectros de CD (figura 8.1) se observa que el péptido está desestructurado en medio acuoso, pero en presencia de TFE o SDS, experimenta un cambio conformacional consistente con una organización en hélice α de hasta un 60 % (ver tabla 8.1). Los resultados de FTIR son consistentes con los de CD. En medio acuoso, el péptido presenta un 40 % de forma agregada en torno a 1626 cm^{-1} y, al pasar a TFE, o en presencia de LUVs de PC o PC:PA (1:1), el péptido sufre un cambio conformacional caracterizado por una disminución a la mitad de la fracción agregada. En cambio, la distribución de estructuras en la parte no agregada permanece casi igual, con un 60 % de hélice α, un 13 % de giro β y un 27 % de estructura al azar (tabla 8.2). Además, la fracción helicoidal se distribuye en dos bandas, centradas a 1656 (α_1) y 1646 cm^{-1} (α_2). Esta última no aparece en la región típica de las hélices α, pero ha sido descrita en otros péptidos que se unen a membrana, como la melitina (sharon1999). A partir de los espectros polarizados, se calculó la orientación de cada una de las hélices respecto al eje de las cadenas lipídicas: $\alpha_1$presenta una orientación de 59º en PC:PA y 0º en PC, mientras que α_2 presenta 90º en ambos casos (tabla 8.3).

En cambio, el análisis de CD de Bax$\alpha 5$ muestra que este péptido presenta ya un 40 % de hélice en medio acuoso, que aumenta hasta un 90 % en presencia de pequeñas cantidades de SDS o TFE (tabla 8.1). Este cambio conformacional se observa también en los espectros de FTIR a través de la disminución de la forma agregada (figura8.4). En LUVs de PC el máximo de absorción aparece a 1648 cm^{-1}, lo que sugiere la presencia de los dos tipos de hélice descritas para Bax$\alpha 5^K$.

En el caso de Bax$\alpha 6$, de nuevo las valoraciones con TFE y SDS inducen la estructuración del péptido en hélice α, pero en este caso el cambio es gradual y llega hasta el 60 % (tabla 8.1). El análisis cualitativo de los espectros de FTIR muestra que el péptido se encuentra mayoritariamente en forma agregada en medio

acuoso, y, tras la adición de TFE o vesículas de PC:PA se ordena mayoritariamente en estructura helicoidal (figura 8.5).

Péptidos de Bid

Al analizar los espectros de CD obtenidos para Bidα6 (figura 8.6 y tabla 8.5), se observa que, de nuevo, el péptido está desestructurado en ambiente acuoso, y que experimenta una rápida organización en hélice α, que alcanza el 75 %, tras la adición de TFE o SDS. La deconvolución de la banda amida I' de los espectros de FTIR, muestra que este péptido presenta en torno a un 40 % de componente agregado, que disminuye en presencia de vesículas lipídicas dando lugar a estructura helicoidal (que pasa de un 30 % a más de un 70 %) (ver figura 8.8 y tabla 8.4). En este caso, la hélice α está representada por una sola banda típica, centrada a 1655 cm^{-1}. El análisis de los espectros polarizados muestra que Bidα6 se orienta con un ángulo de 34º respecto a las cadenas acílicas de LUVs de PC:PA (tabla 8.3).

En el caso de Bidα7, la valoración con cantidades crecientes de TFE y SDS induce la formación gradual de estructura helicoidal en los experimentos de CD, que alcanza cerca del 60 % (tabla 8.5). En los espectros de FTIR aparece de nuevo un alto porcentaje de péptido agregado. El mayor cambio estructural respecto al medio acuoso, lo induce la presencia de LUVs de PC:PA, que aumenta significativamente la porción de hélice α.

Péptidos de Bcl-xL

Bcl-xLα5 presenta un espectro de CD típicamente desestructurado en medio acuoso (figura 8.10). La titulación con cantidades crecientes de TFE induce un 50 % de estructura helicoidal. En cambio, el péptido no alcanza más de un 30 % de hélice α en presencia de SDS (tabla 8.6). En los experimentos de FTIR se observa que el péptido se encuentra mayoritariamente en estado agregado, y en este caso, la presencia de TFE o vesículas lipídicas induce cambios estructurales menores que en otros péptidos.

En el caso de Bcl-xLα6, el cambio conformacional inducido por la adición de TFE o SDS se observa en los espectros de CD (figura 8.11), y la fracción helicoidal alcanza en torno al 60 %. Los espectros de FTIR muestran que el péptido está predominantemente en estado agregado en medio acuoso, pero en este caso, la presencia de LUVs de PC:PA induce claramente la aparición de una banda correspondiente a hélice α típica, y la fracción agregada prácticamente desaparece (8.11).

14. Discusión y conclusiones

14.1. Dominios de inserción en membrana

A pesar de que la asociación de las proteínas de la familia Bcl-2 a las membranas celulares es esencial para su función, se sabe muy poco sobre las características de esta interacción. La determinación de los segmentos que pueden estar directamente implicados en la inserción en la membrana proporciona información importante sobre la estructura de las formas activas de estas proteínas.

El fragmento C-terminal de Bcl-xL ha sido descrito como una cola de anclaje específico a la OMM, lo que está de acuerdo con la inserción observada en nuestros resultados. En el caso de Bax, la hélice C-terminal homóloga es necesaria y suficiente para dirigir a esta proteína a la OMM (29). Al menos en el contexto de Lep, nuestros resultados indican que esta secuencia puede actuar como un fragmento TM.

En cuanto a la parte N-terminal de las proteínas estudiadas, el fragmento más hidrofóbico corresponde a la hélice α1 de Bid. Esta secuencia muestra una baja tendencia TM en nuestros experimentos, de acuerdo con los datos de la bibliografía que indican que el fragmento N-terminal de Bid procesada no se asocia a la membrana (53). Por otro lado, en el caso de Bcl-xL y Bax, solo la hélice α1 de Bax es TM en el contexto de Lep. Se ha descrito que este fragmento es capaz de dirigir proteínas quiméricas a la OMM, pero sin asociación fuerte a la membrana (28). Sin embargo, empieza a estar claro (18) que la inserción y activación de Bax en la membrana es un proceso en varios pasos con varios estados de asociación/inserción intermedios.

En cuanto a las horquillas propuestas como dominios putativos de formación de poros, estudios de mutagénesis dirigida y deleción sugieren que las horquillas α5-α6 de Bcl-xL, Bcl-2 y Bax son importantes en su función en apoptosis (36,62,46,63,64). Nuestros resultados muestran que la primera hélice de las horquillas de Bcl-xL, Bax y Bid son capaces de insertarse en la membrana en el contexto de las quimeras de Lep. Sin embargo, la segunda hélice de estas horquillas, se inserta sólo en presencia de la primera. Estos resultados están básicamente

de acuerdo con los datos de inserción de Bcl-2, Bax y Bid publicados recientemente en la bibliografía (65, refBid, refBax), y con los estudios preliminares de NMR realizados con Bcl-xL (66). El efecto sinergístico observado en la inserción simultánea de la horquilla con respecto a las hélices por separado indica la existencia de complementariedad en la inserción de las hélices. Esta complementariedad podría deberse a interacciones electrostáticas favorables entre los residuos cargados de las hélices, pero también a las restricciones impuestas por el giro entre las dos hélices. De acuerdo con esto último, existe un gran número de aminoácidos con tendencia a formar giros (88) en las secuencias que separan las hélices de la horquilla, tal y como se muestra en la figura 9.2.

En cuanto a la inserción TM o no de las horquillas putativas formadoras de poros, los estudios de inserción de tBid por EPR muestras que en este caso la horquilla se inserta en la membrana, pero no la atraviesa (ref). Esto es difícil de conciliar con las funciones descritas para tBid (refs), a menos que se suponga la existencia de distintos estados de inserción, o la existencia de fase no lamelares, cada vez más relacionadas con las proteínas Bcl-2s (refbidneg.curv). En el caso de Bax, la inserción de la horquilla $\alpha 5\alpha 6$ probablemente va acompañada de la formación de un poro toroidal (refs), en el que las hélices tendrían acceso a ambos lados de la membrana sin atravesarla según el concepto tradicional de fragmento transmembrana. Tal disposición justificaría, además, la corta longitud de la región apolar y la presencia de residuos cargados en las hélices de la horquilla. Estas ideas, junto los datos reportados recientemente en la bibliografía (refsbid,bax), están de acuerdo con nuestros resultados, lo que indica su fiabilidad, a pesar de ser obtenidos con proteínas quiméricas.

14.2. Relación estructura/función en los péptidos derivados del dominio putativo de formación de poros

La regulación de la salida de los factores apoptóticos de la mitocondria implica la alteración de las propiedades de permeabilidad de la membrana externa de este orgánulo. La familia de proteínas Bcl-2 está implicada en este proceso. Anteriormente hemos mostrado que las hélices $\alpha 5$ de Bcl-xL y de Bax, y su homóloga $\alpha 6$ de Bid son capaces de insertarse en la membrana en ausencia del resto de la proteína, y que las horquillas completas interaccionan fuertemente con membranas lipídicas. Continuando con esta estrategia reduccionista, hemos analizado la actividad de formación de poros de los péptidos derivados de las hélices $\alpha 5$ y $\alpha 6$ de Bcl-xL y de Bax, y sus homólogas $\alpha 6$ y $\alpha 7$ de Bid.

Los estudios estructurales de CD muestran que, en la mayoría de los casos, los péptidos se encuentran desestructurados en medio acuoso y se organizan mayoritariamente en hélice α en presencia de TFE y SDS. En los estudios de FTIR se observan también cambios conformacionales comparables al pasar de un medio acuoso a otro con TFE o vesículas lipídicas.

Péptidos de Bax

En el caso de Bax, se sintetizaron dos versiones con la secuencia de la hélice $\alpha 5$. A pesar de las diferencias en la secuencia (ver tabla ...), ambos péptidos presentan una actividad similar y permeabilizan las membranas a través de mecanismos similares. La presencia de las lisinas parece, además, tener un ligero efecto desestabilizador sobre la estructura del péptido.

Tanto en el caso de Bax$\alpha 5$ como en el de Bax$\alpha 6$, la permeabilización de la membrana ocurre a concentraciones en el rango de nanomolar, tal y como se ha descrito para la proteína Bax. Además, los poros formados por estos péptidos son sensibles a la presencia de lípidos con curvatura intrínseca, y son capaces de liberar dextranos de 70 kDa, en un mecanismo que promueve la difusión de lípidos entre las monocapas. La acción concertada de Bax y tBid produce efectos similares, que se han interpretado como la formación de un poro de naturaleza lipídica o toroidal.

En el caso de Bax$\alpha 5^K$, los estudios en bicapas planas sugieren que el péptido permeabiliza las membranas en un proceso de dos pasos: inicialmente se produce la asociación a la membrana, que va acompañada de un incremento constante de la conductividad a potenciales positivos, y, probablemente cuando el péptido alcanza una concentración crítica en la membrana, se forma un poro de gran tamaño que es independiente del potencial aplicado. Este comportamiento, junto con el hecho de que la selectividad del poro depende de la carga neta de la membrana (lo que indica que los lípidos están expuestos en la pared del poro), están de acuerdo con el modelo de poro toroidal.

La presencia de dos tipos de hélices en Bax$\alpha 5^K$, una orientada paralela al plano de la membrana, y otra perpendicular, apoyan también el modelo propuesto. Puesto que la proporción entre ambas no varía entre los medios acuoso y lipídico, ambos tipos de hélices deben encontrarse ya la misma molécula de péptido, lo que está a favor del modelo B de la figura 9.4.

Estos resultados indican que los péptidos derivados de Bax, Bax$\alpha 5$ y Bax$\alpha 6$, son capaces de reproducir parcialmente, de manera individual y en ausencia de tBid, la actividad de la proteína completa Bax.

Péptidos de Bid

La permeabilización de membranas promovida por los péptidos de Bid es muy diferente de la actividad observada en los péptidos de Bax. Sólo Bidα6 es capaz de formar canales permeables a calceína a concentraciones en el rango de nanomolar similares a las descritas para tBid. Además, esta actividad depende de la presencia de lípidos cargados negativamente, lo que pone de manifiesto la importancia de las interacciones electrostáticas entre el péptido y la membrana. Al igual que tBid, Bidα6 es incapaz de liberar moléculas de gran tamaño, como los dextranos usados en los experimentos, y de inducir la difusión lipídica entre las monocapas de la membrana. En bicapas planas con carga neta negativa, este péptido forma canales discretos de unos 13-15 pS. Además, de los experimentos de FTIR se deduce que se inserta en la membrana con un ángulo de unos 34º. Estos resultados indican que Bidα6 no forma poros lipídicos en su interacción con las membranas, sino que modifica su permeabilidad probablemente a través de canales tipo "barrel-stave". Los datos de la bibliografía sugieren que Bidα6 podría estar implicado en la interacción con la CL y en la reorganización de la membrana mitocondrial que se produce durante la apoptosis (refs), de modo que su la alteración que produce en la permeabilidad de la membrana podría ser una consecuencia de estas funciones.

En el caso de Bidα7, se necesitan concentraciones del orden de micromolar para afectar la permeabilidad de las membranas y la presencia de lípidos produce cambios conformacionales menos importantes que en los otros ejemplos, lo que indica que este péptido interacciona débilmente con la bicapa.

Péptidos de Bcl-xL

A pesar del alto nivel de homología con los péptidos derivados de Bax y de formar parte del dominio putativo de formación de poros de Bcl-xL, los péptidos Bcl-xLα5 y Bcl-xLα6 afectan a la permeabilidad de la membrana sólo a concentraciones del orden de micromolar. En el caso de Bcl-xL, esto puede deberse al bajo nivel de estructura helicoidal que presenta incluso en presencia de LUVs. Otra posibilidad podría ser la necesidad de un pH ácido para su actividad, como se ha descrito para Bcl-xL, o que estos péptidos sean responsables de la actividad antiapoptótica independiente de BH3 descrita para Bcl-xL (Ref.).

Consideraciones adicionales

En cuanto a las implicaciones en la comprensión general del mecanismo de acción de Bax, Bid y Bcl-xL, los resultados obtenidos con estos péptidos ilustran las diferencias funcionales entre las proteínas de las que forman parte, a pesar de su

alto nivel de homología. El hecho de que pequeñas porciones pueden reproducir en parte la actividad de la proteína completa pone de manifiesto la importancia del estudios de pequeños fragmentos para la compresión del todo. Además, sugiere la existencia de vínculos funcionales entre péptidos formadores de poros sencillos, como los antimicrobianos, y proteínas más complejas como las toxinas bacterianas o las proteínas de la familia Bcl-2.

14.3. Conclusiones

De los estudios de inserción en membrana utilizando quimeras basadas en Lep, se puede concluir que los fragmentos C-terminal de Bcl-xL y de Bax, y la hélice α1 de Bax son capaces de insertarse en la membrana, al menos en nuestro sistema de estudio. En cuanto a las hélices de la horquilla putativa de formación de poros, la primera de ellas, α5 en el caso de Bcl-xL y Bax, y α6 en el caso de Bid, es capaz de insertarse en el contexto de Lep, mientras que la segunda necesita la presencia de la primera para hacerlo. Además, estas horquillas contienen la información suficiente para asociarse a la membrana e integrarse en ella mediante interacciones de tipo hidrofóbico, lo que parece indicar que constituyen dominios de inserción en membrana en las proteínas parentales.

Los estudios funcionales y estructurales llevados a cabo con los péptidos derivados de las horquillas de Bax, Bcl-xL y Bid permiten concluir que péptidos con la secuencia de las hélices α5 y α6 de Bax son capaces de reproducir individualmente, y en parte, la formación de poros toroidales de gran tamaño descritos para la acción concertada de Bax y tBid. En el caso de los péptidos derivados de Bid, sólo Bidα6 presenta una actividad de permeabilización de la membrana similar a la descrita para tBid. Mientras que la actividad formadora de poros de Bidα7 y de los péptidos derivados de Bcl-xL es mucho menor, siendo difícil de relacionar con las funciones biológicas de las proteínas de las que forman parte.

Bibliografía

Adams, J. M. and S. Cory, **2001**. Life-or-death decisions by the bcl-2 protein family. *Trends Biochem Sci* 26: 61–66. B26 R26.

Adler, A. J., N. J. Greenfield and G. D. Fasman, **1973**. Circular dichroism and optical rotatory dispersion of proteins and polypeptides. *Methods Enzymol* 27: 675–735.

Anderluh, G., M. Dalla Serra, G. Viero, G. Guella, P. Macek and G. Menestrina, **2003**. Pore formation by equinatoxin ii, a eukaryotic protein toxin, occurs by induction of nonlamellar lipid structures. *J Biol Chem* 278: 45216–23. Pr.

Antonsson, B., F. Conti et al., **1997**. Inhibition of bax channel-forming activity by bcl-2. *Science* 277: 370–372.

Antonsson, B., S. Montessuit, S. Lauper, R. Eskes and J. C. Martinou, **2000**. Bax oligomerization is required for channel-forming activity in liposomes and to trigger cytochrome c release from mitochondria. *Biochem J* 345: 271–278. B82.

Ashkenazi, A. and V. M. Dixit, **1998**. Death receptors: signaling and modulation. *Science* 281: 1305–1308. Pr.

Assuncao Guimaraes, C. and R. Linden, **2004**. Programmed cell deaths. apoptosis and alternative deathstyles. *Eur J Biochem* 271: 1638–50.

Axelsen, P. H., B. K. Kaufman, R. N. McElhaney and R. N. Lewis, **1995**. The infrared dichroism of transmembrane helical polypeptides. *Biophys J* 69: 2770–81.

Basanez, G., A. Nechushtan, O. Drozhinin, A. Chanturiya, E. Choe, S. Tutt, K. A. Wood, Y. Hsu, J. Zimmerberg and R. J. Youle, **1999**. Bax, but not bcl-xl, decreases the lifetime of planar phospholipid bilayer membranes at subnanomolar concentrations. *Proc Natl Acad Sci U S A* 96: 5492–5497. Pr.

Basanez, G., J. C. Sharpe, J. Galanis, T. B. Brandt, J. M. Hardwick and J. Zimmerberg, **2002**. Bax-type apoptotic proteins porate pure lipid bilayers through a mechanism sensitive to intrinsic monolayer curvature. *J Biol Chem* 277: 49360–49365. Pr.

Basanez, G., J. Zhang, B. N. Chau, G. I. Maksaev, V. A. Frolov, T. A. Brandt, J. Burch, J. M. Hardwick and J. Zimmerberg, **2001**. Pro-apoptotic cleavage products of bcl-xl form cytochrome c-conducting pores in pure lipid membranes. *J Biol Chem* 276: 31083–91. Pr.

Basu, A. and S. Haldar, **2003**. Identification of a novel bcl-xl phosphorylation site regulating the sensitivity of taxol- or 2-methoxyestradiol-induced apoptosis. *FEBS Lett* 538: 41–7.

Ben-Efraim, I. and Y. Shai, **1997**. The structure and organization of synthetic putative membranous segments of romk1 channel in phospholipid membranes. *Biophys J* 72: 85–96.

Bibi, E. and H. R. Kaback, **1990**. In vivo expression of the lacy gene in two segments leads to functional lac permease. *Proc Natl Acad Sci U S A* 87: 4325–9.

Binder, W. H., V. Barragan and F. M. Menger, **2003**. Domains and rafts in lipid membranes. *Angew Chem Int Ed Engl* 42: 5802–27.

Boise, L. H., M. Gonzalez-Garcia, C. E. Postema, L. Ding, T. Lindsten, L. A. Turka, X. Mao, G. Nunez and C. B. Thompson, **1993**. bcl-x, a bcl-2-related gene that functions as a dominant regulator of apoptotic cell death. *Cell* 74: 597–608.

Bordier, C., **1981**. Phase separation of integral membrane proteins in triton x-114 solution. *J Biol Chem* 256: 1604–7.

Borgese, N., S. Colombo and E. Pedrazzini, **2003**. The tale of tail-anchored proteins: coming from the cytosol and looking for a membrane. *J Cell Biol* 161: 1013–9. Pr.

Botelho, A. V., N. J. Gibson, R. L. Thurmond, Y. Wang and M. F. Brown, **2002**. Conformational energetics of rhodopsin modulated by nonlamellar-forming lipids. *Biochemistry* 41: 6354–68.

Bouillet, P. and A. Strasser, **2002**a. Bax and bak: back-bone of t cell death. *Nat Immunol* 3: 893–894.

Bouillet, P. and A. Strasser, **2002**b. Bh3-only proteins - evolutionarily conserved proapoptotic bcl-2 family members essential for initiating programmed cell death. *J Cell Sci* 115: 1567–1574. Pr.

Cantor, C. and P. Shimmel, **1980**. *Biophysical Chemistry Part II*. W.H. Freeman and Co, New York.

Cartron, P. F., H. Arokium, L. Oliver, K. Meflah, S. Manon and F. M. Vallette, **2004**. Distinct domains control the addressing and the insertion of bax into mitochondria. *J Biol Chem* .

Cartron, P. F., M. Priault, L. Oliver, K. Meflah, S. Manon and F. M. Vallette, **2003**. The n-terminal end of bax contains a mitochondrial-targeting signal. *J Biol Chem* 278: 11633–41. Pr.

Chai, J., Q. Wu, E. Shiozaki, S. M. Srinivasula, E. S. Alnemri and Y. Shi, **2001**. Crystal structure of a procaspase-7 zymogen: mechanisms of activation and substrate binding. *Cell* 107: 399–407.

Chang, H. Y. and X. Yang, **2000**. Proteases for cell suicide: functions and regulation of caspases. *Microbiol Mol Biol Rev* 64: 821–46. URL `http://mmbr.asm.org/cgi/content/full/64/4/821`. Pr.

Chen, F. Y., M. T. Lee and H. W. Huang, **2002**. Sigmoidal concentration dependence of antimicrobial peptide activities: A case study on alamethicin. *BIOPHYSICAL JOURNAL* 82: 908–914.

Cheng, E. H., M. C. Wei, S. Weiler, R. A. Flavell, T. W. Mak, T. Lindsten and S. J. Korsmeyer, **2001**. Bcl-2, bcl-x(l) sequester bh3 domain-only molecules preventing bax- and bak-mediated mitochondrial apoptosis. *Mol Cell* 8: 705–11.

Chou, J. J., H. L. Li, G. S. Salvesen, J. Y. Yuan and G. Wagner, **1999**. Solution structure of bid, an intracellular amplifier of apoptotic signaling. *Cell-* 96: 615–624. B48.

Chung, C. T., S. L. Niemela and R. H. Miller, **1989**. One-step preparation of competent escherichia coli: transformation and storage of bacterial cells in the same solution. *Proc Natl Acad Sci U S A* 86: 2172–5.

Claros, M. G. and G. von Heijne, **1994**. Toppred ii: an improved software for membrane protein structure predictions. *Comput Appl Biosci* 10: 685–6.

Cramer, W. A., J. B. Heymann, S. L. Schendel, B. N. Deriy, F. S. Cohen, P. A. Elkins and C. V. Stauffacher, **1995**. Structure-function of the channel-forming colicins. *Annu Rev Biophys Biomol Struct* 24: 611–641. B34 R34.

Cserzo, M., E. Wallin, I. Simon, G. vonHeijne and A. Elofsson, **1997**. Prediction of transmembrane alpha-helices in prokaryotic membrane proteins: the dense alignment surface method. *Protein-Engineering* 10: 673–676.

Dalla Serra, M. and G. Menestrina, **2003**. Liposomes in the study of pore-forming toxins. *Methods Enzymol* 372: 99–124.

Degli Esposti, M., **2002**. Sequence and functional similarities between pro-apoptotic bid and plant lipid transfer proteins. *Biochim Biophys Acta* 1553: 331–40.

Desagher, S., A. Osen-Sand, A. Nichols, R. Eskes, S. Montessuit, S. Lauper, K. Maundrell, B. Antonsson and J. C. Martinou, **1999**. Bid-induced conformational change of bax is responsible for mitochondrial cytochrome c release during apoptosis. *J Cell Biol* 144: 891–901. B80.

Deverman, B. E., B. L. Cook et al., **2002**. Bcl-xl deamidation is a critical switch in the regulation of the response to dna damage. *Cell* 111: 51–62.

Du, C., M. Fang, Y. Li, L. Li and X. Wang, **2000**. Smac, a mitochondrial protein that promotes cytochrome c-dependent caspase activation by eliminating iap inhibition. *Cell* 102: 33–42.

Dufourcq, J., J. F. Faucon, G. Fourche, J. L. Dasseux, M. Le Maire and T. Gulik-Krzywicki, **1986**. Morphological changes of phosphatidylcholine bilayers induced by melittin: vesicularization, fusion, discoidal particles. *Biochim Biophys Acta* 859: 33–48.

Earnshaw, W. C., L. M. Martins and S. H. Kaufmann, **1999**. Mammalian caspases: structure, activation, substrates, and functions during apoptosis. *Annu Rev Biochem* 68: 383–424.

Ekert, P., J. Silke, C. Hawkins, A. Verhagen and D. Vaux, **2001**. Diablo promotes apoptosis by removing miha/xiap from processed caspase 9. *J Cell Biol* 152: 483–490. Pr.

Elkins, P., A. Bunker, W. A. Cramer and C. V. Stauffacher, **1997**. A mechanism for toxin insertion into membranes is suggested by the crystal structure of the channel-forming domain of colicin e1. *Structure* 5: 443–458. B44.

Epand, R. F., J. C. Martinou, M. Fornallaz-Mulhauser, D. W. Hughes and R. M. Epand, **2002**a. The apoptotic protein tbid promotes leakage by altering membrane curvature. *J Biol Chem* 277: 32632–9.

Epand, R. F., J. C. Martinou, S. Montessuit, R. M. Epand and C. M. Yip, **2002**b. Direct evidence for membrane pore formation by the apoptotic protein bax. *Biochem Biophys Res Commun* 298: 744–9.

Eskes, R., S. Desagher, B. Antonsson and J. C. Martinou, **2000**. Bid induces the oligomerization and insertion of bax into the outer mitochondrial membrane. *Molecular and cellular biology* 20: 929–935. B86.

Esposti, M. D. and C. Dive, **2003**. Mitochondrial membrane permeabilisation by bax/bak. *Biochem Biophys Res Commun* 304: 455–61. Pr.

F. Gonzalvez, P. D. I. B. M. L. B. A. P. D. S. M. J. M. M. G. X. W. S. B., F. Pariselli and P. Petit, **2005**. tbid interaction with cardiolipin primarily orchestrates mitochondrial dysfunctions ans subsequently activates bax and bak. *Cell Death Differenciation* in press.

Fisher, L. E. and D. M. Engelman, **2001**. High-yield synthesis and purification of an alpha-helical transmembrane domain. *Anal Biochem* 293: 102–8.

Franzin, C. M., J. Choi, D. Zhai, J. C. Reed and F. M. Marassi, **2004**. Structural studies of apoptosis and ion transport regulatory proteins in membranes. *Magn Reson Chem* 42: 172–179. URL `http://www3.interscience.wiley.com/cgi-bin/fulltext/106601068/PDFSTART`.

Frey, S. and L. K. Tamm, **1991**. Orientation of melittin in phospholipid bilayers. a polarized attenuated total reflection infrared study. *Biophys J* 60: 922–30.

Frickenhaus, S. and R. Heinrich, **1999**. Kinetic and thermodynamic aspects of lipid translocation in biological membranes. *Biophys J* 76: 1293–309.

Garcia Fernandez, M., L. Troiano, L. Moretti, M. Nasi, M. Pinti, S. Salvioli, J. Dobrucki and A. Cossarizza, **2002**. Early changes in intramitochondrial cardiolipin distribution during apoptosis. *Cell Growth Differ* 13: 449–55.

Gazit, E., D. Bach, I. D. Kerr, M. S. Sansom, N. Chejanovsky and Y. Shai, **1994**. The alpha-5 segment of bacillus thuringiensis delta-endotoxin: in vitro activity, ion channel formation and molecular modelling. *Biochem J* 304 (Pt 3): 895–902.

Gazit, E. and Y. Shai, **1993**. Structural and functional characterization of the alpha 5 segment of bacillus thuringiensis delta-endotoxin. *Biochemistry* 32: 3429–36.

Gong, X. M., J. Choi, C. M. Franzin, D. Zhai, J. C. Reed and F. M. Marassi, **2004**. Conformation of membrane-associated pro-apoptotic tbid. *J Biol Chem* .

Goormaghtigh, E., V. Raussens and J. M. Ruysschaert, **1999**. Attenuated total reflection infrared spectroscopy of proteins and lipids in biological membranes. *Biochim Biophys Acta* 1422: 105–85.

Goormaghtigh, E., L. Vigneron, M. Knibiehler, C. Lazdunski and J. M. Ruysschaert, **1991**. Secondary structure of the membrane-bound form of the pore-forming domain of colicin a. an attenuated total-reflection polarized fourier-transform infrared spectroscopy study. *Eur J Biochem* 202: 1299–305.

Goping, I. S., A. Gross, J. N. Lavoie, M. Nguyen, R. Jemmerson, K. Roth, S. J. Korsmeyer and G. C. Shore, **1998**. Regulated targeting of bax to mitochondria. *J Cell Biol* 143: 207–215. B74.

Gordon, L. M., P. W. Mobley, R. Pilpa, M. A. Sherman and A. J. Waring, **2002**. Conformational mapping of the n-terminal peptide of hiv-1 gp41 in membrane environments using (13)c-enhanced fourier transform infrared spectroscopy. *Biochim Biophys Acta* 1559: 96–120.

Goyal, L., **2001**. Cell death inhibition: keeping caspases in check. *Cell* 104: 805–8. Pr.

Greenfield, N. and G. D. Fasman, **1969**. Computed circular dichroism spectra for the evaluation of protein conformation. *Biochemistry* 8: 4108–16.

Greenfield, N. J., **2004**. Analysis of circular dichroism data. *Methods Enzymol* 383: 282–317.

Gross, A., X. M. Yin, K. Wang, M. C. Wei, J. Jockel, C. Milliman, H. Erdjument-Bromage, P. Tempst and S. J. Korsmeyer, **1999**. Caspase cleaved bid targets mitochondria and is required for cytochrome c release, while bcl-xl prevents this release but not tumor necrosis factor-r1/fas death. *J Biol Chem* 274: 1156–1163.

Halestrap, A. P., G. P. McStay and S. J. Clarke, **2002**. The permeability transition pore complex: another view. *Biochimie* 84: 153–66.

Hanada, M., C. Aime-Sempe, T. Sato and J. C. Reed, **1995**. Structure-function analysis of bcl-2 protein. identification of conserved domains important for homodimerization with bcl-2 and heterodimerization with bax. *J Biol Chem* 270: 11962–11969.

Hanahan, D., **1983**. Studies on transformation of escherichia coli with plasmids. *J Mol Biol* 166: 557–80.

Haris, P. I. and D. Chapman, **1988**. Fourier transform infrared spectra of the polypeptide alamethicin and a possible structural similarity with bacteriorhodopsin. *Biochim Biophys Acta* 943: 375–80.

Heimlich, G., A. D. McKinnon, K. Bernardo, D. Brdiczka, J. C. Reed, R. Kain, M. Kronke and J. M. Jurgensmeier, **2004**. Bax-induced cytochrome c release from mitochondria depends on alpha-helices-5 and -6. *Biochem J* 378: 247–55. Pr.

Heller, W. T., A. J. Waring, R. I. Lehrer, T. A. Harroun, T. M. Weiss, L. Yang and H. W. Huang, **2000**. Membrane thinning effect of the beta-sheet antimicrobial protegrin. *Biochemistry* 39: 139–45.

Hengartner, M. O., **1997**. Apoptosis and the shape of death. *Developmental-Genetics* 21: 245–248.

Hessa, T., H. Kim, K. Bihlmaier, C. Lundin, J. Boekel, H. Andersson, I. Nilsson, S. H. White and G. von Heijne, **2005**. Recognition of transmembrane helices by the endoplasmic reticulum translocon. *Nature* 433: 377–81.

Heuck, A. P., R. K. Tweten and A. E. Johnson, **2001**. Beta-barrel pore-forming toxins: intriguing dimorphic proteins. *Biochemistry* 40: 9065–73.

High, S. and B. M. Abell, **2004**. Tail-anchored protein biosynthesis at the endoplasmic reticulum: the same but different. *Biochem Soc Trans* 32: 659–62.

Higy, M., T. Junne and M. Spiess, **2004**. Topogenesis of membrane proteins at the endoplasmic reticulum. *Biochemistry* 43: 12716–22.

Hockenbery, D., G. Nunez, C. Milliman, R. D. Schreiber and S. J. Korsmeyer, **1990**. Bcl-2 is an inner mitochondrial membrane protein that blocks programmed cell death. *Nature* 348: 334–336.

Hsu, Y. T., K. G. Wolter and R. J. Youle, **1997**. Cytosol-to-membrane redistribution of bax and bcl-x(l) during apoptosis. *Proc Natl Acad Sci U S A* 94: 3668–3672. B72.

Hu, X., Z. Han, J. H. Wyche and E. A. Hendrickson, **2003**. Helix 6 of tbid is necessary but not sufficient for mitochondrial binding activity. *Apoptosis* 8: 277–89. Pr.

Huang, H. W., **2000**. Action of antimicrobial peptides: two-state model. *Biochemistry* 39: 8347–52.

Huang, H. W., F. Y. Chen and M. T. Lee, **2004**. Molecular mechanism of peptide-induced pores in membranes. *Phys Rev Lett* 92: 198304. Pr.

Huang, Q., Q. L. Deveraux, S. Maeda, G. S. Salvesen, H. R. Stennicke, B. D. Hammock and J. C. Reed, **2000**. Evolutionary conservation of apoptosis mechanisms: lepidopteran and baculoviral inhibitor of apoptosis proteins are inhibitors of mammalian caspase-9. *Proc Natl Acad Sci U S A* 97: 1427–32. URL `http://www.pnas.org/cgi/content/full/97/4/1427`.

Huang, Y., Y. C. Park, R. L. Rich, D. Segal, D. G. Myszka and H. Wu, **2001**. Structural basis of caspase inhibition by xiap: differential roles of the linker versus the bir domain. *Cell* 104: 781–90. Pr.

Janiak, F., B. Leber and D. W. Andrews, **1994**. Assembly of bcl-2 into microsomal and outer mitochondrial membranes. *J Biol Chem* 269: 9842–9849. B118.

Jeong, S. Y., B. Gaume, Y. J. Lee, Y. T. Hsu, S. W. Ryu, S. H. Yoon and R. J. Youle, **2004**. Bcl-x(l) sequesters its c-terminal membrane anchor in soluble, cytosolic homodimers. *EMBO J* 23: 2146–55.

Jiang, X. and X. Wang, **2004**. Cytochrome c-mediated apoptosis. *Annu Rev Biochem* 73: 87–106.

J.M. Berg, L. S. N. C., J.M. Tymoczko, **2002**. *Biochemistry*, chap. 12. Michelle Julet.

Johnstone, R. W., A. A. Ruefli and S. W. Lowe, **2002**. Apoptosis: a link between cancer genetics and chemotherapy. *Cell* 108: 153–64. Pr.

Kagawa, Y., L. W. Johnson and E. Racker, **1973**. Activation of phosphorylating vesicles by net transfer of phosphatidyl choline by phospholipid transfer protein. *Biochem Biophys Res Commun* 50: 245–51.

Karatekin, E., O. Sandre, H. Guitouni, N. Borghi, P. H. Puech and F. Brochard-Wyart, **2003**. Cascades of transient pores in giant vesicles: line tension and transport. *Biophys J* 84: 1734–49. URL `http://www.biophysj.org/cgi/reprint/84/3/1734.pdf`. Pr.

Karbowski, M., Y. J. Lee, B. Gaume, S. Y. Jeong, S. Frank, A. Nechushtan, A. Santel, M. Fuller, C. L. Smith and R. J. Youle, **2002**. Spatial and temporal association of bax with mitochondrial fission sites, drp1, and mfn2 during apoptosis. *J Cell Biol* 159: 931–938.

Kaufmann, T., S. Schlipf, J. Sanz, K. Neubert, R. Stein and C. Borner, **2003**. Characterization of the signal that directs bcl-xl, but not bcl-2, to the mitochondrial outer membrane. *J Cell Biol* 160: 53–64.

Keenan, T. W. and D. J. Morre, **1970**. Phospholipid class and fatty acid composition of golgi apparatus isolated from rat liver and comparison with other cell fractions. *Biochemistry* 9: 19–25.

Kelekar, A., B. S. Chang, J. E. Harlan, S. W. Fesik and C. B. Thompson, **1997**. Bad is a bh3 domain-containing protein that forms an inactivating dimer with bcl-xl. *Mol Cell Biol* 17: 7040–7046.

Keller, J. N., M. S. Kindy, F. W. Holtsberg, D. K. St Clair, H. C. Yen, A. Germeyer, S. M. Steiner, A. J. Bruce-Keller, J. B. Hutchins and M. P. Mattson, **1998**. Mitochondrial manganese superoxide dismutase prevents neural apoptosis and reduces ischemic brain injury: suppression of peroxynitrite production, lipid peroxidation, and mitochondrial dysfunction. *J Neurosci* 18: 687–97.

Kerr, J. F., A. H. Wyllie and A. R. Currie, **1972**. Apoptosis: a basic biological phenomenon with wide-ranging implications in tissue kinetics. *Br J Cancer* 26: 239–57.

Kim, P. K., M. G. Annis, P. J. Dlugosz, B. Leber and D. W. Andrews, **2004**a. During apoptosis bcl-2 changes membrane topology at both the endoplasmic reticulum and mitochondria. *Mol Cell* 14: 523–9. Pr.

Kim, P. K., F. Janiak-Spens, W. S. Trimble, B. Leber and D. W. Andrews, **1997**. Evidence for multiple mechanisms for membrane binding and integration via carboxyl-terminal insertion sequences. *Biochemistry* 36: 8873–82.

Kim, T. H., Y. Zhao, W. X. Ding, J. N. Shin, X. He, Y. W. Seo, J. Chen, H. Rabinowich, A. A. Amoscato and X. M. Yin, **2004**b. Bid-cardiolipin interaction at mitochondrial contact site contributes to mitochondrial cristae reorganization and cytochrome c release. *Mol Biol Cell* .

Kudla, G., S. Montessuit, R. Eskes, C. Berrier, J. C. Martinou, A. Ghazi and B. Antonsson, **2000**. The destabilization of lipid membranes induced by the

c-terminal fragment of caspase 8-cleaved bid is inhibited by the n-terminal fragment. *Journal of biological chemistry, The* 275: 22713–22718. B87.

Kutay, U., G. Ahnert-Hilger, E. Hartmann, B. Wiedenmann and T. A. Rapoport, **1995**. Transport route for synaptobrevin via a novel pathway of insertion into the endoplasmic reticulum membrane. *EMBO J* 14: 217–23.

Kuwana, T., M. R. Mackey, G. Perkins, M. H. Ellisman, M. Latterich, R. Schneiter, D. R. Green and D. D. Newmeyer, **2002**. Bid, bax, and lipids cooperate to form supramolecular openings in the outer mitochondrial membrane. *Cell* 111: 331–342. A Pr.

Kyte, J. and R. F. Doolittle, **1982**. A simple method for displaying the hydropathic character of a protein. *J Mol Biol* 157: 105–32.

La Rocca, P., Y. Shai and M. S. Sansom, **1999**. Peptide-bilayer interactions: simulations of dermaseptin b, an antimicrobial peptide. *Biophys Chem* 76: 145–59.

Lan, L., S. Isenmann and B. W. Wattenberg, **2000**. Targeting and insertion of c-terminally anchored proteins to the mitochondrial outer membrane is specific and saturable but does not strictly require atp or molecular chaperones. *Biochem J* 349: 611–621. B76.

Lazebnik, Y., **2001**. Why do regulators of apoptosis look like bacterial toxins? *Curr Biol* 11: R733–4. Pr.

Lee, M. T., F. Y. Chen and H. W. Huang, **2004**. Energetics of pore formation induced by membrane active peptides. *Biochemistry* 43: 3590–9. URL `http://pubs.acs.org/cgi-bin/article.cgi/bichaw/2004/43/i12/pdf/bi036153r.pd` Pr.

Li, H., H. Zhu, C. J. Xu and J. Yuan, **1998**. Cleavage of bid by caspase 8 mediates the mitochondrial damage in the fas pathway of apoptosis. *Cell* 94: 491–501.

Li, H. M., M. J. Cocco, T. A. Steitz and D. M. Engelman, **2001**. Conversion of phospholamban into a soluble pentameric helical bundle. *BIOCHEMISTRY* 40: 6636–6645.

Liu, J., A. Weiss, D. Durrant, N. W. Chi and R. M. Lee, **2004**. The cardiolipin-binding domain of bid affects mitochondrial respiration and enhances cytochrome c release. *Apoptosis* 9: 533–41.

Liu, X., C. N. Kim, J. Yang, R. Jemmerson and X. Wang, **1996**. Induction of apoptotic program in cell-free extracts: requirement for datp and cytochrome c. *Cell* 86: 147–57.

Liu, Z. H., C. H. Sun, E. T. Olejniczak, R. P. Meadows, S. F. Betz, T. Oost, J. Herrmann, J. C. Wu and S. W. Fesik, **2000**. Structural basis for binding of smac/diablo to the xiap bir3 domain. *Nature*- 408: 1004–1008. Pr.

Losonczi, J. A., E. T. Olejniczak, S. F. Betz, J. E. Harlan, J. Mack and S. W. Fesik, **2000**. Nmr studies of the anti-apoptotic protein bcl-xl in micelles. *Biochemistry* 39: 11024–11033. B52.

Ludtke, S. J., K. He, W. T. Heller, T. A. Harroun, L. Yang and H. W. Huang, **1996**. Membrane pores induced by magainin. *BIOCHEMISTRY* 35: 13723–13728.

Luo, X., I. Budihardjo, H. Zou, C. Slaughter and X. Wang, **1998**. Bid, a bcl2 interacting protein, mediates cytochrome c release from mitochondria in response to activation of cell surface death receptors. *Cell* 94: 481–490. B84.

Lutter, M., M. Fang, X. Luo, M. Nishijima, X. Xie and X. Wang, **2000**. Cardiolipin provides specificity for targeting of tbid to mitochondria [in process citation]. *Nat Cell Biol* 2: 754–761.

Malovrh, P., G. Viero, M. D. Serra, Z. Podlesek, J. H. Lakey, P. Macek, G. Menestrina and G. Anderluh, **2003**. A novel mechanism of pore formation: membrane penetration by the n-terminal amphipathic region of equinatoxin. *J Biol Chem* 278: 22678–85.

Matsuyama, S., S. L. Schendel, Z. Xie and J. C. Reed, **1998**. Cytoprotection by bcl-2 requires the pore-forming alpha5 and alpha6 helices. *J Biol Chem* 273: 30995–31001. Pr.

Mattson, M. P., **2000**. Apoptosis in neurodegenerative disorders. *Nat Rev Mol Cell Biol* 1: 120–129.

McDonnell, J. M., D. Fushman, C. L. Milliman, S. J. Korsmeyer and D. Cowburn, **1999**. Solution structure of the proapoptotic molecule bid: a structural basis for apoptotic agonists and antagonists. *Cell* 96: 625–634. B49.

Melen, K., A. Krogh and G. von Heijne, **2003**. Reliability measures for membrane protein topology prediction algorithms. *J Mol Biol* 327: 735–44. Pr.

Melnyk, R. A., A. W. Partridge and C. M. Deber, **2001**. Retention of native-like oligomerization states in transmembrane segment peptides: Application to the escherichia coli aspartate receptor. *BIOCHEMISTRY* 40: 11106–11113.

Menestrina, G., **2000**. Use of fourier-transformed infrared spectroscopy for secondary structure determination of staphylococcal pore-forming toxins. *Methods Mol Biol* 145: 115–32.

Menestrina, G., V. Cabiaux and M. Tejuca, **1999**. Secondary structure of sea anemone cytolysins in soluble and membrane bound form by infrared spectroscopy. *Biochem Biophys Res Commun* 254: 174–80.

Menikh, A., M. T. Saleh, J. Gariepy and J. M. Boggs, **1997**. Orientation in lipid bilayers of a synthetic peptide representing the c-terminus of the a1 domain of shiga toxin. a polarized atr-ftir study. *Biochemistry* 36: 15865–72.

Minn, A. J., C. S. Kettlun, H. Liang, A. Kelekar, M. G. V. Heiden, B. S. Chang, S. W. Fesik, M. Fill and C. B. Thompson, **1999**. Bcl-xl regulates apoptosis by heterodimerization-dependent and -independent mechanisms. *Embo J* 18: 632–643. B61.

Minn, A. J., P. Velez, S. L. Schendel, H. Liang, S. W. Muchmore, S. W. Fesik, M. Fill and C. B. Thompson, **1997**. Bcl-x(l) forms an ion channel in synthetic lipid membranes. *Nature* 385: 353–357. B64.

Monne, M., M. Hermansson and G. von Heijne, **1999**a. A turn propensity scale for transmembrane helices. *J Mol Biol* 288: 141–5. Pr.

Monne, M., I. Nilsson, A. Elofsson and G. von Heijne, **1999**b. Turns in transmembrane helices: determination of the minimal length of a "helical hairpin.ªnd derivation of a fine-grained turn propensity scale. *J Mol Biol* 293: 807–14. Pr.

Moscowitz, A., **1960**. *Optical Rotatory Dispersion*. McGrau-Hill Book Co.

Muchmore, S. W., M. Sattler et al., **1996**. X-ray and nmr structure of human bcl-xl, an inhibitor of programmed cell death. *Nature* 381: 335–341. B45.

Muller, P., S. Schiller, T. Wieprecht, M. Dathe and A. Herrmann, **2000**. Continuous measurement of rapid transbilayer movement of a pyrene-labeled phospholipid analogue. *Chem Phys Lipids* 106: 89–99.

Muzio, M., B. R. Stockwell, H. R. Stennicke, G. S. Salvesen and V. M. Dixit, **1998**. An induced proximity model for caspase-8 activation. *J Biol Chem* 273: 2926–30.

Nechushtan, A., C. L. Smith, Y. T. Hsu and R. J. Youle, **1999**. Conformation of the bax c-terminus regulates subcellular location and cell death. *Embo J* 18: 2330–2341.

Nguyen, M., D. G. Millar, V. W. Yong, S. J. Korsmeyer and G. C. Shore, **1993**. Targeting of bcl-2 to the mitochondrial outer membrane by a cooh-terminal signal anchor sequence. *J Biol Chem* 268: 25265–25268.

Nicholson, D. W., **2000**. From bench to clinic with apoptosis-based therapeutic agents. *Nature* 407: 810–816. B13 R13.

Nielsen, H., J. Engelbrecht, S. Brunak and G. von Heijne, **1997**. Identification of prokaryotic and eukaryotic signal peptides and prediction of their cleavage sites. *Protein Eng* 10: 1–6.

Nilsson, I., A. E. Johnson and G. von Heijne, **2002**. Cleavage of a tail-anchored protein by signal peptidase. *FEBS Lett* 516: 106–8. Pr.

Nilsson, I. and G. von Heijne, **1998**. Breaking the camel's back: proline-induced turns in a model transmembrane helix. *J Mol Biol* 284: 1185–9.

Nilsson, I., P. Whitley and G. von Heijne, **1994**. The cooh-terminal ends of internal signal and signal-anchor sequences are positioned differently in the er translocase. *J Cell Biol* 126: 1127–32.

Nilsson, I. M. and G. von Heijne, **1993**. Determination of the distance between the oligosaccharyltransferase active site and the endoplasmic reticulum membrane. *J Biol Chem* 268: 5798–801.

Nouraini, S., E. Six, S. Matsuyama, S. Krajewski and J. C. Reed, **2000**. The putative pore-forming domain of bax regulates mitochondrial localization and interaction with bcl-x(l). *Mol Cell Biol* 20: 1604–1615. Pr.

Nutt, L. K., J. Chandra, A. Pataer, B. Fang, J. A. Roth, S. G. Swisher, R. G. O'Neil and D. J. McConkey, **2002**. Bax-mediated ca2+ mobilization promotes cytochrome c release during apoptosis. *J Biol Chem* 277: 20301–20308.

Oakes, S. A. and S. J. Korsmeyer, **2004**. Untangling the web: mitochondrial fission and apoptosis. *Dev Cell* 7: 460–2.

Oakes, S. A., J. T. Opferman, T. Pozzan, S. J. Korsmeyer and L. Scorrano, **2003**. Regulation of endoplasmic reticulum ca2+ dynamics by proapoptotic bcl-2 family members. *Biochem Pharmacol* 66: 1335–40.

O'Connor, L., A. Strasser, L. A. O'Reilly, G. Hausmann, J. M. Adams, S. Cory and D. C. Huang, **1998**. Bim: a novel member of the bcl-2 family that promotes apoptosis. *Embo J* 17: 384–395.

Oh, K. J., S. Barbuto, N. Meyer, R. S. Kim, R. J. Collier and S. J. Korsmeyer, **2005**. Conformational changes in bid, a pro-apoptotic bcl-2 family member, upon membrane binding. a site-directed spin labeling study. *J Biol Chem* 280: 753–67. URL `http://www.jbc.org/cgi/content/full/280/1/753`.

Oh, K. J., N. Meyer and S. J. Korsmeyer, **2003**. Interaction of bid, a pro-apoptotic bcl-2 family member, with lipid membranes: A site-directed spin labeling study. *BIOPHYSICAL JOURNAL* 84: 205A–206A. Pr.

Oltvai, Z. N., C. L. Milliman and S. J. Korsmeyer, **1993**. Bcl-2 heterodimerizes in vivo with a conserved homolog, bax, that accelerates programmed cell death. *Cell* 74: 609–619.

Orzaez, M., J. Salgado, A. Gimenez-Giner, E. Perez-Paya and I. Mingarro, **2004**. Influence of proline residues in transmembrane helix packing. *JOURNAL OF MOLECULAR BIOLOGY* 335: 631–640.

Petros, A. M., A. Medek, D. G. Nettesheim, D. H. Kim, H. S. Yoon, K. Swift, E. D. Matayoshi, T. Oltersdorf and S. W. Fesik, **2001**. Solution structure of the antiapoptotic protein bcl-2. *Proc Natl Acad Sci U S A* 98: 3012–7. URL `http://www.pnas.org/cgi/content/full/98/6/3012`. Pr.

Pinton, P., D. Ferrari, E. Rapizzi, F. Di Virgilio, T. Pozzan and R. Rizzuto, **2002**. A role for calcium in bcl-2 action? *Biochimie* 84: 195–201.

Popot, J. L., J. Trewhella and D. M. Engelman, **1986**. Reformation of crystalline purple membrane from purified bacteriorhodopsin fragments. *EMBO J* 5: 3039–44.

Priault, M., N. Camougrand, B. Chaudhuri and S. Manon, **1999**. Role of the c-terminal domain of bax and bcl-xl in their localization and function in yeast cells. *FEBS Lett* 443: 225–228. B75.

R.B. Cornell, R. A., **1996**. Modulation of the activities of enzymes of membrane lipid metabolism by non-bilayer-forming lipids. *CHEMISTRY AND PHYSICS OF LIPIDS* 81: 215 –227.

Reed, J. C. and K. J. Tomaselli, **2000**. Drug discovery opportunities from apoptosis research. *Curr Opin Biotechnol* 11: 586–592. B18 R18.

Rodionova, N. A., S. A. Tatulian, T. Surrey, F. Jahnig and L. K. Tamm, **1995**. Characterization of two membrane-bound forms of ompa. *Biochemistry* 34: 1921–9.

Rothschild, K. J. and N. A. Clark, **1979**. Anomalous amide i infrared absorption of purple membrane. *Science* 204: 311–2.

Roucou, X., T. Rostovtseva, S. Montessuit, J. C. Martinou and B. Antonsson, **2002**. Bid induces cytochrome c-impermeable bax channels in liposomes. *Biochem J* 363: 547–52. URL `http://www.biochemj.org/bj/363/0547/bj3630547.htm`.

Saito, M., S. J. Korsmeyer and P. H. Schlesinger, **2000**. Bax-dependent transport of cytochrome c reconstituted in pure liposomes. *Nature-Cell-Biology* 2: 553–555. B71.

Santos, N. C. and M. A. Castanho, **1996**. Teaching light scattering spectroscopy: the dimension and shape of tobacco mosaic virus. *Biophys J* 71: 1641–50.

Sattler, M., H. Liang et al., **1997**. Structure of bcl-xl-bak peptide complex: recognition between regulators of apoptosis. *Science* 275: 983–986. B47.

Saxena, V. P. and D. B. Wetlaufer, **1971**. A new basis for interpreting the circular dichroic spectra of proteins. *Proc Natl Acad Sci U S A* 68: 969–72.

Scarlata, S., **2004**. *Membrane protein structure*, chap. 1. http://www.biophysics.org/btol/Scarlata.html.

Schaad, M. C., P. E. Jensen and J. C. Carrington, **1997**. Formation of plant rna virus replication complexes on membranes: role of an endoplasmic reticulum-targeted viral protein. *EMBO J* 16: 4049–59.

Schendel, S. L., R. Azimov, K. Pawlowski, A. Godzik, B. L. Kagan and J. C. Reed, **1999**. Ion channel activity of the bh3 only bcl-2 family member, bid. *J Biol Chem* 274: 21932–21936.

Schendel, S. L., Z. Xie, M. O. Montal, S. Matsuyama, M. Montal and J. C. Reed, **1997**. Channel formation by antiapoptotic protein bcl-2. *Proc Natl Acad Sci U S A* 94: 5113–5118. B62.

Schinzel, A., T. Kaufmann, M. Schuler, J. Martinalbo, D. Grubb and C. Borner, **2004**. Conformational control of bax localization and apoptotic activity by pro168. *JOURNAL OF CELL BIOLOGY* 164: 1021–1032.

Schlesinger, P. H., A. Gross, X. M. Yin, K. Yamamoto, M. Saito, G. Waksman and S. J. Korsmeyer, **1997**. Comparison of the ion channel characteristics of proapoptotic bax and antiapoptotic bcl-2. *Proceedings-of-the-National-Academy-of-Sciences-of-the-United-States-of-America* 94: 11357–11362. B63.

Scorrano, L., M. Ashiya, K. Buttle, S. Weiler, S. A. Oakes, C. A. Mannella and S. J. Korsmeyer, **2002**. A distinct pathway remodels mitochondrial cristae and mobilizes cytochrome c during apoptosis. *Dev Cell* 2: 55–67.

Scorrano, L., S. A. Oakes, J. T. Opferman, E. H. Cheng, M. D. Sorcinelli, T. Pozzan and S. J. Korsmeyer, **2003**. Bax and bak regulation of endoplasmic reticulum ca2+: a control point for apoptosis. *Science* 300: 135–9. Pr.

Seddon, J. and R. Templer, **1995**. *Polymorphism in Lipid-Water Systems*, vol. 1, chap. 3. Elsevier Science B.V., 99–160.

Senisterra, G. and R. M. Epand, **1993**. Role of membrane defects in the regulation of the activity of protein kinase c. *Arch Biochem Biophys* 300: 378–83.

Serra, M. D. and G. Menestrina, **2000**. *Characterisation of molecular properties of pore-forming toxins with planar lipid bilayers.*. Human Press, Totowa, New Jersey, 171–188.

Shai, Y., **2002**. Mode of action of membrane active antimicrobial peptides. *Biopolymers* 66: 236–48.

Sharon, M., Z. Oren, Y. Shai and J. Anglister, **1999**. 2d-nmr and atr-ftir study of the structure of a cell-selective diastereomer of melittin and its orientation in phospholipids. *Biochemistry* 38: 15305–16.

Shimizu, S., A. Konishi, T. Kodama and Y. Tsujimoto, **2000**a. Bh4 domain of antiapoptotic bcl-2 family members closes voltage-dependent anion channel and inhibits apoptotic mitochondrial changes and cell death [published erratum appears in proc natl acad sci u s a 2000 aug 1;97(16):9347]. *Proc Natl Acad Sci U S A* 97: 3100–3105. B106.

Shimizu, S., M. Narita and Y. Tsujimoto, **1999**. Bcl-2 family proteins regulate the release of apoptogenic cytochrome c by the mitochondrial channel vdac [see comments]. *Nature* 399: 483–487. B97.

Shimizu, S., Y. Shinohara and Y. Tsujimoto, **2000**b. Bax and bcl-xl independently regulate apoptotic changes of yeast mitochondria that require vdac but not adenine nucleotide translocator. *Oncogene* 19: 4309–4318.

Smaili, S. S., Y. T. Hsu, R. J. Youle and J. T. Russell, **2000**. Mitochondria in ca2+ signaling and apoptosis. *J Bioenerg Biomembr* 32: 35–46.

Sobko, A. A., E. A. Kotova, Y. N. Antonenko, S. D. Zakharov and W. A. Cramer, **2004**. Effect of lipids with different spontaneous curvature on the channel activity of colicin e1: evidence in favor of a toroidal pore. *FEBS Lett* 576: 205–10.

Sreerama, N. and R. W. Woody, **2000**. Estimation of protein secondary structure from circular dichroism spectra: comparison of contin, selcon, and cdsstr methods with an expanded reference set. *Anal Biochem* 287: 252–60.

Sreerama, N. and R. W. Woody, **2004**. On the analysis of membrane protein circular dichroism spectra. *PROTEIN SCIENCE* 13: 100–112.

Srinivasula, S. M., M. Ahmad, T. Fernandes-Alnemri and E. S. Alnemri, **1998**. Autoactivation of procaspase-9 by apaf-1-mediated oligomerization. *Mol Cell* 1: 949–57.

Streicher-Scott, J., R. Lapidus and P. M. Sokolove, **1994**. The reconstituted mitochondrial adenine nucleotide translocator: effects of lipid polymorphism. *Arch Biochem Biophys* 315: 548–54.

Stroud, R. M., K. Reiling, M. Wiener and D. Freymann, **1998**. Ion-channel-forming colicins. *Curr Opin Struct Biol* 8: 525–533. B29 R29.

Susin, S. A., N. Zamzami, M. Castedo, T. Hirsch, P. Marchetti, A. Macho, E. Daugas, M. Geuskens and G. Kroemer, **1996**. Bcl-2 inhibits the mitochondrial release of an apoptogenic protease. *J Exp Med* 184: 1331–1341.

Suzuki, M., R. J. Youle and N. Tjandra, **2000**. Structure of bax. coregulation of dimer formation and intracellular localization. *Cell* 103: 645–654. B51.

Suzuki, Y., Y. Imai, H. Nakayama, K. Takahashi, K. Takio and R. Takahashi, **2001**. A serine protease, htra2, is released from the mitochondria and interacts with xiap, inducing cell death. *Mol Cell* 8: 613–21.

Tamm, L. K. and S. A. Tatulian, **1993**. Orientation of functional and nonfunctional pts permease signal sequences in lipid bilayers. a polarized attenuated total reflection infrared study. *Biochemistry* 32: 7720–6.

Tamm, L. K. and S. A. Tatulian, **1997**. Infrared spectroscopy of proteins and peptides in lipid bilayers. *Q Rev Biophys* 30: 365–429.

Terrones, O., B. Antonsson, H. Yamaguchi, H. G. Wang, J. Liu, R. M. Lee, A. Herrmann and G. Basanez, **2004**. Lipidic pore formation by the concerted action of proapoptotic bax and tbid. *J Biol Chem* 279: 30081–91. URL `http://www.jbc.org/cgi/content/full/279/29/30081`. Pr.

Thompson, C. B., **1995**. Apoptosis in the pathogenesis and treatment of disease. *Science* 267: 1456–62.

Thornberry, N. A. and Y. Lazebnik, **1998**. Caspases: enemies within. *Science* 281: 1312–1316. Pr.

Tinoco, I. and C. Cantor, **1970**. *Circular Dichroism*, vol. 18. John Wiley and Sons, New York.

Tristram-Nagle, S. and J. F. Nagle, **2004**. Lipid bilayers: thermodynamics, structure, fluctuations, and interactions. *Chem Phys Lipids* 127: 3–14. Pr.

Valcarcel, C. A., M. Dalla Serra, C. Potrich, I. Bernhart, M. Tejuca, D. Martinez, F. Pazos, M. E. Lanio and G. Menestrina, **2001**. Effects of lipid composition on membrane permeabilization by sticholysin i and ii, two cytolysins of the sea anemone stichodactyla helianthus. *Biophys J* 80: 2761–74.

van den Brink-van der Laan, E., J. A. Killian and B. de Kruijff, **2004**. Nonbilayer lipids affect peripheral and integral membrane proteins via changes in the lateral pressure profile. *Biochim Biophys Acta* 1666: 275–88.

van Geest, M. and J. S. Lolkema, **2000**. Membrane topology and insertion of membrane proteins: search for topogenic signals. *Microbiol Mol Biol Rev* 64: 13–33.

van Geest, M., I. Nilsson, G. von Heijne and J. S. Lolkema, **1999**. Insertion of a bacterial secondary transport protein in the endoplasmic reticulum membrane. *J Biol Chem* 274: 2816–23. Pr.

van Meer, G., **1989**. Lipid traffic in animal cells. *Annu Rev Cell Biol* 5: 247–75.

Vaux, D. L., G. Haecker and A. Strasser, **1994**. An evolutionary perspective on apoptosis. *Cell* 76: 777–9.

Verhagen, A. M., P. G. Ekert, M. Pakusch, J. Silke, L. M. Connolly, G. E. Reid, R. L. Moritz, R. J. Simpson and D. L. Vaux, **2000**. Identification of diablo, a mammalian protein that promotes apoptosis by binding to and antagonizing iap proteins. *Cell* 102: 43–53. Pr.

Verhagen, A. M., J. Silke et al., **2002**. Htra2 promotes cell death through its serine protease activity and its ability to antagonize inhibitor of apoptosis proteins. *J Biol Chem* 277: 445–54. URL `http://www.jbc.org/cgi/content/full/277/1/445`.

Vilar, M., M. Galleni, T. Solmajer, B. Turk, J. M. Frere and A. Matagne, **2001**. Kinetic study of two novel enantiomeric tricyclic beta-lactams which efficiently inactivate class c beta-lactamases. *Antimicrob Agents Chemother* 45: 2215–23.

Vilar, M., A. Sauri, M. Monne, J. F. Marcos, G. von Heijne, E. Perez-Paya and I. Mingarro, **2002**. Insertion and topology of a plant viral movement protein in the endoplasmic reticulum membrane. *J Biol Chem* 277: 23447–52.

von Heijne, G., **1989**. Control of topology and mode of assembly of a polytopic membrane protein by positively charged residues. *Nature* 341: 456–8.

von Heijne, G., **1992**. Membrane protein structure prediction. hydrophobicity analysis and the positive-inside rule. *J Mol Biol* 225: 487–94.

Wei, M. C., T. Lindsten, V. K. Mootha, S. Weiler, A. Gross, M. Ashiya, C. B. Thompson and S. J. Korsmeyer, **2000**. tbid, a membrane-targeted death ligand, oligomerizes bak to release cytochrome c. *Genes Dev* 14: 2060–2071.

Wei, M. C., W. X. Zong, E. H. Cheng, T. Lindsten, V. Panoutsakopoulou, A. J. Ross, K. A. Roth, G. R. MacGregor, C. B. Thompson and S. J. Korsmeyer, **2001**. Proapoptotic bax and bak: a requisite gateway to mitochondrial dysfunction and death. *Science* 292: 727–730. B89.

Wey, C. L., R. A. Cone and M. A. Edidin, **1981**. Lateral diffusion of rhodopsin in photoreceptor cells measured by fluorescence photobleaching and recovery. *Biophys J* 33: 225–32.

White, S. H. and G. von Heijne, **2004**. The machinery of membrane protein assembly. *Curr Opin Struct Biol* 14: 397–404.

Whitley, P., E. Grahn, U. Kutay, T. A. Rapoport and G. von Heijne, **1996**. A 12-residue-long polyleucine tail is sufficient to anchor synaptobrevin to the endoplasmic reticulum membrane. *J Biol Chem* 271: 7583–6. Pr.

Wiener, M. C. and S. H. White, **1992**. Structure of a fluid dioleoylphosphatidylcholine bilayer determined by joint refinement of x-ray and neutron diffraction data. ii. distribution and packing of terminal methyl groups. *Biophys J* 61: 428–33.

Wolter, K. G., Y. T. Hsu, C. L. Smith, A. Nechushtan, X. G. Xi and R. J. Youle, **1997**. Movement of bax from the cytosol to mitochondria during apoptosis. *J Cell Biol* 139: 1281–1292. B73.

Yang, L., T. A. Harroun, T. M. Weiss, L. Ding and H. W. Huang, **2001**. Barrel-stave model or toroidal model? a case study on melittin pores. *Biophys J* 81: 1475–85.

Yang, L. and H. W. Huang, **2002**. Observation of a membrane fusion intermediate structure. *Science* 297: 1877–9.

Yethon, J. A., R. F. Epand, B. Leber, R. M. Epand and D. W. Andrews, **2003**. Interaction with a membrane surface triggers a reversible conformational change in bax normally associated with induction of apoptosis. *J Biol Chem* 278: 48935–41. URL `http://www.jbc.org/cgi/content/full/278/49/48935`.

Zachowski, A., **1993**. Phospholipids in animal eukaryotic membranes: transverse asymmetry and movement. *Biochem J* 294 (Pt 1): 1–14.

Zakharov, S. D. and W. A. Cramer, **2002**. Insertion intermediates of pore-forming colicins in membrane two-dimensional space. *Biochimie* 84: 465–75. Pr.

Zakharov, S. D., E. A. Kotova, Y. N. Antonenko and W. A. Cramer, **2004**. On the role of lipid in colicin pore formation. *Biochim Biophys Acta* 1666: 239–49.

Zha, H., C. Aime-Sempe, T. Sato and J. C. Reed, **1996**. Proapoptotic protein bax heterodimerizes with bcl-2 and homodimerizes with bax via a novel domain (bh3) distinct from bh1 and bh2. *J Biol Chem* 271: 7440–7444. B55.

Zha, J., S. Weiler, K. J. Oh, M. C. Wei and S. J. Korsmeyer, **2000**. Posttranslational n-myristoylation of bid as a molecular switch for targeting mitochondria and apoptosis. *Science* 290: 1761–1765. B88.

Zimmerberg, J. and L. V. Chernomordik, **1999**. Membrane fusion. *Adv Drug Deliv Rev* 38: 197–205.

Zong, W. X., C. Li, G. Hatzivassiliou, T. Lindsten, Q. C. Yu, J. Yuan and C. B. Thompson, **2003**. Bax and bak can localize to the endoplasmic reticulum to initiate apoptosis. *J Cell Biol* 162: 59–69. Pr.